Università degli Studi di Ferrara

DOTTORATO DI RICERCA IN
SCIENZE DELL' INGEGNERIA

CICLO XXVI

COORDINATORE Prof. Trillo

Shear strengthening of RC beams using the Embedded Through-Section Technique

Settore Scientifico Disciplinare ICAR/09

Dottorando
Dott. Breveglieri Matteo

Tutore
Prof. Aprile Alessandra

Tutore
Prof. Barros Joaquim António Oliveira

Anni 2010/2014

ACKNOWLEDGEMENTS

I would like to express my gratitude to Professor Alessandra Aprile for having given me the possibility to perform this research and to work in an international background, for supporting my work in several occasions, and motivating me to reach this final result.

I would like to express my gratitude to Professor Joaquim Barros for having accepted the supervision of this doctoral thesis, for his important contribution in the development of this research project and for the passion for research he is able to transmit.

I would like acknowledge Ing. Sergio Tralli, Ing. Roberto Lovisetto (Elletipi S.r.l. – Ferrara, Italy) for supporting the experimental program, Ing. Marcello Bolognesi, Prof.Alberto Pellegrinelli, Prof. Paolo Russo from the ENDIF Geomatic Group (University of Ferrara, Italy) for monitoring the experimental program, Ing. Giuseppe Cersosimo (Interbau S.r.l. – Milano, Italy) for applying the ETS strengthening, BASF company Italy for providing the CFRP rods and the Engineering Department of the University of Ferrara for the financial support.

I would also like to express my gratitude to the persons, that I met during my doctoral studies. I would like to thank my parents and my sister for their unconditional support.

The work reported in the present thesis was carried out at the Department Engineering of University Ferrara, Italy, and at the Civil Engineering Department of the University of Minho, Portugal, in accordance with the agreement for a joint research doctoral thesis approved by the University of Minho on February 2nd, 2014 and by the Academic Senate of the University of Ferrara on April 16th, 2014.

A dissertation submitted in partial fulfillment of the requirements for the degree of

Doctoral degree in Science of Engineering by the University of Ferrara
Doctoral degree in Civil Engineering by the University of Minho

THIS THESIS HAS BEEN EVALUATED BY THE FOLLOWING BOARD OF EXAMINERS

Prof. Dr. **Aprile Alessandra**

ENDIF, Department of Engineering, University of Ferrara, Italy

Prof. Dr. **Joaquim Antonio Oliveira de Barros**

ISISE, Department of Civil Engineering, University of Minho, Portugal

Prof. Dr. **Guido Camata**

Department of Engineering and Geology, University "D'Annunzio" of Chieti-Pescara, Italy

Prof. Dr. **Thanasis Triantafillou**

Department of Civil Engineering, University of Patras, Greece

THIS THESIS WAS PRESENTED AND DEFENDED
BEFORE A BOARD OF EXAMINERS AND PUBLIC

09 APRIL 2015
AT UNIVERSITY OF FERRARA

Reading Committee for the additional qualification of "Doctor Europeaus":

Prof. Dr. **Antony Darby**

Department of Architecture and Civil Engineering at the University of Bath, UK

Prof. Dr. **Thanasis Triantafillou**

Department of Civil Engineering, University of Patras, Greece

ABSTRACT

A new shear strengthening technique, designated as Embedded Through-Section (ETS), has been developed to retrofit existing reinforced concrete (RC) elements. This technique calls for holes to be drilled through the beam section; then bars of steel or FRP materials are introduced into these holes and bonded with adhesives to the surrounding concrete. When concrete cover has not the bond and strength requisites to guarantee a strengthening effectiveness for the Externally Bonded and Near Surface Mounted techniques, ETS strategy can be a competitive alternative since it mobilizes the beam's concrete core which is, generally, free of damage. To explore the potentialities of the ETS technique for the shear strengthening of RC beams, an experimental program was carried out, composed of RC T-cross section beams strengthened in shear by using steel bars and ETS CFRP rods. The research was focused on the evaluation of the ETS efficiency on beams with different percentage of existing internal transverse reinforcement (ρ_{sw}=0.0%, ρ_{sw}=0.1% and ρ_{sw}=0.17%) and on the study of the interaction effect between ETS bars and existing steel stirrups. The influence of the inclination and shear strengthening ratio of ETS configurations on the shear strengthening efficiency was also evaluated. The good bond between the strengthening ETS bars and the surrounding concrete allowed the yield initiation of the ETS steel bars and the attainment of high tensile strains in the ETS CFPR rods, leading to significant increase in shear capacity (up to 136%). The attained level of shear capacity was strongly influenced by the inclination of the ETS bars and the percentage of internal transverse: inclined ETS bars provided higher increase of shear resistance than vertical ones.

The predictive performance of two analytical models to calculate the ETS strengthening contribution was assessed by using the experimental results. The first model follows an empirical approach (experimental-based approach), while the second model takes into account the physical and mechanical principles of the technique (mechanical-based approach).

The predictive performance of a numerical model is evaluated simulating the tested beams strengthened with ETS technique. The strategy to simulate the crack shear stress transfer in a fixed smeared crack based finite elements program is crucial to correctly predict the deformational and cracking behavior of RC elements that exhibit shear failure. An alternative strategy to shear retention function is presented in this work, based on the adoption of a bilinear softening diagram $\left(\tau_t^{cr} - \gamma_t^{cr}\right)$ for modeling the sliding component of the crack constitutive law. The parameters influencing the $\tau_t^{cr} - \gamma_t^{cr}$ diagram are individually investigated and analyzed as a function of the mechanical and geometrical properties of the tested beams. A simple rule to estimate the values of the $\tau_t^{cr} - \gamma_t^{cr}$ diagram is provided and its predictive performance is assessed.

SINTESI

La tecnica Embedded Through-Section (ETS) è una nuova tecnica di rinforzo sviluppata per aumentare la resistenza a taglio di strutture esistenti in cemento armato. Questa tecnica consiste nel praticare fori all'interno della sezione dell'elemento da rinforzare, in cui vengono inserite barre di acciaio o FRP, rese successivamente solidali al calcestruzzo circostante per mezzo di un materiale adesivo. Nel caso in cui la superficie esterna della sezione non sia in grado di fornire aderenza e resistenza sufficiente per garantire l'efficienza delle tecniche Externally Bonded Reinforcement (EBR) e Near Surface Mounted (NSM), la tecnica ETS può essere una valida alterativa, infatti quest' ultima mobilita la resistenza del calcestruzzo nell'anima della trave che è in generale priva di danneggiamento. Un programma sperimentale composto da travi di sezione a T in c.a. rinforzate con barre di acciaio e CFRP è stato condotto al fine di esplorare le potenzialità della tecnica ETS per il rinforzo a taglio. La ricerca è focalizzata sullo studio dell'efficienza della tecnica ETS in travi con diversa percentuale di armatura trasversale interna (ρ_{sw} = 0,0%, ρ_{sw} = 0,1% e ρ_{sw} = 0,17%), al fine di esaminare l'interazione tra le barre applicate secondo la tecnica ETS e staffe esistenti in acciaio. Gli altri parametri analizzati nel programma sperimentale sono il materiale, la percentuale e inclinazione del rinforzo. La buona aderenza tra le barre ETS e il calcestruzzo circostante ha permesso il raggiungimento della tensione di snervamento nelle barre di acciaio e di alti valori di tensioni di trazione nelle barre in CFPR, con conseguente notevole aumento della capacità di resistenza taglio (fino a 136%). Il livello di efficienza è stato fortemente influenzato dall'inclinazione delle barre ETS e dalla percentuale di rinforzo trasversale interno. Le barre inclinate hanno fornito maggiore incremento di resistenza al taglio di quelli verticali.

I risultati sperimentali sono stati utilizzati per valutare l'accuratezza due modelli analitici per calcolare il contributo a taglio fornito dal rinforzo ETS. Il primo modello è basato su un approccio empirico (approccio experimental-based), mentre il secondo modello si basa su principi fisici e meccanici che governano la trasmissione degli sforzi tra rinforzo e calcestruzzo nella tecnica ETS (approccio mechanical-based).

Il comportamento delle travi rinforzate tramite la tecnica ETS è stato simulato utilizzando programma ad elementi finiti al fine di valutare le prestazioni del modello costitutivo implementato per simulare l'azione tagliante. L'approccio per simulare questa azione in modelli basati sul "fixed smeared crack model" è fondamentale per stimare correttamente la relazione carico spostamento e stato fessurativo di elementi in c.a. che presentano rottura a taglio. Il tradizionale approccio basato sullo "shear retention factor" è stato sostituito da un' approccio alternativo che si basa su un diagramma sforzo di taglio-deformazione a taglio, $\tau_t^{cr} - \gamma_t^{cr}$, per la modellazione della energia di frattura a taglio. I parametri che influenzano il diagramma sono analizzati individualmente e in funzione delle proprietà meccaniche e geometriche delle travi. Una semplice regola per stimare tali valori del diagramma, $\tau_t^{cr} - \gamma_t^{cr}$, è stata fornita e le sue prestazioni sono state valutate.

Keywords

Shear strengthening

Reinforced concrete beams

Embedded Through-Section technique

ETS steel bars

ETS technique

ETS CFRP bars

Existing stirrups

Analytical model

Experimental-based model

Mechanical-based model

FEM simulation

Material nonlinear analysis

Shear Softening diagram

Table of Contents

Nomenclature

Explanation in the text of notation and abbreviation in direct conjunction to their appearance have preference to what is treated here.

Latin Letters

A_c	=	area of the concrete prism cross section
A_{fw}	=	area of the strengthening
A_{sw}	=	cross sectional area of the two legs of a steel stirrup
b_w	=	beam's width
C_1 , C_2 , C_3	=	integration constants of the bond model
CDC	=	critical diagonal crack (shear crack)
CDC_{avg}	=	average critical diagonal crack (shear crack)
CDC_{tan}	=	Tangent critical diagonal crack (shear crack)
d	=	beam cross section effective depth
$\underline{D}^{co}$	=	elastic constitutive matrix
$\underline{D}^{cr}$	=	crack constitutive matrix
$\underline{D}^{crco}$	=	constitutive matrix for the cracked concrete
D_I^{cr}	=	Constitutive softening/hardening modulus corresponding to crack opening mode I (tensile)
D_{II}^{cr}	=	Constitutive softening/hardening modulus corresponding to crack opening mode II (shear)
$D_{I,i}^{cr}$	=	crack constitutive matrix component relative to the i^{th} crack normal opening mode (mode I)
$D_{t,1}^{cr}$	=	crack shear modulus of the first linear softening branch = D_{II}^{cr}
$D_{t,2}^{cr}$	=	Crack shear modulus of the second linear softening branch
$D_{t,3-4}^{cr}$	=	crack shear modulus of the unloading and reloading branches
EC	=	embedded cable (type of finite element)
E_c	=	concrete Young's modulus
E_{fw}	=	strengthening young's modulus
E_{sw}	=	internal reinforcement Young's modulus
f_c	=	concrete compressive strength (Chapter 5)

f_{cm}	=	concrete average cylindrical compressive strength
f_{ct}	=	tensile strength
f_{ctm}	=	concrete average tensile strength
f_{ctm}^{*}	=	value of average concrete tensile strength for values larger than which concrete fracture does not occur
f_{epox}	=	Epoxy adhesive tensile stress
f_{fe}	=	effective stress in the ETS bar
f_{y}	=	steel yield stress
f_{yk}	=	characteristic steel yield stress
f_{t}	=	steel tensile stress
F	=	applied load
F_{f}	=	force resulting from the tensile stress in the ETS bars crossing the shear failure crack
$F_{\max}$	=	maximum load
F_{Ref}	=	maximum load of the reference beam
G_{c}	=	concrete elastic shear modulus
G_{f}^{I}	=	mode I fracture energy
$G_{f,s}$	=	mode II fracture energy
IP	=	integration point
h_{w}	=	beam cross section height
J_1, J_2, J_3	=	constants of the bond model
k	=	number expressing the safety factor of the model
L_1	=	strengthened beam's shear span length
L_2	=	un-strengthened beam's shear span length
l_{b}	=	crack band width
L_{d}	=	crack length
L_{f}	=	strengthening ETS bar length
L_{fi}	=	available bond length for a single i^{th} ETS bar

L_p	=	bar perimeter
L_{Rfe}	=	effective resisting bond length
L_{Rfi}	=	ith bar resisting bond length
$\overline{L}_{Rfi}$	=	average available bond length
$\overline{L}_{Rfi}^{eq}$	=	equivalent value of the average resisting bond length
n	=	number of installed bars in the considered cross section
n_f	=	number of ETS bars crossed by the shear failure crack
$N_{f,\text{int}}^{l}$	=	minimum integer number of bars that can cross the CDC
p	=	parameter that defines the shape of the last branch of the steel stress-strain curve
p_1	=	shear degradation factor
p_2	=	parameter defining the fracture energy available to the new crack
$PSTE$	=	plane stress element
s_{fw}	=	ETS bars spacing
s_{sw}	=	stirrups spacing
$\underline{T}^{cr}$		matrix that transforms the stress components from the coordinate system
V_f^{ana}	=	ETS analytical contribution
V_f^{I}	=	ETS contribution calculated with the experimental based-approach
V_f^{II}	=	ETS contribution calculated with the mechanical based-approach
V_{fd}^{I}	=	design value calculated using the experimental-based approach
V_{fd}^{II}	=	design value calculated using the mechanical-based approach
V_{f1}^{bd}	=	maximum value of the force transferable through bond by the given ETS bar
$V_{fi}^{bd}\left(L_{Rfi},\delta_{Li}\right)$	=	bond based constitutive law
V_f^{bd}	=	force transferred by bond capacity of a single ETS bars
$V_f^{II,bd}$	=	ETS contribution corresponding to the bond capacity
$V_f^{II,y}$	=	ETS contribution corresponding to the yield strength

V_{fi}^{cf} = concrete tensile fracture capacity

$V_{f}^{\exp}$ = experimental value of the ETS contribution

$V_{fi,eff}^{\max}$ = maximum effective capacity of the average-length bar along the CDC.

V_{Ref} = shear strength of a reference beam

V_{f}^{y} = yielding capacity of a single ETS bars

$V_{\max}$ = Total shear strength

V_{t} = the shear resistance of the ETS strengthened beam (Chapter 4)

u_{L} = deflection

$u_{L\max}$ = deflection at maximum load $F_{\max}$

Greek letters

α = angle between the axis and the generatrices of the concrete conical surface.

α_{i} = fracture parameters used to define the trilinear stress-strain softening diagram

α_{th} = threshold angle

β = shear retention factor

β_{f} = inclination of the strengthening with respect to the beam longitudinal axis.

γ_{f} = partial safety factor

γ_{t}^{cr} = crack shear strain

$\gamma_{t,p}^{cr}$ = peak crack shear strain

$\gamma_{t,u}^{cr}$ = ultimate crack shear strain

δ_{1} = slip corresponding to the free-slipping in the local bond stress-slip relationship.

δ_{Li} = loaded end slip imposed.

$\Delta\underline{\varepsilon}$ = vector of the incremental strain

$\Delta\underline{\varepsilon}_{l}^{cr}$ = local vector of the incremental crack strain

$\Delta\underline{\sigma}$ vector of the incremental stress

$\Delta\underline{\sigma}_{l}^{cr}$ = local vector of the incremental crack stress

ε_{n}^{cr} = crack normal strain

$\varepsilon_{n,i}^{cr}$ = crack normal strain used to define point *i* in the trilinear stress-strain softening diagram

$\varepsilon_{n,u}^{cr}$ = ultimate crack normal strain

ε_{sh} = strain corresponding to point 2 (PT2) of the steel stress-strain relationship

ε_{su} = strain corresponding to point 3 (PT3) of the steel stress-strain relationship

ε_{sy} = strain corresponding to point 1 (PT1) of the steel stress-strain relationship

ε_{fe} = effective strain

ε_{fe}^{I} = effective stain for the evaluation of the shear strengthening contribution of the ETS system

ε_{fd} = design effective strain

$\varepsilon_{F\max}$ = strain measured at $F_{\max}$

$\varepsilon_{\max}$ = maximum strain recorded in the ETS bars or stirrup.

ε_{sy} = steel yield strain

η = reduction factor of the initial average available resisting bond length

θ = critical diagonal crack (CDC) inclination angle

λ = constant entering the governing differential equation for the bond elastic phase

ν_c = poisson's ratio

ξ_i = fracture parameters used to define the trilinear stress-strain softening diagram

ρ_{fw} = percentage of shear strengthening ratio

ρ_{sl} = percentage of steel longitudinal reinforcement.

ρ_{sw} = percentage of shear reinforcement ratio

σ_n^{cr} = crack normal stress

$\sigma_{n,i}^{cr}$ = crack normal stress used to define point *i* in the trilinear stress-strain softening diagram

σ_{sh} = stress corresponding to point 2 (PT2) of the steel stress-strain relationship

σ_{su} = stress corresponding to point 3 (PT3) of the steel stress-strain relationship

σ_{sy} = stress corresponding to point 1 (PT1) of the steel stress-strain relationship

τ_t^{cr} = crack shear stress

$\left(\tau_t^{cr} - \gamma_t^{cr}\right)$ = Softening diagram

$\tau_{t,p}^{cr}$ = crack shear strength

τ_0	=	adhesive-cohesive initial bond strength of the local stress-slip relationship/Peak stress of the local bond stress-slip relationship
ϕ_f	=	ETS bar diameter
ϕ_s	=	stirrups diameter

1

Introduction

1.1 Background and motivation

Strengthening and retrofitting of reinforced concrete (RC) structures are important topics for civil engineering, since their implication has historical, social and economic relevance nowadays. The need to preserve the built heritage does not regard exclusively the masonry buildings belonging to the historical heritage, but also includes an increasing number of relatively new reinforced concrete structures, most of them built after the Second World War. The "list" comprises a large number of strategic, public and residential buildings and infrastructures, which represent the biggest part of the reinforced concrete building stock. There is the need to strengthen the existing reinforced concrete structures such as bridges and buildings in order to meet the changing social needs, the design standard's upgrade, the safety requirement's increase and, finally, the deterioration of materials.

The number of new constructions is progressively reducing and the number of strengthening interventions in civil construction is significantly increasing, indicating this field as a possible expansion of the construction market. Part of the European reinforced concrete buildings stock is obsolete and structurally inadequate with respect to modern building regulations. The problem of obsolete buildings particularly involves a large part of South Europe, where the seismic hazard is considerable (Portugal, Spain, Italy and Greece).

The main problem related to existing RC structures, besides their inadequacy to the new design code, is the lack of structural ductility. In fact, brittle structural behavior can lead to collapse of the structure in extreme situations. The shear resistance of RC elements is an important aspect to assure adequate structural ductility and avoid brittle and unpredictable failures. Unlike the updated codes, which provide a high percentage of transverse steel reinforcement, the old codes did not include strict rules on construction details aiming to increase ductility. As a consequence, one of the main tasks in upgrading

the existing structures that require strengthening interventions is to increase the shear resistance of the beams, columns and joints.

The shear strengthening requires special attention since, unlike the bending strengthening, a unified approach for the calculation of the shear strength of RC elements does not exist. Shear behavior and shear strengthening are challenging topics that have been faced by a considerable number of researchers in the last decades. A large number of beams with and without strengthening systems have been tested, and several analytical formulations have been proposed. Traditional strengthening techniques, such as concrete and steel jacketing or steel plating, have been replaced by innovative techniques based on the use of non-conventional materials for constructions that are presented in Chapter 2. Among these techniques, the shear strengthening using Fiber Reinforced Polymers (FRP) materials has received a considerable attention of the research community dedicated to the structural upgrade, and significant advances have been obtained. The benefits from using composite materials in this context are derived from their following attributes: high strength, lightness, immunity to corrosion, ease of application. However, also disadvantages are well known that mainly regards the vulnerability to acts of vandalism, and the loss of efficiency in case of fire. One of the main drawbacks that limits the efficiency of the FRP strengthening system is related to the premature debonding; in this case, the composite material fails well below its ultimate strain. This means that the high potentialities of the FRP are, in general, not fully exploited.

The Externally Bonded Reinforced (EBR) and the Near Surface Mounted (NSM are the main FRP-based strengthening techniques that have been proposed for the upgrading of RC structures. In the NSM technique the FRP is installed into narrow slits open in the concrete cover, while in the EBR technique the FRP is simply bonded to the external surface of the element to be strengthened. The NSM has been demonstrated to be more effective than the EBR technique since a larger bond strength can be mobilized, due to the higher confinement provided to the FRP by the surrounding concrete.

An alternative approach for the shear strengthening of RC beams, denominated Embedded Through-Section (ETS) technique, was recently proposed. This technique consists of opening holes across the depth of the beam's cross-section, with the desired inclinations, introducing bars into these holes and bonding them to the concrete substrate with adhesives. By using this technique, the bond performance between the strengthening system and the surrounding concrete is improved with respect to the previous FRP-based strengthening techniques, since the strengthening element is deeply embedded in the concrete cross section. The strengthening bars can be made of composite material as well as of steel; the first experimental tests showed that a significant increase of shear strength can be obtained with both of them. Due to high effectiveness of this strengthening technique, the tested beams failed mainly in bending, which made impossible to determine the shear strength contribution provided by the adopted

ETS systems. A further advantage of the ETS is the protection provided by the surrounding concrete to the embedded bars against vandalism acts and ageing effects; in case of ETS steel bar, the corrosion is avoided by providing a small layer of covering material at its extremities.

1.2 Scope and Aim of the Thesis

The purpose of the research work presented in this thesis is to increase the existing knowledge on the structural behavior of RC members strengthened in shear using the ETS technique. For this purposes an experimental program was carried out aiming to analyze and discuss the aspects related to the ETS strengthening effectiveness, mobilized strengthening mechanisms and the types of failures of the ETS system. This work aims also to contribute to a deep understanding on the mutual interaction between the existing steel stirrups and the ETS strengthening, as well as the influence of percentage and inclination of the ETS bars, in the context of shear capacity of RC beams. The shear strengthening effectiveness of different ETS bar material is also investigated. New data are provided by the experimental programs carried out that can be used in the establishment of new design guidelines on the shear strengthening of RC beams using the ETS technique, or to improve those already present in literature.

Another goal of the present work is to develop a simple analytical model for the calculation of the shear resistance contribution provided by steel ETS bars, since a limited research has been dedicated to this topic, and most of the available approaches consist of extremely simplified models based on the existing guidelines for EBR or NSM FRP-based strengthening techniques.

In the context of finite element formulations, the present work also aims to investigate the potentialities of a constitutive model that adopts a shear softening stress-shear strain diagram for modelling the crack shear stress transfer in the framework of modeling the behavior of RC elements that fail in shear. The adopted constitutive model has exhibited a good capacity for predicting the relevant behavioral aspects of RC beams failing in shear, even those shear strengthened with EBR and NSM FRP-based systems, so its applicability to the ETS technique is explored in the present work. For this purpose, the parameters that define this crack shear softening diagram are deeply investigated and discussed by comparing the results obtained experimentally and numerically, in order to contribute for the establishment of possible criteria for the selection of these parameters.

It is expected that this thesis is of interest to structural engineers, composite material suppliers and testing institutions, as well as standardization organizations and technical committees with the charge of developing design codes in the areas of the strengthening of RC structures.

1.3 Thesis Structure

The thesis is divided into six chapters.

In Chapter 1, the principal aim of this research work and an overview of the thesis are presented. Chapter 2 gives fundamental background to understanding the shear mechanism in reinforced concrete beams. Thereafter literature review on shear strengthening techniques is presented. The main section is dedicated to FRP shear strengthening. In the last section, the previous experimental programs on reinforced concrete beams strengthened using the ETS technique are presented.

In Chapter 3, the experimental program is outlined: specimens, materials and test set-up are described. The obtained results of the test carried out on T-cross section RC beams strengthened using the Embedded Through-Section technique are presented and analyzed in terms of their structural behavior, failure modes and strengthening effectiveness. The influence of the investigated parameter is discussed. The contents of this chapter were published in the following ISI Journals:

- *Breveglieri M, Aprile A, Barros J.A.O, 2014. Shear strengthening of reinforced concrete beams strengthened using embedded through section steel bars. Engineering Structures 2014;81:76–87.*
- *Breveglieri M, Aprile A, Barros J,A,O., 2015. Embedded Through-Section shear strengthening technique using steel and CFRP bars In RC beams of different percentage of existing stirrups. Composite Structure 2015; 126; 101-113.*

Chapter 4 presents two analytical models to estimate the steel ETS system by contribution. The first model follows an empirical approach and is denominated “Empirical-based” model. Similarly, the second model follows a mechanical approach and is denominated “physic-mechanical “model. The content of this chapter was submitted for publication was submitted for publication to a ISI Journal with the following title:

- *RC concrete beams strengthened in shear using the Embedded Through-Section technique: experimental results and analytical formulation. Authors: Breveglieri M, Aprile A, Barros J,A,O.*

Chapter 5 deals with the numerical simulation of the tested beams, presenting and discussing the assessment of the shear softening diagram to simulate RC beams failing in shear. A parametric study has been performed to have a better understanding on the implemented constitutive model. Using the aforementioned numerical simulation, a simple rule to estimate the shear softening diagram’s parameters has been proposed. The content of this chapter was submitted for publication to a ISI Journal with the following title:

- *Assessment of a shear - softening FEM-based model for the analysis of RC beams strengthened in shear using the ETS technique. Authors: Breveglieri M, Barros J,A,O, Aprile A.., Ventura-Gouveia A.*

Chapter 6 provides the major concluding remarks and findings of the conducted research program, together with suggestions for future research.

Finally, a complementary section with annexes is also presented. Annex C present the result of a preliminary numerical work developed to simulate the tests performed on ETS strengthened beams by Barros and Dalfré (2012). The obtained results have been published in the conference proceedings FraMCoS-8 Fracture Mechanics of Concrete and Concrete Structures, Toledo, Spain, with the following title

- *Model to simulate the behavior of RC beams shear strengthened with ETS bars. Authors: Barros JAO, Breveglieri M, Ventura-Gouveia A, Dalfré GM, Aprile A. (2013).*

2

Literature Review

2.1 Introduction

This chapter provides a general look on shear in reinforced concrete structures, paying special attention to the shear strengthening of RC elements. The first part of this chapter is dedicated to the understanding of the fundamental concept of shear and shear mechanisms in concrete structures; furthermore, the main parameters influencing the shear resistance are presented. A brief overview of the main theoretical models and the codes formulation to estimate the shear resistance of RC beams is presented. The second part of the chapter deals with the shear strengthening of RC structures by using non-conventional techniques. In order to avoid the occurrence of shear failures several alternative techniques have been proposed by researchers in the last decades. The previous research has focused on the use of Fiber Reinforced Polymers (FRP) material, but, also alternative techniques have been investigated and developed. Those techniques are shortly presented in this section giving particular attention to the Externally Bonded Reinforcement (EBR), Near Surface Mounted (NSM) and Embedded Through-Section (ETS) FRP-based techniques. Previous experimental programs on the ETS technique are summarized here, since the behavior of RC concrete beams using this latter technique is the object of the present research. Existing guidelines formulation for the estimation of the shear contribution of the FRP system are discussed. Finally, a short section is dedicated to the bond behavior of steel and composites bar cast-in place and post-installed into concrete.

2.2 Fundamental concepts of shear

The shear resistance and behavior of RC elements is a complicated problem due to the high number of parameters that can affect the shear resistance. The understanding of the behavior of reinforced concrete elements under shear load and the mechanisms governing the shear stress transfers have involved a large number of researchers and is still a vivid topic in the international research community. In the beginning of the XX century Hennebique (Ritter 1899) presented and patented a construction method to

increase the shear resistance of RC beams, this method consisted of introducing steel strips similar to the current stirrups in the concrete. Simple models were right away developed by Ritter (1899) and Mörsch that in his textbook: Der Eisenbetonbau, seine Theorie und Anwendung (1908), demonstrates that a reinforced concrete beam can be treated as a simple or multiple truss system where the compressive forces are carried out by diagonal struts and the tensile stresses by stirrups or bent-up bars. From the beginning of the XX century, although the "truss concept" proposed by Mörsch still supports most of the design approaches, a huge progress has been made in understanding the concepts on which shear transfer mechanisms and resistance of RC structures are based; the parameters influencing the shear resistance are nowadays clear and several models to take into account these parameters have been developed. Nevertheless, there is a lack of a unified theory for the calculation of the shear force resistance of RC concrete elements.

2.2.1 Concept of shear stress

The state of stress in cracked reinforced concrete member differs considerably from what is predicted by the theory of linear elasticity and the actual distribution of shear stresses over the cross section is not fully clarified. In case of un-cracked concrete, the shear stresses can be calculated from the equilibrium equation (Fig.2.1a) following Jourawsky's formulation, where in case of rectangular beam (beam's width, b_w) the shear stress, τ, describes a parabolic curve along the section's axis. The shear stress along the beams height of a homogeneous, isotropic un-cracked beam, τ, can be derived from considerations of internal equilibrium of flexural stresses with the following equation:

$$\tau_{(y)} = \frac{VS(y)}{b_w I} \tag{2.1}$$

Where S(y) and I are the first and the second moment of area of the section respectively. The shear stress so generated can be combined with the flexural stress parallel to the beam's axis. In absence of cracking, the stress field is represented by a set of diagonal compressive and tensile stresses, inclined at an angle φ with respect to the longitudinal axis. By considering the equilibrium of an infinitesimal element, the magnitude, σ_1, σ_2 and the inclination φ of the principal stresses, resulting from the simultaneous application of a tensile stress σ and a shear stress illustrated τ in Fig. 2.1c can be obtained as follows:

$$\sigma_1 = \frac{\sigma}{2} + \sqrt{\sigma^2 + 4\tau^2} \text{ Principal tension } \sigma_2 = \frac{\sigma}{2} - \sqrt{\sigma^2 + 4\tau^2} \text{ Principal compression} \tag{2.2}$$

The inclination of the tensile stress with respect to the beams' axis is found using the Mohr-Coulomb circle

$$\tan 2\varphi = \frac{2\tau}{\sigma} \text{ or } \tan \varphi = \frac{\tau}{\sigma_1} \tag{2.3}$$

The inclination of the principal stresses is illustrated for the case of a uniformly loaded simply supported rectangular beam in Fig. 2.1c. The stress trajectories intersect the neutral axis at 45°. Concrete can withstand the pure shear stress well; problems arise at the formation of shear crack, caused by the attainment of the concrete tensile strength, in fact, when the principal tensile stress become higher than the tensile stress of the concrete, a crack will form perpendicular to the direction of principal tensile stress. These cracks are generically called diagonal or shear cracks. In real practice, there is little interest in the shear cracking resistance of an un-cracked section of ordinary reinforced concrete, which is important in prestressed members (uncovered in this work) and member subjected to high axial compression. For ordinary reinforced concrete, there is bigger interest in the shear cracking resistance of a cracked section.

The concept of shear stress was extended to the idealized section of a cracked reinforced concrete beams, as shown in Fig. 2.1b, the horizontal force to be transferred across the cracked zone remains constant, as well as the shear stress τ (Park and Paulay 1975). It is assumed that the concrete below the neutral axis is in a state of constant pure shear. From the concepts presented in Fig.2.1a, the incremental tension force is $dT = \tau b_w dx$, it is possible to obtain the value of τ as indicated in Eq. (2.4):

$$\tau = \frac{1}{b_w}\frac{dT}{dx} = \frac{dM}{dx}\frac{1}{b_w jd} = \frac{V}{b_w jd} \tag{2.4}$$

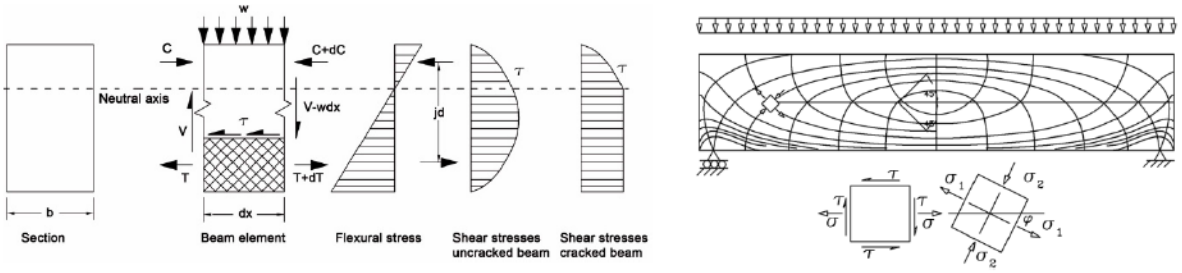

Fig 2.1 Trajectories of principal stresses in a homogeneous isotropic beam. Shear force, shear stresses in a homogeneous isotropic beam (a) assumed shear stress in cracked beam.

In a region of large bending moments, the stresses are greatest at the extreme tensile fiber of the member and are responsible for the initiation of flexural cracks perpendicular to the axis of the member. In the region of high shear force, principal tensile stress generate inclined cracks at approximately 45°

to the axis of the member. Under this hypothesis, Eq. (2.4) has been used as a measure of the shear stress in the cracked tension zone of a reinforced concrete beam, regardless of the presence of flexural cracks, and is still used in many countries as a convenient index to measure shear intensity. However Eq. (2.4) cannot be considered as giving a shear stress at any particular locality in a cracked reinforced concrete beam. This stress called for many years as "nominal stress" has also been considered in the design to evaluate the ultimate load carrying capacity, a reinforced member with no shear reinforcement, assuming that the diagonal crack is governing the failure. ACI guidelines (ACI-318-08) for example adopted an index of shear intensity based on an average stress on the full effective cross section (omitting the reduction of the internal level arm 0.9d) as:

$$\tau = \frac{V}{b_w d} \tag{2.5}$$

2.2.2 Mechanisms of Shear resistance

Shear transfers action and resisting mechanisms in concrete beams are influenced by many parameters which are difficult to clearly identify in fact, a complex stress redistribution occurs after cracking, that makes it impossible to determine which of the resisting mechanism will contribute the most. The 1973 ASCE-ACI Committee 426 (1973) report identified the following four mechanisms of shear transfer: 1) shear stresses in un-cracked concrete-flexural compression zone, 2) interface shear transfer, 3) dowel action of the longitudinal reinforcing bars simulates the dowel effect, 4) arch action and 5) residual tensile stresses transmitted directly across cracks (mechanism identified after the report release) (See Fig.2.2).

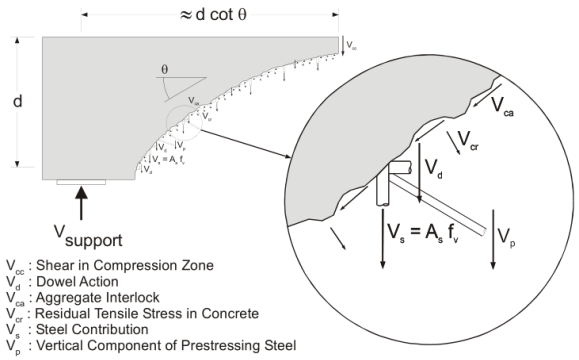

Fig. 2.2 Shear Mechanisms/Actions Contributing to Shear Resistance

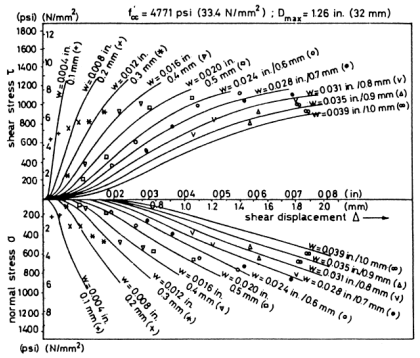

Fig. 4.3—Comparison of Walraven's experimental results and predictions for crack interface shear transfer (Walraven 1981).

Fig. 2.3 Comparison of Walravens' experimental results and prediction for crack interface-shear transfers (Walraven 1981)

Researchers have in general assigned different importance to each of these mechanisms, resulting in different models, mainly for members without shear reinforcement. In fact in beams with the presence

of stirrups each of these mechanisms is participating but its contribution on the total shear resistance is usually smaller, since the truss action is activated by the steel reinforcement.

Shear in the un-cracked concrete and flexural compression zone

In the un-cracked regions of a member, the shear force is transferred by inclined principal tensile and compressive stresses, as visualized by the principal stress-trajectories in Fig. 2.1c. In a cracked sections, this state of stress is still valid in the un-cracked compression zone, which contributes to the shear resistance. The magnitude of the shear resistance is limited by the depth of the compression zone since the integration of the shear stresses over the depth of the compression zone gives the shear force component. Fenwick and Paulay (1968) suggested that shear resistance carried by the compression zone is about 25% of the total shear strength. This contribution has been in general assumed proportional to the concrete strength class. In a slender member without axial compression, the shear force in the compression zone does not contribute significantly to the shear capacity because the depth of the compression zone is relatively small (Taylor 1974; Reineck 1991b).

Interface shear transfers

The interface shear transfer mechanism is based on early works by Fenwick and Paulay (1968), Mattock and Hawkins (1972), and Taylor (1974). The physical explanation relies in the local roughness in the crack plane that provides resistance against slip and allows the shear transfers along the crack. This mechanism was usually referred as “aggregate interlock”, since in a normal concrete class strength the cracks opens in the concrete matrix, enclosing the aggregates, resulting in a highly irregular surface of the crack which provides surface resistance against slip. However, it seems more appropriate to use the terminology as “shear transfers” of “friction”, since this action was observed even if cracks propagation occurs through the aggregate as it does in high strength concrete where the matrix is of similar strength to the aggregates. Dedicated research on this mechanism have evidenced the influence of four parameters: crack interface shear stress, normal stress, crack width, and crack slip. Walraven (1981) developed a model which was able to describe the relationship between the stress and shear displacement at different crack opening Fig. 2.3, this work also assessed the influence of the compressive strength and the aggregate size (normal compressive strength were considered). Other relationships have been proposed based on Walraven’s experimental data (Kupfer et al. 1983; Vecchio and Collins 1986) although large differences may still occur between the constitutive laws of different researchers. This mechanism is now well known and is widely accepted as an important shear-transfer mechanism. The important role of interface shear transfer in the redistribution of diagonal compression fields in beams with stirrups was investigated by Collins 1978; Kupfer et al. 1983; Dei Poli et al. 1990.

The ability of diagonal cracks to transfer shear, explicitly controls the capacity of members without stirrups, otherwise, in presence of stirrups, these offer resistance to crack opening by bridging the crack and improving the interface shear transfer.

Dowel action

The works by Baumann and Rüsch (1970) Vintzeleou and Tassios (1986) and Chana (1987) has analyzed the dowel action of longitudinal reinforcement, showing that, when macro cracks forms across longitudinal bars, a resisting action due to the vertical force induced by the sliding between the surfaces of the crack, is provided by the steel longitudinal bars. The dowel action is mostly influenced by the geometry of the concrete elements, since, it depends on the amount of concrete cover beneath the longitudinal bar and by the concrete tensile strength, which has in general a small influence. Normally, the dowel action is not very significant in members without transverse reinforcement because the maximum shear in a dowel is limited by the tensile strength of the concrete cover supporting the dowel. Otherwise, this action may be significant in the presence of stirrups since the "dowel action" stiffness of the longitudinal bars is increased by the constrained action offered by the stirrups. Dowel action may be significant in members with large amounts of longitudinal reinforcement, particularly when the longitudinal reinforcement is distributed in more than one layer.

Arch action

The shear resistance of a concrete member can be divided into two separate “actions” (Park and Paulay 1975), by decomposing the rate of change of bending moment along the beam in two contributes. The first contribute indicates the change of internal tensile force along the longitudinal reinforcement to balance the external moment. This is called beam action, and describes the behavior of slender unreinforced beams which are characterized by a tension zone that divide concrete into blocks. The mechanical model can be figured as “concrete cantilever” supported at the beams’ top and loaded by the horizontal shear from longitudinal bonded reinforcement (Fig. 2.4a). Regarding beam action, the physical models describing this action can be classified further into tooth models (Kani 1964), in which the resisting action is provided by the bending of the tooth, due to the variation of the tensile force in the longitudinal reinforcement. The second contribution that originates is the arch action Fenwick and Paulay (1968), which is characterized by the change of the internal lever arm (location of longitudinal compression stress resultant in concrete) changes, to balance the moment. The arch action implies, that shear can be sustained by inclined compression in the beam by forming an arch in which the tensile horizontal reaction is provided by the flexural reinforcement in case of simply supported beams (Fig. 2.4b). Due to the high horizontal reaction, the arch action can only occur if an adequate anchorage of

the longitudinal reinforcement is provided. This action characterizes the failure of beams with a relative small shear span to depth ration (a/d) (Section 2.4). In this case, the most used method to analyze the arch action is the adoption of a strut and tie model.

Residual tensile stresses across cracks

In cracked concrete, residual tensile stresses after the formation of the first crack can be transmitted directly across the crack. Small pieces of concrete bridge the crack and continue to transmit tensile force up to crack widths in the range of 0.05 to 0.15 mm. The concept of the residual tensile stress can be compared with the softening branch after the peak tensile stress is reached, typical of the constitutive model describing the behavior concrete in tensions (fib 2013). The deformations are localized in a very small region (the fracture zone); therefore, the response should be expressed in this case in terms of a stress-crack opening relationship and not strain. Fig.2.5 (Gopalaratnam and Shah 1985) shows a typical response of concrete loaded in tension. Due to the presence of these tensile stresses, the cracked concrete, in the vicinity of the tips of inclined and flexural cracks can also carry shear stresses that add to the shear capacity of the concrete.

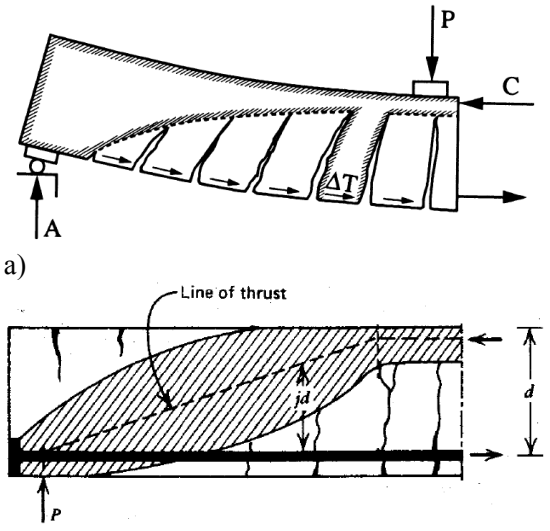

Fig. 2.4 Kani's tooth model for slender beam without shear reinforcement (a), Arch action (b)

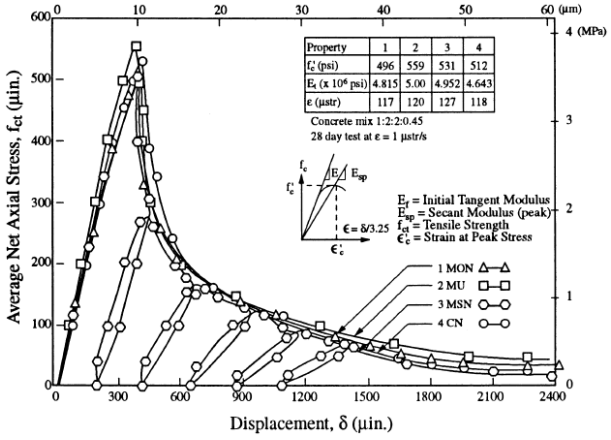

Fig. 2.5 Response of a plain concrete loaded in uniaxial tension (Gopalaratnam and Shah 1985**)**

Reineck (1991a) indicates that the residual tensile stresses provide a significant portion of the shear resistance of very shallow members (that is, depths less than about 100 mm), in that case, the crack opening is small, and the resistance provided by the residual tensile stresses is significant. However, in a large member, the contribution of crack tip tensile stresses to shear resistance is less significant due to the large crack widths that occur before failure in such members.

Shear reinforcement

In members with shear reinforcement, the largest portion of the shear forces is in general carried by the shear reinforcement after diagonal cracks are formed. The presence of the transversal reinforcement allows the formation of the "truss action" in which this carries out the tensile stresses after formation of cracks. Shear reinforcement so, provides a higher interface shear transfers, providing a certain level of restraint against the growth of inclined cracks by bridging the crack. The presence of stirrups also ensure a more ductile behavior. Finally, shear reinforcement provides dowelling resistance to shear displacements along the inclined crack. For these reasons, the presence of shear reinforcement changes the relative contributions of the different shear resisting mechanisms. Depending on the amount of the transverse reinforcement more inclined crack may develop until the stirrups yield. After the yielding of the stirrups, the load may also increase due to flatter inclined struts crossing the cracks. This latter mechanism is possible due to the interface shear of friction along the crack faces. The minimum amount of shear reinforcement required to affect such changes is of fundamental importance, this is taken as a function of the concrete strength in most major design codes.

2.2.3 Parameters influencing shear Capacity and Shear Failure

Depth of member or size effect

The findings on small scale test beams were also applied to big reinforced concrete beams up to 1965, when several US Air Force warehouse beams collapsed under a shear force that was less than one half of the ACI code prediction. After investigation it was found that it was it was possible to explain the results in terms of size effect. Kani (1967) demonstrates that there is a significant size effect for which the shear strength of beams without shear reinforcement decrease, as the effective depth increase. Shioya et al. (1989) extended the available data to beam depths of 3000 mm, confirming Kani's results. As shown in Fig. 2.6, the average shear stress to cause failure of the largest beam was about one-third the average shear stress to cause failure of the smallest beam. There is general agreement that the main reason for this size effect is the larger width of diagonal cracks in larger beams; however, there is disagreement on how best to model this phenomenon for which different formulas have been proposed as presented by Reineck 1991b. Bazant and Kim (1984) proposed a size-reduction factor based on nonlinear fracture mechanics and suggest that the large amount of energy that is released in the cracking of large members leads to the faster propagation of inclined cracks and lower shear failure stress. Others believe that the most important consequence of wider cracks is a reduced ability to transmit crack interface shear stresses, due to the larger cracks widths that occur in larger members. Tests have demonstrated that the size effect is not significant when beams without stirrups contain well distributed longitudinal reinforcement.

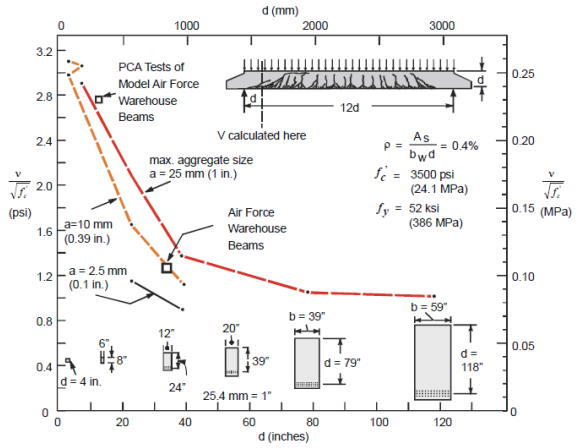

Fig. 2.6 Size effect in shear (Kuchma and Collins. 1998)

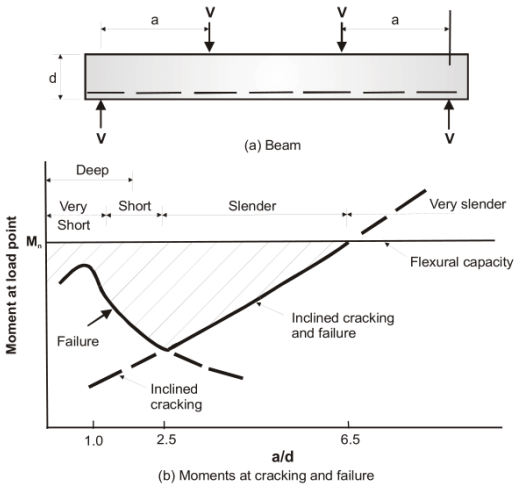

Fig. 2.7 "Kani's shear valley" Influence of the shear-span to depth ratio

Shear Span to Depth Ratio

Extensive research on the behavior of simply supported RC beams failing in shear evidence the influence of shear span to depth ratio (a/d). The shear span is the distance, a, between a support and a point of concentrated load. Kani (1964) conducted a large experimental study to assess the influence of the a/d ratio on the shear resistance of RC beams without shear reinforcement. The results are represented in the so-called "Kani's Valley of Shear Failures" (Fig. 2.7), in this graph the beams have been classified into four types depending on their a/d ratio and depending on the failure that they exhibited. Beams with a/d ratios less than about 2.5 present in general high strength, because a significant portion of the shear may be transmitted directly to the support by an inclined strut. This mechanism is frequently referred to as arch action, for deep beams. The arch action is the dominant mechanism and failure occurs due to crushing or splitting of the concrete, which justifies the use of a strut-and-tie model, rather than a sectional design approach. In beams with a/d ratios between 2.5 and 7 the arch effect is negligible since the arch mechanism is not capable of sustaining the cracking load, and the beam mechanisms commands. In beams without stirrups failure occurs as the diagonal cracking load is applied. It has been recognized that, as members become deep, the average stress at failure become progressively larger than in slender beams. Many empirical formulas for calculating shear strength include an a/d ratio to account for the influence of this parameter. The a/d relates the maximum moment and the maximum shear force for simple beams subject to point loads $M_{max} = V_{max} \times a$ and thus the moment to shear force ratio is $M_{max}/V_{max}\ d = a/d$. For distributed loading this term is also significant, as already pointed out by Kani (1964, 1967), and it gives $M_{max}/V_{max}\ d = l / 4d$, which means

that "a" is the distance to the resultant of the loads in one half of the span. Therefore, the a/d-ratio characterizes the slenderness of a simple beam and the value influences the relationships between the different shear transfer actions.

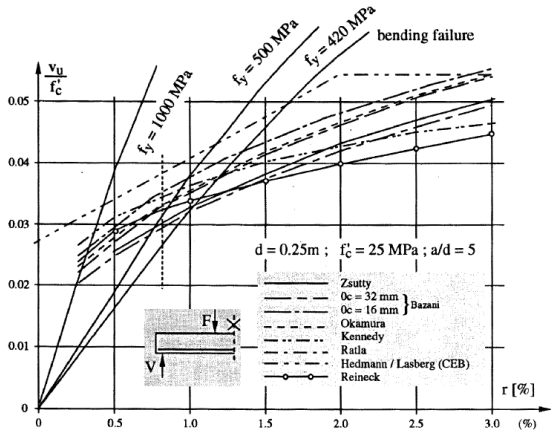

Fig. 2.8 Increase in ultimate shear capacity (dimension less value) with increasing reinforcing ratio according to different proposals (Reineck 1991b)

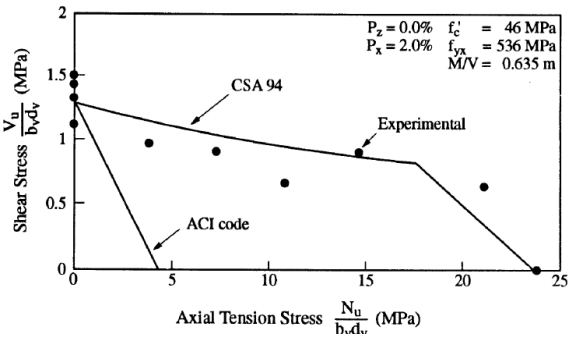

Fig. 2.9 Influence of axial load on shear strength of members without stirrups

Longitudinal reinforcement

The longitudinal reinforcement can affect the shear strength by bridging the cracks, in fact, for a constant amount of load, as the longitudinal reinforcement ratio decreases, flexural stresses and strains increase and the shear strength is lowered. The reduction in shear capacity can be explained by an increased crack width, resulting in lower interface shear transfer, correspondingly longer flexural cracks that reduce the size of the compression zone. Further, as the longitudinal reinforcement ratio decreases, dowel action decreases. It has also been reported that for members having longitudinal bars distributed over their height, crack spacing is smaller and that improves shear strength significantly (Collins and Kuchma, 1999). The design codes also usually require that additional longitudinal reinforcement be provided to resist the large tensile force due to shear in diagonally cracked members without stirrups. Fig. 2.8 compares the predicted influence of the quantity of longitudinal reinforcement from a number of empirical formulas. It was also observed that members with low amounts of longitudinal reinforcement may fail at very low shear stresses. The flexural capacity is also shown for different strengths of longitudinal reinforcement.

Axial force

When a RC element is subjected to that axial tension, its shear strength decreases, otherwise, if axial compression (for example, due to load or pre-stressing) is applied, the shear strength increases. Tensile forces make the crack angle steeper, and longitudinal reinforcement needs to be provided in both the top and bottom of the member. Members without shear reinforcement subjected to large axial

compression and shear, may fail in a very brittle manner at the instance of first diagonal cracking. As a result, a conservative approach should be used for such members. It is in fact not very well understood how much the shear capacity is influenced by the axial load and its influence on member's ductility. Compressive forces on the other hand increase the depth of the compressed un-cracked compression zone, and decrease the shear crack width, resulting in a higher shear capacity. The effect of the axial force may be underestimated for member subjected to axial compression and shear as demonstrated by Gupta and Collins (1993) for the ACI 318 approach (Fig. 2.9). On the other hand, for members without shear reinforcement but containing appropriate longitudinal reinforcement, the ACI 318-08 procedure for members subjected to shear and tension can be very conservative.

Concrete Strength

The shear strength also increases with the increase of concrete strength. The concrete compressive strength in general, is used to estimate the tensile strength of the concrete, because, direct tensile tests are more difficult to perform and the results present in general a higher dispersion than the compression tests. The concrete contribution to shear is usually related to the formation of the shear diagonal cracking, and therefore dependent on the tensile strength of the concrete. The ACI 318-08 shear design approach in which the shear strength is taken as proportional to the square root of f'_c is also shown in the same Fig. 2.10. Other codes as the Eurocode 2 take this contribution portioned to $f'^{1/3}_c$ or $f'_c f'^{2/3}_c$ depending on its version. The shear failure stresses of the beams tested by Moody et al. (1954) increase as the concrete compressive strength increases. ACI 318-08 is shown to provide a reasonable estimate of the influence of f'_c for these beams which were small, heavily reinforced and cast with low-to-medium-strength concrete. Similarly, the ACI provision is only slightly un-conservative for the moderately reinforced and mid-sized members that were tested by Yoon and Cook (1996). However, Collins and Kuchma (1999) Angelakos et al. (2001) did not find a similar increase in shear strength with concrete strength for their tests of larger, more lightly reinforced beams, and cast with high strength concretes with a small maximum aggregate size, as reported by Kuchma and Kim (2001) (Fig. 2.10). The explanation offered by some researchers for why the shear stress at failure does not increase as greatly, or not at all, with increasing concrete compressive strength is that the smoother shear cracks in high-strength concrete members reduce the effectiveness of the interface shear transfer mechanism.

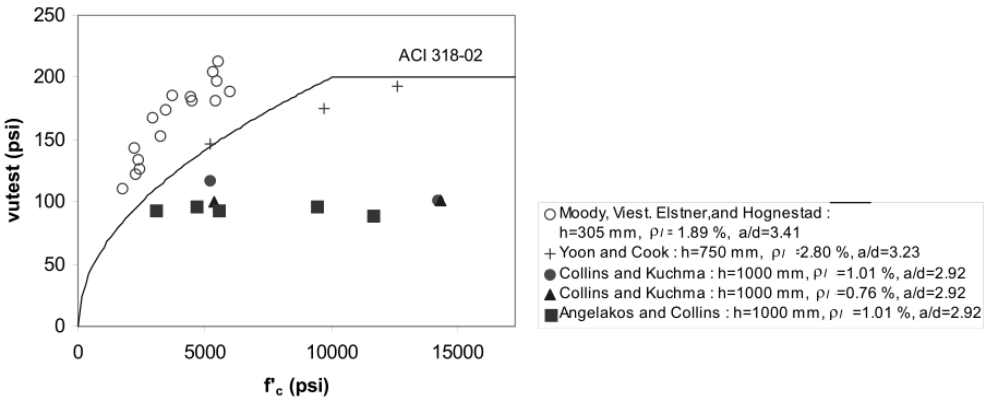

Fig. 2.10 Influence of concrete compressive strength on shear strength (from Kuchma and Kim 2001)

Shear crack pattern and failure

The development of the crack pattern is particularly relevant in case of shear behavior, in fact, for most members without shear reinforcement, the cracking formation is the cause of immediate failure. In case of beams with no transverse reinforcement the shear capacity is low due to the concrete inability to transmit tensile stress. In members with shear reinforcement, the formation of the shear crack do not compromise the shear strength, since stress redistribution and the formation of a "truss action" arise due to the presence of transversal reinforcement. The inclination of the cracks has the tendency to increase in highly reinforced beams. Depending on the amount of the transversal reinforcement, more inclined cracks may develop until the stirrups yield. After yielding of the stirrups, the load may increase due to interface shear transfers along the crack faces up to a stage where the crack width can no longer transfer shear stress and the beam fail. The presence of stirrups leads to a relative ductile failure in comparison to beams without shear reinforcement.

Three types of inclined crack/failure are typical of reinforced concrete beams failing in shear: web-shear cracks and flexure-shear cracks, web-crushing (Fig. 2.11).The web shear failure is common in small shear span ratio beams and beams with a narrow web of beams without shear reinforcement. In this case cracks are formed in sections of the beam's web which are not influenced by flexural cracks. The crack width is relatively small compared to a flexural crack. The cracking process is characterized by the formation of crack initiation in the beam's web and its propagation to the top and bottom of the beams. If shear reinforcement is introduced, diagonal cracks are initiated in a bending crack, initially developed in the tensile zone of the beam. This cracking process is called flexural-shear; the crack is usually larger in the tensile zone of the beam and decreases its width close to the compression area. In this case, the longitudinal reinforcement in tension is required to balance the longitudinal component of the diagonal compression, and the web reinforcement in tension is required to balance the transverse

component of the diagonal compression. Failure occurs after the stirrups have yielded. For large amounts of transverse reinforcement, the concrete in the inclined struts may fail, this "web-crushing" failure occurs when the concrete reaches its resistance in compression before the steel reinforcement reach the yield strain. This type of failure is characterized by an extremely brittle behavior and is very likely in thin webbed members such as I-beams.

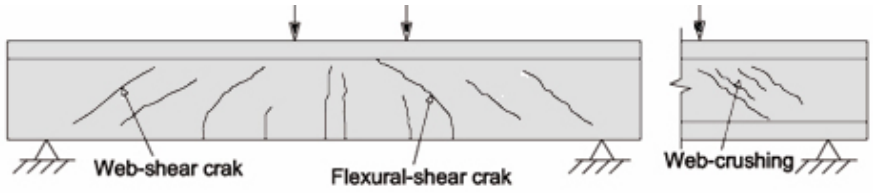

Fig. 2.11 Typical cracks and failure modes

2.3 Theories used to predict shear capacity

An overview on the different theories used to predict the shear capacity of reinforced concrete beams are presented, focusing on models, developed to estimate the shear behavior of beams with shear reinforcement. Despite the variety of proposed methods, a unified approach for calculating the shear capacity has not yet been generally accepted. In this section are presented the theories on which most used design standards are based: truss model introduced by Ritter and Mörsch, the variable angle truss VAT with reference to the theory of the plasticity for RC introduced by Nielsen (1999). The more recent approaches recognized in international codes, as, for example the modified compression field approaches developed by Vecchio and Collins (1986) recently introduced in the Model Code 2010 (fib 2013) are excluded from the discussion since these are conceptually distant to the work presented in this thesis.

2.3.1 The 45° truss model

The truss model to estimate the shear capacity of a cracked reinforced concrete beam under shear and bending loads after cracking was introduced by Ritter (1899) and developed by Mörsch in (1908). The model is based on simple equilibrium equations and considering the cracked beams as a truss where the compressive stressed in the beam's web act as 45° inclined compressed struts and the stirrups are treated as vertical members; the longitudinal tension reinforcement and the flexural compressive zone of the beam act as the bottom and top chord of the truss, respectively. The main assumption of this simplified model lies in neglecting the tensile stresses in the diagonally cracked concrete. The difference between Ritter's and Mörsch's model exists in the assumption made by Mörsch where the

compression diagonals represent a continuous field of stress rather than a discrete diagonal compressive strut as it was initially pointed out by Ritter, assuming that the diagonal struts are extended across more than one stirrups. The equilibrium of the internal forces presented in Fig. 2.12 requires that tensile stresses in the stirrups and compressive strut in concrete to be equal. Assuming an angle of diagonal compression θ =45° and considering that the shear stresses are uniformly distributed over an effective shear area $b_w \cdot jd$, the diagonal compressive force is $\sigma_c b_w jd/\sqrt{2}$. The external shear force V is assumed to be equal to the force in the longitudinal reinforcement resulting considering the equilibrium $\left(\sigma_c b_w jd/\sqrt{2}\right)^2 = V^2 + V^2$, σ_2 can be written:

$$\sigma_c = 2V/b_w jd \tag{2.6}$$

The vertical component of the diagonal compressive force is balanced by the tensile force in the stirrup so the vertical force in the stirrups can be written as:

$$V_s = V = A_{sw}\sigma_s \frac{jd}{s} \tag{2.7}$$

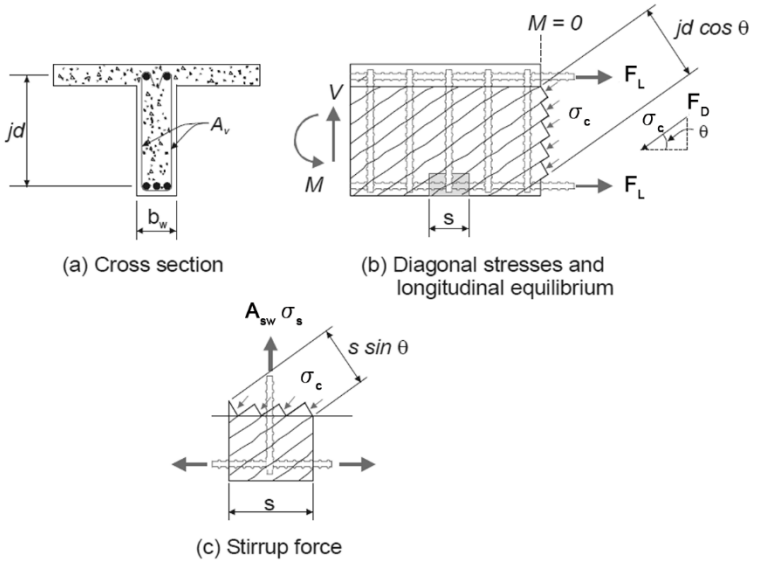

Fig 2.12 Equilibrium Conditions for 45° Truss Model.

Eq. (2.7) is generally used to design the required amount of stirrups and Eq.(2.6) to check the compressive stresses in the concrete. This defines the upper limit of the shear force and is associated with the compressive web shear failure. Mörsch model provides conservative results because the choice of the 45° angle for the compressive strut, provide lower stress values in the stirrups compared to the

experimental tests (Richart 1927; Withey 1907, 1908). The conservative values of shear strength are also due to the fact of having neglected the tensile concrete resistance (Talbot 1909, Hognestad 1952). Several international codes are based on Mörsch theory as for example the US Standard (ACI-318-08). In this case, where this model has adopted a contribution related to the tensile concrete V_c based on empirical formulation is added to the shear resistance V_s as presented in the following section. Furthermore a minimum shear strengthening ratio is required by the code for the truss action activation

2.3.2 Truss approaches with concrete contribution

The large number of tests conducted between 1950 and 1960's, allowed to have a better understanding of mechanisms and contributions due to: aggregate interlock and dowel action on shear resistance, and the compressive stress state above flexural cracks. On the basis of a large amount of research programs, the ACI-ASCE shear committee (1962) recommended the use of a semi-empirical expression for the estimation of the shear strength carried out by the concrete to overcome the inaccuracy by adopting the Mörsh approach. Following this approach the total shear capacity was calculated superimposing the two contribution V_c for the concrete and V_s for the steel stirrups calculated as Eq. (2.8).

$$V = V_c + V_s \tag{2.8}$$

Fig. 2.13 shows how by using this additive approach it is possible to obtain the required total shear strength with a lower percentage of vertical stirrups. The theories based on this approach considered in general one of both the following two mechanisms: 1) existence of tensile stresses in concrete transverse to the struts, 2) shear stresses that are transferred across the inclined crack by aggregate interlock or friction. Both mechanisms are interrelated and results in: 1) angle of the principal compression stress in the web being less than then the crack angle, 2) a vertical component of the force along the crack that contributes to shear strength of the member (ACI-ASCE Committee 445).

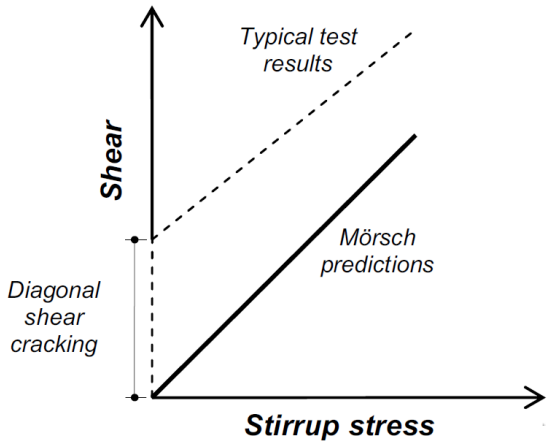

Fig. 2.13 Truss approaches with concrete contribution concept

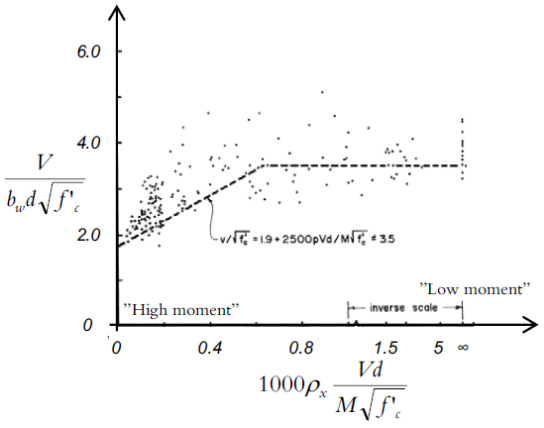

Fig. 2.14 Eq. (11.3.2.1) form ACI 318-08 versions (unit psi) comparison with experimental results.

The first semi-empirical expression proposed by ACI-ASCE shear committee, appeared in the 1963 ACI 318 and still present in the current version is:

$$\frac{V_c}{b_w d} = \tau_{cd} = 0.166\sqrt{f_c'} + 0.17\rho_w \frac{V_d}{M} \le 0.29\sqrt{f_c'}\ (MPa) \tag{2.9}$$

This equation (Fig 2.14) is based on the results of numerous test on RC without shear reinforcement and takes into account the major facts influencing the shear resistance, such as the tensile strength of the concrete in the parameter $\sqrt{f_c'}$, longitudinal reinforcement ρ_w and the shear span to depth ratio M/dV. A simpler and more conservative expression is also accepted:

$$\frac{V_c}{b_w d} = 0.166\sqrt{f_c'}\ \text{(MPa)} \tag{2.10}$$

Eq. (2.9) and Eq. (2.10) represent the ultimate load at which the diagonal crack governing the failure of a beam without shear reinforcement is formed. The V_c contribution of the ACI shear design is in fact equal for beams with and without shear reinforcement. Other formulations for the estimation of the concrete contribution V_c have been proposed, in an attempt to also account other parameters, as for example the arch action (Zsutty 1968) or the possibility that forces are transferred across the cracks by shear friction. Bazant and Kim (1984) also included the maximum size of the aggregates in his formula that is based on fracture mechanics. Okamura and Higai (1980) and Niwa et al. (1986) proposed an empirical formula that tried to consider all the main parameters. Similar approaches has also been adopted in several version of European codes as for example the CEB-FIB Model Code 1990 the Eurocode 2 in its 1991 version. This latter norm presented the concrete contribution using an empirical Eq. (2.11) function of the beam's internal arm, concrete compressive strength and percentage of longitudinal reinforcement (See for more information regarding Eq. (2.11) and (2.12) see Section 2.4.2).

$$V_{Rd1} = 0.0525\beta k \left(f_{ck}\right)^{2/3} \left(1.2 + 40\rho_l\right) b_w d \quad \text{(mm, MPa)} \tag{2.11}$$

In the Eurocode 2 version 2005, the previous equations has been modified in

$$V_{Rd,c} = \left[C_{Rd,c} k \left(100\rho_l f_{ck}\right)^{1/3} + k_1 \sigma_{cp}\right] b_w d \le \left(\nu_{\min} + k_1 \sigma_{cp}\right) b_w d \quad \text{(mm, MPa)} \tag{2.12}$$

A combination of the variable-angle truss (Section 2.3.3) and a concrete contribution has also been proposed. This procedure has been referred to as the modified truss model approach (CEB 1978;

Ramirez and Breen 1991). In this approach, in addition to a variable angle of inclination of the diagonals, the concrete contribution for non prestressed concrete members diminishes with the level of shear stress. This type of approaches abandoned in the Eurocode 2 in its actual version (2004) was reintroduced in the recent Model Code (2012). In this latter case, the approach to calculate contribution carried out by the concrete is based on the Modified compression field theory (Vecchio and Collins 1986).

2.3.3 The variable angle truss model (VAT)

The 45 degree truss model proposed by Mörch often leads to very conservative results, to overcome this problem, an alternative to the truss approach with concrete contribution, is the variable angle truss model. This model adopt a lower angle for the shear crack which is justified by the experimental results that the evidenced an angle θ typically lower than 45°. The previous equation describing the 45° truss model can be rewritten by assuming the angle θ as a variable of the problem. The variable angle truss model (VAT) does not directly account for the components of aggregate interlock/friction, dowel forces in the cracks, and shear carried out by the un-cracked concrete, but a lower inclination for the compression diagonals allows a further mobilization of the stirrups in the reinforcement, resulting in a higher shear resistance. In order to fulfill the equilibrium of the section by assuming an angle θ of the compressive strut the equilibrium conditions can be expressed as in Fig. 2.15. The external shear V is equal to the vertical resultant of principal diagonal compressive stress $F_D = \sigma_c b_w jd \cos\theta$, therefore $V = F_D \sin\theta$. From this equality, the principal compressive stress σ_c can be determined using Eq. (2.13). From the equilibrium at the bottom chord the diagonal compressive force is divided into the longitudinal component of the tensile reinforcement as indicated in Eq. (2.14) and into the vertical component of the stirrups as indicated in Eq. (2.15). The vertical component of the principal diagonal is supposed to be acting in length, "s" equal to the stirrups spacing (Fig. 2-15c). The relationship between the force in the stirrup and the external shear force action on the beam is obtained in Eq. (2.16) by introducing Eq. (2.13) in Eq. (2.15).

$$\sigma_c b_w jd \cos\theta = \frac{V}{\sin\theta} \Rightarrow \sigma_2 = \frac{V}{b_w jd}\left(\tan\theta + \cot\theta\right) \tag{2.13}$$

$$F_L = 0.5 \cdot V \cot\theta \tag{2.14}$$

$$\sigma_2 s b_w \sin^2\theta = A_s \sigma_s \tag{2.15}$$

$$\frac{V}{b_w jd}\frac{1}{\left(\sin\theta\cos\theta\right)} b_w s \cdot \sin^2\theta = A_s\sigma_s \Rightarrow \frac{V}{jd}\tan\theta \tag{2.16}$$

The presented equations are not sufficient to solve the problem for variables (compressive stress, σ_2, tensile force in the longitudinal reinforcement, F_L, stress in the stirrups, σ_s, and inclination, θ, of the principal compressive stress).

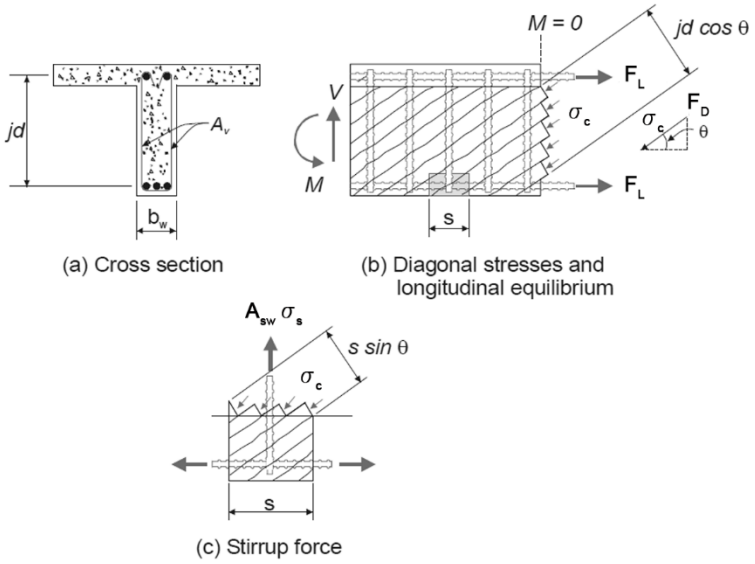

Fig. 2.15 Equilibrium Conditions for Variable-Angle Truss Model

Mörsch (1922) discussed the inclination of the angle θ affirming that "it is absolutely impossible to determine mathematically the slope of the secondary inclined crack according to which you can design the stirrups". Several approaches have been proposed to solve the indeterminate system; however, for design purposes it is necessary to introduce assumption. Kupfer used minimum energy principles to determine the crack angle θ assuming a linear elastic behavior of both steel and concrete. Collins and Vecchio (1986) in continuation of the work of Baumann (1972) assumed in their compression field theory, the yielding of the stirrups ($\sigma_s = f_y$). Solutions based on limit analysis and plasticity methods have been developed by Thürlimann and Grob (1976), and Nielsen (1999). These approaches (Section 2.3.4) assume the yielding of the stirrups and the attainment of the maximum compressive stress in concrete. This approach leads to smaller values of θ; a smaller amount of stirrups is therefore required, but at the same time the tensile force in the longitudinal reinforcement increases.

2.3.4 Limit Analysis and Concrete Plasticity

In the late 70's the theory of plasticity for concrete was developed in Denmark by Nielsen and Braestrup (1975) (see Nielsen (1999) for a complete discussion). For many years, the application of plastic theory in practical design was restricted to Denmark and Switzerland, but the growing interest in

plastic methods has led to the adoption of this approach by Eurocode 2. The theory of plasticity search for the values of carrying capacity, which are lower than or equal to yield load by creating stress fields, which fulfill the equilibrium condition and are safe according to the failure criterions for the materials. Those solutions are named lower bond solution. It is also possible to search the solutions which are greater than or equal to the yield load by creating failure mechanisms and using the work equation on the mechanisms. Those solutions are named upper bond solution. The exact solution of the problem can be found in between of the values provided by the lover-bond theorem and the upper bond theorem; in some cases it is possible to find coincident solutions, in that case the exact solution is obtained. In the plastic approach, concrete is assumed to be a rigid, perfectly plastic material, responding to a modified Coulomb failure criterion with the associated flow rule, the tensile strength is usually neglected. Steel reinforcement is as well assumed as a perfectly plastic material, with the yield strength f_y. The initial approach does not differ from the VAT approach, the beam is considered to have a compressive stringer (compressive zone) taking a compressive force C and a tensile stringer (tensile zone) taking the tensile force T. In the shear zone the stress field can be considered as an idealized model of a cracked web, the cracks being parallel to the uniaxial stress direction. The theory of plasticity assumes that the capacity of the web is achieved by simultaneously reaching the yield of the shear reinforcement and the limiting stress f'_c in the inclined struts (web crushing). This assumption yields to a condition for the angle θ of the inclined struts and a function for the capacity depending on the amount of shear reinforcement. The plastic approach for design purpose was developed as a lower bond approach. However in some cases the two approaches coincide (Nielsen 1999). The lower-bond and bond solution is here presented for simply supported beam symmetrically loaded by two concentrated forces (Fig.2.16).

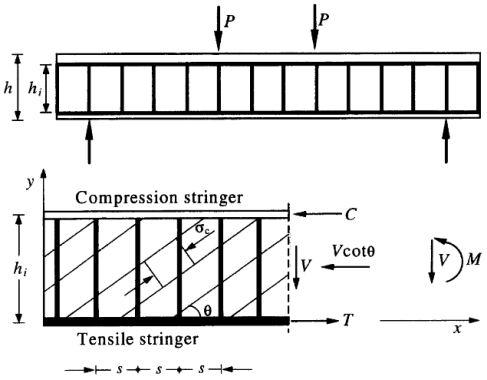

Fig. 2.16 Stress field in the lower bond approach

The compression zone and the tensile zone are idealized as stringer carrying the forces C and T respectively and assumed strong enough to carry the compressive and tensile loads. In the web it is

considered a homogeneous stress field, consisting of a uniaxial compressive stress f'_c in the concrete which forms a constant angle θ, this stress field can be expressed as:

$$\sigma_x = -\sigma_c \cos^2\theta \; \sigma_y = -\sigma_c \sin^2\theta \; \tau = |\tau_{xz}| = f'_c \sin\theta\cos\theta \tag{2.17}$$

the relation between the constants stress and the shear for V is

$$\tau = \frac{V}{b_w jd} \tag{2.18}$$

Vertical stirrups are assumed as vertical forces distributed over the concrete area ($s \cdot b_w$), and assuming that the stirrups stress equals to the yield stress (for vertical stirrups the x-direction and τ_{xy} components are null).

$$\sigma_y = \frac{A_s f_y}{b_w s} = \rho_{sw} f_y \tag{2.19}$$

Where ρ_{sw} is the shear reinforcement ratio. The stresses carried out but the concrete and stirrups are presented in Eq. (2.20)

$$\sigma_x = -f'_c \cos^2\theta \qquad \sigma_y = -f'_c \sin^2\theta + \rho_{sw} f_y \qquad \tau = |\tau_{xz}| = f'_c \sin\theta\cos\theta \tag{2.20}$$

The stress field is statically admissible if the boundary conditions are satisfied. The boundary conditions along the stringers require the total stress to be zero $\sigma_y = 0$. Under this condition the last two equations of Eq. (2.20) lead to:

$$\rho_{sw} f_y = \tau \tan\theta \tag{2.21}$$

And the first and last equation of Eq. (2.20) to

$$\sigma_x = -\tau \cot\theta \tag{2.22}$$

Solving the last two equations for τ and θ it is possible to obtain:

$$\frac{\tau}{f'_c} = \sqrt{\psi(1-\psi)} \tag{2.23}$$

$$\tan\theta = \left(\frac{\psi}{1-\psi}\right)^{1/2} \tag{2.24}$$

Where the mechanical degree of shear reinforcement is defined as

$$\psi = \frac{\rho_{sw} f_y}{f'_c} \tag{2.25}$$

Eq. (2.23) represents a circle as show in Fig. 2.17. The maximum value of 0.5 is obtained when the degree of shear reinforcement is greater than 0.5, in this case, the shear sector of the beam is over-reinforced. Eq. (2.24) expresses the inclination of the angle θ as a function of the mechanical degree of shear reinforcement. The load-carrying capacity Eq. (2.23) is a correct lower bond solution, Nielsen (1999) demonstrated how the upper bond solution coincides with the lower bond solution apart from the region characterized by low degree of shear reinforcement where the solution is governed by the upper bond solution (See Fig. 2.17). When ψ/ν is small, the angle θ must also be small before web crushing can take place. The cracked web region, therefore, may become unstable, resulting in sliding failure along cracks before concrete compressive strength is reached. The possibility of sliding in cracks will be further enhanced by the large stirrup distances normally used when dealing with small reinforcement degrees. In plastic models for shear design of reinforced concrete beams the distinction between two shear failure modes, namely web crushing and crack sliding is fundamental. The first mentioned mode is met in beams with large shear reinforcement degrees. The mode of crack sliding is met in non-shear reinforced beams as well as in lightly shear reinforced beams, in this case the shear strength will, for the reasons given above, be overestimated. This problem has been partly overcome in the "design codes" by introducing a minimum shear reinforcement requirement and by limiting the choice of cot θ, for instance to cot θ=2.5 for beams with constant longitudinal reinforcement (Fig. 2.18).

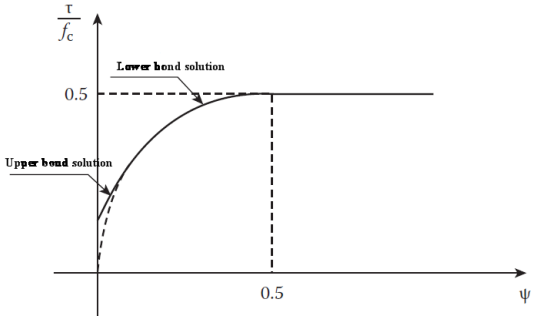

Fig. 2.17 Upper bound solution for the maximum shear capacity of a beam loaded by concentrated forces

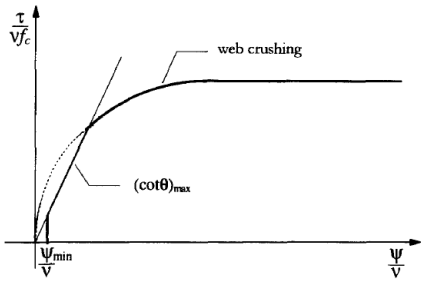

Fig. 3. Code restrictions on maximum cot θ and minimum ψ.

Fig. 2.18 Upper bond solution with the restriction of maximum cot θ and minimum ψ.

If we assume the stringers to be sufficiently strong, the shear capacity of the beam will be exhausted in the following way: at a certain load level the stirrups will reach the yield stress f_y (it is assumed that the beam is not over-reinforced with stirrups). Once the stirrups are yielding, increasing the shear force can only be carried by increasing the compression stress σ_c, which at the same time rotates to smaller

anglesθ. The concrete stress σ_c may increase until it reaches the effective compression strength νf_c and the beam finally fails by crushing of the web concrete. The web crushing criterion and the code restrictions are illustrated as well in Fig. 2.18.

Concrete is not an ideal plastic material, which means that a reduced plastic strength should be used in order to obtain a fair theoretical estimation compared to the experimental results. The reduction factor ν is called effectiveness factorν, and it is a measure of the effectiveness of the concrete at plastic design. The studies on the influence of this parameter show that the dominating parameter is the concrete strength. Concrete exhibits a decrease of ductility with the increase of strength. A safe value was proposed by Nielsen (1999) Eq. (2.26). In EC2 this effectiveness factor was reduced even further (Section 2.4)

$$\nu = 0.7 - \frac{f_c}{200},\ f_c \text{ in MPa.} \tag{2.26}$$

Fig 2.19 show the comparison between the presented models based on the truss analogy. For a given amount of shear reinforcement, much larger capacity are predicted than those based on the traditional Mörsch model with or without introducing the concrete contribution. For comparison Fig. 2.19 shows the predictions using the standard method of EC2. The strut angle in the actual version of the Eurocode is limited to the angle of 21.8°, corresponding to $\cot\cot\theta$ =2.5.

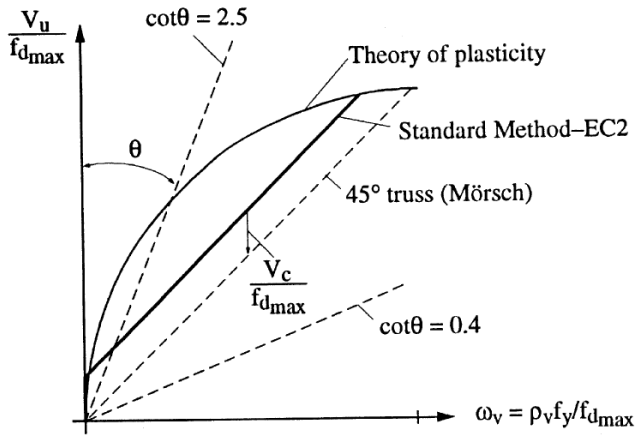

Fig. 2.19 Calculated shear strength as function of ψ and θ for the different models

2.4 Shear design models in standards

2.4.1 ACI 318-08 (2008)

The shear strength in the ACI 318-08 is based on a 45° truss model with concrete contribution. As previously discussed, the introduction of the concrete contribution was introduced since extremely

conservative results were obtained, also economical reason are at the basis of this choice, so that the percentage of steel could be reduced. The total shear strength is calculated as

$$V_n = V_c + V_s \tag{2.27}$$

Where V_c is the nominal shear strength of concrete calculated according to Eq. (2.28) or to the simplified version Eq. (2.29) and Vs is the nominal shear strength provided by the shear reinforcement according to Eq. (2.30).

$$V_c = \left(\sqrt{f'_c} + 120\rho_w \frac{V_u d}{M_u} \right) \frac{b_w d}{7} \leq 0.3\sqrt{f'_c} b_w d \tag{2.28}$$

$$V_c = 0.17\lambda\sqrt{f'_c} b_w d \tag{2.29}$$

where f'_c is the specified concrete compressive strength. λ is a reduction factor of the compressive strength considering lightweight concrete, $\lambda = 1$ for normal concrete. b_w is the width of the web and d is the internal lever arm.

$$V_s = \frac{A_{sw} f_{sy} d}{s} \tag{2.30}$$

Where A_{sw} is the reinforcement area within the longitudinal stirrup spacing s, f_y is the yield strength. To avoid diagonal crushing of the compression chords and to limit diagonal cracking, Vs should not be greater than $V_s = 0.66\sqrt{f'_c} b_w d$. The maximum longitudinal spacing for shear reinforcement perpendicular to the axis of the structure is $s_{\max} = d/2$ or 600mm. The ACI prediction gives in general unconservative results for large members and lightly reinforced members without shear reinforcement, and does not allow the use of concrete compressive strength higher than 69 MPa.

2.4.2 Eurocode 2 Part 1 (1991)

The first version of the Eurocode EC2, Part 1 (1991) is based partly on Plasticity Theory which is presented in section 2.3.4 assumes that the capacity of web is achieved by simultaneously reaching the yielding of the shear reinforcement and the limiting stress in the inclined concrete struts.

The Eurocode 2 Part 1 version (1991) provides two methods, the standard method and the variable strut inclination method. The standard method is basically a combination of a concrete contribution term and a steel contribution term based on the 45° truss model. The method is applicable for concrete strengths ranging from $12 \leq f'_c \leq 50$ MPa.

45° truss or Standard Method

The total shear resistance consists of the concrete contribution V_{cd} and the steel contribution V_{wd}. Thus, the total shear resistance V_{Rd3} is:

$$V_{Rd3} = V_{cd} + V_{wd} \le V_{Rd2,\max} \tag{2.31}$$

Where

V_{cd} =concrete contribution taken as equal to V_{Rd1}, see below

$V_{wd} = \dfrac{A_{sw} f_{ywd} \left(0.9d\right)}{s}$ = the steel contribution

A_{sw} = area of the shear reinforcement within spacing, s

f_{ywd} = yield strength of shear reinforcement

$V_{Rd2,\max}$ = upper limit on shear resistance to prevent web crushing

$V_{Rd1} = \beta \tau_{rd} k \left(1.2 + 40\rho_t\right) b_w d$ (mm, MPa)

or its simplified version

$V_{Rd1} = 0.0525 \beta k \left(f_{ck}\right)^{2/3} \left(1.2 + 40\rho_l\right) b_w d$ (mm, MPa)

Where

$\beta = \dfrac{2.5d}{x}$, $\left(1.0 \le \beta \le 5.0\right)$ is an enhancement factor that can be applied if the member is loaded by a concentrated load situated at distance, $x \le 2.5d$, from the face of the support. Otherwise $\beta = 1$

τ_{rd} =basic design strength ($0.25 f_{ctk0.05}$)

$f_{ctk0.05}$=lower 5% fractile characteristic tensile strength (=0.7 f_{ctm})

f_{ctm} =mean value of the concrete tensile strength (=0.30 $\left(f_{ck}\right)^{2/3}$

f_{ck} = characteristic cylinder compressive strength of concrete

$k = \left(1.6 - d/1000\right) \ge 1.0$ (mm unit)

$\rho_l = \dfrac{A_{sl}}{b_w d} \le 0.02$

A_{sl}= area of longitudinal reinforcement in tension

b_w = effective wed width

d =effective depth

The shear strength V_{Rd1} increases as the amount of longitudinal reinforcement increase, and decreases as the depth of the member increases. The value τ_{rd} and consequently the shear strength V_{Rd1} could

provide unsafe values, which led country like Germany to reduce the value τ_{rd}. The upper limit on the total shear resistance is determined by the resistance V_{Rd2} which is the web crushing shear force based on the Plasticity theory. The maximum value of V_{Rd2} is expressed in terms of the effective stress in the compression strut:

$$V_{Rd2,\max} = 0.5\upsilon f_{cd} b_w \left(0.9d\right) \tag{2.32}$$

Where f_{cd} =the factored design strength, takes as $f_{cd} = f_{ck}/1.5$ and $\upsilon = 0.7 - \frac{f_{ck}}{200} \geq 0.5$ is the effectiveness factor. The minimum amount of shear reinforcement depends on the concrete compressive strength and the steel yield strength.

Variable strut inclination method

The variable strut inclination method is based on a variable-angle truss. This method assumes that transverse reinforcement carries the entire shear. The concrete contribution to shear resistance is considered using flatter truss angles. The shear resistance of members with shear reinforcement is:

$$V_{Rd3} = \frac{A_{sw} f_{ywd} \left(0.9d\right)}{s} \cot\theta \tag{2.33}$$

Where

$0.4 < cot\theta < 2.5$: For beams with constant longitudinal reinforcement, or

$0.5 < cot\theta < 2.0$: For beams with curtailed longitudinal reinforcement

The maximum shear resistance provided by a section, based on the crushing of struts, can be obtained from equilibrium at a section as:

$$V_{Rd2} = \frac{\upsilon f_{cd} b_w \left(0.9d\right)}{\cot\theta + \tan\theta} \tag{2.34}$$

Eq. (2.33), shows that smaller the angle, the higher is the shear capacity provided by the shear reinforcement. However, the shear capacity given by Eq. (2.34) decreases as θ decreases below 45°. From the lower-bound theory of plasticity, therefore, a limitation on the effectiveness of the shear reinforcement is given as:

$$\frac{A_{sw} f_{ywd}}{b_w s} \leq 0.5\upsilon f_{cd} \tag{2.35}$$

In design, the actual failure condition can be obtained by equating the applied shear force to the resistance V_{Rd2} and finding the largest value of cotθ which requires the least amount of shear reinforcement. Once cotθ is found, the shear resistance, V_{Rd3}, can be calculated from the Eq.(2.33). For analysis purpose, the angle θ can be found by equating V_{Rd3} to V_{Rd2} as follows:

$$\tan\theta \geq \frac{1}{\sqrt{\left(\frac{\upsilon f_{cd}}{\rho_{sw} f_{ywd}} - 1\right)}} \quad \cot\theta \leq \frac{1}{\sqrt{\left(\frac{\upsilon f_{cd}}{\rho_{sw} f_{ywd}} - 1\right)}} \tag{2.36}$$

Where θ should be calculated using Eq. (2.36) and those conditions applied to Eq. (2.33).

2.4.3 Eurocode EN 1992-1-1 (2004)

In this version of the Eurocode, which consists a revision of the previous version, the "additive approach" has been eliminated and only the design method based on the truss model with variable angles are available.

Members Not Requiring Shear Reinforcement

The design value for the shear resistance $V_{Rd,c}$ for member that does not require shear reinforcement (in N) is given by:

$$V_{Rd,c} = \left[C_{Rd,c} k \left(100\rho_l f_{ck}\right)^{1/3} + k_1 \sigma_{cp}\right] b_w d \leq \left(\nu_{\min} + k_1 \sigma_{cp}\right) b_w d \quad \text{(mm, MPa)} \tag{2.37}$$

Where, f_{ck} is characteristic compressive strength.

$$k = 1 + \sqrt{\frac{200}{d}} \leq 2.0 \text{ mm unit} \tag{2.38}$$

$$\rho_l = \frac{A_{sl}}{b_w d} \leq 0.02 \tag{2.39}$$

A_{sl} = area of longitudinal reinforcement in tension

b_w = smallest width of the cross section

$\sigma_{cp} = N_{ed} / A_c < 0.2 f_{cd}$

N_{ed} = the axial force in the cross section due to loading or pre-stressing (N)

A_c = the area of concrete cross section (mm^2).

The value of $C_{Rd.c}, k_1, \nu_{\min}$ are indicated in the national annex the recommended value for $C_{Rd.c}$ and k_1 are $0.18/\gamma_c$ and 0.15, respectively, the value $\nu_{\min}$ is presented in Eq. (2.40)

$$\nu_{\min} = 0.035k^{3/2} f_{ck}^{1/2} \tag{2.40}$$

Members Requiring Shear Reinforcement

The design of the members with shear reinforcement is based on a truss model, whereby the values for the angle θ of the inclined struts in the web are limited as follows: $1 \le \cot\theta \le 2.5$ For members with vertical shear reinforcement, the shear resistance, V_{Rd}, is the smaller of

$$V_{Rd,s} = \frac{A_{sw}}{s} z f_{ywd} \cot\theta \tag{2.41}$$

And

$$V_{Rd,\max} = \left[\alpha_{cw} \upsilon_1 f_{cd} / \left(\cot\theta + \tan\theta\right)\right] b_w z \tag{2.42}$$

Where: A_{sw} = the cross-sectional area of the shear reinforcement

s = spacing of the stirrups

f_{ywd} = the design yields strength of the shear reinforcement

f_{ywk} = the characteristic yield strength of the shear reinforcement

$\upsilon_1 = 0.6$ (Recommended values for $f_{ck} \le 60MPa$, different values for each country can be adopter (see National Annexes

α_{cw} = a coefficient taking account of the interaction of the stress in the compression chord and any applied axial compressive stress (α_{cw}=1 is recommended for non-pre-stressed structures).

θ = inclination of concrete struts

b_w =the minimum width between tension and compression chords

z =inner arm, for a member with constant depth. (approximate values z=0.9d may be used.

The maximum spacing between shear stirrups should not exceed $s_{\max} = 0.75d\left(1 + \cot\alpha\right)$ or 300 mm.

2.5 Shear strengthening of concrete structures with non-conventional techniques

2.5.1 Introduction

Reinforced concrete beams need to be strengthened when they are insufficiently reinforced in shear and become subjected to higher loads, or when their shear capacities fall below their flexural capacity after flexural strengthening. Shear failure should be avoided because of its brittle and unpredictable nature. The relatively recent approaches for shear strengthening of RC beams made use of composite materials. Structural strengthening have seen a constantly growing numbers of strengthening system, that are not necessarily based on the use of FRPs. Alternative strengthening methods based on the use, for example, of strain hardening cementitious materials, textile reinforced mortar and prestressed steel strips have been developed starting from traditional strengthening techniques, thanks to the scientific progress in material research and the possibility to adopt advanced technology.

2.5.2 Traditional strengthening technique

One of the simplest concepts of strengthening is based on the idea to increase the cross section of the element to be strengthened by adding traditional construction material as normal reinforced concrete to increase stiffness, shear and bending resistance. This type of intervention is known as concrete jacketing and consists of casting a new cross-section that incorporates the existing concrete elements (Fig. 2.20a). The lack of steel is simply filled up by adding new bars or stirrups on the outside of the structure before the new cast. The method is economical since it uses common construction material and the workers do not require any particular skill beyond those used in normal constructions. In case of compressed elements, a higher confinement is provided by the new cast. The shear resistance is increased and load-bearing capacity similar to newly constructed beams or columns can be obtained. However, the addition of extra material to the structure adds extra load, and this rehabilitation method can be rather inefficient at increasing the structure's global capacity. By using this technique it is also necessary to improve the bond between the old and the new material, which is a very complex problem that involve several uncertainties (Wittmann 1998; Li 1998). If applied in a big scale in case of seismic strengthening, this technique implies the change of the structure's natural frequency due to the increase of self-weight and stiffness. Steel Jacketing is also adopted for strengthening of reinforced concrete elements, by assembling steel in L-shape profile and plates around the concrete element (Fig. 2.20b). The steel cage can provide a higher confinement and the shear resistance can significantly increase. Generally smaller increase of cross section can be obtained in comparison to concrete jacketing but the increase of self-weight can be significant as well. Nowadays, in case of concrete jacketing, it is possible

to reduce the thickness of the concrete jacket by using self-compacting concrete (SCC) characterized by higher flowability (Overview in section 2.5.3). Shotcrete can also be an alternative to the traditional casting. The most advantageous feature of shotcrete is that it can be applied to big area in a short time, the applied mortar can also contain fibers of steel or polymer materials.

An alternative strengthening technique to the section jacketing is the steel plate bonding (Fig. 2.20c), this technique firstly applied by (Dussek 1974) in the mid '60's and developed in the early '70's by L'Heremite and Bresson (L'Hermite 1967; Bresson 1971). The strengthening approach is based on the application of steel plates to the tension side of the reinforced concrete element using the adhesive material; the bond performance can also be increased by using bolts. Due to the fact that concrete has a relatively low tensile strength the introduction of a high tensile and stiffness strength material functions as extra reinforcement. This technique exhibits several drawbacks since steel plates are heavy to mount and to transport on site. They are difficult to apply if placed in sagging region of the beams, as they might need extra pressure during the curing of the adhesive to withstand their self-weight. Since steel is applied the risk of corrosion is high, making this technique expensive to maintain. Furthermore, steel plates may be difficult to apply to curved surfaces.

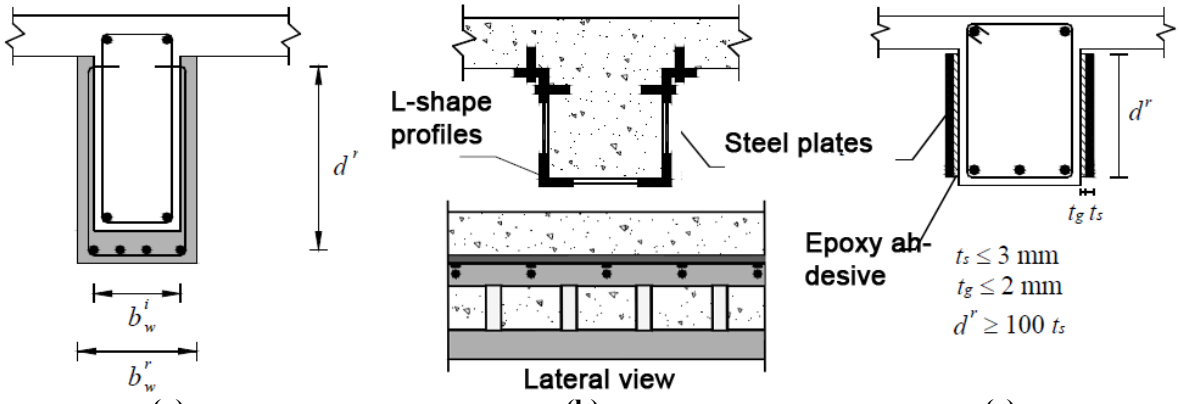

Fig.2.20 Traditional techniques (a) Concrete jacketing (b) steel jacketing (c) steel plate bonding - form (Dias 2008), recommended dimension for steel plating by (Appleton and Gomes 1997)

2.5.3 Non-conventional techniques -Overview

Most of the proposed strengthening techniques relies their effectiveness on the ability to transfer the stress by bond between the concrete surface and the strengthening system, but there are also several experimental program dedicated to investigate unbonded-type of strengthening in which the strengthening effectiveness lies in internal stress-state change, induced by an external prestressed or post-tensioned system. However, it is also possible to combine the two "types" of strengthening

approaches which has been demonstrated for example in case of flexural strengthening using pre-stressed CFRP laminates (Mostakhdemin Hosseini et al. 2014).

Unbonded types of strengthening have been investigated mainly for flexural strengthening. The post-tensioning by using metallic materials can be for example a possible solution in cases where the properties of the steel in tension has deteriorated (corroded), additional tensile forces need to be carried. In bending, this method works in the same way as prestressed or post-tensioned concrete elements. Strengthening of prestressed concrete beams by steel external post-tensioning systems was presented in (Ionel 1996); The great advantage of this technique is to increase not only the ultimate state resistance but as well as to improve the service limit state by limiting the crack width or in case of structure presenting large deformation by reducing or limiting the deflection, an example of strengthening intervention was executed on the cantilever terrace of the Fallingwater House designed by Frank L. Wright by Silman Associated (2001). The method requires that the tension forces are transferred to the concrete by use of anchoring system, which can represent a problem in limited intervention spaces or small size structural element. This technique is limited by the compressive strength of the concrete. One important consideration is to prevent the corrosion of new strands, as well as in protecting the external cable from vandalism or accidents. Advantages can also be obtained by using FRPs (Nakai et al. 1994; Meier 1992).

(a) **(b)** **(c)**

Fig.2.21 Prestressed technique for shear strengthening: (a) Tendons placed internally into drilled holes, (b) Externally prestressed wire (Kim et al. 2007; Yang et al. 2009), (c) Prestressed metal straps (Helal et al. 2014; Garcia et al. 2014)

A limited number of post-tensioning (Shehata 1996) or pre-stressing application has been investigated to increase shear capacity. Tendons for shear strengthening can be placed externally or internally in drilled holes Fig. 2.21a. Teng et al. (1996) strengthened RC and prestressed beam by using steel clamping units (no stress applied), acting as external stirrups. External pre-tensioned wire have been recently investigated for shear strengthening (Fig.2.21b) (Kim et al. 2007; Yang et al. 2009). Post-tensioned metal straps (Fig. 2.21c) have been tested for strengthening of short splices (Helal et al. 2014), and for the enhancement of seismic behavior of RC buildings, providing confinement to the beam-columns joint and increasing its shear resistance (Garcia et al. 2014). The advantages relies in a

light strengthening system and in the possibility to provide an active confinement provided by the pretensioning of the metal straps surrounding the concrete element. Prestressed CFRP straps has also been successfully employed for shear strengthening of RC concrete rectangular and T-beams (Hoult and Lees 2009; Lees et al. 2002).

Traditional concrete jacketing adopts a layer of thickness usually greater than 60-70mm that can excessively increase the section geometry and the structure's self-weight. Concrete technology development has allowed to reduce the layer thickness of RC jacketing system. By using of self-compacting concrete (SCC), it is in fact possible to obtain an effective and thinner layer of concrete to repair and strengthen the RC element. (Chalioris et al. 2013) repaired pre-damaged beams with a U-configuration jacket of self-compacting concrete SCC and U-formed stirrups; the layer thickness of the self-compacting concrete was 25 mm, which was the minimum thickness to provide an adequate steel bar cover (Fig. 2.22a). The results illustrates that the thinner reinforced concrete jacket combines a higher performance than conventional RC jackets, with an increase of load in the range 35% - 50% improving as well the deflection ductility. New possibilities have been introduced also by application of a High Performance Fiber Reinforced Concrete HPFRC, which is characterized by high compressive strength and hardening behavior in tension (Naaman and Reinhardt 2006; Carpinteri et al. 2007). The latter properties allows to use this cementitious material in substitution of the traditional steel reinforcement. (Beschi et al. 2009; Martinola et al. 2007) demonstrated how for a thickness of 30-40 mm of HPFRC jacket similar results to traditional RC jacketing can be obtained. Researcher at the University of Minho developed a shear and flexural strengthening technique, which was called hybrid composite plate (HPC) (Esmaeeli et al. 2013). This technique combines the structural effectiveness of prefabricated strain hardening cementitious composite (SHCC) plates with carbon fiber polymer (CFRP sheets or laminates). (Esmaeeli et al. 2013) tested the performance of these panels on small deep beams failing in shear. They obtained significant increase of shear resistance, which was also attributed by the authors to the contribution of the SHCC plate to the resistance of the compressive strut, and not exclusively to the tensile properties of the HPC panel. Subsequently (Esmaeeli et al. 2014) showed that by testing a repaired beam with HCP panel in which CFRP laminates were installed (Fig.22), the maximum load carrying capacity increased of 99% in respect to the virgin un-strengthened beams (the testes beams had no stirrups). Failure occurred usually at the existing concrete-panel interface even in case of bolted connection (Fig 2.23c). Retrofitting of beam column-joint by using HPC panels (Esmaeeli et al. 2015) showed that a thin HPC panel conjugate the benefits of the ultra-high ductility of strain hardening cement composites (SHCC) with the high strength, elasticity modulus and durability of carbon fiber reinforced polymer (CFRP) reinforcement systems increasing the shear resistance of the

joint region and energy dissipation capacity which is a fundamental aspect in case of seismic retrofitting.

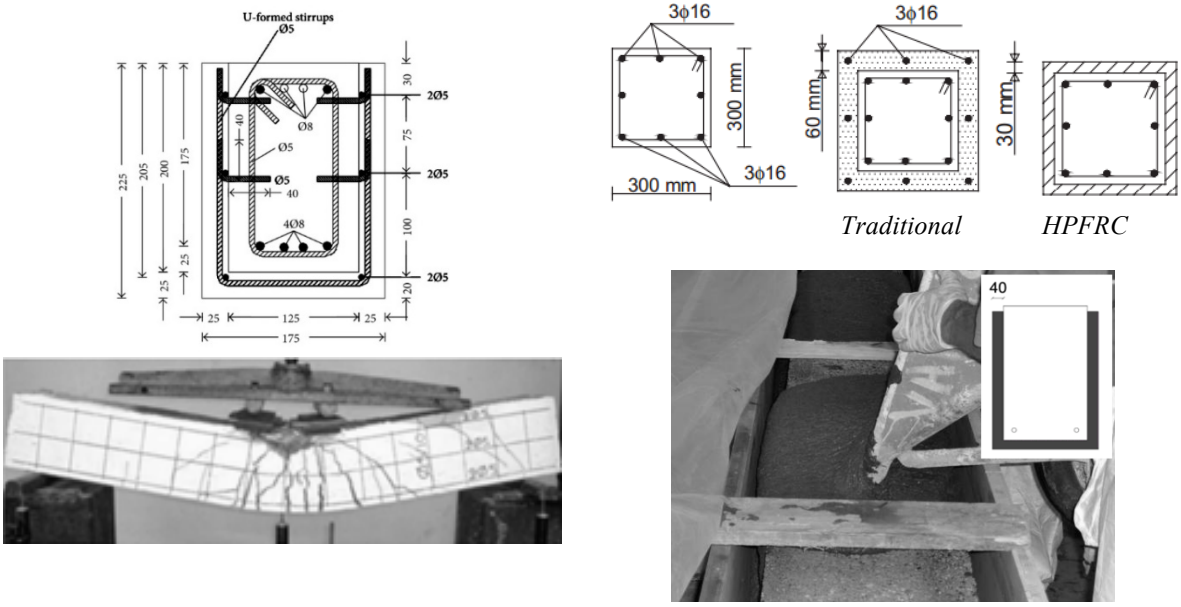

(a) **(b)**

Fig. 2.22 (a) Cross-sectional dimensions and steel reinforcement arrangement of the jacketed beam, Jacketing layer 25mm (Chalioris and Constantin, 2012) - dimensions are given in mm. (b) comparisons between traditional RC jacketing and HPFRC jacketing, casting of the HPFRC layer (Beschi et al. 2009; Martinola et al. 2007).

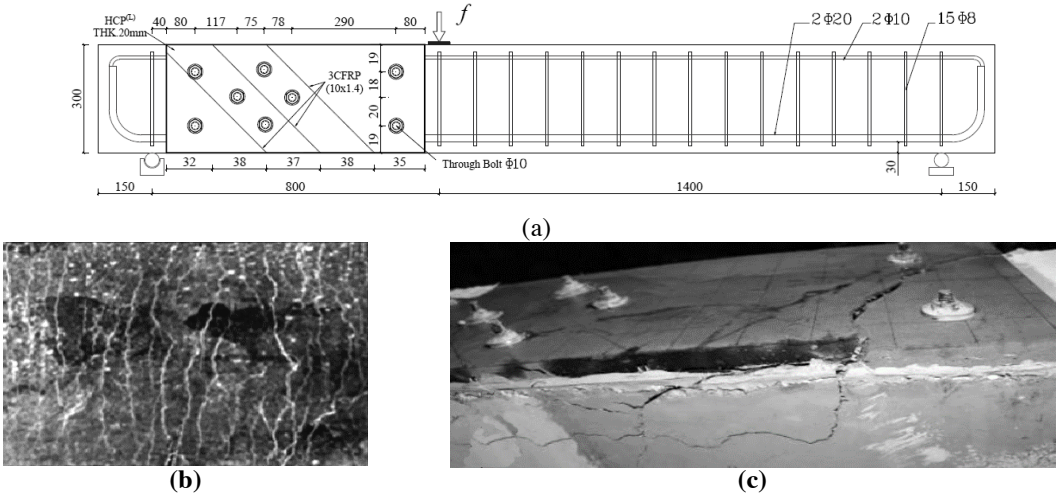

(a)

(b) **(c)**

Fig.2.23 From: (Esmaeeli et al. 2014) (a) Details of repaired beam (there was no transverse steel reinforcement in the critical shear span of the beam; a combination of epoxy adhesive and through bolts were used to fix the HCP reinforced with 3 CFRP laminates. (b)Multiple cracking during tensile test for SHCC (c) lateral HCP detachment of the strengthened specimen.

An alternative to the aforementioned techniques is the Fabric-reinforced cementitious matrix (FRCM) system. An FRCM is a composite material consisting of one or more layers of (inorganic) cement-based matrix reinforced with dry fibers in the form of open mesh or fabric; its development was possible thanks to the recent advances in textile engineering (ACI Committee 549 2013). FRCM has also been

identified as Textile-reinforced concrete (TRC) in RILEM Technical Committee 201 (2006), mineral-based composite (MBC) in Blanksvärd et al. (2009) and Textile Reinforced Mortar (TRM) in Triantafillou and Papanicolaou (2006). Different types of mortar were used to assure the bond between the existing concrete and the strengthening system; FRCM is a system where all constituents are developed and tested as a unique combination. The shear resistance of RC members strengthened with closed-type of textile reinforced mortar under monotonic or cyclic loading were tested by (Triantafillou and Papanicolaou 2006) demonstrating that TRM jacketing provides substantial gain in shear resistance. The effectiveness level, depending on the number of applied layers, It was shown that this technique is able to convert a shear-type failure into flexural failure.

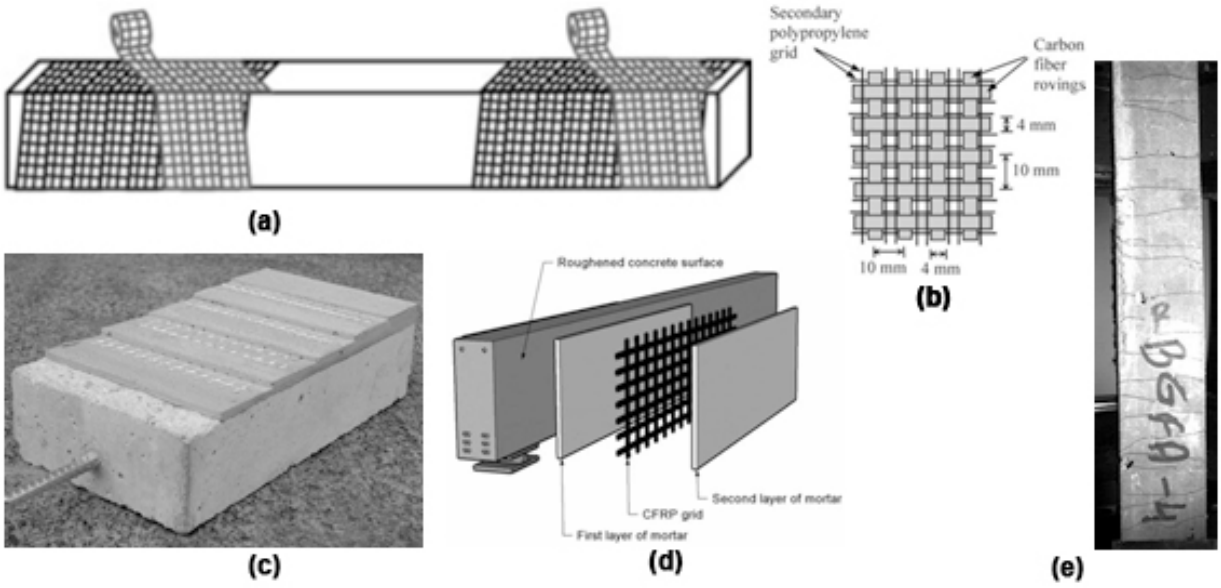

Fig. 2.24 From Triantafillou and Papanicolaou 2006 (a) Application of spirally strips of textile-reinforced mortar jackets in (b)Architecture of bi-directional textile, (c) example of TRC, (d) Side bonded mineral-based composite (Blanksvärd et al. 2009), (d) Distributed cracking pattern in AR glass-FRCM (ACI Committee 549 2013).

Test on RC rectangular beams side bonded with mineral based composites conducted by Blanksvärd et al. 2009 showed significant increase of shear strength without debonding failure between the base concrete and the cementitious bonding agent during the experimental program. The exploited failure comprise: shear failure in concrete, shear failure with rupture of CFRP, shear failure and debonding of CFRP, compression failure at the top of the concrete beam due to yielding of the tensile reinforcement. Complementary benefits of using this type of strengthening are: i) heat resistance, ii) compatibility with the substrate, ii) long-term durability.

2.5.4 Fiber Reinforced Polymers (FRP) shear strengthening

Fiber Reinforced Polymers (FRP) strengthening follows the path opened by the steel plate bonding technique and eliminates most of the drawbacks related to the use of metallic material, like for example the high weight and corrosion problems; however, weak points as the fire resistance or occurrence of brittle failure with consequent lack of ductility in some strengthening cases are unsolved. The pioneering work done in the case of flexural strengthening (Meier 1987; Kaiser 1989; Meier et al. 1992; Triantafillou and Plevris 1992; Täljsten 1994; Van Gemert 1996) by replacing steel with FRP plates, made of FRP materials, an attractive solution for structural strengthening, which gained wide acceptance in the international research community. Competitive strengthening solutions using materials like carbon or glass fiber reinforced polymers (CFRP or GFRP) have been nowadays developed due to the high strength-to weight ratio, high durability (not corrodible), electromagnetic neutrality, ease of handling, rapid execution with low labor costs and low impact on architectural and aesthetic appearance (Bakis et al. 2002; Teng et al. 2003; De Lorenzis and Teng 2007; Choudhury et al. 2013). FPRs are high strength materials with relatively high Young's modulus, characterized by a linear elastic behavior up to failure, which occurs in a brittle manner. The most popular techniques based on the use of FRP reinforcements are the Externally Bonded Reinforcement (EBR) and the Near Surface Mounted (NSM). Experimental studies conducted worldwide on RC beams strengthened in shear with FRPs clearly demonstrate the reliability and effectiveness of such techniques for structural strengthening and retrofitting. According to the EBR technique, sheets or plate/laminates of carbon fiber reinforced polymers (CFRP) are bonded on the faces of the elements to be strengthened. In case of the NSM technique, CFRP laminates or bars are installed into slit/grooves sawed into the beams' concrete cover and bonded to the concrete substrate by an epoxy adhesive. Fig. 2.25 shows a laboratory application for shear strengthening using both techniques. The oldest known study on the shear strengthening with EBR FRP was carried out by (Berset 1992), that strengthened reinforced concrete beams of different percentage of internal stirrups beams using GFRP sheets inclined at 45°. The EBR technique for RC shear strengthening has been largely investigated (Triantafillou 1998; Khalifa 1999; Khalifa and Nanni 2000; Pellegrino and Modena 2002; Bousselham and Chaallal 2006; Chaallal et al. 1998; Monti and Liotta 2007; Barros et al. 2007), and it was demonstrated that the shear strength can considerably increase by applying this technique. However, due to the premature debonding occurring to the externally bonded FRP strips or sheets, the maximum stress mobilized in the strenghtening material is quite lower than its ultimate strength. The common shear strengthening configurations for the EBR technique are presented in Fig. 2.26. The use of flexible fiber sheets allows to adopt several

strengthening configuration: Full wrapping of the cross section (O), U jacketing (U) and side bonding on the beam web (S).

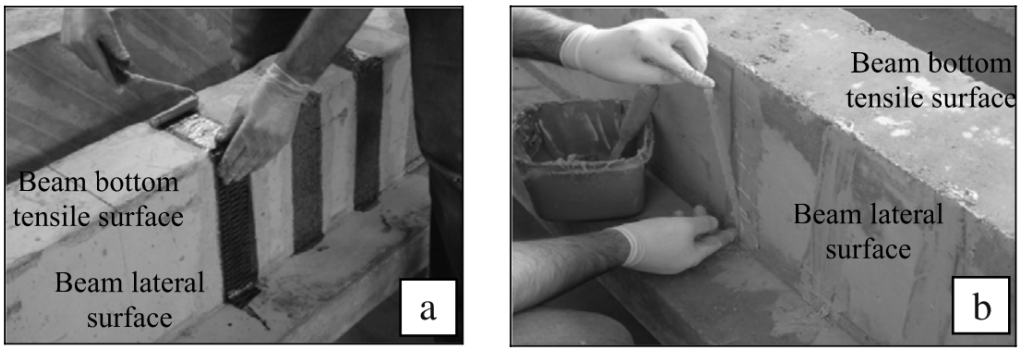

Fig. 2.25 Shear strengthening techniques with CFRP: (a) External bonded reinforcement (EBR), (b) Near surface mounted (NSM)(Dias and Barros 2010)

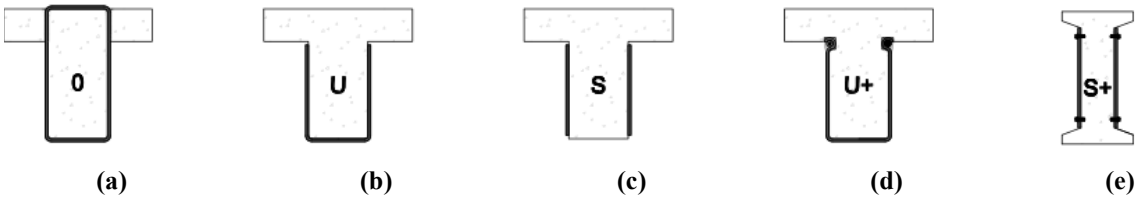

Fig.2 26. Common externally bonded FRP strengthening configurations: Full wrapping of the cross section, O (a), U jacketing (b) and side bonding on the beam web, S (c). Additional mechanical anchorage systems can be provided to enhance the effectiveness of U or S configurations when the available bond length is short (U+ and S+).

It has been demonstrated that the highest increase of shear strength can be obtained when a close configuration of the FRP is provided (Jirsa et al. 2011), this is the only case where the composite is, in general, able to exploit its full tensile capacity by reaching its ultimate strain. The problem related to the full wrapping are technical, in fact for existing RC beams the presence of integrated slabs make this strengthening intervention high-priced and time demanding. By adopting a U and S strengthening configuration usually low increase of load carrying capacity are obtained since these two systems are more prone to debonding failure. Side bonding configuration has been recently removed from the latest version of the Italian guidelines (National Research Council CNR-DT 200-2012), since experimental programs that adopted this strengthening configuration have demonstrated that debonding occurred at low level of shear strength increment. In the U strengthening configuration a larger bond length is provided by bending the FRP around the bottom edge of the beam. (Khalifa 1999) showed that the increment of shear capacity for the tested beams (the tested beams were without shear reinforcement) was 35% and 80%, for S and U strengthening configuration, respectively. Fig 2.28a shows a typical failure of the EBR strengthening using the U configuration. The increment of shear strength in the

aforementioned experimental program increased more than 145 % when an anchorage system was provided to the U strengthening configuration, in this case the FRP was able to convert a shear-type failure into a flexural failure. It results, that a mechanical anchorage system is a fundamental requirement in case of small bond transfers length. The variety of proposed anchorage systems available in literature is wide, those can be made of metal or composite material; handmade anchors have also been proposed and investigated (Kim and Smith 2009).

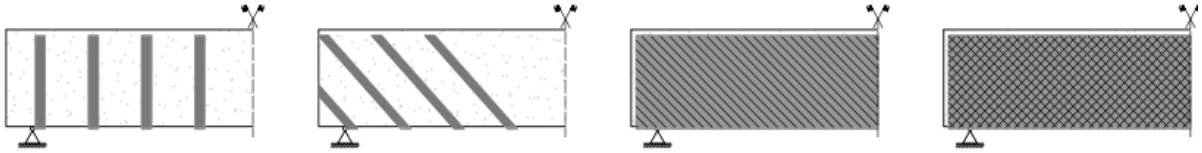

(a) **(b)** **(c)** **(d)**

Fig. 2.27. Possible arrangements for externally bonded FRP strengthening systems including variations in the fiber orientation (a-b), the use of discrete strips or continuous sheets (a-d), and the overlay of sheets with different fiber orientations (d).

Each of the aforementioned strengthening configurations may be set in several possible arrangements (Fig.2.27). The orientation of the fiber (usually between 90° and 45°), and different layer can be overlaid with a different fiber inclination, resulting in a mono-bi or multidirectional system. By using the EBR technique, it is possible to adopt a continuous or a discrete strengthening configuration. A higher increase of shear strength is generally achieved by bonding the FRP strengthening systems with the fibers orthogonal to the critical shear crack plane. An extensive database on EBR-FRP strengthened beams has been developed by the Structural Composites Research Group at the University of Minho (Lima and Barros 2011) with the purpose of collecting data, to be used for the appraisal of the predictive performance of the available analytical models (Section 2.8). An extension of the EBR technique was developed at the EMPA laboratory in partnership with SIKA by using prefabricated L-shaped CFRP plates to limit the occurrence of debonding of the strengthening system in the lower part of the beam's web (Czaderski 2002; Czaderski and Motavalli 2004).

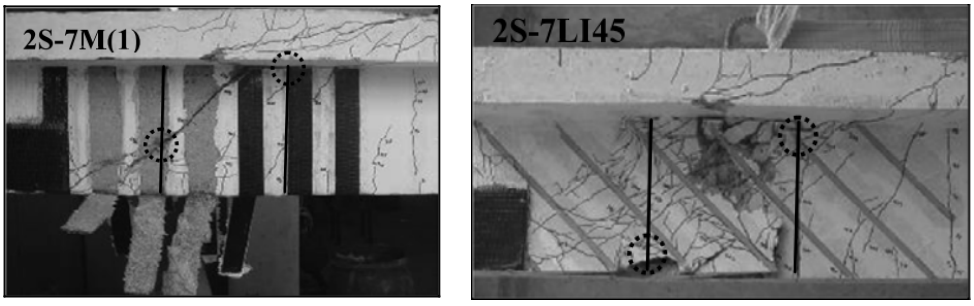

(a) **(b)**

Fig. 2. 28 RC T-beams at failure (a) EBR technique and (b) NSM technique.

Maximum efficiency using composite materials is obtained when the strengthening system is able to exploit its full tensional strain. Both EBR and NSM technique rely on the stress transfer capacity between FRP and concrete substrate, however, this last one is usually the most damaged part of the RC elements. As previously reported, the main problem of FRP strengthening lies in the fact that the FRP fail mostly by debonding in a EBR strengthened element. Unlike the case of EBR simply glued on the concrete surface, a certain confinement provided in the NSM FRP strips due to the insertion into thin slits open in the concrete cover allows to develop higher bond stress (Sena-Cruz and Barros 2004; Barros et al. 2007; Bilotta et al. 2011; Seo et al. 2013). Oehlers et al. (2008), Costa and Barros (2012) and Barros and Dias (2013) demonstrated experimentally that by installing NSM strips into deeper grooves the bond performance can be improved.

The available experimental research showed that the NSM technique is more effective than EBR for both the flexural (De Lorenzis et al. 2000; Carolin et al. 2001; Hassan and Rizkalla 2003; El-Hacha, Raafat, Rizkalla 2004; Barros et al. 2007) and shear strengthening (De Lorenzis and Nanni 2001; Dias and Barros 2008, 2010, 2011a, 2011b; 2012; Anwarul Islam 2009; Rahal and Rumaih 2011).

When using NSM technique, the current failure modes are concrete fracture, followed by debonding of the FRP systems (Fig. 2. 28b). Haskett et al. (2008), reported that the interfacial fracture energy of externally bonded (EB) FRP plates is approximately 1 N/mm and increased up to approximately 5 N/mm for near surface mounted (NSM) FRP laminates. FRP bars of circular, square and rectangular cross section have been used for the NSM shear strengthening of RC beams. Due to the largest bond area, CFRP laminates of rectangular cross section are proved as being the most effective strengthening elements for the NSM shear strengthening of RC beams. It also has been demonstrated that strips laminates of CFPR are preferable than CFRP bars due to their lower stiffness in the orthogonal direction to the element axis. By applying the NSM technique, the full tensile capacity of the CFRP reinforcements can only be attained when these reinforcements are surrounded by relatively high strength concrete and an adequate bond transference length is assured (Dias and Barros 2013). NSM does not require surface preparation work and after cutting the slit, requires minimal installation time compared to the EBR technique, the susceptibility to acts of vandalism is also reduced by using the NSM technique.

The number of tests on reinforced concrete beams strengthened in shear using the NSM technique available in literature is smaller than the one for EBR strengthened beams, but the efficacy of this technique has been assessed by several research carried out in the last decade, (De Lorenzis and Nanni 2001; Barros et al. 2007; Lee and Lim 2008; Rizzo and De Lorenzis 2009; Anwarul Islam 2009; Rahal and Rumaih 2011). These experimental programs show that the NSM technique can significantly increase the shear strength of RC beams up to 157% as demonstrated by Lee and Lim (2008) by testing

a RC beam without stirrup and 45° inclined NSM FRP. For both EBR and NSM the maximum effectiveness is obtained when the fibers are oriented along the principal tensile direction, or rather for cracked elements in the orthogonal direction the potential cracks. As already shown for the EBR technique, when the bond is assured by an anchorage system, the shear strength increases significantly as well for the NSM technique. Higher increment of shear strength can be obtained using the NSM technique in comparison with unanchored EBR technique. Moreover the NSM technique exhibits a less brittle failure in comparison with the EBR technique. A comprehensive study on the shear strengthening of RC concrete beams was carried out by Dias and Barros (2008, 2010, 2011a; 2011b; 2012; 2013). In this context, the influence of several parameters was investigated: concrete strength, percentage of existing stirrups, percentage and inclination of the CFRP, existence of cracks. The shear strength has increased by increasing the concrete compressive strength, due to the higher bond performance that could be achieved. Fig. 2.29a shows the influence of the concrete strength class as presented in Dias and Barros 2013, the average value of the NSM system contribution for the highest class of concrete strength ($f_{cm} = 39.7$) is 2.7 times higher the one obtained with the lowest strength class ($f_{cm} = 18.6$). The tested beams evidenced a clear detrimental effect of the steel stirrups on the shear strengthening effectiveness of the NSM, as it is possible to observe in Fig. 2.29b for all the tested strengthening solution lower NSM system contribution has been provided with the highest percentage of transverse reinforcement, however, the level of the influence of the percentage of existing steel stirrups seems to be larger, as smaller the concrete strength. The influence of the existing stirrups on the strengthening effectiveness was already evidenced for EBR strengthening by (Khalifa and Nanni 2002; Grande et al. 2009, Triantafillou 1998; Pellegrino and Modena 2002) that observed reduction of effectiveness with the increase of the transverse reinforcement ratio and the stiffness of the FRP system.

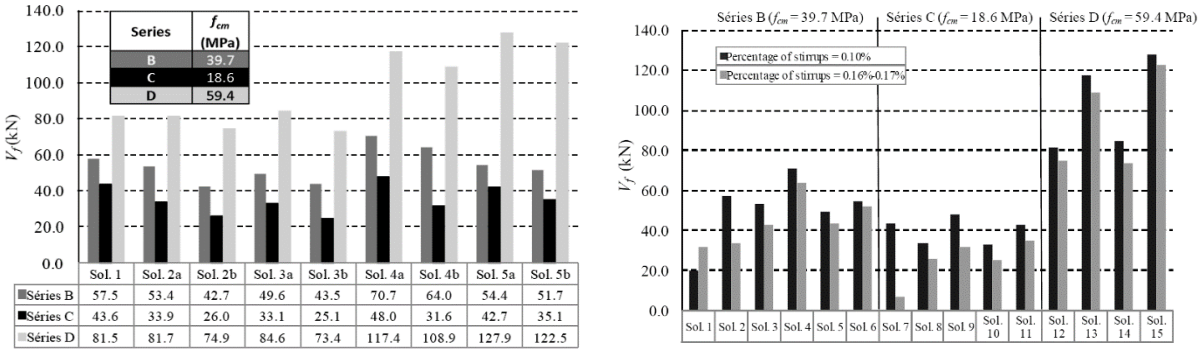

(a) **(b)**

Fig. 2.29 Influence of the concrete strength (a) and percentage of existing stirrups (b) on the effectiveness of the shear strengthening technique using NSM CFRP laminates (Dias and Barros 2013).

When the percentage of strengthening NSM-reinforcement is relatively high, the concrete cover including the FRP reinforcement has the tendency to detach; this failure mode is even more visible in the case of low strength concrete beams. Even when a small percentage of CFRP laminates is used, it was observed that the concrete had fractured around the CFRP strip, which indicated that failure did not occur exclusively by debonding. A subsequent experimental-analytical investigations (Bianco et al. 2006, 2007) demonstrated, even by means of an analogy with adhesive anchors (Cook et al. 1993, 1998), that the NSM failure mode can be ascribed to a semi conical tensile fracture surface of concrete surrounding each NSM strip (Fig. 2.30c). Depending on the relative mechanical and geometrical properties of the possible failure mode affecting the behavior, at ultimate, of NSM strip compromise: debonding, tensile rupture of the strip itself, concrete semi-conical tensile fracture and mixed shallow-semi-cone-plus-debonding failure mode Fig.2.30

A mechanical explanation of the interaction between the NSM strengthening was found by Bianco et al. (2009), that developed a complex three dimensional model for the estimation of the shear strength contribution of NSM shear strengthened beams. The model was also able to simulate the deeper embedment of the laminate into the beam's web surface; the concrete fracture failure surface has in this case higher fracture area, resulting in a higher concrete fracture force. The detrimental effect induced by the interference of consecutive laminates (group effect) observed in the experimental programs carried out by Dias and Barros (2012) and (Rizzo and De Lorenzis 2009) Fig. 2.31, was accounted by the model. This interaction results in a reduced strength when compared with the sum of the single bars/strip resistance (Bianco 2008).

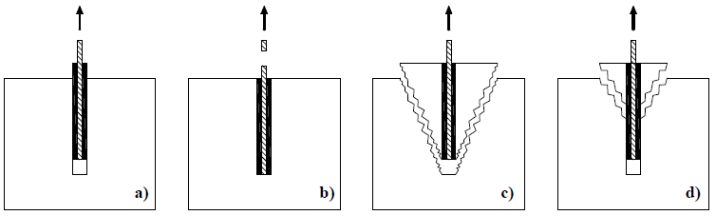

Fig. 2.30 Possible failure modes of an NSM strip: (a) debonding, (b) strip tensile rupture, (c) concrete semi-conical fracture, (d) mixed shallow semi-cone plus debonding

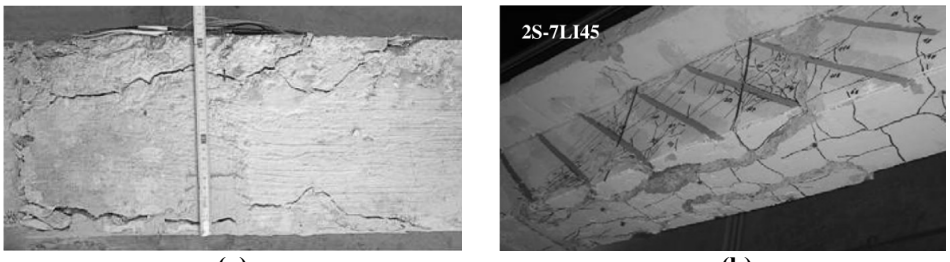

(a) **(b)**

Fig. 2.31 "Group Effect "of failure mode due to the interaction of high percentage of strengthening (a) (Rizzo and De Lorenzis 2009) (b) (Dias and Barros 2011b)

Recently an alternative NSM technique using manually made FRP rods (MMFRPs) has been proposed (Jalali et al. 2012). This "handmade" CFRP strengthening bars was obtained by wrapping and impregnating a carbon fiber textile around a wooden core. In order to delay the occurrence of debonding the MM-NSM can be fabricated with end anchors as shown in Fig. 2.32. This anchor consists in extra dry carbon fibers at both ends of the bar that are wrapped and impregnated around a wooden core orthogonal (in vertical MM-NSM) to the bars axis. The proposed MMFRP rods and end anchorage enhanced the shear capacity of the beams between 25% and 48% over the control specimen. Furthermore the proposed end anchorage of MMFRP rods significantly enhanced the ductility of the test specimens. The main drawbacks regarding this application is the time that needs to be dedicated to prepare the MMFRP; moreover even if "ready to install" FRP with similar shape as the proposed MMFRP could be provided by companies, the labor to install the strengthening is time-consuming.

(a) **(b)**

Fig. 2.32 Manually made FPR rods (MMFRP) proposed by (Jalali et al. 2012): (a) MM-NSM (b) groove prepared for the FRP installation.

2.5.5 Embedded through section technique for shear strengthening

A new strengthening technique, designated as Embedded Through-Section (ETS), has recently been investigated for the shear strengthening of RC beams (Valerio et al. 2009; Chaallal et al. 2011; Barros and Dalfré 2012). According to this technique, steel or FRP bars are inserted into holes bored through the cross section and bonded with an epoxy adhesive (Fig. 2.33). Like any FRP-based strengthening technique, the ETS technique relies its efficiency on the bond between the concrete substrate and the strengthening element; furthermore, the bond effectiveness is influenced by the provided confinement (Bianco et al. 2009; Mohamed Ali et al. 2008; Yuan et al. 2004). This technique can be highly effective for the shear strengthening due to even higher confinement provided by the concrete surrounding the bars deep embedded into the core of the element to be strengthened, which entails advantages on the bond strength. Furthermore, a larger concrete fracture surface is mobilized during the pullout process applied to the ETS bars crossing the shear crack, when compared to the case of a EBR and NSM FRP strengthening system. When concrete cover has not the bond strength requisites to guarantee the aimed strengthening effectiveness for the EBR or NSM techniques, ETS strategy can be a technical and

economic alternative since it mobilizes the beam's concrete core that is generally the less damaged zones of a beam. Moreover ETS strengthening provide a better protection from fire, environmental aggressive agents and vandalism acts than EBR and NSM techniques. The main steps of the ETS technique as presented in The main steps of the ETS technique as reported in (Barros and Dalfré 2012) are presented in Fig. 2.34

(a) **(b)** **(c)**

Fig. 2.33 Embedded Through-Section (ETS) technique (a) schematic concept and bars position in (a) (Valerio et al. 2009) and (b) (Chaallal and Mofidi 2011)

Fig. 2.34 Embedded Through-Section (ETS) strengthening technique as reported in (Barros and Dalfré 2012): (a) drilling of the holes, (b) cleaning of the holes with compressed air, (c) hole filled with adhesive and ETS strengthening bar.

Significant increase of shear capacity has been pointed out by Valerio et al. (2007, 2009) who investigated the use of the ETS technique for the shear strengthening of RC existing bridges, performed pullout tests for assessing the strengthening effectiveness of adhesive materials, and different embedment lengths for the ETS bars. The shear stress transfer mechanisms developed in an ETS bar were studied by Barros et al. (2008) using similar specimens to the ones tested by Mattock and Hawkins (1972) for traditional embedded steel bars. In this context, direct shear tests were executed with the purpose of capturing the main features of FRP/steel ETS bars as they contribute to the shear resistance, and to provide data for a rational decision about the most effective bars and adhesives for this type of application. From the results, a significant increase in shear strength was obtained with a relatively low shear reinforcement ratio, and it was verified that steel bars were very effective for this purpose.

Chaallal et al. (2011) carried out tests to assess the effectiveness of the ETS technique using vertical CFRP bars by comparing the performance of the ETS, EBR and NSM techniques on beams with different percentages of internal steel stirrups. It was demonstrated that the ETS technique provided the highest efficiency and was able to convert shear failure into a flexural failure. In the continuation of a comprehensive research project initiated by Barros et al. (2008) on the ETS shear strengthening effectiveness, an experimental program was carried out by Barros and Dalfré (2012) with RC beams shear strengthened with ETS steel bars. The variables examined in this experimental program were the width of the beam's web, the percentage and inclination of the ETS bars, the spacing of existing steel stirrups and their interaction with the strengthening bars. A significant increase of load carrying capacity was obtained (between 14% and 124%), proving that the use of ETS steel bars can be a very effective and cost-competitive shear strengthening technique. By analyzing the previous experimental tests it can be observed that the beams with the higher percentage of ETS bars failed in bending, despite the very high percentage of flexural reinforcement used, which evidence the feasible use of this technique, but makes it impossible to use the results of beams failing in bending for the assessment of an analytical model to calculate the ETS strengthening contribution.

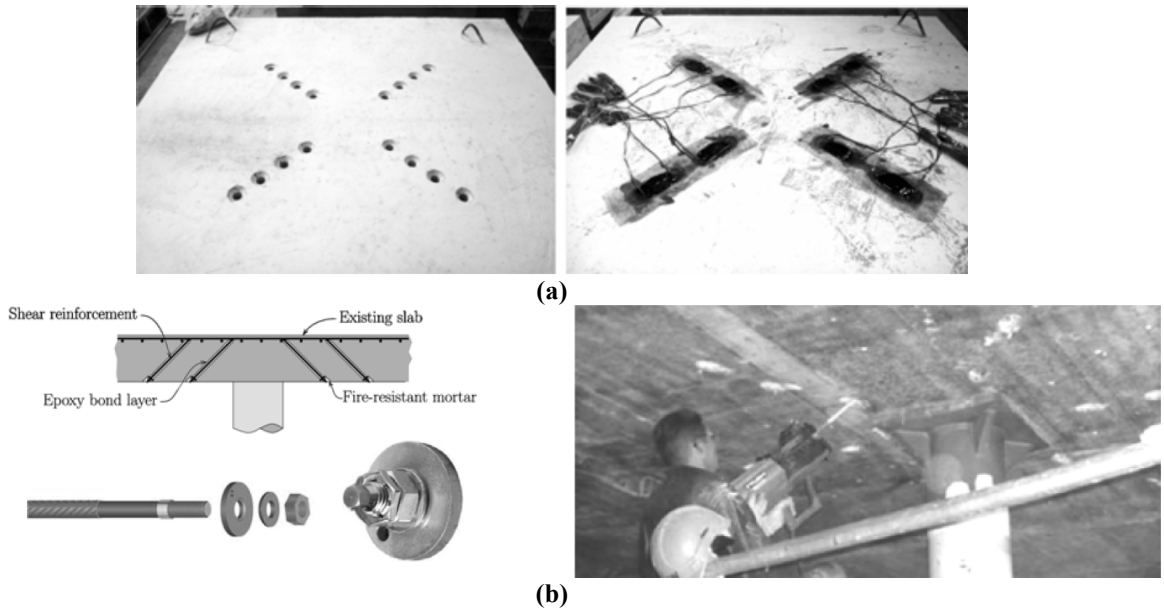

Fig. 2.35(a) Application of carbon fiber reinforced polymer for punching shear strengthening (Sissakis and Sheikh 2007), (b) Post-installed shear reinforcement, typical cross section, detail of the strengthening bar, drilling of the inclined holes (Fernàndez Ruiz et al. 2010)

The ETS technique concept can also be extended for the punching shear strengthening of concrete slabs. To increase the critical shear perimeter in the slab-column connections, steel bars bonded with adhesive can be introduced in drilled holes at 45-degree (Hassanzadeh and Sundqvist 1998; Fernàndez

Ruiz et al. 2010). Bolts to act as shear reinforcement (El-Salakawy et al. 2003), and carbon fiber reinforced polymer (Binici 2003; Sissakis and Sheikh 2007; Meisami et al. 2015) can also be used to increase resistance of this type of elements (Fig. 2.35). The experimental program on RC beams strengthened using the ETS technique are here briefly presented.

Valerio et al. (2007, 2009)

Valerio et al. (2007, 2009) performed a series of tests on RC and pre-stressed rectangular beam strengthened with the ETS method. The experimental program comprises small-scale and large scale beams. The beams were designed to match a common typology of beam used for railway bridges in the UK. The small scale beams had a cross section of 110mm x 190 mm and a length of 3000 mm. Four 7 mm diameter wires were adopted as longitudinal reinforcement; in some of the beams two wires were pre-tensioned to 45 kN. All the beams did not have stirrups with the only exception of beam SSB Rst3d-C6@0.7d, where two-leg 3mm diameter vertical stirrups spaced at 100 mm stirrups were used (ρ_{sw}=0.129 %). The large-scale beams had a cross section of 450mm x 340mm and a length of 4000 mm. Fourteen 12.5 mm diameter tendon each of them pre-tensioned to 70 kN were adopted as longitudinal reinforcement, shear reinforcement was absent in this group of strengthened tested beams. The cube compression strength was 55-60 MPa. The beams were loaded under a four point bending systems at different shear span lengths (a/d ratio equal to 3 and 4). The small beams were strengthened using vertical carbon or steel bars of 6, 7.5, 8mm diameter spaced at 0.35d, 0.d5, 0.7d and d (Fig. 2.36). The large scale pre-stressed beams were strengthened using vertical 7.5 mm carbon or 8 mm steel bars spaced at length d. In general, one bar was placed in the cross section, with the exception of the large scale beams SLB P4d-2C7.5@0.5d and SLB P4d-2S8@d in which two bars were placed in each cross section. The thickness of the adhesive layer was 1 mm. One large-scale beam was strengthened with the NSM technique for comparison. Table 2.1 shows the specimens' details and the test results for the strengthened beams where SSB stands for strengthened small beams and SLB for strengthened large beams, C and S indicates a Carbon and Steel bars respectively. Small pre-stressed beams with a strengthening ratio ρ_{fw} between 0.17% and 0.38% exhibit flexural failure rather than shear failure demonstrating the potentialities of this technique; in this case the gap between the two types of failure for the un-strengthened beams was low, which justify the relatively low increase of shear strength provided by the strengthening. Higher increase of load carrying capacity (between 79% and 127%) have been obtained in non-prestressed reinforced beams (percentage of strengthening ranged between 0.24% and 0.49%). All the large scale beams failed in shear with maximum increase of load carrying

capacity of 14.6% in the beam with higher percentage of strengthening (ρ_{fw}=0.15%). Both materials used for the strengthening were effective and no significant differences in the used material have been noticed. Thus it was concluded by the authors that the proposed shear strengthening method is feasible and effective for both prestressed and RC beams, even in the presence of transverse steel reinforcement.

Table 2.1 Specimend detail and results of strengthened beams Valerio et al. 2009

Specimen	Type	a/d	ϕ	s	ρ_{fw} [%]	Capacity [kN]	V_f [kN]
SSB P4d-C7.5@0.7d	Prestr.	4	7.5	0.7d	0.38	41.1 (f)	≥ 4.3 (+10.4%)
SSB P4d-S8@0.7d	Prestr.	4	8	0.7d	0.44	43.8 (f)	≥5.9 (+15.7%)
SSB P4d-C6@0.7d	Prestr.	4	6	0.7d	0.24	43.2 (f)	≥ 5.3 (+14.7%)
SSB P4d-S6@0.7d	Prestr.	4	6	0.7d	0.24	41.9 (f)	≥ 4.0 (+10.5%)
SSB P4d-C6@d	Prestr.	4	6	d	0.17	43.3 (f)	≥ 5.4 (+14.3%)
SSB P4d-S6@d	Prestr.	4	6	d	0.17	42.7 (f)	≥ 4.8 (+12.8%)
SSB R3d-C6@0.7d	No-prestr	3	6	0.7d	0.24	46.4 (f)	22.9 (+97 %)
SSB R3d-C6@0.5d	No-prestr	3	6	0.5d	0.34	50.5 (s)	27 (+114%)
SSB R3d-C6@0.35d	No-prestr	3	6	0.35d	0.49	53.5 (f)	≥ 30.0 (+127%)
SSB Rst3d-C6@0.7d	No-prestr.	3	6	0.7d	0.24	56.5 (f)	≥ 25.0 (+79%)
SLB P4d-2C7.5@0.5d	Prestr.	4	7.5	0.5d	0.15	339.1 (s)	43.2 (+14.6%)
SLB P4d-C7.5@0.5d	Prestr.	4	7.5	0.5d	0.08	315.0 (s)	19.1 (+6.5%)
SLB P4d-2S8@d	Prestr.	4	8	d	0.09	349.1 (s)	53.2 (+18 %)

(s) = shear failure, (f) = flexural failure

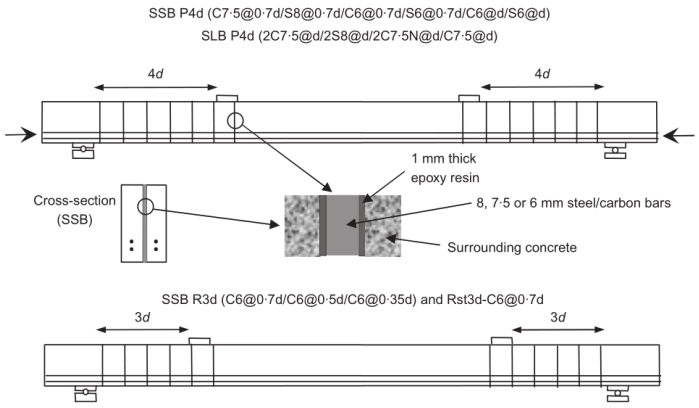

Fig. 2.36 Test layout for strengthened beams Valerio et al. (2009)

Barros et al. (2008)

The shear stress transfer mechanisms developed in a ETS bar were studied by Barros et al. (2008), using similar specimens to the ones tested by Mattock and Hawkins (1972) for traditional embedded steel bars. The performed short beams test is presented in Fig. 2.37. In this context, direct shear tests were executed with the purpose of capturing the main features of FRP/steel ETS bars on the contribution for the shear resistance, and to provide data for a rational decision about the most effective bars and adhesives for this type of application. Different type of material (CFRP, GFRP, steel),

diameter of the bar (8 and 12mm) and type of adhesive (Epoxy and Grout) has been tested. A significant increase in shear strength was obtained with a relatively low shear reinforcement ratio, and it was verified that steel bars were very effective for this purpose.

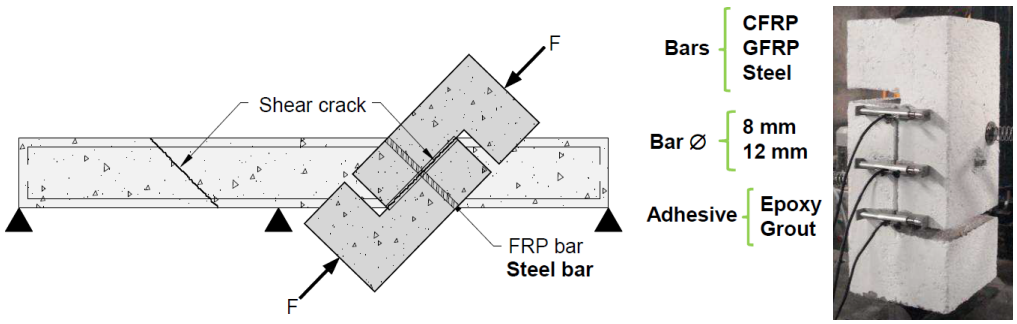

Fig. 2.37 Short beam shear test (Barros et al. 2008)

Chaallal et al. (2011)

Chaallal et al. (2011) carried out experimental test on T-cross section RC beams strengthened with vertical CFRP rods to investigate the effectiveness of this technique and to compare the results with beam strengthened with the Externally Bonded (EBR) and Near Surfaces Mounted (NSM) techniques. One of the main investigated parameter was the percentage of transverse steel. The experimental program consisted of 12 beams divided in three different series, each of them characterized by a different percentage of internal transverse reinforcement, equal to ρ_{sw}= 0.0%, ρ_{sw}= 0.38% (8mm@d/2 - 175 mm) and ρ_{sw}= 0.25% (8mm@ 3/4d - 260 mm), for S0, S1, S3, respectively. The T-cross section had dimensions, 508mm (width of the flange) by 406mm (total depth). The T beams are 4520 mm long, the thickness of the web and the width of the flange are 152mm and 102mm, respectively, (Fig. 2.22). The longitudinal steel reinforcement consists of four bars with diameter of 25.2 mm laid in two layers at the bottom and six bars with diameter of 10.3 mm laid in one layer at the top. The total load was applied at a distance a=3d. The cylindrical compressive strength was 25 Mpa for S0 and S1 series and 35 MPa for S3 Series. The diameter of the vertical holes for the ETS rods installation are 18mm. Sand coated CFRP rods with nominal diameters of 9.5 mm and 12.7 mm are used for NSM and ETS strengthening methods, respectively. The FRP bars presented average tensile strength and modulus of elasticity of 1870 MPa and 143.9 GPa, respectively. A commercially available epoxy paste was used for embedding the rods. The CFRP sheet used for EB series was a unidirectional carbon fiber fabric (Sika Wrap Hex 230C, ply thickness 0.381mm) and presented an ultimate stress and young´s modulus of 3650 MPa and 231 GPa, respectively.

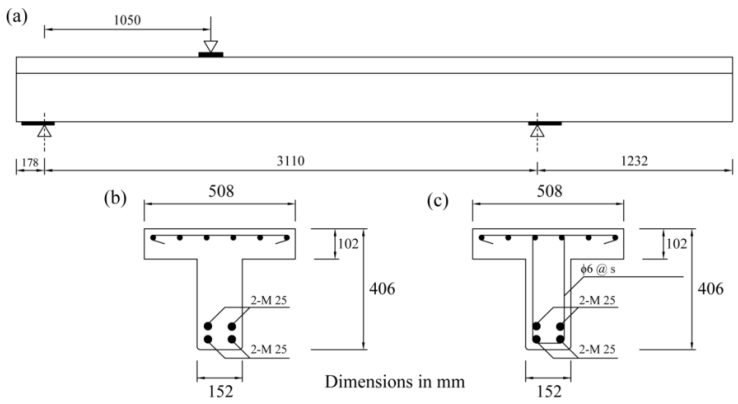

Fig. 2.38 Details of concrete beams: a) elevation; b) cross section with no transverse steel; and c) cross section with transverse steel.

Table 2.2 Specimend detail and results (Chaallal et al. 2011)

Beam ID	Tech.	Series	ρ_{sw} [%]	ρ_{sw} [%]	F_{max} [kN]	V_t [kN]	V_f [kN]	$\Delta F_{max}/F_{fe\,f,max}$ [%]	Failure mode
S0-CON		S0	0.00		122.7	81.3	0	0	Shear
S1-CON		S1	0.38		350.6	232.2	0	0	Shear
S3-CON	--	S3	0.25		294	194.7	0	0	Shear
S0-EB		S0	0.00		181.2	120	38.7	48	Shear
S1-EB		S1	0.38	0.50	378.5	250.7	18.5	8	Shear
S3-EB	EB	S3	0.25		335.2	222	27.3	14	Shear
S0-NSM		S0	0.00		198	131.1	49.8	61	Shear
S1-NSM		S1	0.38	0.72	365	241.7	9.5	4	Shear
S3-NSM	NSM	S3	0.25		380	251.6	56.9	29	Shear
S0-ETS		S0	0.00		273	180.8	99.5	122	Shear
S1-ETS		S1	0.38	0.64	397	262.9	30.7	13	Flexure
S3-ETS	ETS	S3	0.25		425.5	281.8	87.1	45	Flexure

Table 2.2 presents the main results. It is shown that EBR U-jacket sheet, NSM FRP rods, and ETS FRP rods have provided increase in shear capacity of 61%, 48% and 122%, respectively for specimens with no transverse steel. The presence of stirrups decreased the gain of load carrying capacity and shear strength; for the ETS beam with the highest percentage of stirrups (S1-ETS) this increment was limited to 13%. Additionally, the ETS technique was more efficient in terms of mobilizing the tensile capacity of the FRP systems, since the CFRP bars have failed due to the attainment of their tensile strength when applied according to the ETS technique, while the EBR systems failed by debonding, and the NSM rods by the separation of the concrete cover. At the failure of the FRP systems applied according to the EBR and NSM techniques, the maximum tensile strain was much lower than its ultimate tensile strain. It should be noted that the ETS contribution could have been higher if it was not for the concrete cross

section limitation, since beams with stirrups and ETS strengthening failed in bending rather than shear. The effect of transverse steel in inhibiting the effectiveness of FRP was less pronounced in the ETS method in comparison to EBR method and NSM method. In (Mofidi et al. 2012), the result of additional ETS strengthened beams were presented. The same cross section geometry and internal steel arrangement of (Chaallal 2011) was adopted; in this tests the influence of the spacing of the reinforcement and the type of CFRP coating were investigated.

Barros and Dalfré (2011)

Barros and Dalfré (2011) carried out experimental tests on rectangular cross section RC beams strengthened with vertical and inclined ETS steel bars to investigate the effectives of this technique and study the influence of the percentage of internal steel stirrups, inclination and spacing of the strengthening. The experimental program consisted of 2 series of beams with different cross section. Series A and Series B are characterized by concrete cross section 150x300mm^2 and 300x300mm^2, respectively, with a total length of 2450mm and shear span 900mm (ratio a/d=3.44). The longitudinal steel reinforcement consists of two and three steel bars of 25mm diameter (ϕ 25mm), respectively (ρ_{sl}=2.50% for Series A, ρ_{sl}=1.88% for Series B. Steel stirrups of two vertical arms and 6mm diameter were used. Each series is made up of a beam without any shear reinforcement and a beam for each of the following shear reinforcing systems: (i) steel stirrups of ϕ6 mm at a spacing of 300mm, (ii) ETS strengthening bars at 45° and 90° in relation to the beam's axis, with a spacing of 300mm, (iii) steel stirrups of ϕ 6mm at a spacing of 300mm and ETS strengthening bars at 45° or 90° with a spacing of 300mm. Additionally for the A series, two other shear reinforcing systems were also tested: (iv) steel stirrups of ϕ6 mm at spacing of 225mm and (v) steel stirrups of ϕ6 mm at a spacing of 225mm and ETS strengthening bars at 90° with a spacing of 225mm. For the series A and series B, ETS bar of ϕ10 and ϕ8 were used. In case of B-Series two ETS bars were introduced in the cross section. The compressive strength of the tested beams rage between 28.81 and 30.78 MPa. The use of ETS bars for shear strengthening provided significant increase in the load-carrying capacity of RC beams, in particular with inclined strengthening. The deflection capacity was also improved. Table 2.3 shows the percentage of internal transverse steel and of the applied strengthening and the main results of the experimental program: maximum load, percentage of load increment and shear force (calculated as percentage increment compared toA1-Reference and B1-Reference) and the ETS strengthening system contribution to shear strengthening (V_f). For Series A, the strengthening percentage ranged between 0.17% and 0.25%, these beams presented a V_f in the interval between 31.15 and 57.97 kN. For Series B the strengthening percentage ranged were 0.11% and 0.16%, these beams presented a V_f in the interval

between 21.31 kN and 98.52 kN. The effectiveness of the ETS strengthening depended on percentage of internal stirrups.

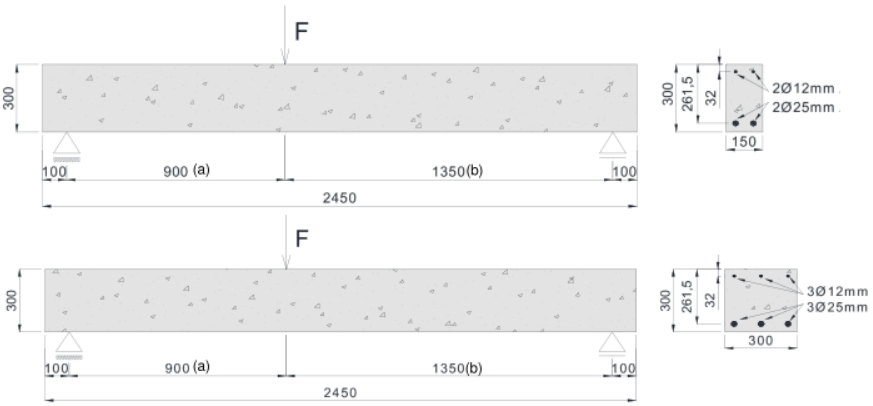

Figure 7.1: Test configuration. All dimensions are in mm.

Fig. 2.39 Test configuration of the beams tested by Barros and Dalfré (2012)

Table 2.3 Specimend detail and results (Barros and Dalfré 2012)

	ρ_{sl}	ρ_{sw}	ρ_{fw}	$F_{\max}$	$\Delta F_{\max} / F_{\mathrm{Re}f,\max}$	V_f
	[%]	[%]	[%]	[kN]	[%]	[kN]
A.1 -Reference	2.5	--	--	108.86	--	--
A.2-S300.90	2.5	0.13	--	164.67	51	--
A.3-E300.90	2.5	--	0.17	160.7	48	31.15
A.4-E300.45	2.5	--	0.25	203.98	87	57.07
A.5-S300.90/E300.90	2.5	0.13	0.17	231.83	113	40.3
A.6-S300.90/E300-45	2.5	0.13	0.25	244.41	125	47.85
A.7-S225.90	2.5	0.17	--	180.31	66	--
A.8-S225.90/E225.90	2.5	0.17	0.23	244.17	124	38.31
B.1-Reference	1.88	--	--	203.36	--	--
B.2-S300.90	1.88	0.06	--	232.31	14	--
B.3-E300.90	1.88	--	0.11	238.88	17	21.31
B.4-E300.45	1.88	--	0.16	326.19	65	79.69
B.5-S300.90/E300.90	1.88	0.06	0.11	390.11	92	94.68
B.6-S300.90/E300-45	1.88	0.06	0.16	396.51	95	98.52

2.6 Design guidelines for FRP shear strengthening

The increasing interest by the research community in FRP strengthening and the continuous growth in field applications, led to several analytical formulations for the estimation of the shear strengthening contribution carried out by EBR (Triantafillou 1998; Monti and Liotta 2007; Chen and Teng 2003a, 2003b), and NSN (De Lorenzis and Nanni 2001, 2002; Nanni et al. 2004; Bianco et al. 2009, 2011, 2014, Dias and Barros 2013) systems. The parameters that influence the shear behavior of a strengthened RC element were already identified (Lima and Barros 2007; Bousselham and Chaallal 2008; Belarbi et al. 2012). Several authors have evidenced that the stress in the FRPs is strongly influenced by the axial rigidity $E_f \rho_f$ of the FRP composite, (Carolin and Täljsten 2005; Chaallal et al. 1998; Khalifa et al. 1998; Triantafillou and Antonopoulos 2000; Dias and Barros 2013).

Nowadays, only the EBR technique has been completely implemented in design guidelines and standard around the world, providing the guidance for design, detailing, and installation of this FRP based strengthening systems. In most of the proposed analytical formulations and in all the design guidelines, the shear strength of a strengthened member is attained by the sum of the contributions from concrete, V_c , steel reinforcement, V_s , and FRP, V_f , as follows:

$$V_t = V_c + V_s + V_f \tag{2.43}$$

where V_c and V_s may be calculated according to the provisions existing in current design codes, independently of the adopted FRP strengthening system. The design guidelines are, in general restricted to the calculation of the shear strengthening contribution provided by the strengthening V_f .The methodology to estimate the design value of the FRP contribution the shear V_{fd} requires the adoption of a safety factor generally directly applied to the value V_f . Lima and Barros (2011) developed a web tool, designated DABASUM (**DA**ta**BA**se for FRP-based **S**hear strengthening of reinforced concrete beams- **U**niversity of **M**inho, dabasum-civil.uminho.pt) to collect data on experimental programs dealing with the shear strengthening of RC beams using the EBR technique and to assess the predictive performance of the fib Bulletin 14 (fib 2001), ACI 440 (ACI Commitee 2008), HB 305-2008 (Standard Australian 2008, former CIDAR (2006), and CNR DT-200 (National Research Council 2012) design guidelines. At the time of the analysis (Lima and Barros 2011) the fib design model presented, in average, the lowest safety factor (1.198), while the safest predictions were obtained with the CNR-DT 200 (average safety factor 2.108). The largest scattering was obtained from the CNR model (COV=0.73), while the model with lowest scattering was the fib (COV=0.55). The HB 305-2008 model

globally presented a good performance with an average value of 1.43 and COV = 0.58. A reliability analysis based on structural safety conducted by the authors demonstrated that the fib design model presented the weakest performance, while the best results were attained by the CNR-DT 200, which also provided the highest number of extremely conservative values (32%). Through the analysis of the database it was possible to observe that the aforementioned design models seemed to be not suited for application to low strength concrete beams. None of the design models explicitly consider the influence of the longitudinal reinforcement ρ_{sl} in the prediction of V_f, nevertheless the experimental results evidenced that such parameter should not be neglected. A clear reduction of the model performance was observed with the increase of stirrups percentage, since the interaction between conventional steel reinforcement and FRP strengthening systems is not considered by the models for the calculation of V_f. This evidence indicates that the influence of the existing steel transverse reinforcement should be explicitly considered in the analytical formulations.

2.7 Bond behavior of steel bar cast-in place and post-installed into concrete

The bond behavior of ETS installed bars is not deeply investigated since this is not a purpose of the presented work. However, it is possible to draw an analogy between the bond of ETS installed bars cast in steel bars / post installed steel bars / adhesive steel anchors, for which a large number of experimental programs have been carried out. The work done under the framework of FRP strengthening on the bond between concrete surface and FRP could be used for a better understanding the bond behavior of the ETS technique.

The resistant mechanisms upon which steel bars-to-concrete bond is based are well known, due to the large number of test results that have been performed in the last forty-fifty years by analyzing a wide variety of specimens and testing techniques. Lutz and Gergely (1967) concluded that the load transfer between concrete and steel occurs through the action of three mechanisms: chemical adhesion, friction and mechanical interlock of the ribs on the surrounding concrete in case of deformed bars. The bond resistance of plain bars relies on the chemical adhesion between concrete and bar surface, in this case even low stress can cause a sufficient slip to break the adhesion at the materials interface. Once slip occurs, further bond can be developed only by means of friction. For deformed reinforcement, which are characterized by a higher bond capacity, adhesion is generally negligible and mechanical interaction based on the mechanical interlock of the ribs with the surrounding concrete is the dominant resisting mechanism. Experimental data have evidenced that the mechanical interlock results in a wedge action of the ribs. This wedging action generate radial components of bond forces balanced against tensile rings in concrete (Tepfers 1973). When the confinement is sufficient to prevent the splitting of the

concrete cover the slip of the deformed bars and the successive pull-out failure is caused by the formation of new sliding plane around the bar shearing off the concrete corbels and the force transfer mechanisms changes form rib bearing into friction.

Different models describing the monotonic bond stress-slip behavior analytically were developed in the past, nevertheless most of them are similar to the bond model included in the Model Code 2010 (fib 2013), which is characterized by: i) A total bond strength given by the superposition of mechanical bond and frictional bond which increases until the ultimate bond stress $\tau = \tau_{max}$ is reached at the slip s_1. ii) a horizontal plateau between the slip value s_1 and s_2. iii) the ultimate frictional bond stress $\tau = \tau_f$. For monotonic loading, the bond stresses between concrete and reinforcing bar for pull-out and splitting failure can be calculated as a function of the relative displacements according to Eqs. (2.44) to (2.47) (see Fig. 2.40).

$$\tau_0 = \tau_{max} \left(s/s_1\right)^{\alpha} \quad \text{for } 0 \le s \le s_1 \tag{2.44}$$

$$\tau_0 = \tau_{max} \quad \text{for } s_1 \le s \le s_2 \tag{2.45}$$

$$\tau_0 = \tau_{max} \cdot \left(\tau_{max} - \tau_f\right) \cdot \left(s - s_2\right)/\left(s_3 - s_2\right) \quad \text{for } s_2 \le s \le s_3 \tag{2.46}$$

$$\tau_0 = \tau_f \quad \text{for } s_3 \le s \tag{2.47}$$

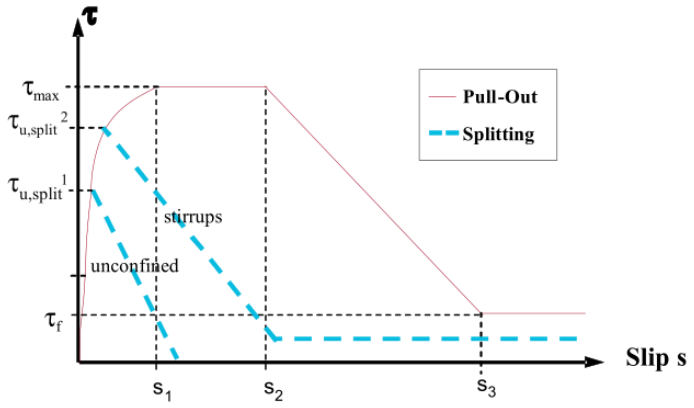

	1	2
	Pull-Out (PO)	
	$\varepsilon_s < \varepsilon_{s,y}$	
	Good bond cond.	All other bond cond.
τ_{max}	$2.5\sqrt{f_{ck}}$	$1.25\sqrt{f_{ck}}$
s_1	1.0mm	1.8mm
s_2	2.0mm	3.6mm
s_3	c_{clear} 1)	c_{clear} 1)
α	0.4	0.4
τ_f	$0.40\,\tau_{max}$	$0.40\,\tau_{max}$

Fig 2.40 Model Code 2010 (fib 2013) bond model.

The first curved part refers to the stage in which the ribs penetrate into the mortar matrix, characterized by local crushing and micro-cracking. The horizontal level occurs only for confined concrete, referring to advanced crushing and shearing off of the concrete between the ribs. This level represents a residual bond capacity, which is maintained by virtue of a large concrete cover or a minimum transverse reinforcement, keeping a certain degree of integrity intact. The decreasing branch refers to the reduction of bond resistance due to shearing of the concrete corbels between the ribs. In case of unconfined concrete, splitting failure occurs, which is reflected by a sudden drop of the bond strength before the horizontal level is reached. Depending on the failure mode, pull-out or splitting, different parameters is

applied. The bond stress-slip curve is considerably influenced by reinforcement yielding and by transverse pressure.

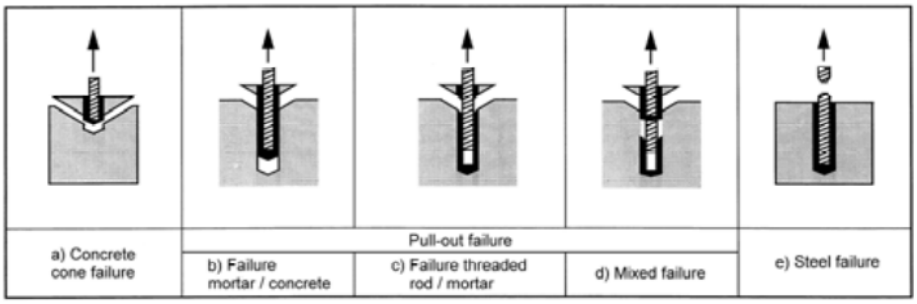

Fig. 2.41 Potential embedment failure modes of bonded anchors, (Cook et al. 2007; Cook et al. 1998)

Otherwise studies on bond of cast-in bars were a bond slip relationship is usually defined (e.g. Eligehausen et al. 1983) that allow the study of local and global behavior of the phenomenon, the study of epoxy adhesive anchors and post-installed rebars has been mostly focused on the calculation of the ultimate strength of the bonded system. Detailed information on the single adhesive anchor behavior is presented in Cook et al. (1998). Fig. 2.40 shows typical failure modes exhibited by bonded anchors and post installed bars. Due to the load-transfers and available bond strength, different failure modes can be observed. If bond strength is high enough to utilize the tension strength of the concrete, concrete failure will occur. This failure is characterized by cone-shaped concrete breakout originating at the base of the anchor (Fig. 2.41a). The slope of the cone envelope with the respect to the surface of the concrete member is approximately 25° to 35°. Normally, this failure mode can be observed at small embedment depth (h_{ef} ~ 3d-5d). For greater embedment depth, the failure mode shifts from a concrete cone to a mixed mode type of failure. A concrete cone with a depth of approximately 2d to 3d forms at the top end of the anchor, and bond failure occurs along the remaining length of the anchor. Bond failure occurs either at the boundary between threaded rod and mortar (Fig. 2.41c) or between the mortar and the sides of the drilled hole (Fig. 40b). Often a mixed interface failure can be observed (Fig. 2.41d). For large embedment depths steel failure can occur. The mechanism of load transfers is shown in Fig 2.42, a tension load is transferred by mechanical interlock from the threaded rod into the mortar and by adhesion and/or micro interlock (due to the roughness of the drilled hole) form the mortar into the concrete.

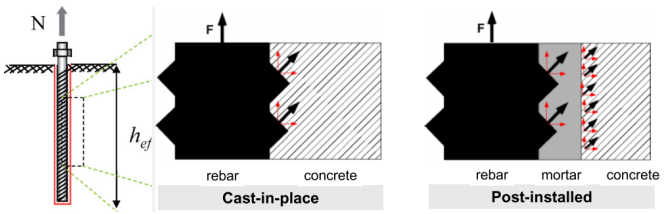

Fig. 2.42 – Mechanism of load transfers of bonded anchor (Eligehausen et al. 2004)

The actual bond stress distribution along the embedment length at peak load is nonlinear with lower bond stresses at the concrete surface and higher bond stresses at the embedded end of the anchor. In the elastic range, adhesive anchors which have been shown in Cook et al. (1993) exhibit a hyperbolic tangent stress distribution along the bonded anchor. In the case of adhesive anchors and post-installed rebars a large number of parameters can influence the performance of the system material: mortar (epoxy, cement, hybrid), cracks in concrete, bar diameter, drilling diameter in relation to bar diameter, embedment depth.

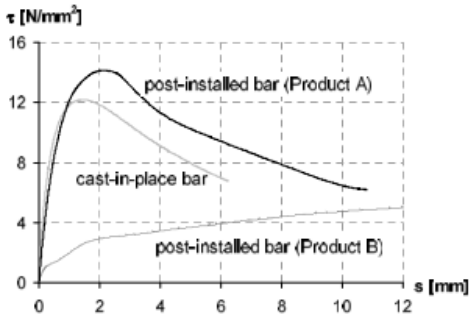

Fig. 2.43 Bond stress-displacement diagram for cast-in-place rebars and post installed rebars in monotonic loading. (Hofacker and Eligehausen 2001).

Hofacker and Eligenhausen (2001) showed that by using a proper adhesive, the post-installed rebars can exhibit a higher bond strength and more ductile behavior that cast-in-place bar (Fig.2.43). The bond stress-displacement curve of the cast in place rebars is similar to that of the post installed bar, which reached a 15% higher maximum bond stress (approximately 14MPa and slip 2.0 mm for post installed rebars) and the bond failure occurred in the interface between rebar and mortar. Also a second adhesive was tested and it exhibit a bond stress about 45% lower than for cast-in-rebars, and bond failure in the mortar /concrete interface.

Annex A presents available data in literature regarding some experimental bond test on steel or FRP bars bonded to a concrete prism with adhesive material. Most of the presented test were conducted within a research on ETS strengthening (Valerio et al. 2009; Dalfré et al. 2011; Godat et al. 2012), instead the work conducted by Owa et al. (2012) and Mahrenholtz (2012) were dedicated to bond performance of post-installed bars for seismic application, only the data relevant for this research have been reported in Annex A. These pull-out tests have shown that the bond behavior between bars and concrete depends on the type of adopted adhesive. A ductile bond-slip response can be provided if the type of adhesive and bar are properly chosen. The bond strength seemed marginally affected by the thickness of the adhesive layer. The test also show that for the same type of adhesive the average bond stress developed by steel and CFRP bars provided in general similar results.

3

Experimental tests on RC beams strengthened in shear using the Embedded Through-Section technique

3.1 Introduction

The Embedded Through-Section (ETS) technique is a promising technique for the shear strengthening of existing (RC) elements, as the experimental work presented in Chapter 2 have already evidenced (Valerio et al. 2009; Chaallal et al. 2011; Barros and Dalfré 2012). According to this technique, holes are drilled through the beam section, and bars of steel or FRP material are introduced into these holes and bonded to the concrete with adhesive materials. When concrete cover has not the bond and strength requisites to guarantee a strengthening effectiveness for the Externally Bonded and Near Surface Mounted techniques (see Chapter 2), ETS strategy can be a competitive alternative since it mobilizes the beam's concrete core which is, generally, free of damage. The present work aims to contribute to a deep understanding of the ETS shear strengthening mechanisms, and the susceptibility of these mechanisms to the interaction between ETS bars and existing steel stirrups. The ultimate purpose of this work is to provide useful data for the establishment of design guidelines on the shear strengthening of RC beams using the ETS technique. To explore the potentialities of the ETS technique for the shear strengthening, an experimental program was carried out, composed of quasi-scale real RC T-cross section beams shear strengthened by using steel and CFRP bars. The experimental program was conceived for assessing the influence on the ETS shear strengthening effectiveness of the percentage, inclination and material type of the ETS systems. To study the interaction between ETS bars and existing steel stirrups, three series of RC T-cross section beams with different percentage of internal transverse reinforcement (ρ_{sw}=0.0%, ρ_{sw}=0.1% and ρ_{sw}=0.17%) were tested. The effectiveness of the ETS technique is finally compared with EBR and NSM techniques. The experimental program is described in detail and the relevant results are presented and discussed. This experimental and

analytical research is a step forward on the already existing information on the use of ETS technique for the shear strengthening of RC elements.

3.2 Test program

Fig 3.1 presents the geometry and the reinforcement arrangements of the nineteen T cross section beams of the experimental program. The reinforcement system was designed according to the Eurocode 2 (European Committee for Standardization 2004), using an high percentage of longitudinal reinforcement (ρ_{sl}=2.79%) in order to force the occurrence of shear failure mode for all the beams of the experimental program. To localize shear failure in one of the beam's shear spans, a three point load configuration was selected, with a different length of the beam shear spans.

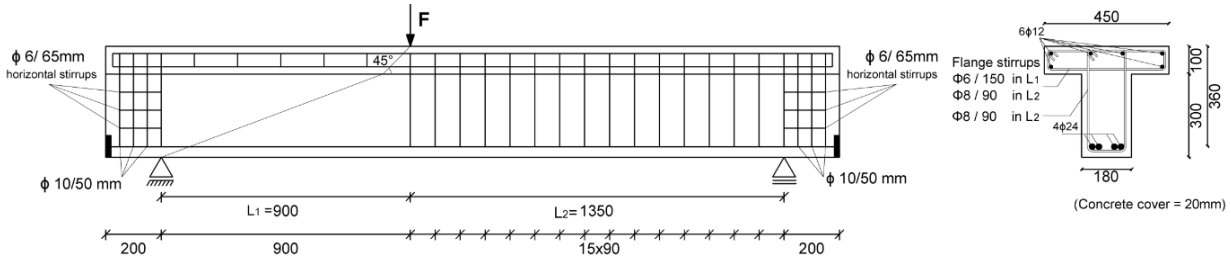

Fig. 3.1. Tested beams: geometry, steel reinforcements applied in all beams (dimensions in mm).

The monitored beam span (L_1 =0.9 m) was 2.5 times the effective depth of the beam's cross section (L_1/d =2.5), since according to the available research (Collins and Mitchell 1997), beyond this limit the arch effect is negligible. To avoid shear failure in the L_2 beam span, steel stirrups ϕ8@90 mm were applied in this span. Different shear reinforcement systems were applied in the L_1 beam's span of the tested beams. In fact, the experimental program consisted of the following three series of beams: 0S-Series that did not have conventional steel stirrups; 2S-Series that had steel stirrups ϕ6@300 mm, corresponding to a shear reinforcement ratio ρ_{sw} =0.10%, 4S-Series that had steel stirrups ϕ6@180 mm, corresponding to a shear reinforcement ratio ρ_{sw} =0.17%, where:

$$\rho_{sw} = \frac{A_{sw}}{b_w \, s_{sw}} \tag{3.1}$$

being A_{sw} the cross sectional area of the two legs of a steel stirrup, s_{sw} the spacing of the steel stirrups, and b_w =180 mm the width of the beam's web.

Each series had a reference beam without any strengthening system (Fig 3.1, Fig 3.2), and four beams with different ETS strengthening configurations (Fig 3.3). The investigated parameters are the shear strengthening ratio (ρ_{fw}) and the inclination (90°, 45°) of the ETS bars, as well as the influence of the percentage of existing steel stirrups. In particular, the shear strengthening ratio of the ETS steel bars and ETS CFRP rods was defined as follows:

$$\rho_{fw} = \frac{A_{fw}}{b_w \, s_{fw} \, \sin\beta_f} \tag{3.2}$$

where A_{fw} is the cross sectional area of ETS bar, s_{fw} and β_f represent the spacing and inclination of this bar, respectively.

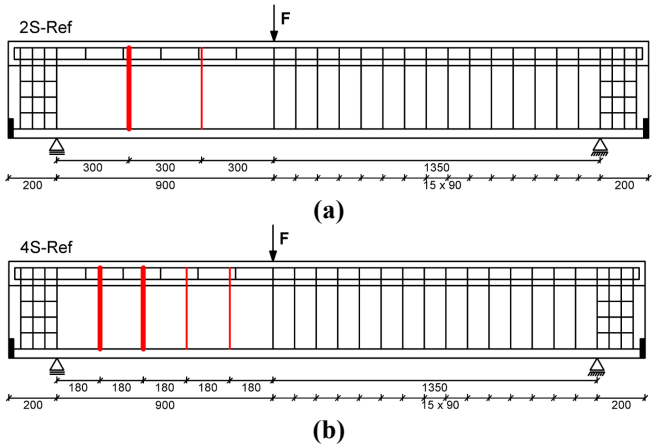

Fig. 3.2. Reference Beams: (a) 2S-Ref (stirrups ϕ6@300), (b) 4S-REF(stirrups ϕ6@180).

Table 3.1 ETS shear strengthening configurations of the tested beams.

Number of bars	Angle [θ_{fw}]	ETS bar spacing [s_{fw}]	ETS Reinforcing ratio [ρ_{fw}]	0S-Ref [c]		2S-Ref [d]		4S-Ref [e]	
d_{ETS}	[°][a]	(mm)	[%][b]	(ρ_{sw}=0.0%)	$\rho_{sw}+\rho_{fw}$ [%]	(ρ_{sw}=0.10%)	$\rho_{sw}+\rho_{fw}$ [%]	(ρ_{sw}=0.17%)	$\rho_{sw}+\rho_{fw}$ [%]
3	90	300	0.15	0S-S300-90	0.15	2S-S300-90	0.25	4S-S300-90	0.32
3	45	300	0.21	0S-S300-45	0.21	2S-S300-45	0.31	4S-S300-45	0.38
5	90	180	0.24	0S-S180-90	0.24	2S-S180-90	0.35	4S-S180-90	0.42
5	45	180	0.34	0S-S180-45	0.34	2S-S180-45	0.45	4S-S180-45	0.52
5	90	180	0.16	--	--	2S-C180-90	0.26	4S-C180-90	0.33
5	90	180	0.22	--	--	2S-C180-45	0.32	4S-C180-45	0.39

[a] Angle between the ETS bar and the beam's axis.
[b] The ETS percentage was obtained from Eq. 3.2.
[c] Series of beams without steel stirrups (0S-Series) (Fig. 3.1).
[d] Series of beams with two stirrups (2S-Series) (Fig. 3.2a).
[e] Series of beams with four stirrups (4S-Series) (Fig. 3.2b).

The influence of the material type of the ETS bars used for the strengthening was also investigated, by having beams strengthened with CFRP and steel bars in both 2S and 4S series of beams. The diameter

of the ETS steel and CFRP bars was 10 and 8 mm, respectively. A smaller diameter for the CFRP bar was chosen in order that the estimated force at the debonding of this bar was similar to the force at yield initiation of the steel bar. Based on previous experiences (Valerio et al. 2009; Chaallal et al. 2011; Barros and Dalfré 2012), it was considered for the strain at debonding of this type of CFRP bars a value in the interval 0.55-0.6%. In the design of the steel ETS configuration it was assumed that the ETS bars work like steel stirrup, and perfect bond for the bars/adhesive/concrete was considered. Table 1 indicates the designation adopted for each beam and the strengthening configurations, namely, the number of applied ETS bars, inclination, spacing, shear strengthening ratio (ρ_{fw}), as well as the percentage of steel stirrups (ρ_{sw}) and total shear reinforcement ($\rho_{sw}+\rho_{fw}$) calculated from Eq. 3.1 and Eq. 3.2. Fig. 3.3 shows the strengthening configurations of the tested series. As previously demonstrated by Barros and Dalfré (2012), the effectiveness of the ETS bars is higher if they are placed in between existing stirrups. Following this approach, the strengthening arrangements indicated in Table 3.1 and Fig. 3.3 were adopted, leading to four different ρ_{fw} values. The ETS strengthening ratio varied between 0.15% (ETS vertical bars spaced at 300 mm) and 0.34% (ETS bars at 45° and spaced at 180 mm). Two strengthening ratio values were adopted in the beams strengthened with ETS CFRP bars, ρ_{fw} = 0.16 (vertical bars spaced at 180 mm), and ρ_{fw}=0.22 (bars at 45° spaced at 180 mm).

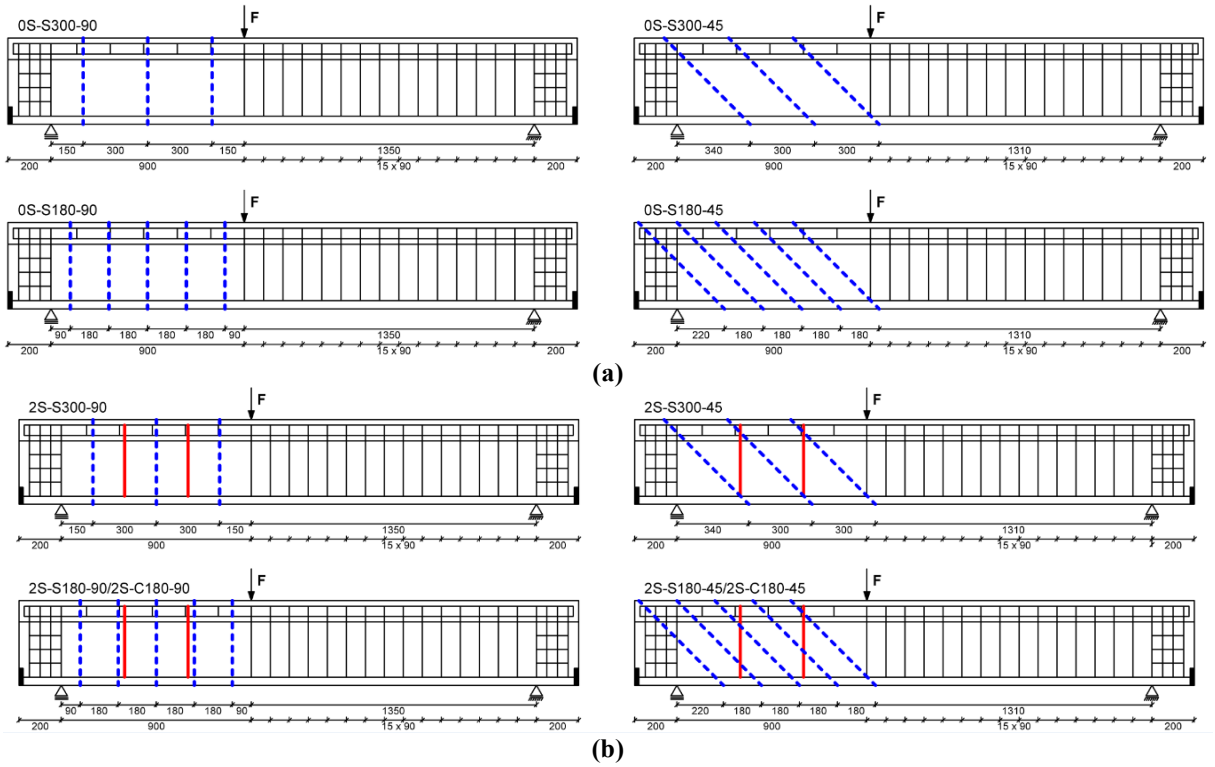

(a)

(b)

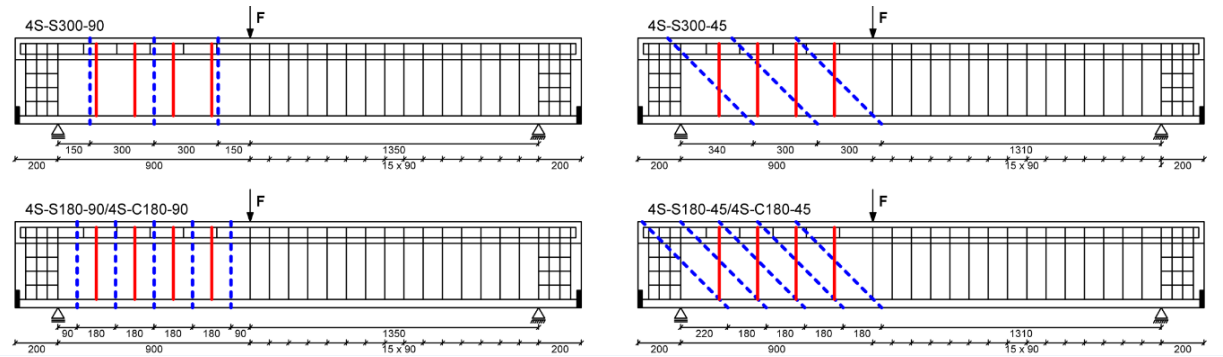

(c)

Fig. 3.3. Strengthening configurations of series: (a) 0S, (b) 2S; (c) 4S (dimensions in mm).

3.3 Material characterization

The concrete average compressive strength (f_{cm}) of the beams was evaluated at 28 days and at the age of the beams' test, by carrying out direct compression tests on cylinder specimens of 150 mm diameter and 300 mm height according to EN 206-1 (2004) (European Committee for Standardization 2001). It was obtained an average compressive strength, f_{cm}, equal to 24.7 and 29.7 MPa at 28 days and at the day of the test (approximately 255 days), respectively, for the first batch (0S-Series and 2S-Series) and 27.6 and 32.3 MPa, at 28 days and at the day of the test (approximately 250 days) for the second batch (4S-Series and CFRP ETS strengthened beams), respectively. For the internal reinforcement of the beams, high bond steel bars of 6, 10, 8, 12, and 24 mm diameter were used. The steel class is B 450 C (f_{yk} =450MPa) according to the Italian Construction Code. (C.S.L.P 2009). The yield stress and tensile strength were obtained by means of uniaxial tensile tests performed according to recommendations of UNI EN ISO 6892-1:2009 (European Committee for Standardization 2009). For the steel bars of 6, 8, 10, 12 and 24 mm diameter it was obtained an average yield stress of 574 (ε_{sy}= 0.287%), 505 (ε_{sy}=0.253%), 549 (ε_{sy}= 0.275%), 527 (ε_{sy}= 0.264%) and 598 (ε_{sy}= 0.299%) MPa, and an average tensile strength of 667, 594, 642, 617 and 708 MPa, respectively. The adopted ETS steel bars were of the same class of the bars used for the flexural reinforcement and steel stirrups applied in the beams. To bond the ETS steel bars to the concrete substrate the Sikadur 32 N epoxy based adhesive was used. The tensile behavior of this adhesive was characterized by carrying out direct tensile tests according to the ISO 527-2 (European Committee for Standardization 2012), having been obtained an average tensile strength of 20.7 MPa and an elasticity modulus of 3.27 GPa. The pultruded carbon fiber sandblasted 8mm rod, MasterBrace BAR 8 CFS (Basf -Technical sheet 2014), has an elasticity modulus of 160 GPa and an ultimate strain of 1.2 %. The material properties are summarized in Table 3.2

Table 3.2 Material properties of the tested beams.

Concrete	**f_{cm}** (at 28 days)	**f_{cm}(** day of the tests)
0S and 2S-Series	24.7	29.7 (255 days)
4S-Series and CFRP strengthened beams	27.6	32.3 MPa (250 days)
Steel		
Young modulus (≈ 200 GPa)	**Yield stress f_y** [MPa]	**Tensile strength f_t** [MPa]
6	573.94	666.67
8	505.35	549.11
10	549.35	641.83
12	527.35	616.48
24	597.88	708.07
CFRP bars	**Young modulus**	**Ultimate strain**
	160 GPa	1.2%
Epoxy resin	**Young modulus**	**Tensile strength**
Ultimate strain>50(%)	3.1 GPa	f_{epox} = 20.1 [MPa]

3.4. Strengthening technique

To simplify the drilling process and to avoid intersecting the longitudinal bars, the ETS strengthening process was executed with the beam's web turned upward. The main steps of the ETS strengthening technique are shown in Fig. 3.4. These steps are: (1) holes of 16 mm diameter for ETS steel bars, and holes of 14 mm of the ETS CFRP bars were drilled through the center of the beams' web up to a depth of 20 mm from the top flange in order to maintain intact the concrete cover and avoid adhesive to flow through the bottom part of the hole (Fig. 3.4a and 3.4b); during the drilling process, the concrete dust was aspirated using a vacuum system; (2) the holes were cleaned by using an helicoidal steel brush capable of removing the particles from the walls of the hole, which were not eliminated by the vacuum system (Fig. 3.4c). The cleaning procedure was repeated until the dust was completely removed; (3) the epoxy resin, which was prepared according to the recommendations of the supplier, was slowly poured into the holes; (4) the steel bars, which were previously cut in the desired length and cleaned with acetone, were slowly introduced into the holes removing the resin in excess (Fig. 3.4d). To guarantee a proper curing of the adhesive, the beams were tested at least two weeks after the ETS application.

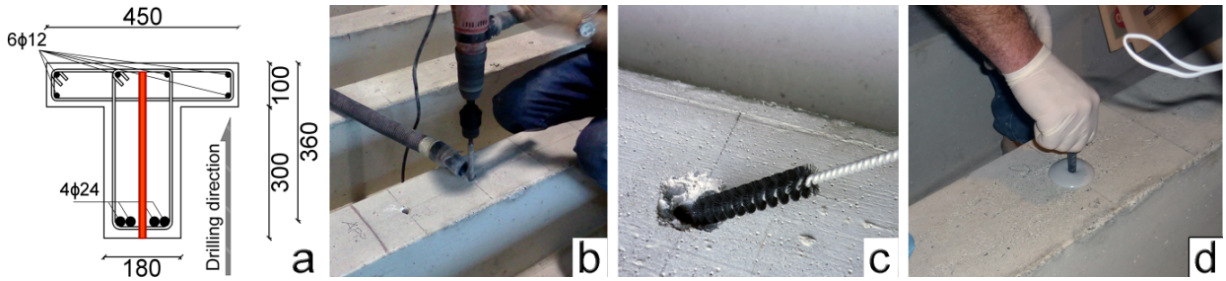

Fig.3.4. Strengthening procedures for the ETS technique.

3.5 Test setup and monitoring system

Fig. 3.5 shows the position of the displacement transducers (LVDTs) and force transducers used for measuring the beam's deflection and applied/reaction forces, respectively. The LVDTs were supported in a bar fixed at the beams supports' sections in order to register displacements only caused by the deflection of the beam. The displacement transducer TR1 was used to control the tests at a displacement rate of 10 μm/s up to the failure of the beams. The beams were loaded under three-point bending configuration with a shear span of 900 mm. The applied load (F) was measured using a force transducer of ±750 kN capacity and accuracy of ±0.1%. A second force transducer of ±500 kN capacity and 0.1% accuracy was under the support corresponding to the longer span (L_2) to complement the information for a full assessment of the shear force in each span of the beam. To obtain the strain variation in steel stirrups and ETS bars, electrical strain gauges (SGs) were bonded on selected cross sections of stirrups and ETS bars that have the highest probability of providing the largest contribution for the shear strengthening of the RC beam. Eight and five SGs for each beam of series without stirrups (0S-Series) and beam with stirrups (2S and 4S Series), respectively, were installed on ETS bars according to the configuration represented in Figs 3.6a and 3.6b. In ETS CFRP strengthened beams, six SGs were installed on a CFRP bar, and two SGs were applied on an internal steel stirrups. The monitoring SGs system in CFRP strengthened beams was slightly different of the one adopted in the steel strengthened beams, and the position of the SGs is indicated in Fig3.6c. In the present study a close-range photogrammetric technique was used to determine the displacement of a range of points on the beams surface at selected load levels up to and after failure. The aim of the photogrammetric measurements was to observe the crack crack pattern evolution.

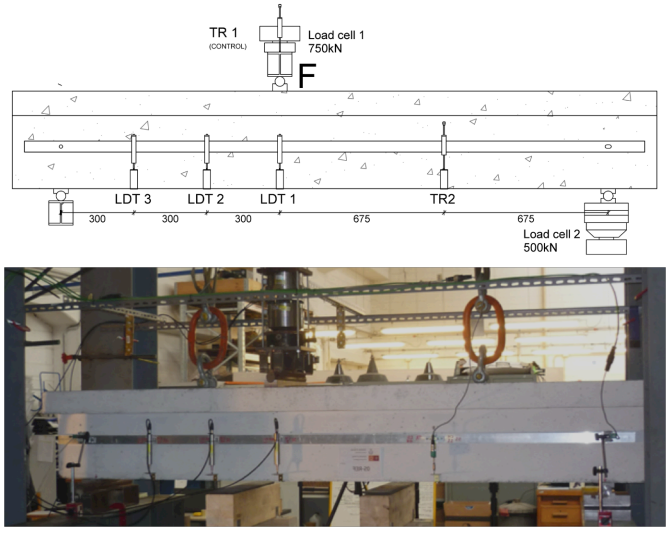

Fig. 3.5. Test set-up.

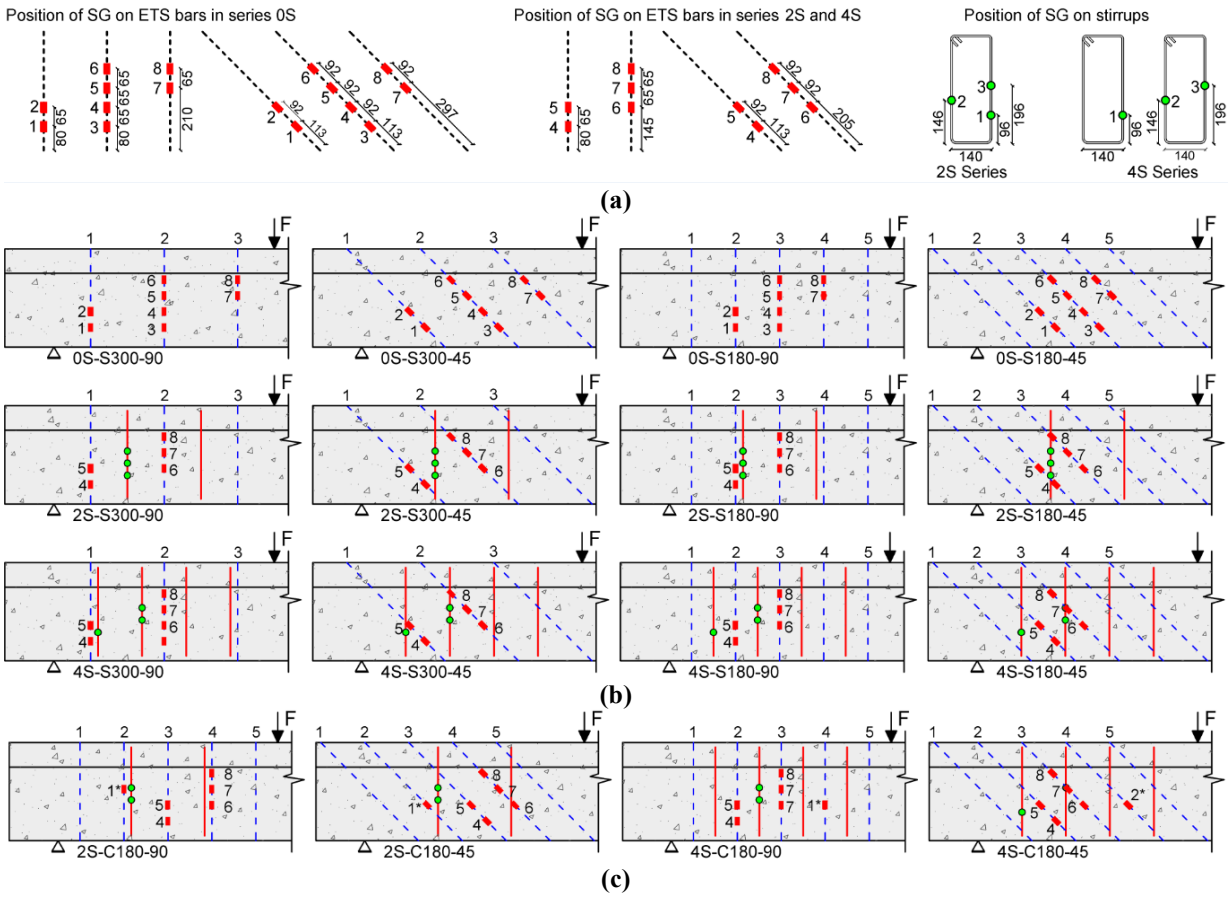

Fig. 3.6. Position of the strain gauges (dimensions in mm), (a) position of the SG on the ETS bars and stirrups, (b) monitored steel ETS strengthening bar (c) monitored CFRP strengthening bar.

3.6 Steel ETS strengthened beams

3.6.1 Load carrying capacity of the tested beams

The load (F)- deflection (u_L) diagrams are presented in Figs 3.7 to 3.9 for 0S Series, 2S Series and 4S Series strengthened with steel ETS bars. All the beams showed the same behavior up to the formation of the first diagonal crack, that has formed at an approximate load of 113 kN (u_L=0.98mm), 100 kN (u_L=0.91mm) and 135 kN (u_L=1.37mm) in case of the reference beams 0S-Ref, 2S-Ref and 4S-Ref, respectively. Fig. 3.10 shows the failure crack patterns at maximum load obtained for all the tested beams. As already observed in beams that have been strengthened in shear with carbon fiber reinforced polymer (CFRP) laminates, installed according to the NSM technique (Dias and Barros 2010), the stiffness degradation of the ETS strengthened beams is generally smaller than that of the reference beams. The ETS steel bars offered resistance to crack opening and sliding by bridging the shear cracks

and enhancing concrete's contribution to the shear resistance due to the aggregate interlock effect, which leads a higher load carrying capacity after shear crack initiation. The ETS strengthening technique increased significantly the maximum load carrying capacity and ultimate deflection capacities of the beams, whose performance level depends on the shear reinforcement/strengthening arrangement. All the beams exhibited a shear failure mode, since a quite high flexural reinforcement was adopted in order to avoid flexural failure mode.

Table 3.3 Experimental results of 0S-Series, 2S-Series and 4S-Series strengthened with steel bars.

	$F_{\max}$	$u_{L\max}$	$\Delta F/F_{Ref}$	$V_{\max}$	$V_f^{\exp}$	$CDC_{tang.}$	$CDC_{avg.}$
	[kN]	[mm]	[%]	[kN]	[kN]	[°]	[°]
0S-Ref	156.1	4.66	--	93.6	--	34	39
0S-S300-90	217.8	4.37	39.5	130.7	37.0	48	42
0S-S300-45	348.6		123.4	209.2	115.5	58	47
0S-S180-90	256.8	4.31	64.6	154.1	60.5	63	44
0S-S180-45	368.8	6.56	136.3	221.3	127.7	35	43
2S-Ref	242.1	4.70	--	145.2	--	45	39
2S-S300-90	315.7	5.32	30.4	189.4	44.2	58	42
2S-S300-45	407.1	7.03	68.2	244.3	99.0	48	39
2S-S180-90	406.8	8.27	68.1	244.1	98.8	73	47
2S-S180-45	504.7	8.37	108.5	302.8	157.6	70	49
4S-Ref	353.8	7.35	--	212.3	--	48	40
4S-S300-90	370.9	7.43	4.8	222.6	10.3	32	46
4S-S300-45	552.4	12.03	56.1	331.5	119.2	61	54
4S-S180-90	413.2	6.32	16.8	247.9	35.6	52	54
4S-S180-45	566.4	11.01	60.1	339.8	127.6	53	40

The main results of the experimental tests are presented in Table 3.3, where $F_{\max}$ is the maximum load attained by the beams and $u_{L\max}$ is the displacement in the loaded section at $F_{\max}$. The strengthening efficiency of the ETS technique can be evaluated by considering the $\Delta F/F_{Ref}$ ratio, where F_{Ref} is the maximum load of the reference beam, and $\Delta F = F_{max} - F_{Ref}$ is the increase of maximum load provided by each ETS arrangement. The Table 2 also includes the maximum shear force $V_{\max} = 0.6 \cdot F_{\max}$ applied in the L_1 beam's span (Fig. 1) and the resisting shear force provided by the ETS arrangement, $V_f^{\exp}$. This last term was determined by considering the shear resistance in the 0S-Ref, 2S-Ref and 4S-Ref reference beams, by assuming as valid the principle that the shear resistance of a beam reinforced with steel stirrups and strengthened with ETS bars is the addition of the contributions of the concrete, steel stirrups and ETS bars. The last two columns in this table include, respectively, the tangent (CDC_{tang}) and the average (CDC_{avg}) inclination of the failure shear crack (CDC), whose evaluation process is schematically represented in Fig. 3.10, for 0S-Ref beam. For the evaluation of the CDC_{tang}, an auxiliary

horizontal line at half distance from the longitudinal reinforcement to the bottom surface of the beam's flange (d_1 represented in 0S-Ref beam in Fig. 3.10) was introduced; then the point of its interception with the CDC was determined. The CDC_{tang} is the inclination of the CDC at this point of interception. The CDC_{avg} is determined by connecting the points of the interception of the CDC with the bottom surface of the beam's flange and the longitudinal reinforcement. According to the obtained results, the CDC_{tang} was usually higher than(CDC_{avg}. The values of CDC_{tan} have ranged from 32° to 73°. By considering all the tested beams, an average value of CDC_{avg} = 44° was obtained. It is possible to notice that the beams with the highest percentage of shear reinforcement ($\rho_{sw}+\rho_{fw}$) and the CFRP strengthened beams exhibited higher inclinations of the CDC_{avg}. Beam 2S-S180-90 presented high inclinations of critical diagonal crack, probably due to the less evenly distributed of the shear reinforcements.

Fig. 3.10 clearly shows that the number of diagonal cracks increased with the percentage of transverse steel reinforcement. The cracks started due to flexural effect achieved by crossing almost orthogonally the flexural reinforcement; however due to the tension stiffening effect the cracks' width remained of minor dimension. During the loading process of the beams, some of these cracks propagated toward the bottom surface of the flange with the average and tangent inclinations reported previously; meanwhile a diffuse pattern of shear cracks of very small inclination formed due to this reinforcement's high dowel resistance.

The load vs. deflection relationship of the beams of 0S-Series is indicated in Fig. 3.7. This series is characterized by the absence of stirrups in the strengthened shear span (ρ_{sw} = 0.0%). The load-displacement relationship of the reference beam (0S-Ref) presented two peaks. The first peak, corresponding to the load level of F =139.2 kN (u_L =1.92mm), occurred when the main shear crack in the beam's web was formed; it was followed by a small decay. This shear crack then progressed at the interface web/flange of the beam and through the web, with an increase of the load carrying capacity up to $F_{\max}$=156.1 kN ($u_{L\max}$=4.66 mm) before completely crossing the web, with an abrupt failure.

Due to the detrimental interaction effect between existing steel stirrups and strengthened systems in the context of the shear strengthening effectiveness (Dias and Barros 2013), the beams of this series presented the highest strengthening efficiency amongst the tested series, with an increase of load carrying capacity that ranged from 40% to 136%. For the ETS vertical bars, the beams with the lowest percentage of ETS bars, ρ_{fw}= 0.15% (0S-S300-90), and with the highest $\rho_{fw=}$ 0.24% (0S-S180-90) presented an increase of load carrying capacity of 39.5% ($F_{\max}$= 217.8 kN; $u_{L\max}$ = 4.37 mm) and 64.6% ($F_{\max}$= 256.8 kN; $u_{L\max}$= 4.31 mm), respectively. The highest increase of load carrying capacity was obtained in the beams with ETS bars inclined at 45°. In fact the beam with the lowest ρ_{fw}

= 0.24% (0S-S300-45) and with the highest ρ_{fw} = 0.34% (0S-S180-45) presented an increase of load carrying capacity of 123.4% (F_{max}=348.6 kN) and of 136.3% (F_{max}= 368.8 kN; $u_{L\,max}$ =6.56 mm), respectively. This indicates that the inclination of the ETS bars seems to have a higher contribution for the strengthening effectiveness that the spacing of these bars, as long as this distance assures that a CDC is crossed by an effective ETS bar (with an enough bond length to avoid premature debonding), which is in agreement with the tendency observed in the NSM technique (Dias and Barros 2013).

Beam 0S-S300-45 exhibits slightly lower force-deflection stiffness than the other beams of 0S-Series. This beam was subjected to preliminary load cycles to overcome some test setup inaccuracies, which had partially pre-cracked this beam, leading to a reduction of initial stiffness of about 15%.

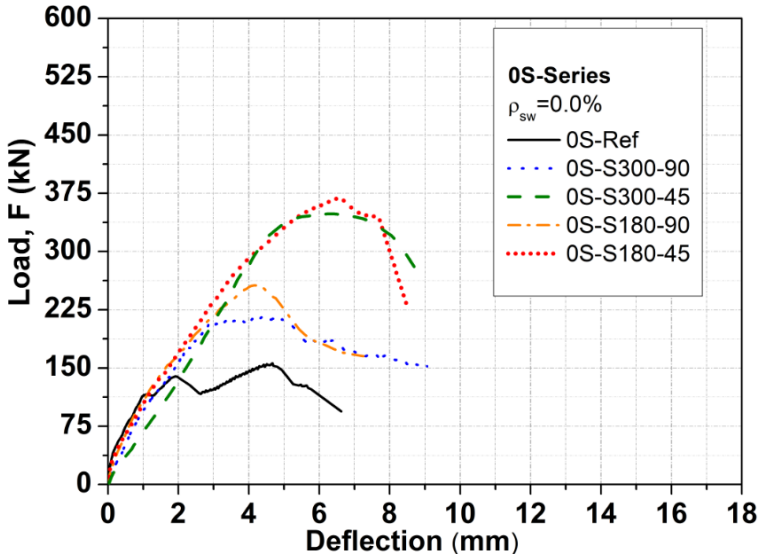

Fig. 3.7 Force vs deflection at the loaded seciton for 0S-Series.

The load vs. deflection relationship of the beams of 2S-Series is depicted in Fig. 3.8. This series is shear reinforced with 2-arms ϕ6mm steel stirrups @300 mm (ρ_{sw} = 0.10%). For the ETS vertical bars, the beams with the lowest percentage of ETS bars, ρ_{fw} = 0.15% (2S-S300-90), and with the highest percentage, ρ_{fw} = 0.24% (2S-S180-90), have presented an increase of load carrying capacity of 30.4% (F_{max}= 315.7 kN; $u_{L\,max}$ =5.32 mm) and 68.1% (F_{max}= 406.8 kN; $u_{L\,max}$=8.27 mm), respectively. Like already occurred in the beams of the 0S-Series, in the 2S-Series the highest strengthening effectiveness has occurred in the beams with ETS bars inclined at 45°. In fact, the beam with the lowest percentage, ρ_{fw} = 0.24% (0S-S300-45), and with the highest percentage, ρ_{fw} = 0.34% (2S-S180-45), presented an increase of the load beam carrying capacity of 68.2% (F_{max} =407.1 kN; $u_{L\,max}$= 7.03 mm) and 108.5% (F_{max}= 504.7 kN; $u_{L\,max}$ =8.37 mm), respectively.

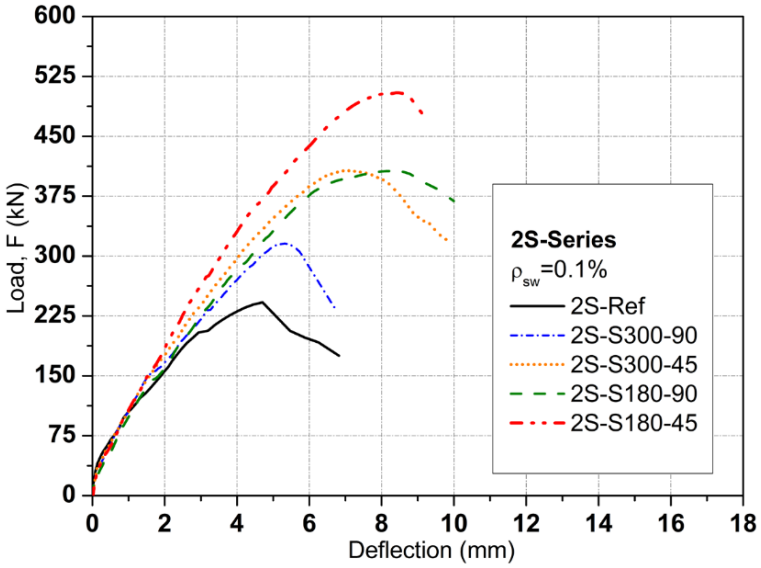

Fig. 3.8 Force vs deflection at the loaded seciton for 2S-Series.

The load vs. deflection relationship of the beams of the 4S-Series is illustrated in Fig. 3.9. This series is shear reinforced with 2-arms ϕ6mm existing steel stirrups @180 mm (ρ_{sw} = 0.17%). For the ETS vertical bars, the beams with the lowest percentage of ETS bars, ρ_{fw} = 0.15% (4S-S300-90), and with the highest percentage, ρ_{fw} = 0.24% (4S-S180-90), presented an increase of load carrying capacity of 4.8% (F_{max} = 370.9 kN; $u_{L\,max}$ = 7.43mm) and 16.8% (F_{max} = 413.2 kN; $u_{L\,max}$ = 6.32mm), respectively. The decrease of the shear strengthening effectiveness with the increase of existing shear reinforcement is quite evident, and will be discussed in more detail in Section 3.7. Furthermore, for configuration 4S-S300-90 a V_f^{exp} of 10.3 kN indicates that the contribution provided by the only ETS bar crossed by the shear crack was low, due to its small resisting bond length (Fig 3.10). The results of this beam showed the importance of the adopted strengthening geometry, revealing that strengthen elements should be placed in between stirrups (Barros and Dalfré 2012; Chaallal and Mofidi 2011). For the beams with ETS bar inclined at 45° a higher increase of load carrying capacity was obtained. In fact, the beams with the lowest percentage of ETS bars, ρ_{fw} = 0.24% (4S-S300-45), and with the highest percentage, ρ_{fw} = 0.34% (4S-S180-45), presented an increase of load carrying capacity of 56.1% (F_{max} =552.4 kN; $u_{L\,max}$ = 12.03 mm) and 60.1% (F_{max} = 566.4kN; $u_{L\,max}$ =11.01mm), respectively. These results indicate that by increasing the percentage of existing steel stirrups, the influence of the inclination of the ETS bars in terms of shear strengthening effectiveness becomes larger, while the influence of the spacing of ETS bars becomes smaller.

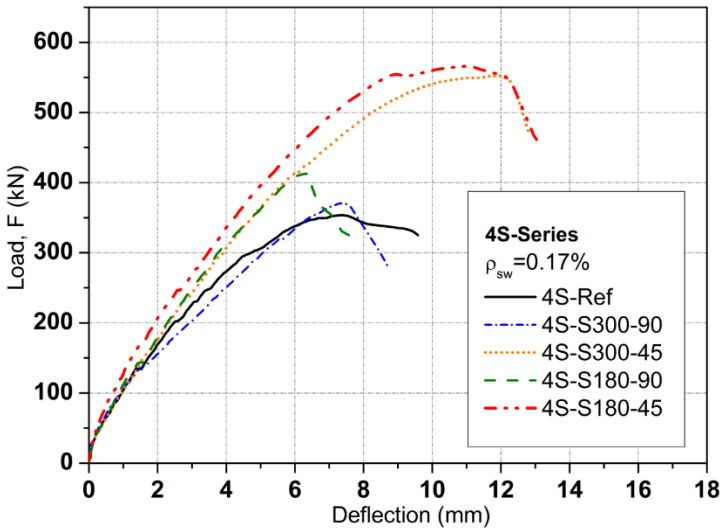

Fig. 3.9 Force vs deflection at the loaded seciton for 4S-Series.

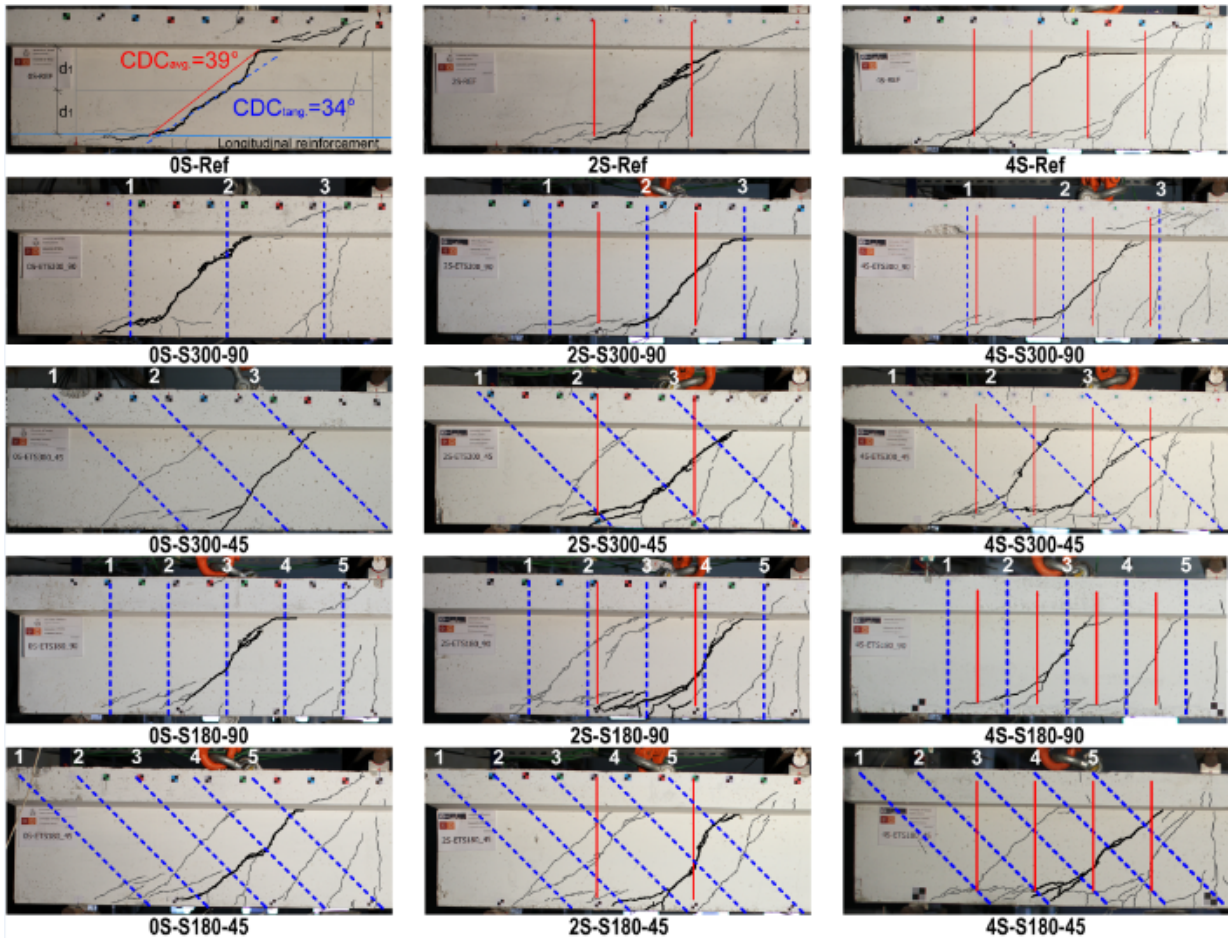

Fig. 3.10 Crack Patterns at Maximum Load.

Fig. 3.11a presents the influence of the inclination and percentage of ETS bars on strengthening efficacy. This is evaluated by considering the $\Delta F/F_{Ref}$ ratio. This figure clearly shows that the ETS

effectiveness is higher when inclined ETS bars are used. For series 0S, and in terms of $\Delta F/F_{Ref}$, the inclined ETS bars were 3.1 and 2.1 times more effective than vertical bars spaced at 300 and 180mm, respectively; this difference increased for 4S-Series up to 11.7 and 3.6 for bars spaced at 300 and 180mm, respectively. This graph also demonstrates that the ETS strengthening efficacy increase by reducing the spacing of the ETS bars, but the effectiveness of using inclined bars is much higher than increasing the percentage of ETS vertical bars. Fig 3.11b represent the influence of the existing stirrups spacing on the ETS strengthening efficacy, showing the important role of the percentage of transverse reinforcement on the ETS effectiveness. A comprehensive discussion of the investigated parameter during the tests is presented in section 3.7 analyzing the strengthening effectiveness in terms of ρ_{sw} and ρ_{fw}, and taking into account the results obtained with CFRP strengthened beams (Section 3.6).

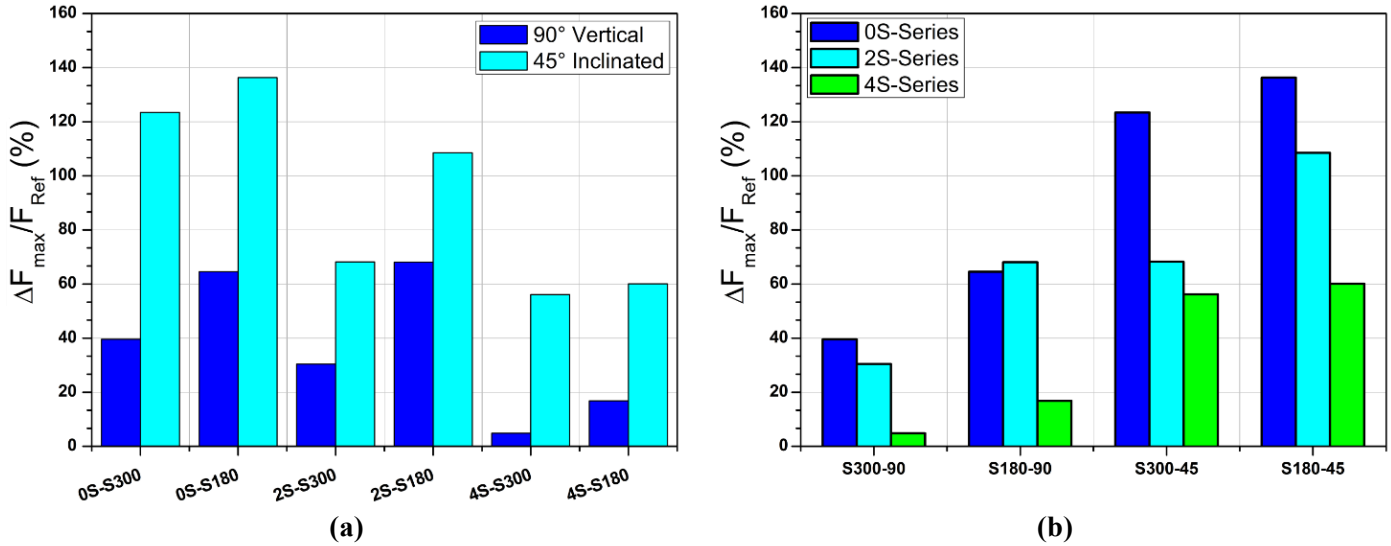

Fig 3.11 Influence of the inclination and percentage of ETS bars (a) and influence of transverse reinforcement (b)

3.6.2 Strains in the ETS bars/rod and steel stirrups

The relationships between the force applied in the beams and the strains registered in the most representative SGs installed in the monitored ETS bars and stirrups are shown in Fig. 3.12, while in Table 3.4 are included the relevant results. In this table, $\varepsilon_{F\max}$ is the strain measured at $F_{\max}$; and $\varepsilon_{\max}$ is the maximum strain recorded in the ETS bars. For this last parameter the value of the $u_L/u_{L\max}$ ratio is also provided in order to indicate if $\varepsilon_{\max}$ occurred in the pre- ($u_L/u_{L\max}$ <1) or post-peak ($u_L/u_{L\max}$ >1) phase of the beam's response. The evaluation of the yield strain, ε_{sy} took into account the yield strain values determined experimentally in coupons of ϕ6 stirrups and ϕ10 steel ETS bars, respectively, ε_{sy}

=0.287% and ε_{sy} =0.275%. In Table 3.4 the designation attributed to the strain gauges (second column), and ETS bars and steel stirrups (third column, where St stands for stirrups and S for ETS steel bar) are represented in Figs. 3.6 and 3.12 in order to highlight the relative position between the SGs and the shear cracks, and to help a better interpretation of the obtained results. The yield initiation process was reflected in the propagation of the crack pattern; the recorded strain values are in fact quite dependent on the distance between the SG and the shear failure crack and on the available bond length of the element they are installed. This effect is quite visible in beams strengthened with vertical ETS bars, in which relatively high strain values have been measured in zones of the ETS bars crossed by a shear crack and sufficient bond length (Figs 3.12a,b,e and h). For instance, large strains at F_{max} have been recorded in SG No.4 of the 0S-S180-90 beam (0.59% at F_{max}) (Fig. 3.12b), SG No.7 for the 4S-S180-90 (ε=88% at F_{max}) (Fig. 3.12h). In the vertical ETS bars the yield strain was usually attained in the elements that crossed the CDC at half of the beam's height (Beam 0S-S180-90, Fig.4) since in this case the available bond length was adequate. The largest strain value was recorded in the SG4 of the 0S-S180-90 beam (ε_{max} =1.06%) because this SG was installed in a zone of the ETS bar crossed by the shear failure crack (Fig. 3.12b). If the available bond length is relatively small, the steel bars cannot attain the yield strain due to slip occurrence, as was the case of SG No.1 of the 0S-S180-90 (ε= 0.16% at F_{max}). (Fig. 3.12a) and SG No.4 of the 4S-S180-90 beam (ε=0.04% at F_{max}) (Fig 3.12h).

Higher strains have been recorded in inclined ETS steel bars, thanks to the adopted strengthening configuration that provided longer force transfer length and favorable orientation of the ETS bars in respect to the crack's inclination, leading consequently to a better mobilization of the bars' reinforcement capacity. It was verified that steel ETS bars have reached the yield strain in the sections where they were crossed by the critical shear crack and also by a secondary diagonal crack, as occurred in the beams 0S-S300-45, 0S-S180-45, 2S-S300-45, 2S-S180-45, 4S-S300-45, and 4S-S180-45. In some of the tested beams, the excellent bond conditions provided by the concrete core allowed the steel yield strain to be exceeded in more than one section of the same ETS bar crossing shear cracks, such was the case, for instance, 4S-S300-45 beam (Fig.3.12i) with ε=0.91% in SG No.6 at 0.75 u_L/u_{Lmax} and ε=0.90% in SG No.8 at 0.82 u_L/u_{Lmax}). By using inclined bars, strain values higher than 0.8% have been usually recorded in at least one of the ETS steel bars after the maximum load reached its peak. The higher number of cracks is a consequence of the higher percentage of the ETS strengthening ratio and the larger effective bond length (in case of inclined ETS bars) that can mobilizes simultaneously bond and concrete resisting fracture mechanisms (Bianco et al. 2010). The maximum strain of ε=0.66% at F_{max} for inclined steel ETS bars was measured in the SG No.5 of beam 2S-S180-45. I can also be

observed that the using inclined ETS bars steel yielding occurred in general at a lower force F compared with vertical ETS installed bars.

Steel stirrups showed a trend in terms of strain variation similar to the ETS bars, attaining relatively high strains in the sections crossed by a diagonal crack, as was the case of SG No.3 in beam 4S-S300-45 (ε=0.89% at 0.68 u_L/u_{Lmax}), or SG No.3 for beam in 2S-S180-90 where a maximum strain of 1% was obtained because this SG was quite close to the section of the steel stirrup crossed by a shear crack (Fig. 3.12e). Moreover, the excellent anchorage conditions provided by the closed configuration of the stirrups, as well as its smaller diameter (when compared to the ETS steel bars diameter), have assured the attainment of the yield strain in several sections monitored with SG, also in stirrups crossed by secondary shear crack as for example beam 2S-S180-90 (Fig 3.12e). In some of the beams, the steel stirrups have even attained its rupture (2S-S300-45, 4S-S180-90).

Table 3.4 Relevant data in terms of strains measured in 0S-2S and 4S-Series, strengthened with steel ETS bars

Beam ID |	SG	Elem.	$\varepsilon_{F\max}$ [%]	$\varepsilon_{\max}$ [%] ($u_L/u_{L\max}$)	Beam ID |	SG	Elem.	$\varepsilon_{F\max}$ [%]	$\varepsilon_{\max}$ [%] ($u_L/u_{L\max}$)
0S-S300-90	1	S1	0.06	0.08 (0.72)	2S-S180-90	3	St1	--	1.00 (0.83)
	5	S2	0.22	0.27 (2.06)		5	S2	0.13	0.14 (1.32)
	6	S2	--	0.29 (0.66)		8	S3	0.20	0.20 (1.00)
	8	S3	0.01	0.27 (2.07)	2S-S180-45	2	St1	0.42	0.56 (1.13)
0S-S300-45	2	S1	0.26	0.29 (1.18)		4	S2	0.13	0.15 (0.78)
	3	S2	--	0.92 (0.62)		5	S2	0.30	0.31 (1.07)
	6	S2	0.27	0.27 (1.00)		7	S3	0.21	0.22 (1.00)
	8	S3	--	0.87 (0.99)		8	S3	0.29	0.31 (1.11)
0S-S180-90	1	S2	0.16	0.17 (1.03)	4S-Ref	1	St1	0.47	0.47 (1.00)
	4	S3	0.59	1.06 (2.23)		2	St2	0.75	0.86 (0.50)
	5	S3	0.28	0.29 (0.99)	4S-S300-90	6	S2	0.16	0.16 (1.00)
	8	S4	0.05	0.05 (1.00)	4S-S300-45	1	St1	0.25	0.31 (1.10)
0S-S180-45	2	S2	0.18	0.19 (0.59)		3	St2	--	0.89 (0.69)
	3	S3	0.46	0.48 (1.03)		4	S1	--	0.38 (0.82)
	5	S3	--	0.26 (0.81)		6	S2	--	0.91 (0.75)
	7	S4	--	0.64 (0.89)		8	S2	--	0.90 (0.82)
	8	S4	0.27	0.36 (1.29)	4S-S180-90	2	St2	0.26	0.38 (1.06)
2S-Ref	1	St1	0.17	0.21 (1.49)		4	S2	0.04	0.05 (1.05)
2S-300-90	1	St1	0.14	0.19 (1.26)		7	S3	0.88	1.00 (1.02)
2S-S300-45	3	St1	0.30	0.95 (1.07)	4S-S180-45	1	St1	0.41	0.48 (1.18)
	4	S1	0.15	0.18 (1.24)		3	St2	--	0.96 (0.92)
	5	S1	0.16	0.73 (1.14)		5	S2	0.66	0.82 (1.20)
	6	S2	0.59	0.84 (0.63)		8	S3	0.26	0.27(1.20)
	8	S2	0.30	0.92 (1.06)					

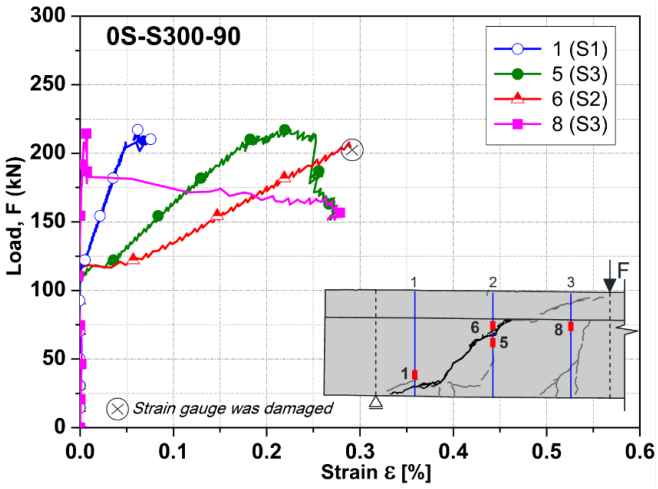
0S-S300-90
1 (S1)
5 (S3)
6 (S2)
8 (S3)
Strain gauge was damaged
Load, F (kN)
Strain ε [%]
F

(a)

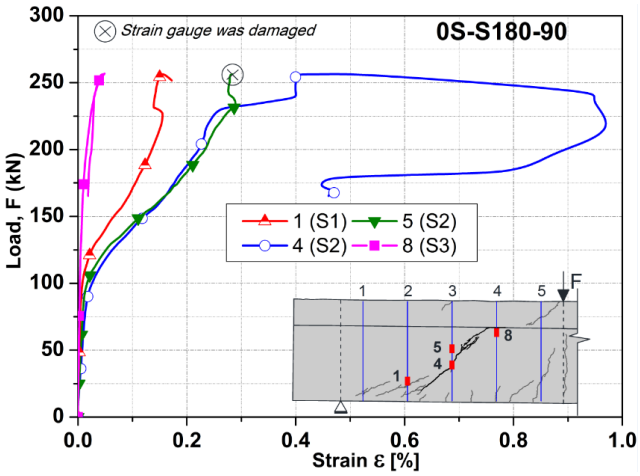
Strain gauge was damaged
0S-S180-90
1 (S1)
5 (S2)
4 (S2)
8 (S3)
Load, F (kN)
Strain ε [%]
F

(b)

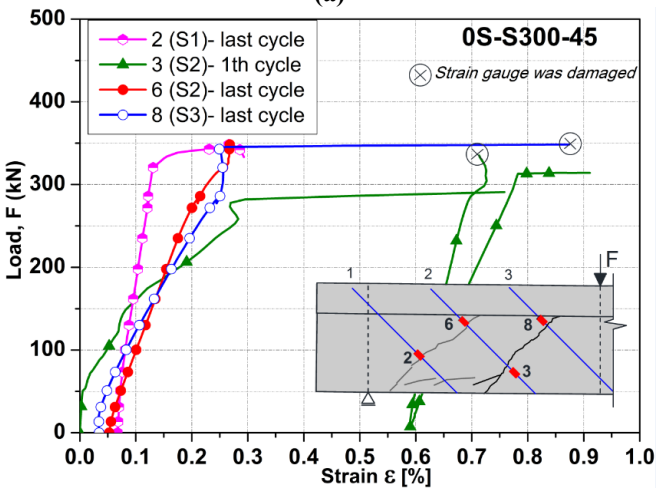
2 (S1)- last cycle
3 (S2)- 1th cycle
6 (S2)- last cycle
8 (S3)- last cycle
0S-S300-45
Strain gauge was damaged
Load, F (kN)
Strain ε [%]
F

(c)

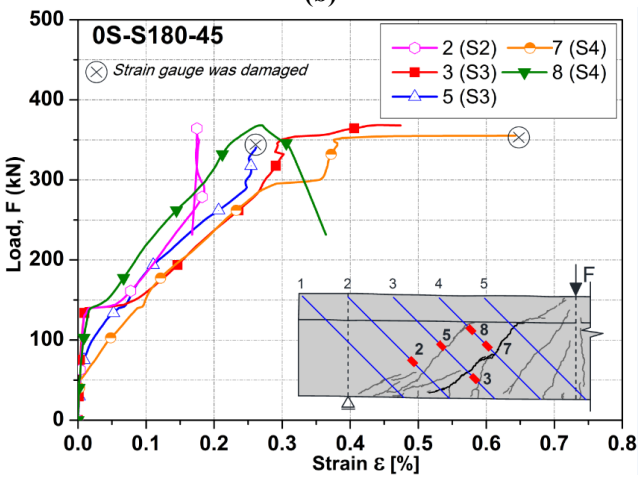
0S-S180-45
Strain gauge was damaged
2 (S2)
7 (S4)
3 (S3)
8 (S4)
5 (S3)
Load, F (kN)
Strain ε [%]
F

(d)

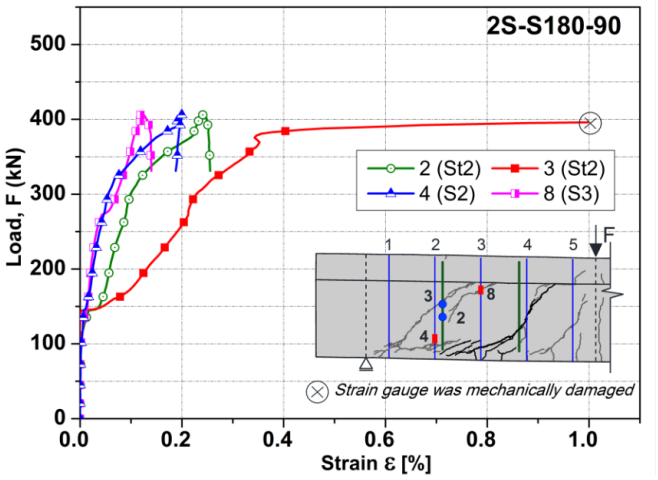
2S-S180-90
2 (St2)
3 (St2)
4 (S2)
8 (S3)
Strain gauge was mechanically damaged
Load, F (kN)
Strain ε [%]
F

(e)

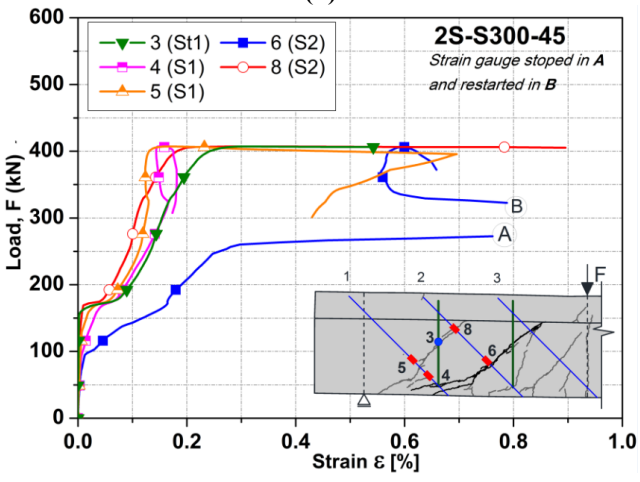
2S-S300-45
Strain gauge stoped in A
and restarted in B
3 (St1)
6 (S2)
4 (S1)
8 (S2)
5 (S1)
A
B
Load, F (kN)
Strain ε [%]
F

(f)

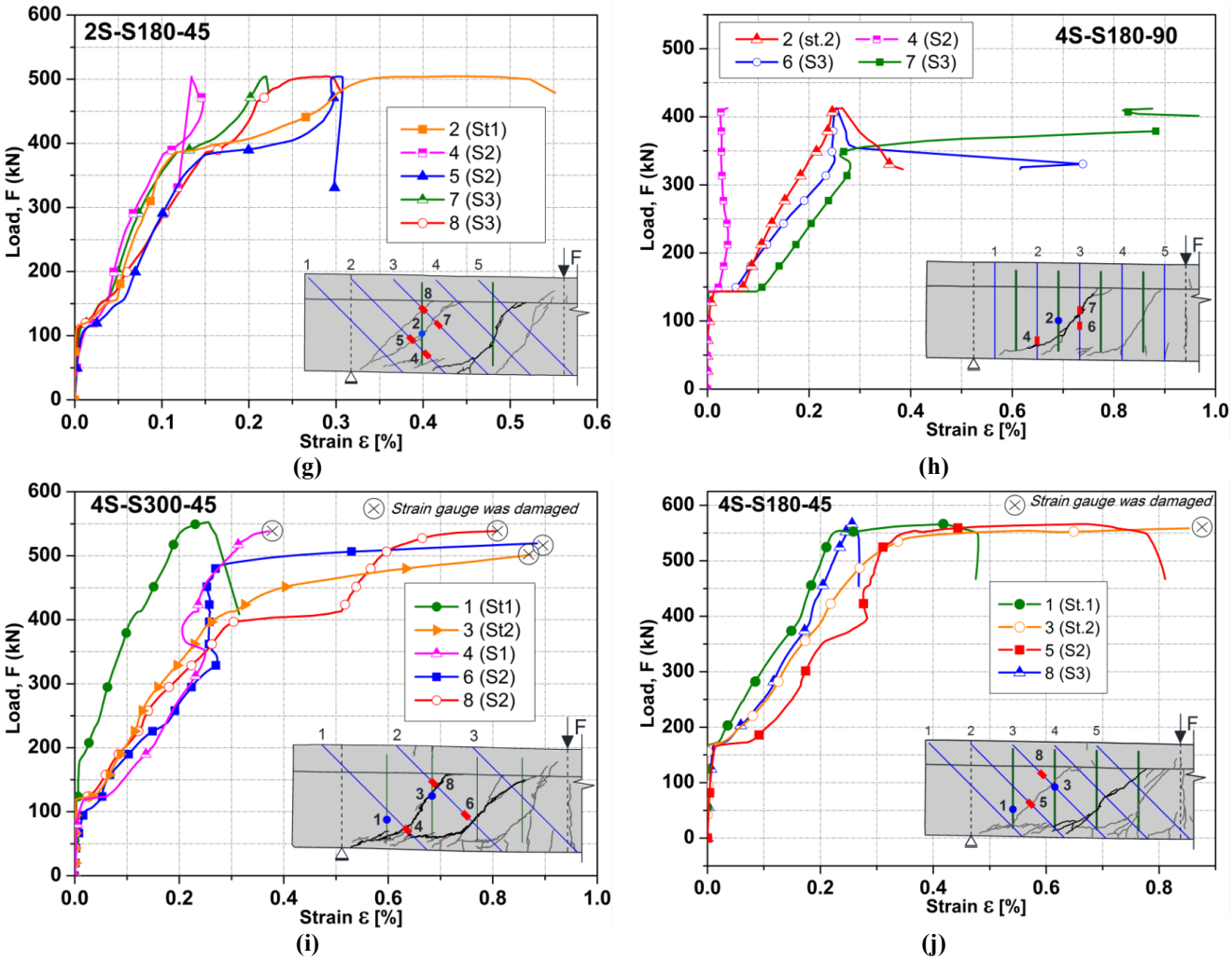

Fig. 3.12 Load versus strains recorded in strain gauges applied in ETS bars and steel stirrups.

3.6.3 Failure modes

After the strengthened beams were tested, inspections on the failure modes of the ETS steel revealed the tendency of debonding at the bar/adhesive interface (Figs. 13a and b). Due to the higher confinement provided to the ETS bars by the web-flange surrounding concrete under compression, debonding which was the governing failure mode occurred in the bond length of ETS bars localized in the bottom part of the beam's cross section (apart 0S-S300-90, see Fig. 3.7), and generally in the shorter embedded length of the two parts in which the crack divides the ETS bar. This type of failure has been observed either in vertical (Fig 3.13a) as well in inclined bars (Fig. 3.13b). It was possible to observe that the stiff steel ribs of the ETS bars scratched the surrounding epoxy adhesive, Fig. 3.13c. Despite this observed behavior, the bond performance was capable to mobilize the yield stress of the steel bars

as reported in the previous section. This type of failure mode might justify the relatively low maximum strains recorded in the vertical ETS bars, and consequently the lower shear strengthening effectiveness when compared to the same strengthening configuration but using inclined steel bars (Table 3.4). These strain values are lower compared the ones obtained using composites material applied according to the NSM technique. (Dias and Barros 2011b; Chaallal et al. 2011).

The average direction of the shear failure crack varied between 39° and 54° with regards to the beam's axis (Table 3.4); so during the opening and sliding process of this type of cracks, the vertical and inclined ETS bars crossing the cracks underwent axial and transversal force components. As already observed in a previous study (Mazaheripour et al. 2013), due to this latter component, the axial force transferred from the bar to the surrounding material increases, leading the ETS bars to scratch the surrounding epoxy adhesive.

The type of failure characterized by the loss of bond between the steel end epoxy adhesive was also found in the bond test conducted by (Valerio et al. 2009), and (Dalfré et al. 2011).

The types of failures reported by (Bianco et al. 2011), namely, concrete fracture, and mixed concrete-fracture-debonding were not observed in the present experimental program. The concrete fracture was not observed due to the relatively high confinement of the core concrete surrounding the ETS bars when using the ETS technique. It is also possible to observe that the group effect, i.e. the tendency for the detachment of the concrete cover with the increase of the shear strengthening percentage, observed when using the NSM technique (Rizzo and De Lorenzis 2009; Dias and Barros 2010, 2011b), did not occur in the ETS technique, neither by using the highest percentage of strengthening. Due to the scratching of the epoxy adhesive, the maximum strain recorded in the ETS bars never attained the steel ultimate strain, and therefore the rupture of the steel ETS bars have never occurred. However, in case of the steel stirrups, due to the excellent anchorage conditions provided by its closed shape, the steel rupture of this reinforcements was observed in some beams like for example 2S-S-300-45 (Fig. 3.13d).

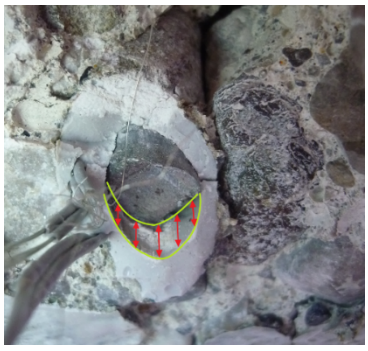

(a)

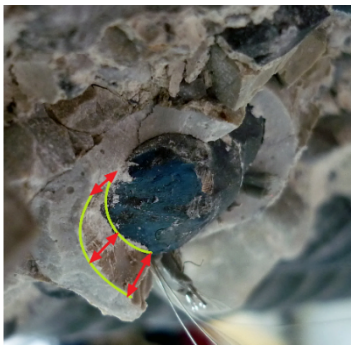

(b)

(c) (d)

Fig. 3.13. Typical failure modes in the transversal reinforcement: (a-b) debond of ETS bars; (c) adhesive scratching due to the action of ETS's ribs; (c) rupture of steel stirrups.

3.7 CFRP ETS strengthened beams

3.7.1 Load carrying capacity of the tested beams

The shear strengthening effectiveness of CFRP bars was also investigated, by strengthening and testing two beams of both 2S-Series and 4S-Series. The tested beams were strengthened with the vertical and inclined configurations that provided highest ρ_{fw}, which corresponded to vertical and inclined ETS bars spaced at 180mm. The resulting strengthening ratios ρ_{fw} were 0.16 and 0.22 for beams 2S-C180-90/4S-C180-90 and 2S-C180-45/4S-C180-45, respectively, as already presented in Table 3.1. Due to the adopted CFRP ETS bar diameter, smaller than in case of steel bars (8mm among 10mm), the percentage of ρ_{fw} for the same strengthening configuration were slightly different between steel and CFRP strengthened beams (Table 3.1). The load vs. deflection relationship of the beams strengthened with ETS CFRP bars is indicated in Figs. 3.14a and in Fig. 3.14b for 2S and 4S-Series respectively; this figures also present the beams strengthened by using steel bars that adopt the same ETS strengthening configuration. ETS CFRP strengthened beams showed, in general, similar behavior, load carrying capacity and ultimate deflection capacities to the beams that have been strengthened with steel ETS bars.

As for ETS steel bars the higher load carrying capacity and higher stiffness after the formation of the shear diagonal cracks is attributable to the ETS bars that bridged the shear cracks surfaces and offered resistance to crack opening and sliding. The exhibited failure mode was in general a shear failure, even if the beam with the highest load carrying capacity (4S-C180-45) has presented a mixed-mode shear-flexural failure. Its crack pattern was characterized by the opening of two large diagonal cracks, followed by the crushing of the concrete at the loaded section at failure (Fig. 3.15).

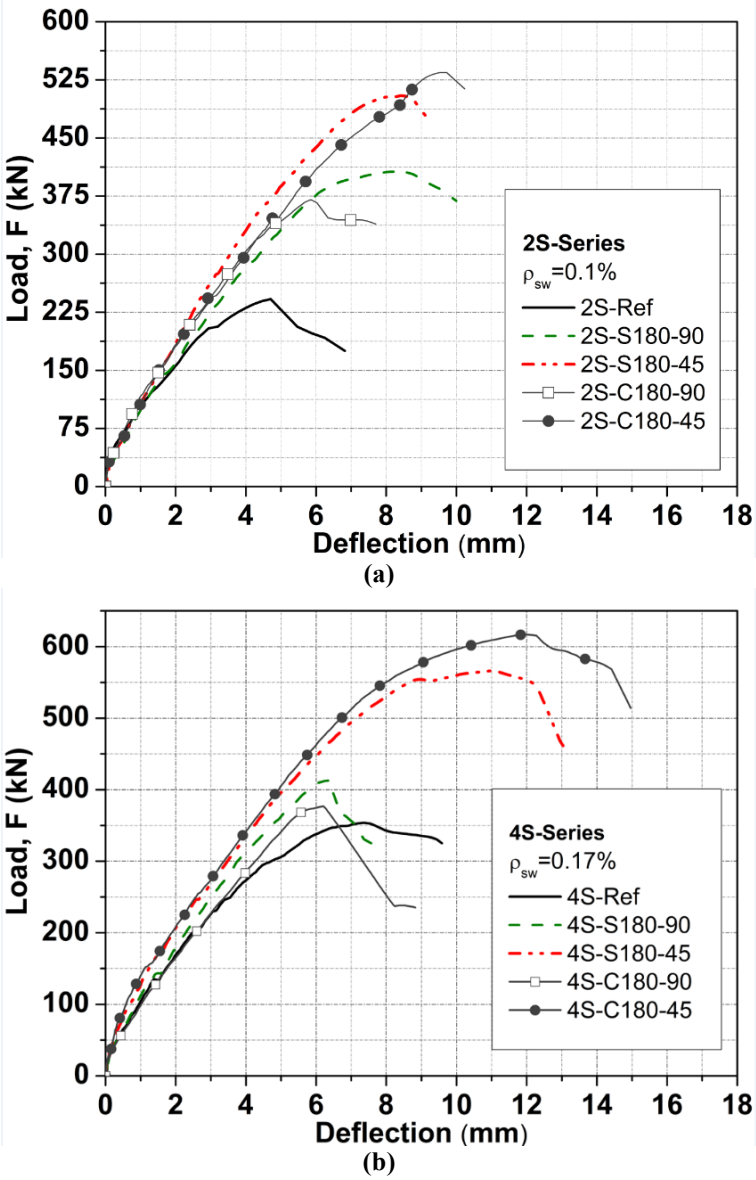

Fig. 3.14 Force vs. deflection at the loaded section for ETS CFRP strengthened beams in (a) 2S- and (b) 4S-Series

Fig. 3.15 shows the failure crack patterns obtained for the CFRP strengthened beams. The main results are presented in Table 3.5 and the same nomenclature as Table 3.3 (Section 3.5.1) is used. In this case the values of (CDC_{tan}) have ranged from 42° to 62°. By considering all the tested beams, an average value of CDC_{avg} = 50° was obtained. It is possible to notice that the beams with vertical CFRP strengthening exhibited higher inclinations of the of both CDC_{tan} and CDC_{avg}. Beam 2S-C180-90 as has happen with beam 2S-S180-90 presented high inclination of critical diagonal crack. From Figs 3.14 and 3.15 it is possible to notice that a high increment of load carrying capacity seems to be related to a diffuse crack pattern, which indicates that a good bond performance of the CFRP ETS bars was attained and the strengthening was effective in transferring the stress to the surrounding concrete. For the CFRP

vertical bars, $\rho_{fw=}$ 0.16% (CFRP180-90), the beams presented an increase of load carrying capacity of 53.1% (F_{max}= 370.49 kN; u_{Lmax} = 6.89 mm) and 6.5% (F_{max}= 376.88 kN; u_{Lmax} = 6.2 mm) for 2S- and 4S-Series, respectively. For the ETS CFRP bars inclined at 45°, $\rho_{fw=}$ 0.22% (CFRP180-45), the beams presented an increase of load carrying capacity of 120.9% (F_{max}= 534.69 kN; u_{Lmax} = 9.53 mm) and 74.4% (F_{max}= 616.86 kN; u_{Lmax} = 12.03 mm) for 2S- and 4S-Series, respectively.

Table 3.5 Experimental results of 2S-Series and 4S-Series strengthened with CFRP bars.

	F_{max} [kN]	u_{Lmax} [mm]	$\Delta F/F_{Ref}$ [%]	V_{max} [kN]	V_f^{exp} [kN]	$CDC_{tang.}$ [°]	$CDC_{avg.}$ [°]
2S-C180-90	370.485	5.89	53.1	222.3	77.1	62	60
2S-C180-45	534.69	9.53	120.9	320.8	175.6	48	46
4S-C180-90	376.875	6.20	6.5	226.1	13.9	49	52
4S-C180-45	616.86	12.03	74.4	370.1	157.8	42	40

A lower strengthening performance was observed for the vertical CFRP bars when compared to the vertical steel bars due the strengthening configuration. In fact, the available bond length of the CFRP bar crossed by the CDC was not sufficient to develop high tensile strains in this type of bars. However, when the strengthening configuration provided an adequate bond length, as was the case of inclined bars, a higher load carrying capacity was obtained by using CFRP bars instead of steel bars. The results obtained in the beams strengthened with ETS CFRP bars demonstrate that the decrease of the shear strengthening effectiveness with the increase of the reinforcement ratio of existing steel stirrups occurs regardless of the type of material adopted for the ETS bars.

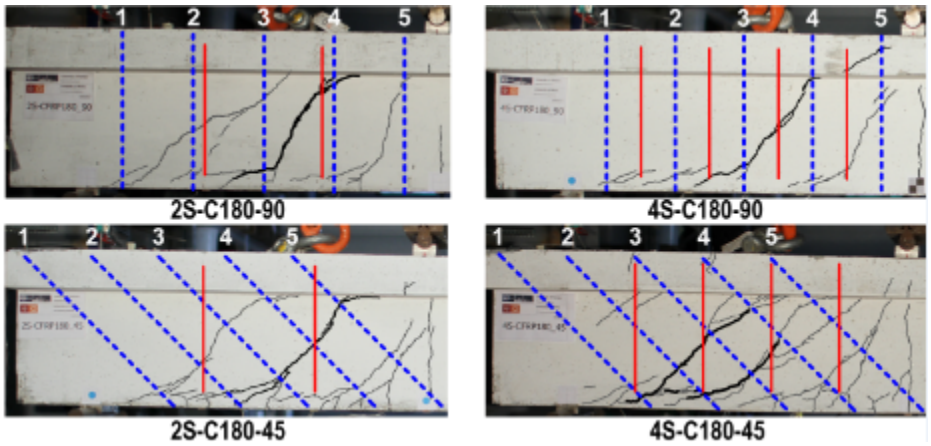

Fig. 3.15 Crack Pattern for ETS CFRP strengthened beams.

3.7.2 Strains in the CFRP ETS rod and steel stirrups

The relationship between the force applied in the beams and the strains in the most representative SGs installed in the monitored CFRP ETS bars are shown in Fig. 3.16, while in Table 3.6 are included the relevant results (same nomenclature as for steel strengthened bars in section 3.5.2 are used). Similar

considerations to the one obtained for the steel strengthened beams can be obtained. The strain values are quite susceptible to the relative distance between the SG and the shear failure crack, and depended on the bond length provided by the strengthening configuration. In case of vertical ETS the significant strain in the CFRP bars can be obtained as shown for SG No 8 ($\varepsilon_{F\max}$=0.67%) for beam 2S-C180-90 (Fig 3.16a) if an adequate bond length is provided, otherwise the strains in the strengthening bar remained low since slip occurs at the bar/adhesive interface and a modest strengthening effectiveness is obtained (beam 4S-C180-90 Fig. 3.16b). Nevertheless CFRP bars can record low strain even if the bars are crossed by the critical shear crack, as was the case of SG No.4 of the 2S-C180-90 beam (ε=0.27% at F_{max}) due to slip occurrence.

In all the monitored elements of the strengthened beams with inclined CFRP bars, as is the case of beams 2S-C180-45 and 4S-C180-45, higher strains were recorded due to the formation of diffuse crack patterns and a higher available bond length (Figs. 3.16c and 3.16d). For instance, in the ETS bars S4 and S3 of beams 2S-C180-45 and 4S-C180-45, relatively high average strains of ε=0.9% ware obtained. The maximum strain of ε=1% at 0.83 u_L/u_{Lmax} was measured in the SG No.7 of beam 2S-C180-45. Considerable strains were also attained in case of a reduced bond length (ε=0.61% at 0.63 u_L/u_{Lmax} in SG No.4 of beam 2S-C180-45). Higher strains were generally recorded in CFRP bars than in steel bars, due to the smaller diameter and lower elasticity modulus of the CFRP. The geometrical closed configuration of the stirrups allowed the steel to yield at lower load than the F_{max}. Yield strain was reached in the monitored stirrups at a percentage of maximum load (F_{max}) that ranged between 0.60% and 0.74% in SG No.3 for beam 4S-C180-45 and SG No.2 for beam 2S-C180-45. As occurred in steel ETS strengthened beams some of the beams steel stirrups have even attained its rupture in 2S-C180-45, 4S-C180-45).

Table 3.6 Significant strains measured for CFRP strengthened beams in 2S- 4S-Series.

Beam ID |	SG	Element	$\varepsilon_{F\max}$ [%]	ε_{max} [%] (u_L/u_{Lmax})	Beam ID |	SG	Element	$\varepsilon_{F\max}$ [%]	ε_{max} [%] (u_L/u_{Lmax})
2S-C180-90	2	St1	--	0.87 (0.79)	4S-C180-90	4	C2	0.15	0.16 (1.05)
	1*	C2	0.40	0.46 (1.31)		6	C3	0.13	0.15 (0.60)
	4	C3	0.27	0.38 (0.82)	4S-C180-45	3	St2	--	0.79 (0.78)
	8	C4	0.67	0.67 (1.00)		5	C2	0.77	0.86 (1.18)
2S-C180-45	2	St1	0.66	0.76 (1.20)		8	C3	0.62	0.89 (1.18)
	1*	C2	0.46	0.56 (0.70)		2*	C4	0.86	0.86 (1.00)
	4	C3	0.24	0.61 (0.63)					
	6	C4	--	0.97 (0.92)					
	7	C4	--	1.00 (0.83)					
	8	C4	0.86	0.86 (1.00)					

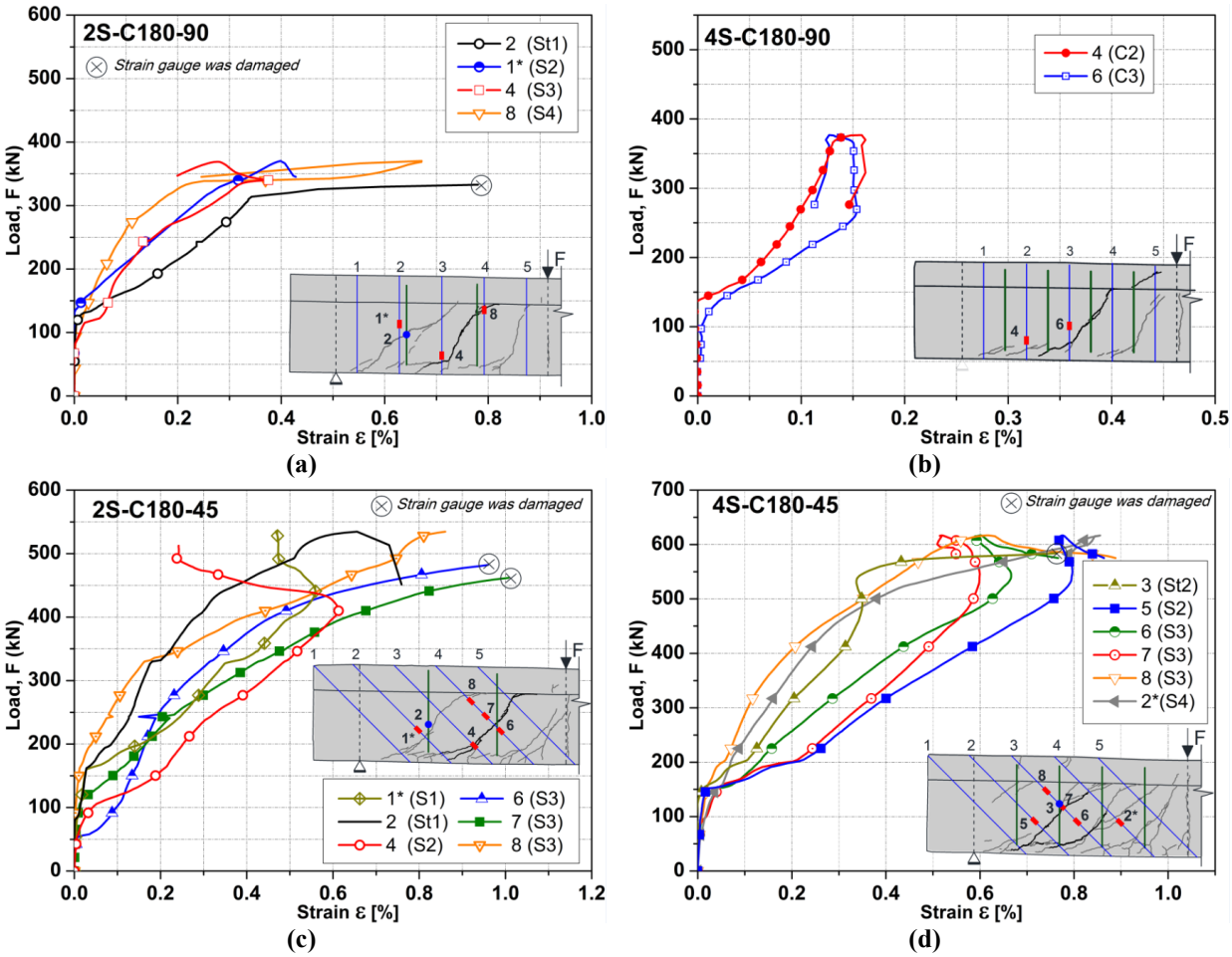

Fig. 3.16 Load vs. strains recorded in strain gauges applied in CFRP bars and steel stirrups.

3.7.3 Failure modes

As for steel bars, the CFRP ETS strengthening system failed by the debond at the bar/adhesive (Fig 3.17a). The scratching effect between bars surface and epoxy adhesive, due to combined tensile and transversal forces along the crack was also observed in the face of the CFRP bars, due to the relatively low shear resistance of the external layer of these bars, in most of cases, the peeling-off of the external layer of the CFRP bars was observed (Fig. 3.17b). This failure is similar to the interlaminar shear failure (i.e. the separation between the bar core and the sanded/coated surface) described in the bond stress carried out by Valerio et al. (2009), which was the dominant failure in case the CFRP bars. The post-test inspection of the failure modes in 2S-C180-45 has revealed that the bars have ruptured, probably not because the ultimate strain was attained, but as a consequence of the combined tensile-shear forces applied in the bar at crack section. Due to the scratching of the epoxy adhesive, the relatively small bond transfer length, and the inexistence of anchorage mechanisms, the maximum strain recorded in the ETS bars never attained the CFRP ultimate strain, and therefore the rupture of the

steel ETS bars has never occurred. Despite this observed behavior, the bond performance was capable to assured relatively high tensile strains in inclined CFRP bars, as reported in the previous section. The reported type of failure mode might justify the relatively low maximum strains recorded in the vertical CFRP ETS bars, and consequently the lower shear strengthening effectiveness when compared to the same strengthening configuration but using steel bars. The bond test presented in Annex A showed that the average bond stress developed by steel and CFRP bars provided in general similar results, but the bond-slip relationship of both steel and CFRP bars should be further investigated.

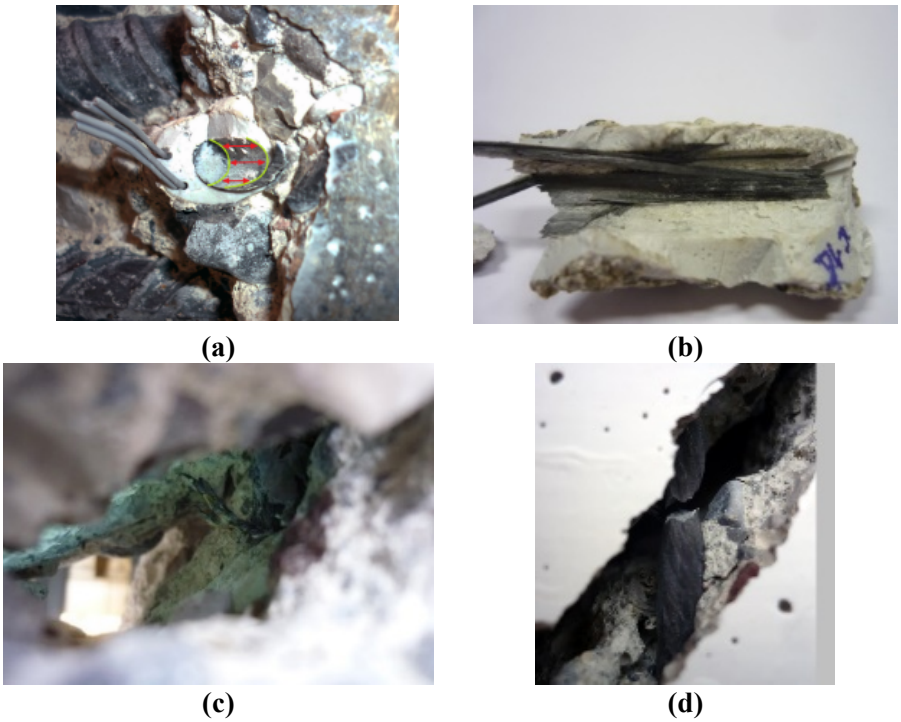

Fig. 3.17 Failure (a) loss of bond CFRP roads, (b) peeling-off of the external layer of the CFRP rod, (c) failure due to combined axial/transversal forced on a CFRP bar (observed in beam 4S-C180-45 (d) stirrup rupture.

Previous research on EBR and NSM techniques revealed that a crack pattern with smaller crack spacing can accelerate the FRP debonding and lead to a premature failure, since the bond length is decreased by the formation of several cracks (Carolin and Täljsten 2005; Mofidi and Chaallal 2011); ETS strengthening is generally characterized by crack spacing larger than EBR and NSM techniques, therefore the CFRP bars embedded in a less cracked concrete core seems less prone to FRP debonding failure than EBR and NSM methods. The types of failures reported by Bianco et al. (2012) for NSM CFRP strengthened beams: (i) concrete fracture, (ii) and mixed-concrete-fracture-debonding were not observed neither in case of CFRP ETS strengthening. Group effects, or interaction effects caused by the mutual interaction, due to the reduced spacing between the strengthening, typical of strengthened elements characterized by high percentage of FRP, when using the NSM technique (Rizzo and De

Lorenzis 2009; Dias and Barros 2010, 2011b), were not observed neither by using the CFRP ETS bars. The stirrups rupture was observed also for the highest percentage of strengthening in beams 2S-C180-45 and 4S-C180-45 (Fig 3.17d).

3.8 Influence of the investigated parameter

3.8.1 Influence of the percentage and inclination of the ETS strengthening

General remarks on the influence of percentage and inclination for beams of 0S, 2S and 4S-Series strengthened with steel ETS bars were reported in section 3.5.1. Taking into account the measured strains and the failure modes a comprehensive discussion of the investigated parameters can be presented also including the results obtained from beams strengthened with CFRP bars (section 3.5.1). The relationship between the strengthening effectiveness ratio provided by the ETS strengthening arrangement ($\Delta F/F_{Ref}$) is plotted versus the total percentage of transverse reinforcement ($\rho_{sw} + \rho_{fw}$) in Fig. 3.18 (see also Tables 3.1 3.3 and 3.5). The $\rho_{sw} + \rho_{fw}$ percentage is in the range of 0.15% to 0.52 %, while the ρ_{fw} is in the interval of 0.15% to 0.34%. Fig. 3.18 clearly shows that the shear strengthening effectiveness decreases with the increase of $\rho_{sw} + \rho_{fw}$. It is also visible that most effective configurations are obtained by adopting inclined ETS bars for both tested strengthening materials. As example it is possible to observe that, in all the tested series the beams adopting the strengthening configurations with vertical ETS bars spaced at 180 mm (ρ_{fw} =0.24) exhibited lower effectiveness than beams with inclined ETS bars spaced at 300 mm (ρ_{fw} =0.21), even if characterized by a larger percentage of strengthening. From this figure it is also possible to observe that and a marginal shear strengthening effectiveness for both steel and CFRP is obtained when vertical ETS bars are applied in RC beams with a reinforcement ratio of steel stirrups higher than of about ρ_{sw} = 0.17%. Indeed beams 4S-S300-90, 4S-180-90 and 4S-C180-90 exhibit a low strengthening effectiveness of 4.8, 16.8 and 6.5%, respectively. The dashed lines identify the tendency lines of beams with the same strengthening solution and different reinforcement ratio, pointing out the importance of the internal shear ratio on the evaluation of the strengthening effectiveness (see section 3.7.2). The higher shear effectiveness showed by the ETS inclined bars can be justified by the orientation of the diagonal cracks that tends to be almost orthogonal to the ETS bars (see also Figs 3.8 and 3.15). Furthermore, for inclined ETS bars, the total resisting bond length of the ETS system is higher than the one for the vertical bars. In was shown in Section 3.5.2 that some inclined ETS bars were crossed by more than one diagonal shear crack; at these intersection points maximum strain levels that exceed the yield strain were recorded (for instance

2S-S300-45 beam, ETS2, SG6 and SG8, Table 3 and Fig. 3.12e), which is also a demonstration of the strengthening effectiveness. As demonstrated in (Bianco et al. 2010, 2011), in the case of shear strengthening elements of non-closed geometric configuration, such is the case of EBR and NSM reinforcements, the effective bond length has a decisive and governing importance on the shear strengthening effectiveness, since a bond length less than the critical one limits the strengthening effectiveness of the system. If the inclination of the dashed line in Fig 3.18 is compared, it is possible to observe that the effectiveness of the inclination on ETS bars effectiveness was even more important when CFRP rods were used.

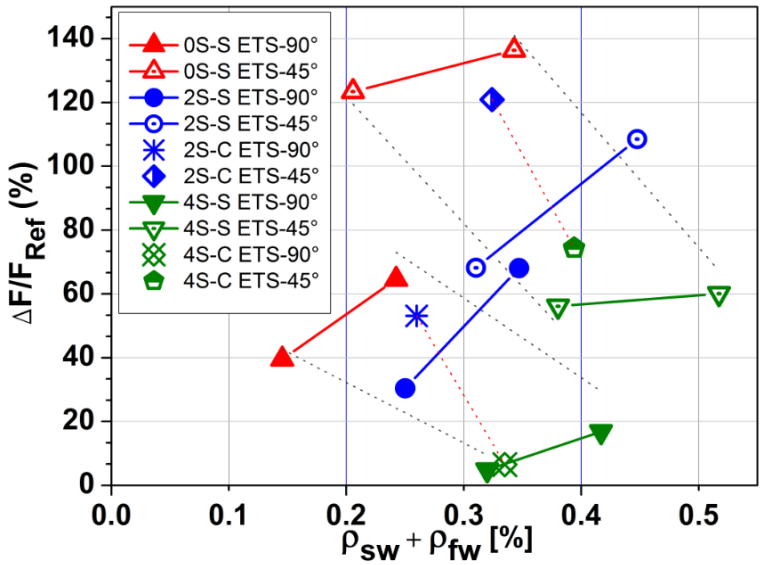

Fig 3.18 Influence of the ρ_{sw}+ ρ_{fw} on the ETS effectiveness.

To have a comprehensive understanding on the influence of the investigated parameters, the information available in previous works (Valerio et al. 2009; Chaallal et al. 2011; Barros and Dalfré 2012) have been considered. From this latter tests only the data regarding beams that failed in shear was considered, which is presented in Table 3.7. The ρ_{sw} of the analyzed beams is in the range of 0.0 to 0.17 % and ρ_{fw} in the interval of 0.04 to 0.64%. Fig. 3.19a shows the influence of ρ_{sw} and ρ_{fw} on the shear strengthening effectiveness of RC beams strengthened with vertical and inclined ETS bars. It is visible the higher strengthening effectiveness of inclined ETS bars, and a tendency for an increase of this effectiveness with ρ_{fw}, while the opposite happens with the increase of ρ_{sw}. By projecting the results presented in Fig 3.19a on a $\Delta F/F_{Ref}$ - ρ_{fw} plane, and attributing to the marker a size diameter proportional to the ρ_{sw} of the beam it represents, the previous conclusions can be also extracted. A relatively high shear strengthening effectiveness with vertical CFRP bars was obtained by Chaallal et

al. (2011), but using an abnormal high shear strengthening ratio (ρ_{fw}=0.64%). Valerio et al. (2009) have also obtained similar high shear strengthening effectiveness with smaller strengthening ratio (ρ_{fw}=0.24% to 0.34%), but using higher concrete strength class ($f_{cm,cube}$= 55 to 60 MPa - cube strength -, instead of f_{cm}=25 MPa (Chaallal et al. 2011)), which reveals the favorable effect of concrete strength on the shear strengthening performance.

Table 3.7 Experimental results of previous experimental tests on beams strengthened with ETS technique.

Valerio et al (2009)	Angle [θ_{fw}]	Material	$f_{cm,cube}/f_{cm}$ [MPa]	ρ_{sw} [%]	ρ_{fw} [%]	$\rho_{sw}+\rho_{fw}$ [%]	$\Delta F/F_{Ref}$ [%]	V_f [kN]
SLB P4d-2S8@d	90°	S	[55-60][a]	0.00	0.09	0.09	18.0	53.2
SSB R3d-C6@0·7d	90°	C	[55-60][a]	0.00	0.24	0.24	97.0	22.9
SSB R3d-C6@0·5d	90°	C	[55-60][a]	0.00	0.34	0.34	114.0	27.0
SLB P4d-2C7·5@d	90°	C	[55-60][a]	0.00	0.08	0.08	14.6	43.2
SLB P4d-C7·5@d	90°	C	[55-60][a]	0.00	0.04	0.04	6.5	19.1
Chaallal et al (2011)								
S0-ETS	90°	C	25.00[b]	0.00	0.64	0.64	112.40	99.50
Dalfré and Barros (2013)								
A.3 E300.90	90°	S	30.78 [b]	0.00	0.17	0.17	47.7	31.2
A.4 E300.45	45°	S	28.81 [b]	0.00	0.25	0.25	47.7	57.1
A.5 S300.90/E300.90	90°	S	30.78 [b]	0.13	0.17	0.30	40.8	40.3
B.3 E300.90	90°	S	30.78 [b]	0.00	0.11	0.11	17.5	21.3
B.4 E300.45	45°	S	28.81 [b]	0.00	0.16	0.16	65.3	98.5
B.5 S300.90/E300.90	90°	S	30.78 [b]	0.06	0.11	0.17	67.9	94.7

[a] $f_{cm,cube.}$ Average concrete cube compressive strength
[b] $f_{cm..}$ Average concrete cylindrical compressive strength

However, the results also indicate that when the shear strengthening ratio is relatively small, the influence of the concrete strength on the shear strengthening effectiveness is marginal due to the inexistence of interaction between ETS bars and smaller stress field applied by ETS bars to the surrounding concrete. The trend lines of the results corresponding to the inclined and vertical ETS bars (dotted and dashed line, respectively) evidence the higher effectiveness of the former bars. The inclination of the trend line is higher for vertical ETS bars, which might be justified by a high number of beams tested without shear reinforcement for this strengthening arrangement. From the results in Figs 3.18 and 3.19, the inclined ETS CFRP bars provided higher effectiveness than inclined steel bars of similar ρ_{fw} and ρ_{sw}, but a comprehensive cost competitiveness evaluation of these strengthening solutions should be made for a sustainable decision of the most appropriate one.

3.8.2 Influence of the existing shear reinforcement on the ETS strengthening effectiveness

As already demonstrated in beams strengthened with the ETS (Chaallal et al. 2011; Barros and Dalfré 2012), EBR and NSM techniques (Pellegrino and Modena 2002; Bousselham and Chaallal 2006; Grande et al. 2009; Dias and Barros 2011a, 2011b), the effectiveness of the ETS strengthening system decrease with the increase of the ρ_{sw}. Fig. 3.18 and Fig. 3.19 show this clear tendency for the ETS strengthened beams. This detrimental effect was more pronounced in case of vertical ETS bars; for instance in the case of the presented work, in ETS steel bars, spaced at 180mm, the $\Delta F/F_{Ref}$ can decrease up to 74% (by comparing the results of 0S-Series and 4S-Series).

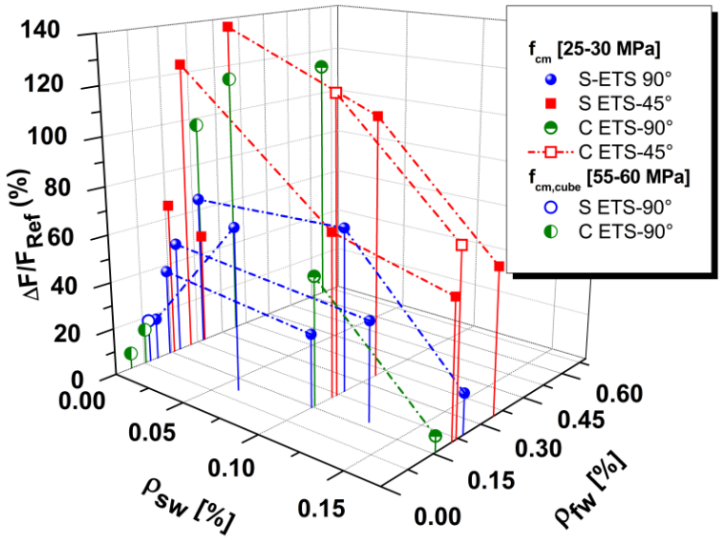

(a)

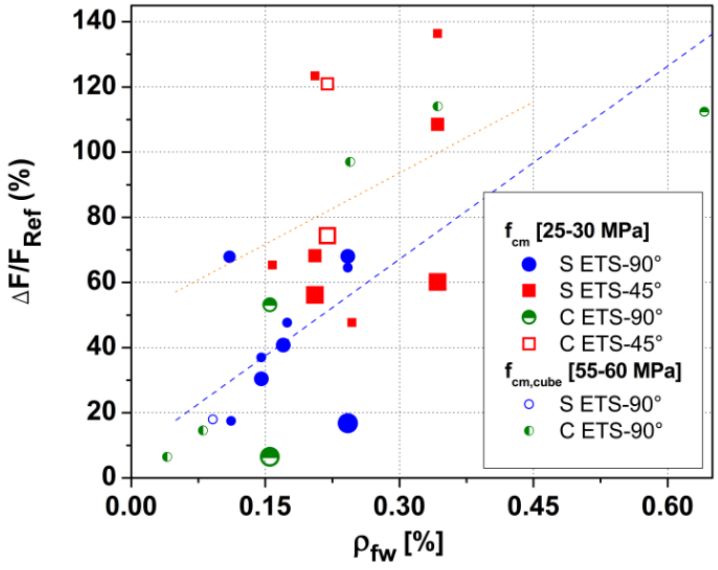

(b)

Fig. 3.19. ETS effectiveness (a) influence of ρ_{sw} and ρ_{fw}, (b) projection on the plane $\Delta F/F_{Ref}$ - ρ_{fw}.

When CFPR ETS bars were used the $\Delta F/F_{\mathrm{Re}f}$ decreased of 88% and 38% in vertical and inclined bars respectively, by increasing ρ_{sw} from 0.1% to 0.17%. Fig. 3.19 show that in two beams characterized by low percentage of transverse reinforcement (2S-S180-90 - Table 3.3 and B.5 S300.90/E300.90 - Table 3.7) the detrimental effect induced by the presence of existing stirrups did not occur, and an higher effectiveness when compared to the same strengthening configuration but in the beams without stirrups (0S-S180-90 and B.3 E300.90) was observed (Fig.3.19). The latter results can be considered an exception since the general behavior contradict these isolated results. The results presented in Fig 3.19 clearly show that the shear strengthening effectiveness is influenced by the shear reinforcement ratio of existing steel stirrups. The detrimental effect induced by the presence of stirrups was recently discussed and a parameter was proposed to simulate this effect (Chen et al. 2013; Pellegrino and Modena 2006). In the present work it was verified that the stirrups have yielded, even in the beams with the highest ρ_{sw} and ρ_{fw}. This indicates that ETS technique using steel bars can mobilize integrally the strength capacity of both shear reinforcements, and consequently, the above parameter can be neglected in this technique. In shallow RC beams shear strengthened with ETS steel bars, the resisting bond length of those bars crossed by the critical shear crack may be not enough to mobilize its yield strain. In this case the applicability of a reduction parameter can be justified. However, no sufficient experimental data is actually available to propose a recommendation for this parameter.

3.9 Comparison with EBR and NSM techniques

An higher strengthening effectiveness than other FRP-based strengthening techniques was expected for the ETS technique. A comparison between EBR, NSM, ETS techniques was presented by Chaallal et al. (2011) for a limited number of beams. The results showed that this latter technique was able to obtain the highest increase of shear strength. In two of the three specimen strengthened with CFRP bars the ETS technique was able to transform a brittle shear failure into flexural failure, as also occurred in several ETS strengthened beams tested by Valerio et al. (2009).

The beams tested in the presented experimental program are characterized by a similar design to the beams tested by Dias and Barros (2008,2010, 2011a, 2011b). This fact allows to compare the obtained results with some of the beams of the above-mentioned experimental programs, which were characterized by similar concrete compressive strength (Dias and Barros 2011a). The data regarding the experimental tests carried out by Dias and Barros are reported in Table 3.8. Fig. 3.20 compares the $\Delta F/F_{\mathrm{Re}f}$ obtained when using ETS, NSM and EBR techniques. The beams tested by Dias and Barros (2011a) had ρ_{sw}=0.1 and ρ_{sw} =0.17%, which is the same shear reinforcement ratio used for the beams tested in the present work. In Fig. 3.20 it is possible to observe that the highest strengthening efficiency

of the ETS technique is clearly visible, mainly when using inclined ETS bars. When comparing the results of beams 2S-10LV (Table 3.8) and 2S-C180-90 in Table 3.5, which are characterized by same percentage of internal stirrup are strengthened with similar percentage ρ_{fw} of CFRP at 90° the effectiveness of using the ETS technique is 1.7 times higher than the one using the NSM technique. By considering the level of strengthening effectiveness and the flexural capacity of the tested beams possible to obtain with the ETS technique, it can be concluded that by using the presented technique a much higher increase of shear strength can be obtained when compared with other FRP-based shear strengthening thechnique. This evidence makes of the ETS technique an optimum solution in structural element where the geometry allows the drilling of the concrete core.

Table 3.8 Strengthening efficacy ($\Delta F/F_{\mathrm{Re}f}$ (%)) versus CFRP percentage (ρ_{fw}) (from - Dias and Barros 2011a)

NSM strengthening at 90° $\rho_{sw} = 0.10\%$		
	ρ_{fw}	$\Delta F/F_{\mathrm{Re}f}$ (%)
2S-4LV	0.08	16.4
2S-7LV	0.13	23.1
2S-10LV	0.18	30.8
NSM strengthening at 60° $\rho_{sw} = 0.10\%$		
	ρ_{fw}	$\Delta F/F_{\mathrm{Re}f}$ (%)
2S-4LI60	0.07	27.2
2S-6LI60	0.11	29.8
2S-9LI60	0.16	35.8
NSM strengthening at 45° $\rho_{sw} = 0.1\%$		
	ρ_{fw}	$\Delta F/F_{\mathrm{Re}f}$ (%)
2S-4LI45	0.08	29.3
2S-7LI45	0.13	38.8
2S-10LI45	0.19	47.0

NSM strengthening at 90° $\rho_{sw} = 0.17\%$		
	ρ_{fw}	$\Delta F/F_{\mathrm{Re}f}$ (%)
4S-4LV	0.08	14.3
2S-7LV	0.13	15.1
NSM strengthening at 60° $\rho_{sw} = 0.17\%$		
	ρ_{fw}	$\Delta F/F_{\mathrm{Re}f}$ (%)
4S-4LI60	0.07	19.5
4S-6LI45	0.11	23.2
NSM strengthening at 45° $\rho_{sw} = 0.17\%$		
	ρ_{fw}	$\Delta F/F_{\mathrm{Re}f}$ (%)
4S-4LI45	0.08	19.1
4S-7LI45	0.13	28.7

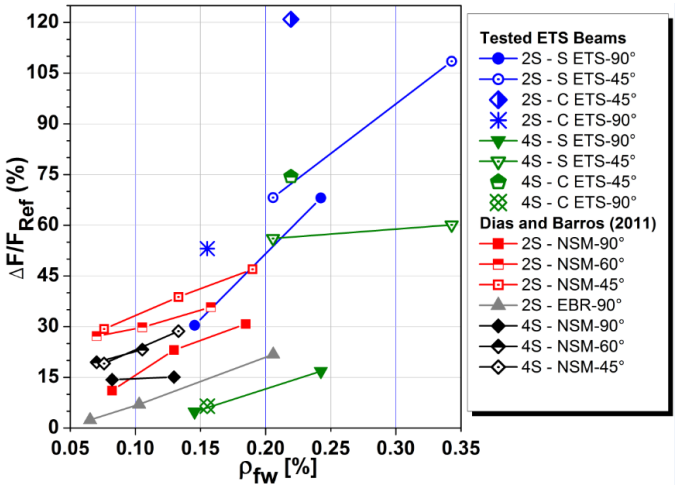

Fig. 3.20. Comparison of shear strengthening efficiency between ETS, NSM and EBR techniques (Dias and Barros 2011a).

3.10 Conclusion

An experimental program on reinforced concrete (RC) T cross section beams shear strengthened with a recent technique denominated Embedded Through-Section (ETS) was described, and the relevant results are presented and discussed. The influence of the percentage of existing steel stirrups (ρ_{sw}) on the ETS shear strengthening effectiveness when using ETS steel or carbon fiber reinforced polymer was investigated. The inclination of these bars (90° and 45°) on this effectiveness was also analyzed. For this purpose three series of beams with different ρ_{sw} (0.0, 0.10, and 0.17%) were tested.

From the obtained results it can be concluded that in general, a significant increase of load carrying capacity was obtained by using the proposed technique, regardless the material type of ETS bars. Vertical ETS bars provided an increase of load carrying capacity in the interval of 5% to 68%. The inclined ETS bars have assured a higher strengthening effectiveness, since an increase of load carrying capacity from 53% to 136% was obtained. The inclined ETS bars were also more effective in assuring larger deflection capacity at the failure of the beams. The higher effectiveness of inclined ETS bars is attributable to the larger available resisting bond length, and their better orientation regarding the inclination of the shear failure crack, since the average inclination of the shear failure crack of the strengthened beams was 45° (varying between 39° and 60°) with the beam's axis, therefore the ETS bars were almost orthogonal to this crack.

When comparing the results from the series of beams with different ρ_{sw} it was verified that the strengthening effectiveness has decreased with the increase of ρ_{sw}, and this tendency was more prone in the series with vertical ETS bars. Information in this respect was collected from available bibliography, which has confirmed the aforementioned tendency.

By comparing the shear strengthening effectiveness obtained with the ETS technique proposed in the present work and the one assured by using the externally bonded reinforcement (EBR) and the near surface mounted (NSM) techniques it was verified that the former one is more effective. In fact, due to the good bond conditions of ETS bars assured by the concrete core of the beams, which also introduced some favorable confinement to these bars, those made of steel have yielded, and the CFRP bars have attained a relatively high maximum tensile strain, mainly the inclined ones. For similar shear strengthening ratio, the CFRP bars provided higher shear strengthening effectiveness than steel bars, due to the larger ultimate force capable to be mobilized in inclined bars. It was also verified that the steel stirrups have exceeded its yield strain, even in the beams with the highest percentage of steel stirrups.

4

Analytical models for the estimation of the ETS strengthening system contribution

4.1 Introduction

Considering the experimental results presented in Chapter 3 and previous experimental works (Valerio et al. 2009; Barros and Dalfré 2012), two different analytical formulations are assessed and presented herein in order to predict the contribution of the steel ETS bars for the shear strengthening of RC beams. The first approach, named *experimental-based,* is supported by the concept of effective strain, like the most of the existing approaches. The calculation of the effective strain can be performed using empirical equations (Triantafillou 1998; Triantafillou and Antonopoulos 2000; Chaallal et al. 1998; Dias and Barros 2013) or using a bond model (Khalifa et al. 1998). The second approach, named *mechanical-based*, is derived by modifying the simplified formulation proposed by Bianco et al. (2014), originally developed for CFRP strips applied according to the NSM technique. This latest is a comprehensive three-dimensional model developed fulfilling equilibrium, kinematic compatibility and constitutive laws of the materials involved, as well as the local bond between the involved materials. (Bianco et al. 2009a, 2009b, 2010).

4.2 Strategy for the development of the analytical formulation

Two models are proposed for the prediction of the contribution of ETS bars for the shear strengthening of RC beams. For the assessment of the predictive performance of these models, the strengthening contribution of the ETS bars, V_f^{ana}, is determined by applying the following (Eq.4.1):

$$V_f^{ana} = V_t - V_{Ref} \tag{4.1}$$

Where V_{Ref} is the shear resistance of the reference beam, and V_t is the shear resistance of the ETS strengthened beam. Following this approach, it is assumed that the steel stirrups offer the same contribution in the strengthened and in the corresponding reference beams.

In Fig. 4.1a the influence of ρ_{fw} on the contribution of the ETS strengthening system, $V_f^{\exp}$ (see Chapter 3) is represented. It was observed in Chapter 3 that for a given value of ρ_{fw}, the ETS strengthening effectiveness increased with the decrease of ρ_{sw}, being this tendency attenuated when inclined ETS bars were used. However, the influence of the shear reinforcement results less relevant on the contribution of the ETS strengthening $V_f^{\exp}$ (Fig. 4.1b)

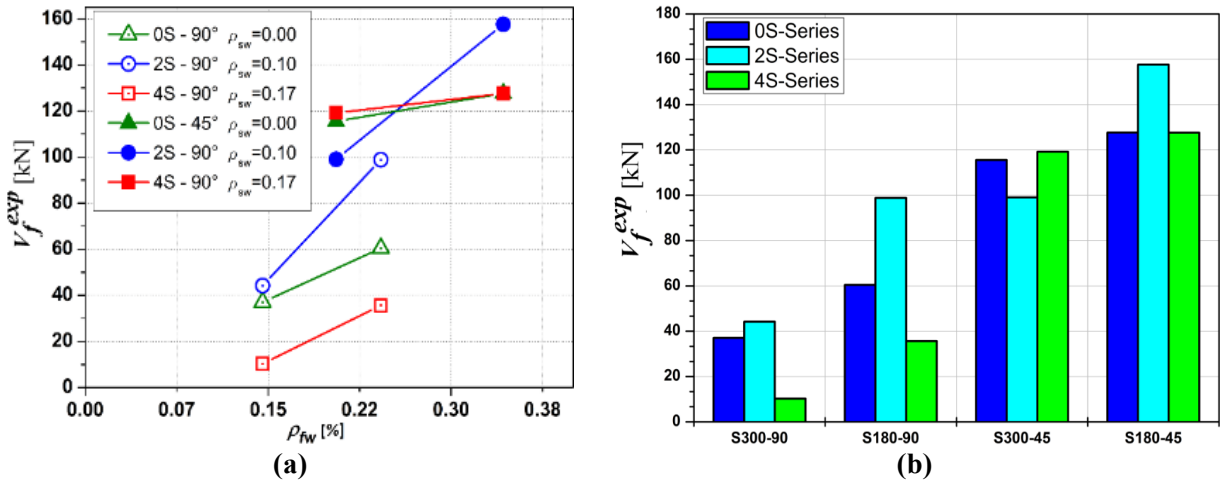

Fig. 4.1. (a) Influence of ρ_{fw} and ρ_{sw} on $V_f^{\exp}$, (b) Influence of the of the stirrups spacing and the adopted strengthening configuration on $V_f^{\exp}$

One model, herein designated as *experimental-based approach* (Section 4.3), is based on the evaluation of the effective strain ε_{fe}, which is estimated through an empirical approach that takes into account the total stiffness of the shear reinforcement and strengthening $\left(E_{fw}\rho_{fw} + E_{sw}\rho_{sw}\right)$ and the concrete strength, f_{cm}. Similar approaches have been used to evaluate the shear resistance of NSM and EBR systems (Dias and Barros 2013; Triantafillou 1998; Triantafillou and Antonopoulos 2000; Chaallal et al. 1998), and have also been adopted by international codes (fib 2001; CAN/CSA-S806-02 2002). The other model, herein designated as *mechanical-based model* (Section 4.4), follows the modeling strategy described by Bianco et al. (2014). This latter is a simplified version of a more sophisticated three-dimensional mechanical model developed to predict the NSM-FRP shear strengthening contribution for RC beams, by considering different physical phenomena, such as debonding and progressive concrete fracture

process (Bianco 2008; Bianco et al. 2009a, 2009b, 2011). The *mechanical-based model* is based on the evaluation of an equivalent average bond length that takes into account the concrete fracture as a reduction effect of the average resisting bond length. This model also adopts a simplified bilinear rigid-softening bond-slip diagram. This formulation, presented in Section 4.4, will be modified herein in order to be applicable for the ETS technique. Both approaches have been developed adopting the variable angle truss model (Paulay 1971). As reported by Bianco et al. (2014), the CDC inclination is a function of the shear span-depth ratio (L_1/d) (Bousselham and Chaallal 2004; Cao et al. 2005), of the shear reinforcement ratio ρ_{sw}, and of the percentage of shear strengthening ratio ρ_{fw}. As shown in Table 3.3, the average inclination of the CDC of the tested beams was 44°. Therefore, the critical diagonal crack inclination, $\theta = 45°$ is adopted for both approaches, like typically assumed in the current design guidelines (Chapter 2).

4.3 Experimental-based model

The experimental-based model estimates the contribution of the ETS strengthening system for the shear resistance of a RC element by determining the effective strain in the ETS bars ε_{fe}, which corresponds to the average strain in steel when the strengthened RC beam reaches its shear capacity. This empirical approach follows the procedure proposed by Dias and Barros (2013) for the NSM technique. The force resulting from the tensile stress in the ETS bars crossing the shear failure crack, F_f, is given by the following (Eq. 4.2):

$$F_f = n_f \cdot A_{fw} \cdot f_{fe} \tag{4.2}$$

where f_{fe} is the effective stress in the ETS bar, which is obtained multiplying the Young's modulus of the bars, E_{fw} by the effective strain, ε_{fe} and A_{fw} is the cross sectional area of the shear reinforcement, given by Eq. (4.3):

$$A_{fw} = n\frac{\pi \cdot \phi_f^2}{4} \tag{4.3}$$

where ϕ_f is the ETS bar diameter and n is the number of bars installed in the considered cross section. The number of ETS bars crossed by the shear failure crack (n_f), is given by Eq. (4.4):

$$n_f = \frac{h_w \cdot \left(\cot\beta_f + \cot\theta\right)}{s_{fw}} \tag{4.4}$$

where h_w (Fig. 4.2) is the depth of the cross section, θ is the orientation of the shear failure crack (CDC), β_f is the inclination of the ETS bar with respect to the beam's axis, and s_{fw} is the spacing of ETS bars.

The vertical projection of the force, F_f, is the contribution of the ETS bars for the shear resistance of the beam, V_f^I:

$$V_f^I = F_f \cdot \sin\beta = n_f \cdot A_{fw} \cdot f_{fe} \cdot \sin\beta_f \tag{4.5}$$

Introducing Eq. (4.4) into Eq. (4.5) and considering the constitutive law for the ETS bars $\left(f_{fe} = E_{fw} \cdot \varepsilon_{fe}\right)$ it results:

$$V_f^I = h_w \cdot \frac{A_{fv}}{s_{fw}} \cdot \varepsilon_{fe} \cdot E_{fw} \cdot \left(cot\ \theta + cot\ \beta_f\right) \cdot \sin\beta_f \tag{4.6}$$

By considering for V_f^I the values obtained experimentally, ($V_f^I = V_f^{\exp}$) the previous equation can be used for determining the effective strain:

$$\varepsilon_{fe} = V_f^{\exp} \Bigg/ \left(h_w \cdot \frac{A_{fv}}{s_{fw}} \cdot E_{fw} \cdot \left(cot\theta + cot\beta\right) \cdot \sin\beta_f \right) \tag{4.7}$$

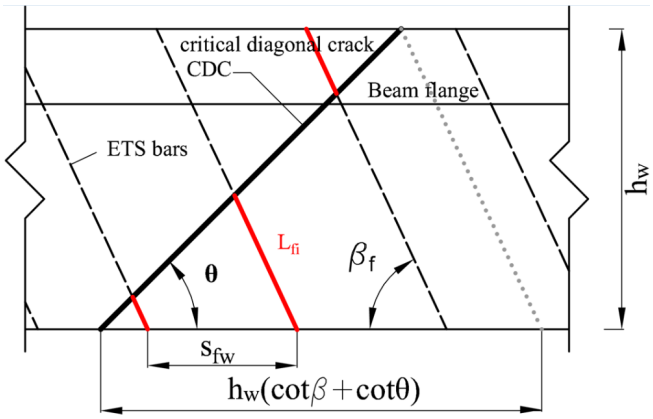

Fig. 4.2 Data for the analytical definition of the effective strain of the ETS system**.**

The concept of effective strain to evaluate the shear contribution of the strengthening is usually applied to FRP strengthened elements (Dias and Barros 2013; Triantafillou 1998; Triantafillou and Antonopoulos 2000; Chaallal et al. 1998), in which the strengthening material exhibits a linear elastic behavior up to failure. In the case of steel ETS bars, the strengthening material exhibit an elastic-plastic behavior and the effective stress, $f_{fe} = E_{fw} \cdot \varepsilon_{fe}$, is limited by the yield stress f_y. In section 4.1 the

effective strain $\left(\varepsilon_{fe}^{I}\right)$ to be used for the evaluation of the shear strengthening contribution of the ETS system, V_f^I, will be obtained by best fitting the experimental ε_{fe} recorded values.

4.4 Mechanical based model

The mechanical-based approach herein proposed follows the main simplifications proposed by Bianco et al. (2014) to their original model (Bianco et al. 2010). The CDC can be modeled as an inclined plane dividing the beam in two parts, joined together by the ETS bars crossing the plane. For the presented approach it is assumed that the inclined critical diagonal crack (CDC) at each load step assumes a constant opening along its entire length (Mohamed Ali et al. 2006), unlike what adopted by (Monti and Liotta 2007; Bianco 2008). At each load step the two parts moves apart and the opening of the crack, i.e. distance between these parts, increases. The ETS bars oppose to the crack opening by anchoring to the surrounding concrete and transferring the bond force originated by the imposed slip δ_{Li}. The capacity of an ETS bar depends on its available bond length L_{fi} that is the shorter between the two parts into which the crack divides its actual length L_f (Fig. 4.3a). The local bond stress-slip is represented by a simplified bi-linear curve (Fig. 4.3b), in which it is possible to identify the "rigid", "softening friction", "free-slipping" phases (Bianco 2008; Bianco et al. 2014). The rigid branch $(0-\tau_0)$ represents the initial shear strength, for which the value τ_0 expresses and average strength of the physical properties of the steel-adhesive-concrete interface. For an imposed slip, it is assumed that the stresses are transferred by friction and micromechanical interlock. These shear reinforcement mechanisms decrease with the increase of the slip (softening friction) up to the point $\delta_{Li}=\delta_1$ in which the friction resisting mechanism is exhausted, leading to a free-slipping phase with the evolution of the crack opening. The constitutive bond law $V_{fi}^{bd}\left(L_{Rfi},\delta_{Li}\right)$ is determined by simulating the behavior of a simple ETS bar within a concrete prism (Fig. 4.3c and d), whose dimensions are limited by the spacing between adjacent bars and half of the web cross section width, $b_w/2$. With this assumption, the interaction effect between ETS bars in the beam's axis direction is neglected due to its low contribution for this type of technique and high complexity of the phenomenon for an engineer-design framework. If more than one ETS bars are installed in the cross section, it is possible to have an interaction effect in the orthogonal direction to the beams' axis, and the value $b_w/2$ should be reduced taking into account the geometry of the cross section. However, this is expected to be a non-current situation for the majority of RC beams requiring shear strengthening intervention.

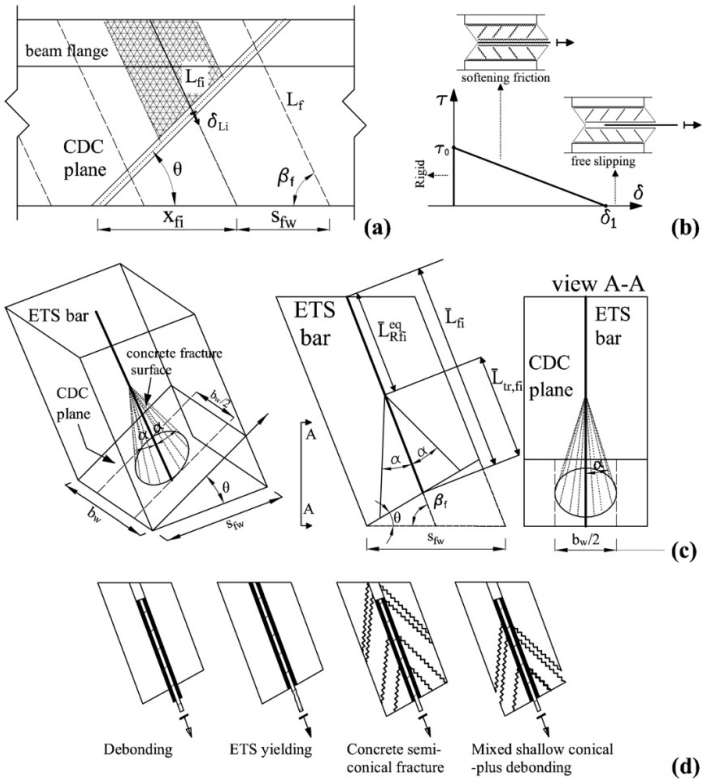

Fig. 4.3 Main mechanical features on the theoretical model and calculation procedure: (a) average-available-bond-length ETS bar and concrete cone of influence, (b) adopted bond stress-slip relationship, (c) ETS confined to the corresponding concrete prism of influence and conical surface fracture surface and area of the concrete cone at the CDC intersection, (d) Failure modes.

The interaction with existing stirrups is neglected, due to the complexity of the phenomenon (this topic requires additional dedicated research). The steel embedded bar-concrete prism system can exhibit the failure modes represented in Fig. 4.3d: debonding, bar yielding, concrete conical fracture and mixed shallow conical-plus-debonding. The fracture occurs when the stress in the concrete surrounding the bar attains the tensile strength. The shape of this surface can be conventionally assumed as a cone with the principal generatrices inclined of an angle α with respect to the bar longitudinal axis (Bianco 2008; Bianco et al. 2014). The cracking propagation increases with the imposed slip, and the resisting bond length decreases progressively. In this simplified approach the concrete fracture process is accounted by reducing the bar resisting bond length L_{Rfi} by using the factor η $\left(0 \le \eta \le 1\right)$. The factor η is a function of the average tensile strength f^*_{ctm} that is calculated imposing the equality between the maximum force that can be transferred through bond stress, and the force corresponding to the concrete conical fracture. For values of $f_{ctm} \ge f^*_{ctm}$ concrete does not fracture, and $\eta = 1$. The effective capacity $V^{\max}_{fi,eff}$

of a single ETS bar is obtained adopting the minimum value between the yield strength and the bond strength and using the equivalent value of the average bond length, $\overline{L}_{Rfi}^{eq} = \eta L_{Rfi}$ (Bianco et al. 2014).

4.4.1 Proposed design formula

The input parameters include the following geometrical and mechanical data: i) the beam cross-section web's height h_w and width b_w; ii) inclination angle of both CDC and ETS bars with respect to the beam's longitudinal axis, θ and β_f, respectively; iii) bars spacing measured along the beam's axis, s_{fw}; iv) diameter ϕ_f of the ETS bar; v) concrete average compressive strength f_{cm}, vi) steel yield strength f_y and Young's modulus E_{fw}. Other parameters strictly related to the proposed model are: the angle α ETS bar's axis and principal generatrices of the semi-conical fracture surface (Fig. 4.3c-d), bond stress τ_0 and slip δ_1 defining the adopted local bond stress-slip relationship (Fig. 4.3b). The algorithm of this model is described in Fig. 4.4, which will be detailed in the following sections.

Input parameters

$$h_w;\ b_w;\ \alpha;\ f_{cm};\ s_{fw};\ n;\ \beta_f;\ f_y;\ E_f;\ \phi_f;\ \tau_0;\ \delta_1;\ \theta$$

Evaluation of the average available resisting bond length and the minimum integer number of ETS bars effectively crossing the CDC

$$\overline{L}_{Rfi} = f\left(h_w;\ \theta;\ \beta_f;\ s_{fw}\right);\ N_{f,\text{int}}^{l}$$

Evaluation of constants

$$L_p;\ A_c;\ V_f^y;\ V_{f1}^{bd};\ J_1;\ \lambda$$

Evaluation of the average available resisting bond length reduction factor, and the equivalent average resisting bond length

$$\eta = \left(s_{fw};\ b_w;\ f_{ctm};\ \overline{L}_{Rfi}\right);\ \overline{L}_{Rfi}^{eq}$$

Evaluation of the maximum effective capacity for one ETS bar

$$V_{fi,eff}^{\max} = \min\left(V_f^{bd}\ ;\ V_f^y\right)$$

Evaluation of the ETS bars contribution

$$V_{fd}^{II} = \frac{V_f^{II}}{\gamma_f} = \frac{1}{\gamma_f}\cdot\left(n\cdot N_{f,\text{int}}^{l}\cdot V_{fi,eff}^{\max}\cdot\sin\beta_f\right)$$

Fig. 4.4 Calculation procedure of the mechanical-based approach.

4.4.2 Average value of the available resisting bond length $\bar{L}_{Rfi}$ and minimum number of bars $N^{l}_{f,\text{int}}$ effectively crossing the CDC

The average value of the available bond length $\left(\bar{L}_{Rfi}\right)$, and the minimum integer number of bars effectively crossing the CDC $\left(N^{l}_{f,\text{int}}\right)$ are determined according to the recommendations of Bianco et al. (2011). The $N^{l}_{f,\text{int}}$ is obtained by rounding off the real number to the lowest integer as follows:

$$N^{l}_{f,\text{int}} = \text{round off}\left[h_w \cdot \frac{\left(\cot\theta + \cot\beta_f\right)}{s_{fw}}\right] \tag{4.8}$$

while $\bar{L}_{Rfi}$ is determined from:

$$\bar{L}_{Rfi} = \frac{1}{N^{l}_{f,\text{int}}} \cdot \sum_{i=1}^{N^{l}_{f,\text{int}}} L_{fi} \tag{4.9}$$

where (Fig. 4.3a):

$$L_{fi} = \begin{cases} i \cdot s_{fw} \cdot \dfrac{\sin\theta}{\sin(\theta+\beta_f)} & for \quad x_{fi} < \dfrac{h_w}{2} \cdot \left(\cot\theta + \cot\beta_f\right) \\ L_f - i \cdot s_{fw} \cdot \dfrac{\sin\theta}{\sin(\theta+\beta_f)} & for \quad x_{fi} \geq \dfrac{h_w}{2} \cdot \left(\cot\theta + \cot\beta_f\right) \end{cases} \tag{4.10}$$

and:

$$x_{fi} = i \cdot s_{fw} \tag{4.11}$$

If $s_f \geq h_w$, the calculation of the average value of the available bond length gives a null length (Eq. 4.9); in these cases $\bar{L}_{Rfi} = \left(h_w \cdot \sin\theta \cdot \left(\cot\theta + \cot\beta_f\right)\right) \Big/ \left(4 \cdot \left(\sin\theta + \sin\beta_f\right)\right)$ is adopted (Bianco et al. 2014).

4.4.3 Evaluation of Constants

The geometrical and integration constants characterizing the bond transfer mechanism are obtained from Eq. (4.12) to Eq. (4.19).

The perimeter of the bar cross section:

$$L_p = \phi_f \pi \tag{4.12}$$

The cross section area of the relevant prism of surrounding concrete:

$$A_c = s_f \cdot \frac{b_w}{2} \tag{4.13}$$

$$L_d = \frac{h_w}{\sin\theta} \tag{4.14}$$

The ETS bar yield force:

$$V_f^y = \frac{\pi \cdot \phi_f^{\,2}}{4} f_y \tag{4.15}$$

Concrete's mean tensile strength:

$$f_{ctm} = 1.4 \cdot ((f_{cm} - 8)/10)^{\frac{2}{3}} \tag{4.16}$$

Concrete's Young's modulus:

$$E_c = 2.15 \cdot 10000 \cdot (f_{cm}/10)^{\frac{1}{3}} \tag{4.17}$$

where both E_c and f_{ctm} are herein evaluated by means of the CEB-FIP Model Code 1990 formulation (CEB-FIB 1990), with f_{ctm} in MPa.

The bond-modeling constants are obtained from the following Eqs. 4.18 and 4.19.

Integration constants regarding the bond transfer mechanism J_1, $1/\lambda^2$:

$$J_1 = \frac{L_p}{A_{fw}} \cdot \left[\frac{1}{E_{fw}} + \frac{A_f}{A_c \cdot E_c} \right];\ \frac{1}{\lambda^2} = \frac{\delta_1}{\tau_0 \cdot J_1} \tag{4.18}$$

The effective resisting bond length L_{Rfe}, and the corresponding maximum bond force V_{f1}^{bd}:

$$L_{Rfe} = \frac{\pi}{2 \cdot \lambda};\ V_{f1}^{bd} = \frac{L_p \cdot \lambda \cdot \delta_1}{J_1} \tag{4.19}$$

More details on the evaluation of these model's constants are reported in Annex B.

4.4.4 Shear strength contribution provided by a system of ETS steel bars

The reduction factor can be evaluated as follows:

$$\eta\left(s_f; b_w; f_{cm}; \bar{L}_{Rfi}\right) = \begin{cases} \left(f_{ctm}/f_{ctm}^*\right)^{0.5} & if \quad f_{ctm} < f_{ctm}^* \\ 1 & if \quad f_{ctm} \geq f_{ctm}^* \end{cases} \tag{4.20}$$

where, (see Annex B):

$$f_{ctm}^{*} = \frac{L_p \cdot \lambda \cdot \delta_1 \cdot \sin\left(\lambda \cdot L_{Rfi}\right)}{J_1 \cdot \pi \cdot \min\left\{L_{Rfi} \cdot \tan\alpha; \frac{b_w}{4}\right\} \cdot \frac{\sin\left(\theta+\beta_f\right)}{2} \cdot \left(\min\left\{ \frac{s_{fw} \cdot \sin\beta_f}{2 \cdot \sin\left(\theta+\beta_f\right)}; \frac{L_{Rfi} \cdot \sin\alpha}{\sin\left(\beta_f+\theta+\alpha\right)} \right\} + \min\left\{ \frac{s_{fw} \cdot \sin\beta_f}{2 \cdot \sin\left(\theta+\beta_f\right)}; \frac{L_{Rfi} \cdot \sin\alpha}{\sin\left(\beta_f+\theta-\alpha\right)} \right\} \right)} \tag{4.21}$$

in which L_{Rfi} is set equal to:

$$L_{Rfi} = \begin{cases} \bar{L}_{Rfi} & if \quad \bar{L}_{Rfi} \le L_{Rfe} \\ L_{Rfe} & if \quad \bar{L}_{Rfi} > L_{Rfe} \end{cases} \tag{4.22}$$

The function that defines the reduced embedded length, η, has relevant influence on the results of the model. In the present approach, η is assumed to be a square root function of f_{ctm}/f_{ctm}^{*} when $f_{ctm} < f_{ctm}^{*}$ (Eq. 4.20), while a linear function was adopted by Bianco et al. (2014). This option provides higher value for $\bar{L}_{Rfi}^{eq}$, which is in agreement with the experimental results, where a visible concrete cone failure was never observed. The equivalent value of the average resisting bond length is given by Eq. (4.23):

$$\bar{L}_{Rfi}^{eq} = L_{Rfi} \cdot \eta\left(s_{fw}; b_w; f_{cm}; \bar{L}_{Rfi}\right) \tag{4.23}$$

4.4.5 Shear strength contribution provided by a system of ETS steel bars

Once the equivalent value of average resisting bond length is calculated, the effective capacity of the ETS bar $V_{fi,eff}^{\max}$ can be evaluated, as the minimum between the resisting bond force, V_f^{bd}, and the yield force, V_f^{y}, of the ETS bar:

$$V_{fi,eff}^{\max} = \min\left(V_f^{bd}; V_f^{y}\right) \tag{4.24}$$

where V_f^{y} is obtained from Eq. (4.15) and V_f^{db} is determined according to the simplified the bond-based constitutive law (Annex B):

$$V_f^{bd}\left(\bar{L}_{Rfi}^{eq}\right) = L_p \cdot \frac{1}{J_1} \cdot \lambda \cdot \left\{\delta_1 \cdot \sin\left(\lambda \cdot \bar{L}_{Rfi}^{eq}\right)\right\} \tag{4.25}$$

Finally, the ETS shear strength contribution can be obtained as follows:

$$V_f^{II} = n \cdot N_{f,\text{int}}^{l} \cdot V_{fi,eff}^{\max} \cdot \sin\beta_f \tag{4.26}$$

where n is the number of installed bars in the cross section.

4.5 Models appraisal

The proposed formulations were used to calculate the ETS contribution of the tested beams presented in section 2, as well as the RC beams tested by Valerio et al (2009) and Barros and Dalfré (2012). Those two experimental programs were characterized by different test set-up, amount of longitudinal and transversal reinforcement, percentage and inclination of the strengthening system, and concrete compressive strength. Only the specimens failed in shear were considered in this study, and beams with unexpected behavior (for example 4S-S300-90- see Chapter 3) were also not considered. Valerio et al. (2009) tested RC beams with a cross section 350x450mm^2, a steel flexural reinforcement ratio of ρ_{sl} =0.93% and a L_1/d ratio of 4. Barros and Dalfré (2012) tested two series of RC beams: A Series (150x300mm^2) and B series (300x300mm^2), with a ρ_{sl} of 2.5% and 1.88%, respectively, and a constant L_1/d ratio of 3.44. The main data of these experimental programs are reported in Table 4.1.

Table 4.1 Experimental results of previous experimental tests on beams strengthened with ETS technique.

	β_f	Compressive strength	ρ_{sw}	ρ_{fw}	$\rho_{sw}+\rho_{fw}$	ϕ_s	s_{sw}	ϕ_f	s_{fw}
	[°]	[MPa]	[%]	[%]	[%]	[mm]	[mm]	[mm]	[mm]
Valerio et al 2009									
SLB P4d-2S8@d	90°	[55-60][a]	0.00	0.09	0.09	--	--	2ϕ8	260
Dalfré and Barros 2012									
A.3 E300.90	90°	30.78 [b]	0.00	0.17	0.17	--	--	ϕ10	300
A.4 E300.45	45°	28.81 [b]	0.00	0.25	0.25	--	--	ϕ10	300
A.5 S300.90/E300.90	90°	30.78 [b]	0.13	0.17	0.30	2ϕ6	300	ϕ10	300
B.3 E300.90	90°	30.78 [b]	0.00	0.11	0.11	--	--	2ϕ8	300
B.4 E300.45	45°	28.81 [b]	0.00	0.16	0.16	--	--	2ϕ8	300

[a] cubical compressive strength
[b] cylindrical compressive strength

4.5.1 Validation of the Experimental based model

The values of ε_{fe} calculated with Eq. (4.7) are plotted in Fig. 4.5 as a function of $\left(E_{fw}\rho_{fw}+E_{sw}\rho_{sw}\right)/\left(f_{cm}^{2/3}\right)$, and for the two considered inclinations of the ETS bars (β_f). The term $\left(E_{fw}\rho_{fw}+E_{sw}\rho_{sw}\right)$ expresses the stiffness of the internal shear reinforcement and the shear strengthening; $\left(f_{cm}^{2/3}\right)$ reflects the influence of the concrete tensile strength. The equation for the evaluation of ε_{ef} that best fits the experimental results is the following one:

$$\varepsilon_{fe}^{I} = -0.099 \cdot \left\{ \left(E_{fw}\rho_{fw} + E_{sw}\rho_{sw} \right) / \left({f_{cm}}^{2/3} \right) \right\} - 0.003 \cdot \beta_f + 0.456 \qquad (4.27)$$

The values of ε_{ef} (Eq. 4.7) and the analytical values of the steel effective strain ε_{fe}^{I} (Eq.4.27) are calculated for all of the beams presented in Table 3.3 and Table 4.1; the obtained results are collected in Table 4.2. Fig 4.5 shows the comparison between the experimental effective strain, ε_{fe}, and the analytical effective strain, Eq. 4.27 provides a different ε_{fe}^{I}-$\left(E_{fw}\rho_{fw} + E_{sw}\rho_{sw} \right) / \left({f_{cm}}^{2/3} \right)$ relationship for different β_f values, with larger ε_{fe}^{I} values for the β_f=45°, as was observed experimentally.

Table 4.2 Experiemental-based model assessemnt.

Beam ID	$V_f^{\exp}$	$\frac{\left(E_{fw}\rho_{fw} + E_{sw}\rho_{sw}\right)}{{f_{cm}}^{2/3}}$	ε_{fe}	V_f^{I}	$\varepsilon_{fd} = \frac{\varepsilon_{fe}}{\gamma_f}$	V_{fd}^{I}	k^{I} γ_f=1[a] (γ_f=1.3[b])
	[kN]	--	[%]	[kN]	[%]	[kN]	
Vertical							
0S-S300-90	37.017	0.030	0.18	39.60	0.14	30.46	0.93 (1.22)
0S-S180-90	60.453	0.051	0.17	65.30	0.13	50.23	0.93 (1.20)
2S-S300-90	44.199	0.052	0.21	39.14	0.13	30.11	1.13 (1.47)
2S-S180-90	98.847	0.072	0.28	64.54	0.13	49.65	1.53 (1.99)
4S-180-90	35.64	0.087	0.10	64.04	0.12	49.26	0.56 (0.72)
A-3 E300.90	31.15	0.036	0.19	30.37	0.14	23.36	1.03 (1.33)
A.5 S300.90/E300.90	40.3	0.063	0.25	29.94	0.13	23.03	1.35 (1.75)
B.3 E300.90	21.31	0.024	0.10	40.49	0.14	31.15	0.53 (0.68)
SLB P4d-2S8@d	53.2	0.030	0.20	51.63	0.14	39.72	1.03 (1.75)
Inclined							
0S-S300-45	115.53	0.043	0.39	81.5	0.25	72.9	1.42 (1.58)
0S-S180-45	127.66	0.071	0.26	135.8	0.24	120.5	0.94 (1.06)
2S-S300-45	99.036	0.065	0.33	81.5	0.25	72.4	1.22 (1.37)
2S-S180-45	157.6	0.093	0.32	135.8	0.24	119.6	1.16 (1.32)
4S-S300-45	119.18	0.079	0.40	81.5	0.24	72.1	1.46 (1.65)
4S-S180-45	127.58	0.108	0.26	135.8	0.23	119.1	0.94 (1.07)
A.4 S300.45	57.07	0.054	0.25	60.2	0.25	55.9	0.95 (1.02)
B.4 E300.45	98.52	0.036	0.33	80.3	0.25	74.5	1.23 (1.32)

[a]Average k^{I} (γ_f =1):1.08

[b]Average k^{I}(γ_f =1.3):1.30

The available data is relatively small for this type of approach, and the dispersion of results is high; a larger number of specimens is required for a better model assessment. The ε_{fe} for inclined ETS bars exceeded the yield strain, having reached 0.40%. In general, vertical ETS bars present average effective strain lower than the yield strain. The values of ε_{fe}^{I} exhibited a tendency to slightly decrease with the increase of $\left(E_{fw}\rho_{fw} + E_{sw}\rho_{sw} \right) / \left({f_{cm}}^{2/3} \right)$.

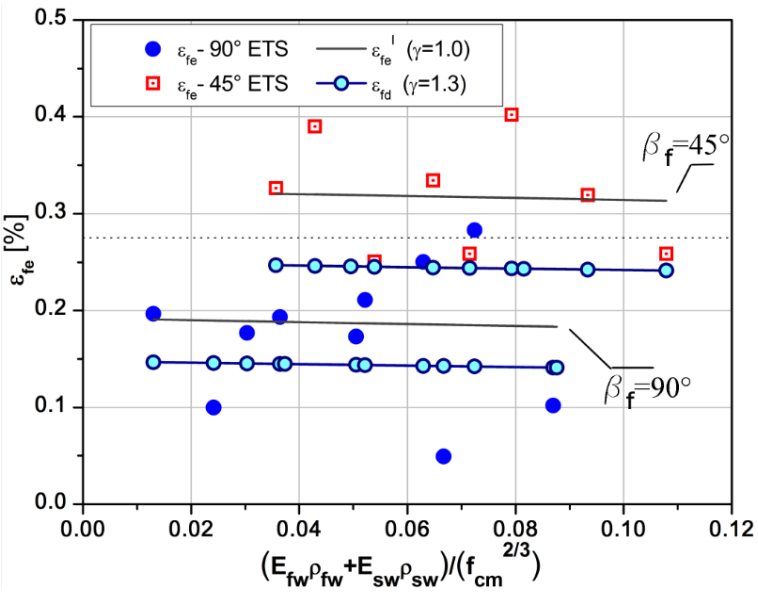

Fig. 4.5 Effective strain versus $\left(E_{fw}\rho_{fw}+E_{sw}\rho_{sw}\right)/\left(f_{cm}{}^{2/3}\right)$ from experimental data and obtained analitically.

The higher shear strengthening effectiveness of inclined ETS is captured by the model as is clearly shown in Fig. 4.5. The decay of the effective strain with the increase of $\left(E_{fw}\rho_{fw}+E_{sw}\rho_{sw}\right)/\left(f_{cm}{}^{2/3}\right)$ is much smaller than in FRP-based techniques (Triantafillou 1998; Dias and Barros 2013).

In Fig. 4.5 the dotted line indicates the yield strain of the ETS bars, that limits the steel stress. The following equation is introduced for the calculation of the ETS contribution:

$$f_{fe}=\begin{cases}\varepsilon_f^I\cdot E_f & if \quad \varepsilon_f^I\le\varepsilon_{sy}\\ f_y & if \quad \varepsilon_f^I>\varepsilon_{sy}\end{cases} \tag{4.28}$$

In the evaluation of V_f^I according to Eq. (4.5), the effective stress installed in the ETS bars is calculated respecting Eq. (4.28). The analytical values, V_f^I, and the corresponding experimental values, $V_f^{\exp}$, are included in Table 4.2. The graphical comparison between V_f^I and $V_f^{\exp}$ is presented in Fig. 4.6. Two lines limiting the deviation of the predicted values from the experimental ones at $\pm$ 30% are also depicted in Fig 4.6. It is easy to recognize that almost all of the results fall within these bounds. By determining the value of the $k^I=V_f^{\exp}/V_f^I$ ratio for all considered beams, also included in Table 4.2, an average value of 1.08 with a standard deviation of 0.28 were obtained.

The design value V_{fd}^{I} can be calculated introducing the partial safety factor γ_f to the ε_{fe}^{I}, resulting a design effective strain $\varepsilon_{fd} = \varepsilon_{fe}^{I} / \gamma_f$, whose values are also indicated in Table 4.2. A value $\gamma_f = 1.3$ is adopted in order to obtain design values for the ETS shear strengthening contribution, V_{fd}^{I}, lower than the experimental ones for the 90% of the analyzed beams, assuring a proper design safety format for this model. The V_{fd}^{I} vs $V_f^{\exp}$ is also represented in Fig. 4.6, and the values of V_{fd}^{I} are presented in Table 4.2, resulting an average value of 1.30 for the $V_f^{\exp} / V_{fd}^{I}$ ratio, which seems acceptable for a technique where the strengthening reinforcements are protected from the aggressiveness of environment agents and vandalism acts.

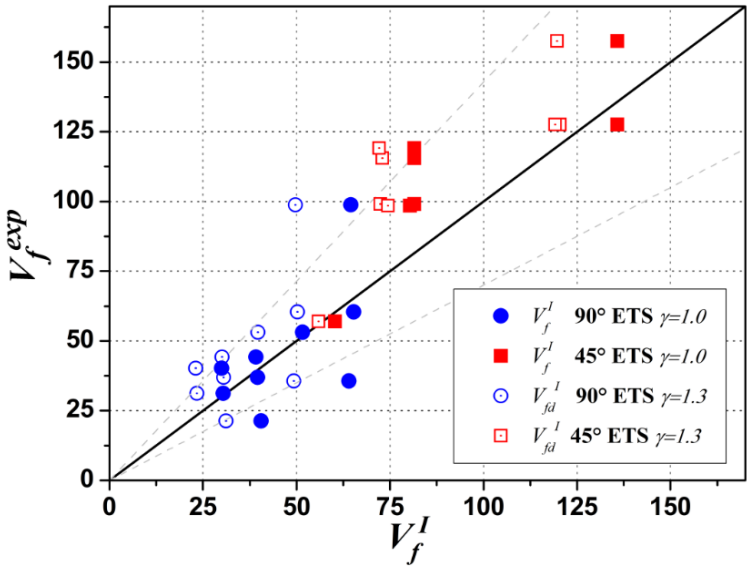

Fig. 4.6 V_f^I and V_{fd}^I vs $V_f^{\exp}$ according to the experimental-based approach**.**

4.5.2 Validation of the Mechanical based model

According to Bianco et al. (Bianco 2008), the angle α defining the opening of the concrete fractured cone is set equal to 28.5°, but an interval between 20° and 30° was found in the literature (Teng et al. 2006; Bianco et al. 2006). The simplified bond model is characterized by τ_0 =16 MPa and δ_1=6 mm. The value of bond strength τ_0 and free-end slip δ_1 are selected taking into account the bond constitutive model for cast-in ribbed bars presented in the Model Code 2010 (fib 2013), and the experimental tests of embedded bars glued to concrete with epoxy adhesive available in literature

(Mahrenholtz 2012; Valerio et al. 2009; Dalfré et al. 2011; Owa et al. 2012; Godat et al. 2012) and reported in Annex A.

Regarding the present model, a sensitivity analysis to study the influence of each input parameter has been carried out by Bianco et al. (2014), demonstrating that using the proposed simplified bond model the results are not significantly affected by changing the values of τ_0 and δ_1, but they are significantly affected by the values attributed to θ and α.

The predicted values V_f^{II} obtained by the formulation proposed in section 4.4 are presented in Table 4.3. Where V_f^{II} is the minimum between $V_f^{II,bd}$, and $V_f^{II,y}$, the strengthening contribution of the ETS system corresponding to the debonding and steel yielding of the ETS bars, respectively.

Table 4.3 Mechanical-based model assessemnt.

Beam ID	V_f^{exp}	$V_f^{II,bd}$	$V_f^{II,y}$	Failure[a]	V_{fd}^{II}	k^{II} γ_f=1[b] (γ_f=1.3[c])
	[kN]	[kN]	[kN]		[kN]	
Vertical						
0S-S300-90	37.017		43.2	D	27.54	1.03 (1.34)
2S-S300-90	44.199	35.8				1.23 (1.60)
0S-S180-90	60.453					0.79 (1.02)
2S-S180-90	98.847	76.9	86.4	D	59.15	1.29 (1.67)
4S-S180-90	35.64					0.46 (0.60)
A-3 S300.90	31.15	24.9	42.5	D	19.18	1.25 (1.62)
A.5 S300.90/300.90	40.3					1.62 (2.1)
B.3 E300.90	21.31	46.5	56.9	D	35.73	0.46 (0.60)
SLB P4d-2S8@d	53.2	71.73	53.28	Y	40.99	1.00 (1.3)
Inclined						
0S-S300-45	115.53					1.89 (2.46)
2S-S300-45	99.036	94.6	61.1	Y	47.00	1.62 (2.11)
4S-S300-45	119.18					1.95 (2.54)
0S-S180-45	127.66					1.04 (1.36)
2S-S180-45	157.6	147.6	122.2	Y	94.00	1.29 (1.68)
4S-S180-45	127.58					1.04 (1.36)
A.4 E300.45	57.07	40.7	60.1	D	31.31	1.40 (1.82)
B.4 E300.45	98.52	89.99	80.5	Y	61.89	1.22 (1.59)

[a] Failure type based on the analytical results: D, debonding, Y, yielding

[b] Average k^{II} (γ_f =1):1.21

[c] Average k^{II}(γ_f =1.3):1.57

The design values V_{fd}^{II} are also presented in Table 4.3, where a γ_f partial safety factor equal to 1.3 is assumed, in order to obtain design values lower than the experimental values for the 90% of the analyzed beams. The analytical predictions, V_f^{II}, their corresponding design values, V_{fd}^{II}, and the experimental results, $V_f^{\exp}$, are compared in Fig.4.7. The two lines limiting the deviation of the predicted values from the experimental values to $\pm$ 30% are also represented in Fig 4.7. Almost all of the results fall within these bounds. The values of the ratio $k^{II} = V_f^{\exp} / V_f^{II}$, included in Table 4.3, have an average value of 1.21 and a standard deviation of 0.42, while when using the design values V_{fd}^{II}, an average value of 1.57 was obtained for the k^{II} ratio (values within round brackets in Table 4.3).

In the cases where more than one ETS bar is installed in a cross section, a detrimental interaction effect on the strengthening capacity of each bar should be considered. For the analyzed beams the present model can simulate this interaction by limiting the width of the concrete prims to $b_w/2$; this assumption can be generalized by limiting the width of the concrete prism to the space between the bars in the same section of the beam, and checking for geometric compatibility.

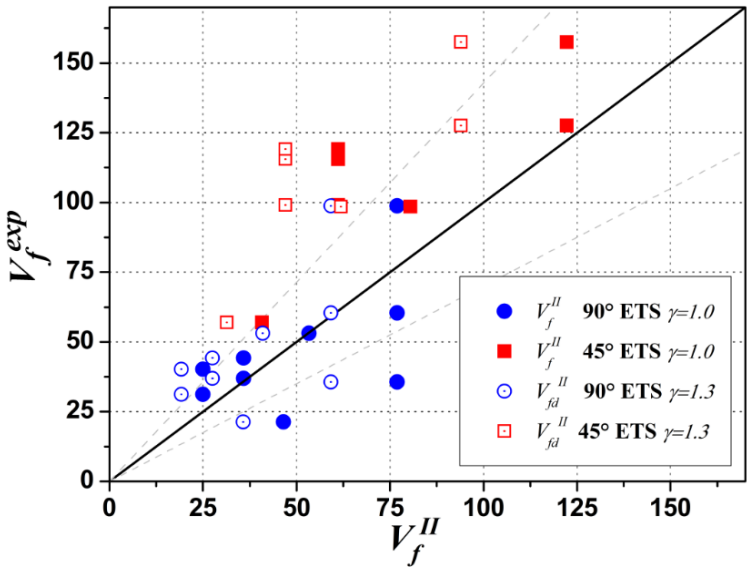

Fig. 4.7. V_f^{II} and V_{fd}^{II} vs $V_f^{\exp}$ according to the mechanical-based approach.

Since this mechanical model neglects the influence of the existing steel stirrups on the ETS strengthening contribution, for each ETS strengthening solution there is a single V_f^{II}, independent from the percentage of existing stirrups, which is not supported by the experimental results (Fig 4.1). A

reduction factor, function of the internal transverse steel reinforcement, could be introduced, as proposed for EBR and NSM strengthening (Chen et al. 2013; Chen et al. 2010; Chaallal and Mofidi 2011; Li and Delmas 2001; Pellegrino and Modena 2006). Like the experimental-based model, the mechanical-based model is able to differentiate between yield and debonding failure, as proved by the results reported in Table 4.3.

4.6 Conclusion

This Chapter presents the results of an experimental program on RC beams strengthened in shear using the ETS technique. The effectiveness of this technique was evaluated by studying the influence of three shear reinforcement ratio of existing steel stirrups (ρ_{sw}= 0%, 0.10%, 0.17%), spacing (300mm and 180mm) and inclination (90° and 45°) of steel ETS bars. The data obtained in the experimental program carried out, together with the experimental results available in literature dealing with the ETS technique were used to assess the predictive performance of two analytical approaches, denominated as *experimental-based* and *mechanical based* that were herein proposed for the estimation of the shear strengthening contribution assured by steel ETS bars.

The tested strengthened ETS beams exhibited a significant increase of load carrying capacity and deflection capacity for both vertical and inclined bars. However, the configuration with inclined bars has assured a much higher effectiveness, which is justified by the fact that for this latter configuration a higher available bond length was assured. Inclined bars were able to mobilize integrally the strength capacity of the ETS shear reinforcement, while in vertical ETS bars the resisting bond length of the bars crossed by the critical shear crack may have been not enough to mobilize its yield strain. As expected, the effectiveness of the ETS technique has decreased with the percentage of existing steel stirrups, especially for vertical ETS bars. The obtained results demonstrate that the ETS shear strengthening technique is an effective and competitive solution.

In terms of analytical models, the so called "experimental-based approach" is based on the concept of effective strain $\left(\varepsilon_{fe}^{I}\right)$, and an equation was proposed to obtain ε_{fe}^{I}. This equation is dependent of the ETS orientation β and of the parameter $\left(E_{fw}\rho_{fw} + E_{sw}\rho_{sw}\right)/\left(f_{cm}^{2/3}\right)$ that includes the percentage of ETS $\left(\rho_{fw}\right)$, the percentage of steel stirrups $\left(\rho_{sw}\right)$ and the concrete compressive strength $\left(f_{cm}\right)$. The analytical $\left(V_f^I\right)$ and the experimental $\left(V_f^{\exp}\right)$ results of the ETS shear contribution were compared considering the ratio k $\left(k^I = V_f^{\exp}/V_f^I\right)$, whose average value was 1.08. This formulation provided

satisfactory results, and evidenced the clearly different behavior between vertical and inclined strengthening, by detecting the steel yielding only in 45° installed bars.

The so-called "mechanical-based approach" is derived from a previous analytical model developed for NSM shear strengthened beams. This model is conceptually more reliable since it considers a bond constitutive law to evaluate the contribution of a single ETS bar, as well as the concrete fracture by reducing the available resisting bond length with the progress of the concrete fracture. The formulation provided satisfactory results, and the analytical $\left(V_f^{II}\right)$ and the experimental $\left(V_f^{\exp}\right)$ results of the ETS shear contribution were compared, and an average value of 1.21 for the $k^{II} = V_f^{\exp} \big/ V_f^{II}$ ratio was obtained.

The two conceptually different approaches have predicted values with similar level of accuracy, however the experimental-based approach has provided a dispersion of results lower than the mechanical-based model. Nevertheless, in terms of structural safety, by adopting for both approaches a partial safety factor of γ_f=1.3, the shear strengthening contribution of 90% of the analyzed beams is less than the one recorded experimentally.

5

Assessment of the behavior of ETS strengthened beams by FEM-based material nonlinear analysis

5.1 Introduction

The evaluation of the predictive performance through the finite element method (FEM) of reinforced concrete (RC) elements failing in shear requires a material nonlinear constitutive model able to simulate the progressive shear stiffness degradation of the cracked concrete. In case of a smeared crack FE model that adopt a fix-crack model (Rots et al. 1985; de Borst and Nauta 1985) a reasonable approach to simulate the shear stress sliding along the crack is a fundamental factor (Maekawa et al. 2003; Rots 2002). The load-deflection response up to ultimate load as well as the failure mode could be accurately simulated if the assumption on the crack stiffness is properly chosen.

A widely used procedure to simulate the shear stiffness degradation in RC concrete structures consists in the introduction of a cracked shear modulus by the adoption of a "shear retention factor" In the past, the shear retention factor was assumed as a constant value (Kwak and Filippou 1990; Hu and Schnobrich 1990; ASCE 1982), nevertheless this involved possible "stress locking" and uncertainty on the parameter to be chosen. Afterwards, the shear retention was often assumed as a function that reduces the shear stress transfer between the crack planes as the normal crack strain increases (Cedolin and Dei Poli 1977; Kolmar and Mehlhorn 1984; Rots 1988; Barros 1995; Sena-Cruz 2004;). This model takes into account the fact that friction (aggregate interlock) between the two surfaces of a crack diminishes with the increase of the crack opening. Kolmar and Mehlhorn (1984) suggested several expressions for the shear retention factor function concluding that a sharp drop followed by a continuous shear stiffness reduction is the most appropriate. Shear retention factor model can also implemented by using different function based on shear stress-strain or shear stress-slip relationship, taking into account parameters as compressive strength, crack width, crack slip and maximum

aggregate size as presented in (Teng et al. 2013). (Kolmar 1986) proposed also to express the shear retention function taking into account the percentage of steel reinforcement crossing the shear plane.
This adoption of a shear retention function leads to accurate results with the exception of structures that fail by the formation of a critical shear crack; in fact in this case the response results too stiff, a too high load carrying capacity is usually obtained and the occurrence of a shear failure is not is correctly predicted.
A shear softening diagram was also introduced to simulate the shear fracture process (Rots and de Borst 1987) as an alternative to the shear-retention function. This Chapter is dedicated to the assessment of the shear-crack diagram ($\tau_t^{cr} - \gamma_t^{cr}$) proposed to model the sliding component of the crack constitutive law implemented into a multi-directional fixed smeared crack model (Ventura-Gouveia 2008, 2011). The constitutive model is briefly described in this work. A deep investigation on the parameters influencing the proposed model is carried out by simulating the experimental tests performed on RC beams strengthened for shear according to the Embedded Through-Section (ETS) technique.

5.2 Numerical Model

5.2.1 Introduction

In a previous work (Barros et al. 2011) implemented a total crack shear stress-shear strain approach with the aim to reproduce numerically the decrease of shear stress transfers with the increase of the crack sliding and crack opening in order to obtain better simulation of the strengthened beams failing in shear and in flexural/shear. Although, for stress states where pronounced shear is present, a more sophisticated approach must be used.

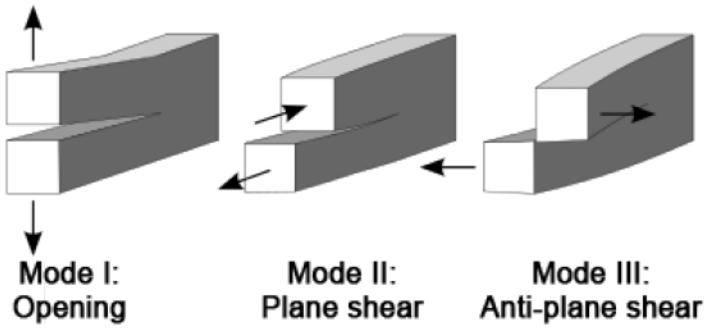

Fig. 5.1 Fracture mode I, II and III, adapted form (ACI Committee 446 1992).

(Ventura-Gouveia et al. 2008) introduced in the previous model an important aspect in the treatment of the concrete fracture mode II (Fig. 5.1), by adopting a softening diagram to simulate the crack shear

stress vs. crack shear strain (Rots and de Borst 1987). This model, presented in section 5.2, is capable of simulating with high accuracy RC beams failing in shear (Barros, et al. 2013a, 2013b). This enhancement on the constitutive model allows capturing the maximum carrying capacity, deformational response, and crack pattern of RC beams failing in shear. A preliminary assessment of the potentials of the model was performed and the result are reported in Annex C.

In the following sections, a briefly description of the formulation of the multi-directional fixed smeared crack model is presented and the crack shear stress vs. crack shear strain softening diagram developed by Ventura-Gouveia (2011) is described. The model is implemented in FEMIX, a FEM-based computer program (Sena-Cruz et al. 2007).

5.2.2. Multi-directional fixed smeared crack model

At the domain of an integration point (IP) of a plane stress finite element and for the case of cracked concrete, the constitutive law is defined by the following equation:

$$\Delta\underline{\sigma} = \underline{D}^{crco}\ \Delta\underline{\varepsilon} \tag{5.1}$$

being $\Delta\underline{\sigma}$ and $\Delta\underline{\varepsilon}$ the vectors of the incremental stress and incremental strain components. In Eq. 5.1, $\underline{D}^{crco}$ is the cracked concrete constitutive matrix, obtained by the following equation (Sena-Cruz 2004):

$$\underline{D}^{crco} = \underline{D}^{co} - \underline{D}^{co}\left[\underline{T}^{cr}\right]^{T}\left(\underline{D}^{cr} + \underline{T}^{cr}\,\underline{D}^{co}\left[\underline{T}^{cr}\right]^{T}\right)^{-1}\underline{T}^{cr}\,\underline{D}^{co} \tag{5.2}$$

where $\underline{D}^{co}$ is the constitutive matrix for concrete between cracks, assumed with a linear elastic behaviour, $\underline{T}^{cr}$ is the matrix that transforms the stress components from the coordinate system of the finite element to the local crack coordinate system, and $\underline{D}^{cr}$ is the crack constitutive matrix:

$$\underline{D}^{cr} = \begin{bmatrix} D_{I}^{cr} & 0 \\ 0 & D_{II}^{cr} \end{bmatrix} \tag{5.3}$$

Where D_{I}^{cr} and D_{II}^{cr} are the constitutive softening/hardening modulus corresponding to crack opening mode I (tensile) and crack sliding mode II (shear), respectively. The behaviour of non-completely closed cracks formed in an *IP* is governed by the following relationship:

$$\Delta\underline{\sigma}_{1}^{cr} = \underline{D}^{cr}\,\Delta\underline{\varepsilon}_{1}^{cr} \tag{5.4}$$

being $\Delta\underline{\sigma}_1^{cr}$ and $\Delta\underline{\varepsilon}_1^{cr}$, respectively, the local vector of the incremental crack stress components and the local vector of the correspondent incremental crack strain components in the coordinate system of the crack.

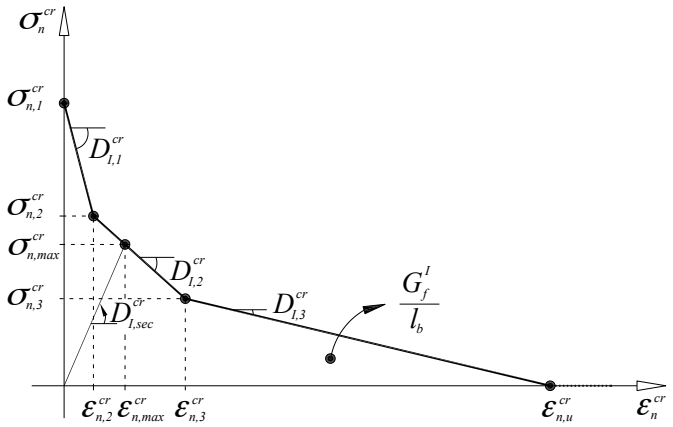

Fig. 5.2 Trilinear stress-strain diagram to simulate the fracture mode I crack propagation ($\sigma_{n,2}^{cr} = \alpha_1\ \sigma_{n,1}^{cr}$, $\sigma_{n,3}^{cr} = \alpha_2\ \sigma_{n,1}^{cr}, \varepsilon_{n,2}^{cr} = \xi_1\ \varepsilon_{n,u}^{cr}, \varepsilon_{n,3}^{cr} = \xi_2\ \varepsilon_{n,u}^{cr}$).

A simple Rankine criterion is used to detect crack initiation. When the maximum principal tensile stress exceeds the tensile strength at an IP of a finite element, the material contained in its influence volume changes from uncracked to cracked state. The crack propagation is mainly controlled by the shape of the tensile-softening diagram represented in Fig. 5.2 and the material fracture energy (Mode I) . The trilinear diagram is defined by the normalized stress, α_i, and strain, ξ_i, parameters that represent the transitions points between the linear segments of this diagram. The ultimate crack strain, $\varepsilon_{n,u}^{cr}$, is defined as a function of the parameters α_i and ξ_i, fracture energy, G_f^I, tensile strength, $f_{ct} = \sigma_{n,1}^{cr}$, and crack band width, l_b, as follows (Bazant and Oh 1983; Sena-Cruz 2004);

$$\varepsilon_{n,u}^{cr} = \frac{2}{\xi_1 + \alpha_1\xi_2 - \alpha_2\xi_1 + \alpha_2}\frac{G_f^I}{f_{ct}l_b} \tag{5.5}$$

The fracture Mode II modulus, D_{II}^{cr}, is obtained from:

$$D_{II}^{cr} = \frac{\beta}{1-\beta}G_c \tag{5.6}$$

where β is the shear retention factor and G_c the concrete elastic shear modulus. The parameter β is defined as a constant value or as a function of the actual crack normal strain, ε_n^{cr} and of the ultimate crack normal strain, $\varepsilon_{n,u}^{cr}$ as follows,

$$\beta = \left(1 - \frac{\varepsilon_n^{cr}}{\varepsilon_{n,u}^{cr}}\right)^{p_1} \tag{5.7}$$

When a linear decrease of β with the increase of ε_n^{cr} is assumed, then $p_1 = 1$. Values of the exponent p_1 larger than the unit correspond to a faster decrease of the parameter (Sena-Cruz 2004).

Although, the description of the model is made using the formation of one crack in an IP, the multi-directional fixed smeared crack model implemented in FEMIX computer program is capable of simulating the formation of multi-cracks in each IP (Sena-Cruz 2004; Ventura-Gouveia 2011).

5.2.3 Shear-Softening diagram

The use of softening diagrams to reproduce the fracture mode I process is common in smeared and discrete crack models, but the use of softening diagrams to model the shear stress transfer across the crack is less usual. As described in the previous section, to simulate the fracture mode II process a shear retention factor is currently used (Rots and de Borst 1987). According to this approach, the shear stress transfer between the crack planes decreases with the increase of the normal crack strain (see Eq. 5.7). In most structures assumed to be in a state of plane stress, this strategy leads to simulations with reasonable accuracy. Exceptions occur in structures that fail by the formation of a critical shear crack. For these cases the simulation of the structural softening with high accuracy requires the adoption of a softening crack shear stress vs. crack shear strain relationship (Rots and de Borst 1987).

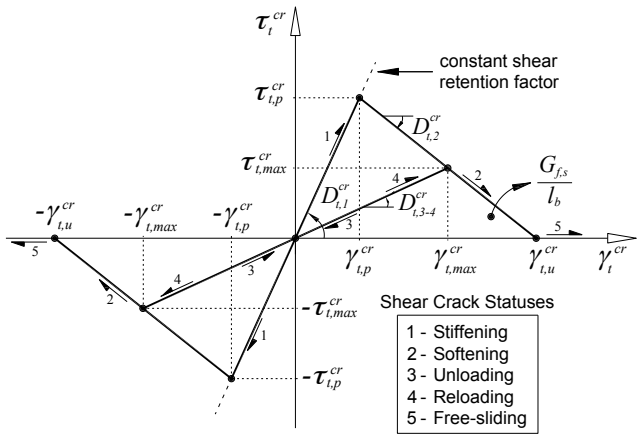

Fig. 5.3: Diagram to simulate the relationship between the crack shear stress and crack shear strain component, and possible shear crack statuses.

In this section a softening diagram to simulate the crack shear stress strain behaviour is described. The proposed crack shear diagram is represented in Fig. 5.3. The shear softening diagram starts at the origin because, according to the crack initiation criterion, when a crack initiates the crack shear stress is null.

As a consequence of the rotation of the directions of principal stresses, shear stresses can develop across the surfaces of the crack (Rots and de Borst 1987). The crack shear stress increases linearly until the crack shear strength is reached (first branch of the shear crack diagram), followed by a decrease in the shear residual strength (softening branch).

The diagram represented in Fig. 5.3 is defined by the following expressions. The positive part of the diagram is explained here, being the treatment of the negative part straightforward.

$$\tau_t^{cr}\left(\gamma_t^{cr}\right)=\begin{cases} D_{t,1}\,\gamma_t^{cr} & 0<\gamma_t^{cr}\le\gamma_{t,p}^{cr} \\ \tau_{t,p}^{cr}-\dfrac{\tau_{t,p}^{cr}}{\left(\gamma_{t,u}^{cr}-\gamma_{t,p}^{cr}\right)}\left(\gamma_t^{cr}-\gamma_{t,p}^{cr}\right) & \gamma_{t,p}^{cr}<\gamma_t^{cr}\le\gamma_{t,u}^{cr} \\ 0 & \gamma_t^{cr}>\gamma_{t,u}^{cr} \end{cases} \tag{5.8}$$

The shear fracture modulus, $D_{t,1}^{cr}$ is defined by Eq. 5.6, being D_{II}^{cr} replaced by $D_{t,1}^{cr}$, with the shear retention factor, β assuming a constant value in the range]0,1[. The peak crack shear strain, $\gamma_{t,p}^{cr}$ is obtained by the following equation:

$$\gamma_{t,p}^{cr}=\frac{\tau_{t,p}^{cr}}{D_{t,1}^{cr}} \tag{5.9}$$

being, $\tau_{t,p}^{cr}$, the crack shear strength acquired from the input data.

The ultimate crack shear strain, $\gamma_{t,u}^{cr}$ is obtained by Eq. 5.9) and depends on the crack shear strength, $\tau_{t,p}^{cr}$, on the shear fracture energy (mode II fracture energy), $G_{f,s}$ and on the crack bandwidth, l_b as follows:

$$\gamma_{t,u}^{cr}=\frac{2G_{f,s}}{\tau_{t,p}^{cr}\,l_b} \tag{5.10}$$

It is assumed in the present approach that the crack bandwidth, used to assure that the results are independent of the mesh refinement, can also be used to define the dissipated energy in the mode II fracture process. As a consequence of the formation of other cracks in the neighbourhood of existing cracks, these existing cracks can close or reopen. The model must take into account this change of crack status. For the opening mode I the model takes this into account (Sena-Cruz 2004) and for the crack shear component a similar approach is used. So, five shear crack statuses are proposed and their meaning is schematically represented in Fig. 5.3. As shown in Fig. 5.3 the evaluation of the fracture mode II softening modulus D_{II}^{cr} of Eq. 5.3, depends on the branches defining the diagram. The crack

mode II modulus of the first linear branch of the diagram is defined by Eq. 5.6, the second linear softening branch is defined by

$$D_{II}^{cr} = D_{t,2}^{cr} = -\frac{\tau_{t,p}^{cr}}{\gamma_{t,u}^{cr} - \gamma_{t,p}^{cr}} \tag{5.11}$$

and the crack shear modulus of the unloading and reloading branches is obtained from

$$D_{II}^{cr} = D_{t,3-4}^{cr} = \frac{\tau_{t,\max}^{cr}}{\gamma_{t,\max}^{cr}} \tag{5.12}$$

being $\gamma_{t,\max}^{cr}$ and $\tau_{t,\max}^{cr}$ the maximum crack shear strain already attained and the corresponding crack shear stress determined from the softening linear branch. Both components are stored to define the unloading/reloading branch (see Fig 5. 3).

In free-sliding status, $\left|\gamma_t^{cr}\right| > \left|\gamma_{t,u}^{cr}\right|$ the crack mode II stiffness modulus, $D_{II}^{cr} = D_{t,5}^{cr}$ is null. To avoid numerical instabilities in the calculation of the stiffness matrix, when the crack shear status is free-sliding a residual crack shear stress value is assumed for this phase of sliding. A free-sliding status is also assigned to the shear crack status when $\varepsilon_n^{cr} > \varepsilon_{n,u}^{cr}$. The details about how the shear crack statuses are treated can be found elsewhere (Ventura-Gouveia 2011). The crack shear stress vs. shear strain diagram represented in Fig. 5.3 was adopted in the simulations performed in the present work, but other more sophisticated diagrams were also implemented in FEMIX computer program, and their corresponding formulations can be found elsewhere (Ventura-Gouveia 2011). The accuracy of the model was already demonstrated for NSM CFRP shear strengthened beams (Barros et al. 2013b).

5.3 Predictive performance of the numerical model

5.3.1 Finite element mesh, integration schemes and constitutive laws for the materials

The predictive performance of the presented model is assessed using the experimental tests presented in Chapter 3 on T-cross section reinforced concrete (RC) beams shear strengthened according to the Embedded Through-Section (ETS) technique using steel bars. For modeling the concrete part of the RC beams 8-noded serendipity plane stress (PSTE) finite elements of average size of 25x25mm were used in all the numerical simulations. The longitudinal steel bars, stirrups and the ETS strengthening bars were modeled with 3-nodes embedded cable (EC) type element (one degree-of freedom per each node) that were assumed perfectly bonded to the surrounding concrete. A Gauss-Legendre integration scheme

was adopted for both PSTE and EC elements, of 2x2 integration points (IP) in case of PSTE, and 2 IP for ECs. Two sets of smeared cracks were allowed to be formed at each integration point, according to a threshold angle of 30° for crack opening criterion (Sena-Cruz and Barros 2004). A modified version of the Newton Rapson method was adopted, i.e. the stiffness matrix of the structure in the iterations of a load increment is the one evaluated in the first iteration, $K_T^i = K_T^0$. The loading process was controlled by the arch length technique (Ventura-Gouveia et al. 2006) by imposing an increment of vertical displacement in point P (Fig. 5.4) that varied between 0.1 and 0.3 mm, and an energy convergence criteria of 1.0 ‰ was adopted. An example of a finite element mesh used for the simulation of 4S-S180-45 beam is represented in Fig. 5.4. The values that define the concrete constitutive model discussed in section 5.2 are indicated in Table 5.1. The trilinear tension-softening diagram represented in Fig. 5.2 was adopted to simulate the concrete fracture mode I process. The value of the concrete tensile strength and fracture energy were obtained according to the Model Code recommendations (CEB-FIB 1990).

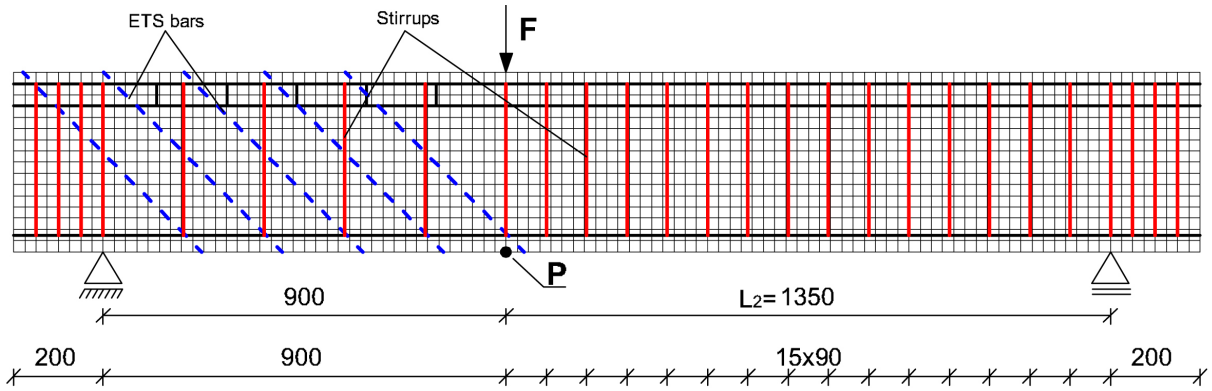

Fig. 5.4 Finite element mesh for beam 4S-S180-45 (dimensions are in mm)

Table 5.1: Values of the parameters of the concrete constitutive model

Poisson's ratio (ν_c)	0.15
Initial Young's modulus (E_c)	30.7 N/mm^2
Compressive strength (f_c)	29.7 N/mm^2
Trilinear tension-softening diagram	f_{ct} = 1.9N/mm^2, G_f = 0.07 N/mm ξ_1 = 0.004, α_1 =0.3, ξ_2 = 0.05, α_2 =0.2
Parameter defining the mode I fracture energy available to the new crack [Sena-Cruz 2004]	p_2 = 2
Crack bandwidth (l_b)	Square root of the area of Gauss integration point
Threshold angle	α_{th}=30°
Maximum number of cracks per integration point [Sena-Cruz 2004]	2
Ultimate crack shear sliding	MAXIMUM_CRACKWIDTH

For modeling the crack shear behavior, the $\tau_t^{cr} - \gamma_t^{cr}$ diagram represented in Fig. 5.3 was used, and the influence on the beam's response of the parameters that define this diagram was investigated, since the load carrying and deflection capacity, as well as the crack pattern of this type of beams are quite dependent on the values adopted for this crack shear softening diagram. Furthermore, and according to the knowledge of the author of the present work, this type of analysis is not available in the literature, therefore valuable contribution can be done in this respect. For assessing the values for the $\tau_t^{cr} - \gamma_t^{cr}$ of the concrete model of the tested beams (β, $\tau_{t,p}^{cr}$, $G_{f,s}$), an inverse analysis was executed by fitting as much as possible, not only the load versus deflection and the load versus strain relationships registered experimentally, but also the crack pattern observed in the failure stage of the beams. From this inverse analysis, it was obtained the interval of values obtained for β, $\tau_{t,p}^{cr}$ and $G_{f,s}$ that assured simulations of acceptable accuracy under the compromise of the deflection response and crack pattern. These values are indicated in Table 5.2, was well as the values that best fit (in bold) the behavior of the tested beams. It is observed that $\tau_{t,p}^{cr}$ can be assumed equal to 1.0 MPa ($\tau_{t,p}^{cr} \approx 0.2\sqrt{f_{cm}}$), which is in agreement with the values adopted in Barros et al (2013a, 2013b).

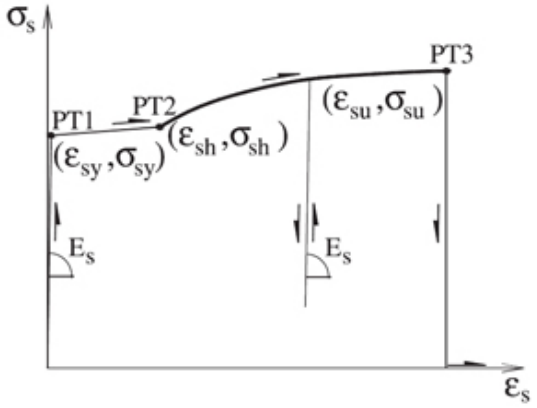

Fig. 5.5 Uniaxial constitutive model for the internal reinforcement and ETS bars

For modeling the behavior of the longitudinal steel bars, stirrups and ETS bars, both in tension and in compression, a trilinear stress-strain diagram was adopted (Fig 5.5) (Sena-Cruz 2004). This diagram is defined by the points PT1= ($\varepsilon_{sy}, \sigma_{sy}$), PT2= ($\varepsilon_{sh}, \sigma_{sh}$) and PT3= ($\varepsilon_{su}, \sigma_{su}$), and a parameter *p* that defines the shape of the last branch of the diagram (Fig 5.5). Unloading and reloading linear branches with slope $E_s = \left(\sigma_{sy} / \varepsilon_{sy}\right)$ are assumed in the present approach. The values for defining this diagram were obtained from tensile tests, and the obtained values are those indicated in Table 5.3.

Table 5.2. Values of the performed numerical simulation, minimum and maximum used value.

	β	$\tau_{t,p}^{cr}$	$G_{f,s}$
0S-REF	**0.175**	**1.00**	**0.07**
min	0.150	0.85	0.07
max	0.22	1.00	0.1
0S-S300-90	**0.15**	**1.00**	**0.08**
Min	0.141	0.85	0.07
Max	0.150	1	0.14
0S-S180-90	**0.144**	**1.00**	**0.1**
Min	0.1	1.00	0.1
Max	0.150	1.1	0.2
0S-S300-45	**0.10**	**1.00**	**0.50**
Min	0.03	0.85	0.14
Max	0.15	1	1.3
0S-S180-45	**0.10**	**1.00**	**0.2**
Min	0.064	1	0.1
max	0.15	1	0.768
2-REF	**0.15**	**1.00**	**0.08**
min	0.05	0.85	0.08
max	0.15	1.00	0.15
2S-S300-90	**0.12**	**1.00**	**0.12**
Min	0.10	1	0.12
Max	0.15	1	0.182
2S-S180-90	**0.1**	**1.00**	**0.18**
Min	0.10	1	0.14
Max	0.15	1.25	0.45
2S-S300-45	**0.075**	**1.00**	**0.6**
Min	0.03	0.85	0.14
Max	0.15	1.00	1.3
2S-S180-45	**0.017**	**1.00**	**1.00**
Min	0.017	1	0.89
Max	0.2	1.25	1.75
4S-REF	**0.1**	**1.00**	**0.22**
Min	0.05	1.00	0.1
max	0.15	1.25	0.25
4S-S300-90	**0.09**	**1.00**	**0.14**
Min	0.09	1.00	0.14
Max	1.15	1.0	0.213
4S-S180-90	0.075	1.00	0.45
Min	0.075	1.00	0.14
Max	0.15	1.50	0.50
4S-S300-45	**0.02**	**1.00**	**0.9**
Min	0.01	0.85	0.51
Max	0.07	1.75	2.0
4S-S180-45	**0.030**	**1.00**	**1.5**
Min	0.012	1	0.3
Max	0.200	3	2.5

Table 5.3: Values of the parameters of the steel constitutive model (Sena 1994)

Steel bar diameter (mm)	PT1		PT2		PT3		p
	$\varepsilon_{sy}[-]$	$\sigma_{sy}(MPa)$	$\varepsilon_{sh}[-]$	$\sigma_{sh}(MPa)$	$\varepsilon_{su}[-]$	$\sigma_{su}(MPa)$	
6	2.870×10^{-3}	573.94	2.870×10^{-3}	573.94	6.925×10^{-2}	666.67	1
8	2.530×10^{-3}	505.35	2.759×10^{-2}	505.35	1.28×10^{-1}	594.11	1
10	2.747×10^{-3}	549.35	2.750×10^{-2}	549.35	1.125×10^{-1}	641.83	1
12	2.637×10^{-3}	527.30	2.830×10^{-2}	527.30	1.000×10^{-2}	616.48	1
24	2.989×10^{-3}	597.88	2.989×10^{-3}	597.88	6.000×10^{-2}	708.07	1

5.3.2 Simulation and discussion

The load-deflection relationships obtained experimentally and numerically are compared in Fig. 5.6. The curves at red color and including circle markers were obtained by using for the $\tau_t^{cr} - \gamma_t^{cr}$ diagram the values in bold in Table 5.2. A shadow region is also indicated in this figure for each beam, which corresponds to the analysis where the minimum and the maximum values for the $\tau_t^{cr} - \gamma_t^{cr}$ parameters, indicated in Table 5.2, were used. Fig.5.6 shows that the numerical model is able to capture with good accuracy the load-deflection response of the beams. However, for some beams strengthened with vertical ETS bars, even the best simulations (using the bold values in Table 5.2) have predicted an ultimate load higher than the load registered experimentally, which may indicate that for this strengthening arrangement some further improvements should be adopted in the $\tau_t^{cr} - \gamma_t^{cr}$ diagram. Above a deflection of about 1.4 mm, the 4S-S300-90 beam exhibited an abnormal high decrease of stiffness during the experimental test, when the 4S-Ref reference beam is taken for comparison purposes, and therefore the model was not capable of matching with the same accuracy the behavior of this beam in this loading stage.

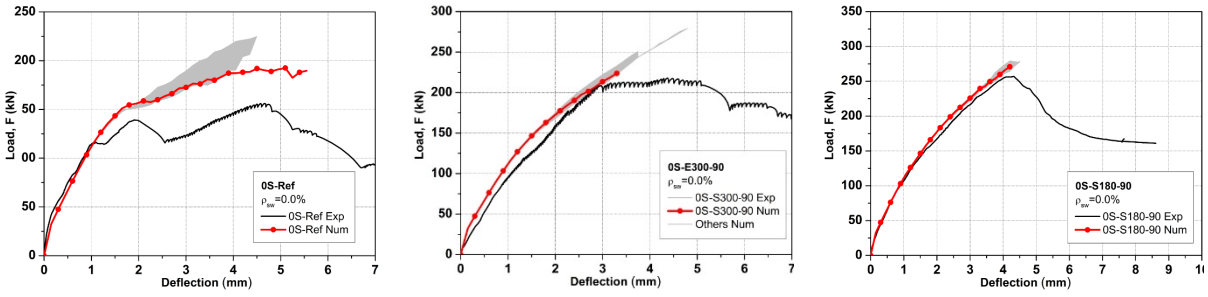

(a) 0S-REF **(b)** 0S-S300-90 **(c)** 0S-S180-90

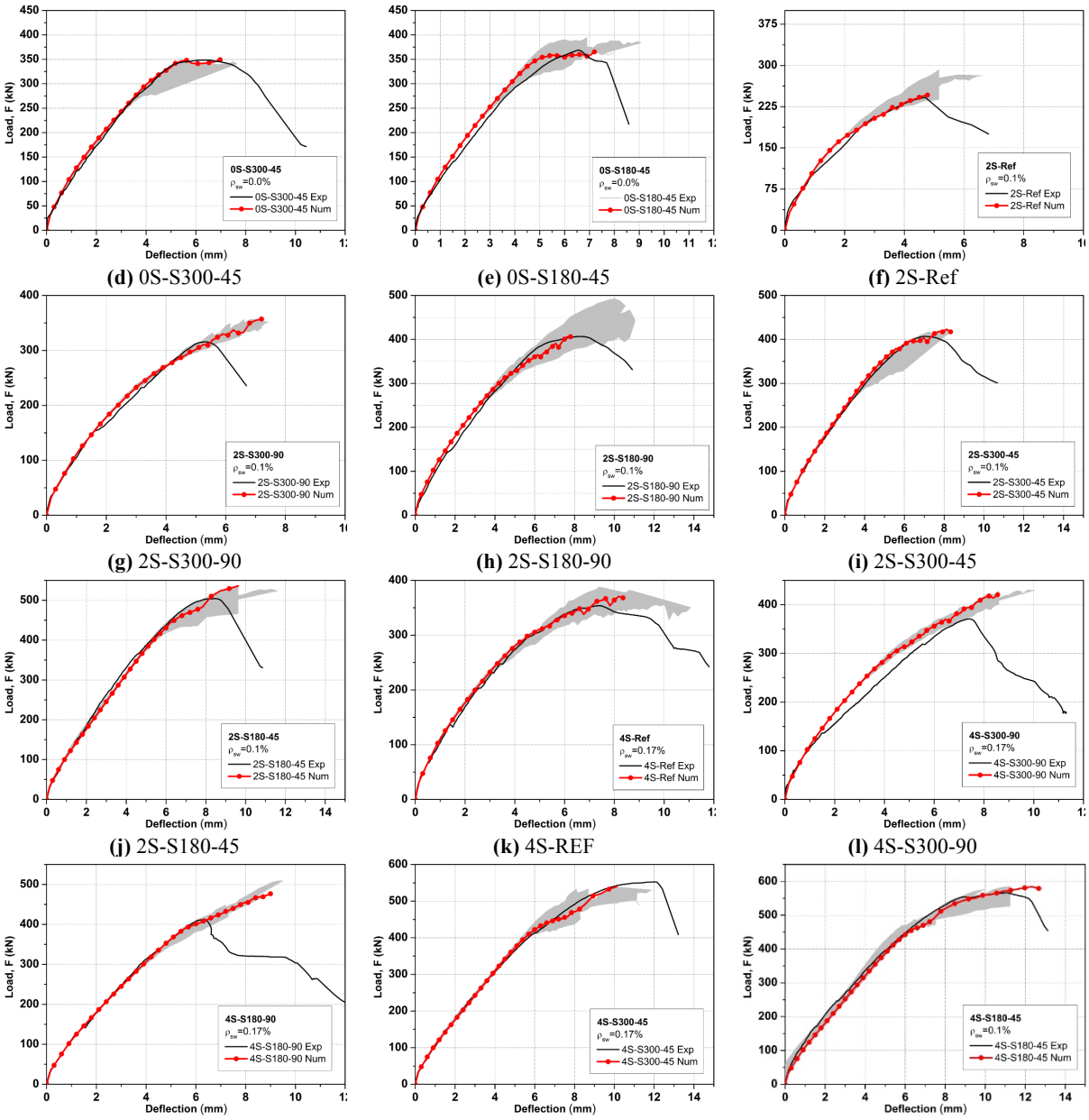

(d) 0S-S300-45 **(e)** 0S-S180-45 **(f)** 2S-Ref

(g) 2S-S300-90 **(h)** 2S-S180-90 **(i)** 2S-S300-45

(j) 2S-S180-45 **(k)** 4S-REF **(l)** 4S-S300-90

(m) 4S-S180-90 **(n)** 4S-S300-45 **(o)** 4S-S180-45

Fig. 5.6 Comparison between experimental and numerical Load vs. deflection at the loaded section relationships.

In Fig. 5.7 the crack patterns obtained from the numerical simulations are superimposed with the crack patterns registered experimentally at peak load (only macro-cracks are indicated). The experimental crack patterns were captured using a close-range photogrammetric technique. The localizations and inclinations of the shear failure crack and secondary cracks are captured with good accuracy. Furthermore, the shear failure mode registered experimentally in all the tested beams was successfully predicted, as it is possible to notice by observing the localization and profile of the cracks of "fully open crack status" (Sena-Cruz 2004) , those with no capacity of transferring any type of crack stress

component. The model was able of simulating the relevant aspects of the crack formation and propagation during the loading process. In fact, the first cracks were of flexural nature by crossing almost orthogonally the flexural reinforcement; however, due to the tension stiffening effect the width of these cracks remained relatively small. During the loading process of the beams, some of these cracks propagated towards the bottom surface of the flange with an average inclination of 45°; meanwhile a diffuse pattern of shear cracks of very small inclination formed and propagated just above the longitudinal reinforcement due to its high dowel resistance. (Chapter 3). The model was also able to catch the formation of higher number of shear cracks with the increase of reinforcing ratio of steel stirrups. By taking the results on the 4S-S180-45 beam, as representative, Fig. 5.8 evidences that the model is also capable of predicting the strain evolution in the ETS bars and steel stirrups with acceptable accuracy, since it should be taken into account the local character of the strain measurements and the perfect bond assumption considered for these reinforcements.

Based on the obtained results it seems acceptable to assume perfect bond between strengthening material and surrounding concrete, mainly if high rigor on the crack width evaluation is not of paramount relevance, such is the case. In fact, when steel shear reinforcements are crossed by a shear crack, due to their excellent bond conditions to the surrounding concrete, a gradient of strain in these reinforcements occur in the cracked section, and the yield stress is attained with a relatively small sliding and debonding length. However, the numerical simulations of RC beams shear strengthened with FRP-systems evidence the relevance of modeling the debond between FRPs and surrounding medium, due to the lower bond performance of FRP systems to the concrete substrate (Yuan et al. 2004; Bianco et al. 2009; Seracino et al. 2007; Mohamed Ali et al. 2008). This is assured by using a tau-slip constitutive model with interface finite elements, and is especially relevant when using the Externally Bonded Reinforcement (EBR) technique (Sayed et al. 2014; Zhang and Teng 2014; Teng et al. 2013; Manos et al. 2014; Godat et al. 2007; Hu et al. 2004). When NSM technique is used, due to the higher ratio between contact surface and cross section area of the currently used FRP laminates, as well as the confinement provided by surrounding concrete to the laminates that are installed into grooves open on the concrete cover of the beam's lateral faces, good predictive simulations were also obtained assuming perfect bond for these FRP or ETS systems (Barros et al. 2013a, 2013b).

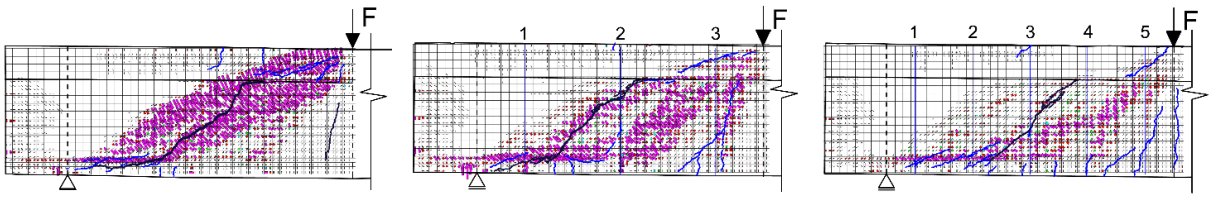

(a) 0S-REF **(b)** 0S-S300-90 **(c)** 0S-S180-90

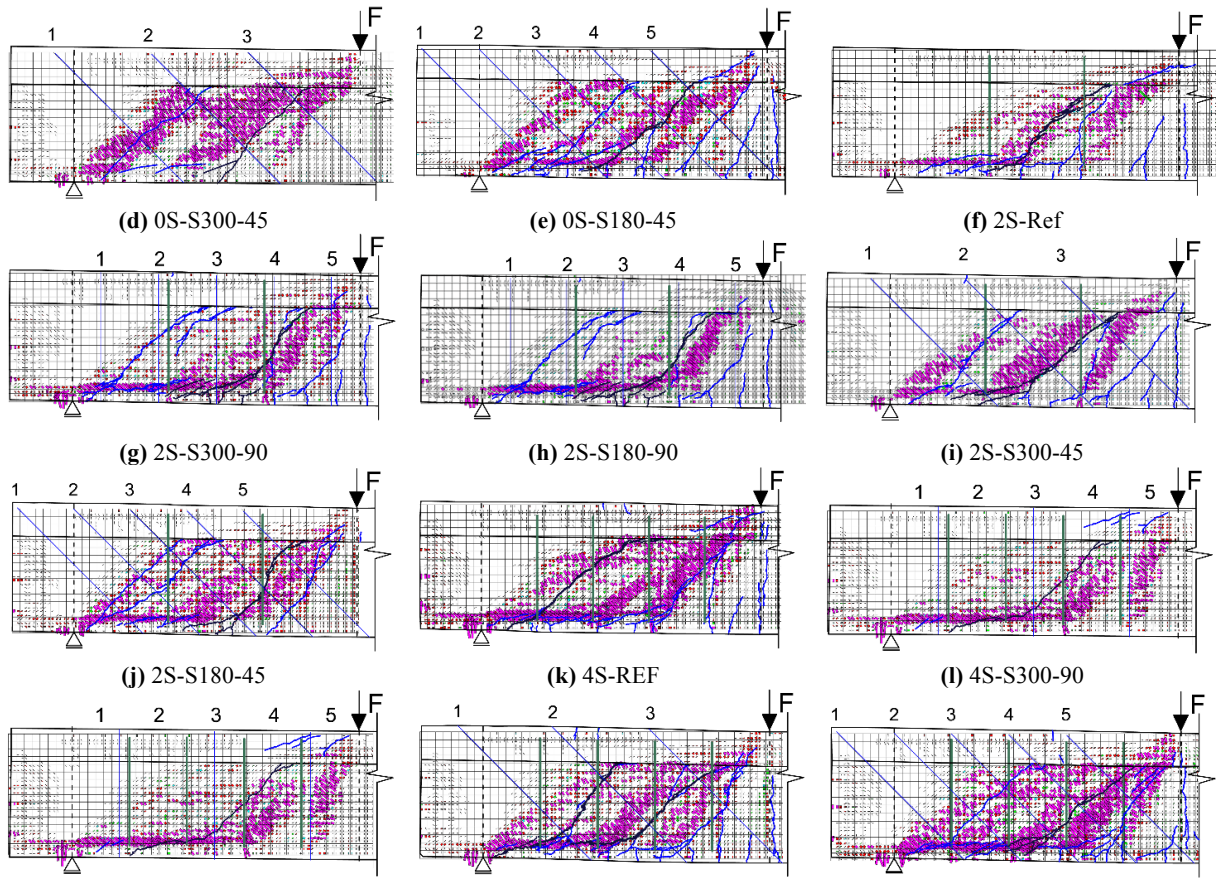

(d) 0S-S300-45 **(e)** 0S-S180-45 **(f)** 2S-Ref

(g) 2S-S300-90 **(h)** 2S-S180-90 **(i)** 2S-S300-45

(j) 2S-S180-45 **(k)** 4S-REF **(l)** 4S-S300-90

(m) 4S-S180-90 **(n)** 4S-S300-45 **(o)** 4S-S180-45

Fig. 5.7 Comparison between the experimental an numerical crack patterns

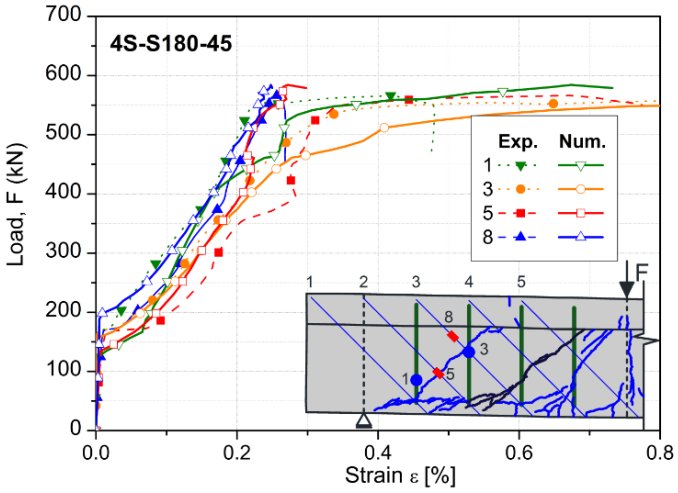

Fig. 5.8 Comparison between numerical and experimental strain measurement for beam 4S-S180-45.

5.4 Sensitivity analysis of the numerical model

5.4.1 Influence of the parameters of the crack shear softening diagram

The numerical simulations presented in the previous section have indicated that the force-deflection and the crack pattern are susceptible to the values adopted for the parameters that define the crack shear softening diagram, namely, $\tau_{t,p}^{cr}$, β and $G_{f,s}$ (Fig. 5.3). To have a better understanding on how these parameters influence the predictive behavior of the type of beams analyzed in the present work, a parametric study was executed by considering the 2S-REF beam. For each selected parameter a set of values are considered, while maintaining constant all the values adopted for the remaining parameters of the multi-directional fixed smeared crack. It is necessary to highlight that difficulties on the convergence procedure were observed in the simulation of beam 2S-REF (red curve indicated by arrow) obtained by using for the $\tau_t^{cr} - \gamma_t^{cr}$ diagram the values in bold in Table 5.2.

Influence of fracture energy mode II, $G_{f,s}$

Fig. 5.9 compares the load vs. deflection at loaded section obtained for three different values of the fracture energy mode II ($G_{f,s}$): 0.01, 0.08 and 1.5 N/mm (all the remaining parameters were maintained the same).

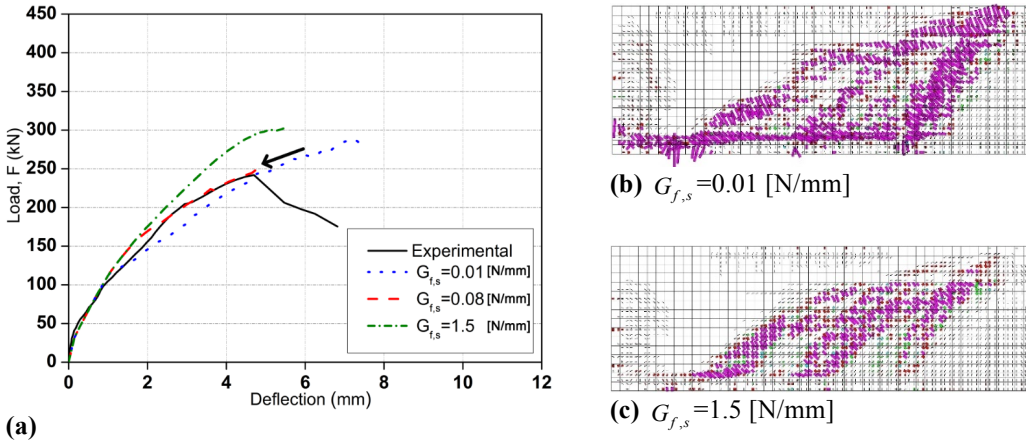

Fig. 5.9 Influence of $G_{f,s}$ on the: (a) relationship between the force and the deflection at the loaded section and (b–d) crack pattern corresponding to the assumed $G_{f,s}$.

This figure also compares the crack patterns obtained in the simulations corresponding to the $G_{f,s}$ of 0.01 and 1.5 N/mm. As expected, by decreasing $G_{f,s}$ the stiffness of the beam's response also decrease, since more cracks enter in the shear softening stage at smaller deflection. In terms of load carrying capacity, a tendency to a small decrease with the decrease of $G_{f,s}$ seems exist, since the analysis

corresponding to the $G_{f,s}$=0.08 N/mm was interrupted due to difficulties on the convergence procedure. By using a low value of $G_{f,s}$ wider cracks are formed, with a tendency to be localized just above the longitudinal reinforcement (Figs 5.9c-d)

Influence of Crack shear strength, $\tau_{t,p}^{cr}$

Fig. 5.10 compares the load vs. deflection at loaded section obtained for three different values of the crack shear strength $\tau_{t,p}^{cr}$ =0.5, 1.0 and 3.0 MPa (all the remaining parameters were maintained the same). The stiffness of the force-deflection response just after the formation of the critical shear crack is as higher as larger is the $\tau_{t,p}^{cr}$, since the entrance of the cracks in the shear softening stage is postponed, but after the cracks have entered in this stage the stiffness degradation is higher as larger is $\tau_{t,p}^{cr}$ due to the more abrupt shear stress decay. Since in these analysis the $G_{f,s}$ is maintained constant, the softening response for this diagram is as brittle as higher is $\tau_{t,p}^{cr}$, due to the decrease of the ultimate crack shear strain, $\gamma_{t,u}^{cr}$ (Fig 5.10b). The $\tau_{t,p}^{cr}$ seems do not have relevant influence on the maximum load carrying capacity of this type of RC beams. The crack patterns for the analysis with $\tau_{t,p}^{cr}$ of 0.5 and 3.0 MPa also support these conclusions, since for the smaller $\tau_{t,p}^{cr}$ (0.5 MPa) a few number of well-defined shear failure cracks (completely open) were formed compared to the crack pattern of the larger $\tau_{t,p}^{cr}$ (3.0 MPa), Fig. 5.10d. Furthermore, for the $\tau_{t,p}^{cr}$=0.5 MPa the shear failure crack has the tendency of propagating just above the longitudinal reinforcement.

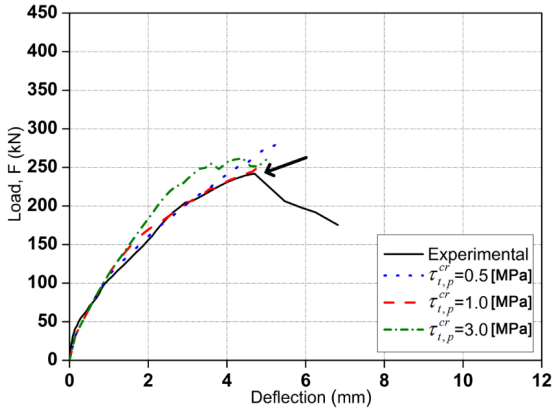

(a)

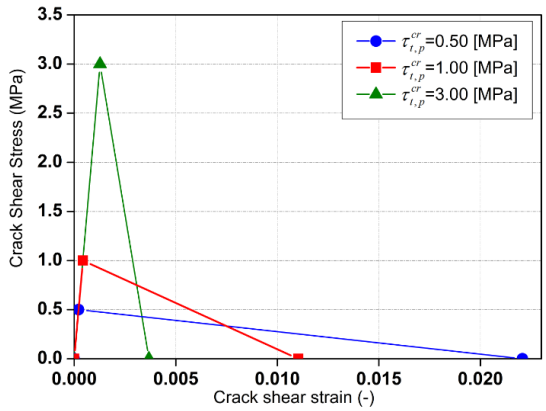

(b)

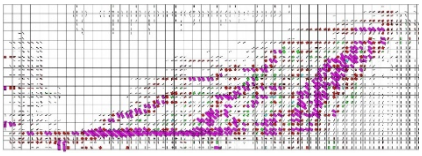

$\tau_{t,p}^{cr}$=0.5 (MPa)

(c)

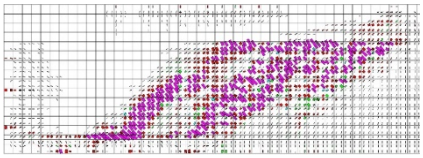

$\tau_{t,p}^{cr}$=3.0 (MPa)

(d)

Fig. 5.10 Influence of $\tau_{t,p}^{cr}$ on the: (a) relationship between the force and the deflection at the loaded section, (b) representation of the crack shear stress-shear strain diagram for the adopted $\tau_{t,p}^{cr}$, (c–d) crack pattern corresponding to the assumed $\tau_{t,p}^{cr}$.

Influence of beta β parameter

Fig. 5.11 compares the load vs. deflection at loaded section obtained for three different values of the shear retention parameter that influences the inclination of the first branch the $\tau_t^{cr} - \gamma_t^{cr}$ diagram: β =0.015, 0.15 and 0.6 (all the remaining parameters were maintained the same).

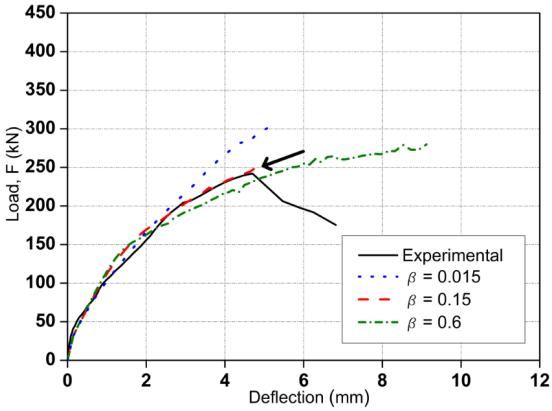

(a)

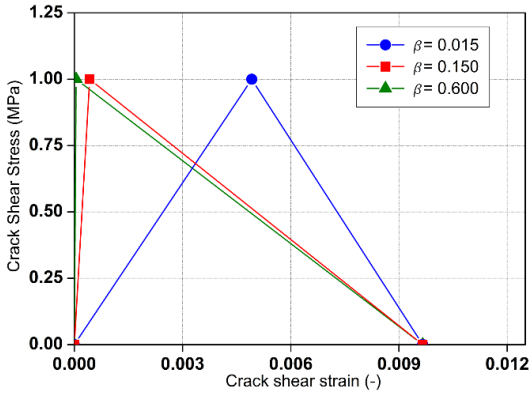

(b)

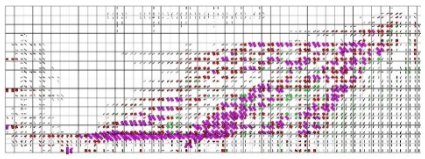

β =0.015

(c)

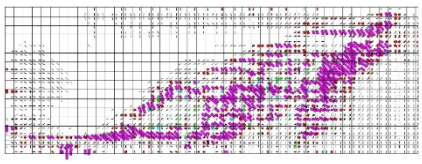

β =0.6

(d)

Fig 5.11 Influence of β on the: (a) relationship between the force and the deflection at the loaded section, (b) representation of the crack shear stress-shear strain diagram for the adopted β, (c–d) crack pattern corresponding to the assumed β.

The inclination of this first branch, $D_{t,I}^{cr}$, is defined by the value adopted for the β parameter according to Eq. (6), by obtaining the peak crack shear strain, γ_t^{cr}, from Eq. (9). Fig. 5.11b shows that the gradient of crack shear stress in this first branch decreases with β (smaller inclination of this branch with the

lower values of β). In consequence, the stiffness of the force-deflection just after the formation of the critical shear crack also decreases with β . However, since the peak crack shear strain, $\gamma_{t,p}^{cr}$, is as larger as smaller is β (Fig. 5.11), the entrance of the cracks in their softening stage is postponed, resulting a larger stiffness of the force-deflection response for smaller β values in the final stage of the response of the beams. Fig. 5.11 shows how the values of β can significantly affect the stiffness and load carrying capacity of the beam. The crack patterns for β =0.015 and β =0.6 are presented in Figs 5.11c-d, where the formation of wider cracks is visible for β =0.6 due to the larger deflection of the beam at its failure.

5.4.2 Comparison between the shear retention factor and the shear softening approach

Fig. 5.12 compares the force-deflection relationship at loaded section for beam 2S-Ref when using the shear retention function (Eq. 5.6 with $p_1 = 3$) and adopting the $\tau_t^{cr} - \gamma_t^{cr}$ diagram presented in Section 5.3. Up to a deflection of about 1 mm (that corresponds to the formation of the diagonal shear crack) the responses are quite similar; up to this stage, the curve is governed by the tensile behavior of the concrete. For higher values of deflection, the two approaches differ significantly. The shear retention factor approach, implemented with an incremental model, is not able to simulate the stiffness degradation induced by the shear deformation, i.e. cannot simulate a decrease of the crack shear stress transfer $\left(\tau_t^{cr}\right)$with the increase of the crack shear$\left(\gamma_t^{cr}\right)$As Fig. 5.12 clearly shows, this approach predicts a load carrying capacity much higher than the experimental one, while the proposed $\tau_t^{cr} - \gamma_t^{cr}$ diagram allows predicting correctly the expected results.

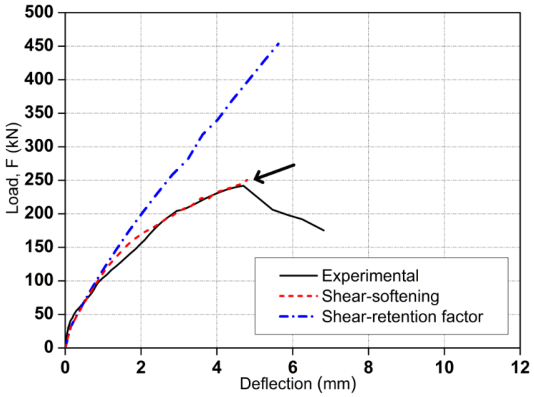

(a)

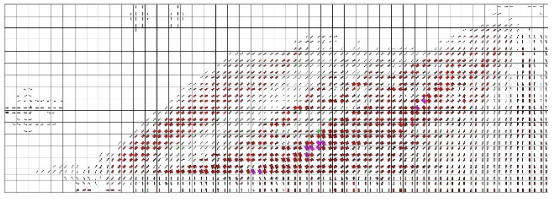

(b)

Fig. 5.12 Comparison between shear softening diagram and shear retention factor-based numerical models (a) force-deflection relationship at the loaded section for beam 2S-Ref, (b) crack pattern using the shear-retention factor.

5.5 Analytical evaluation of the beta parameter and shear fracture energy

5.5.1 β factor and shear fracture energy $G_{f,s}$ as a function of the total shear reinforcement stiffness and concrete compressive strength

In order to simulate the tested beams, different values of the parameters β and $G_{f,s}$ have been used. It has been observed that these parameters play a relevant role in the softening behavior, affecting the final structural response. Through the parametric study has demonstrated that the $\tau_{t,p}^{cr}$ also influences the numerical response, this value was assumed to be constant ($\tau_{t,p}^{cr}$=1.0 MPa) in the simulations presented and discussed in section 5.3. The use of a different $\tau_t^{cr} - \gamma_t^{cr}$ diagram for each beam can be explained by considering the fact that the constitutive model adopted for the concrete describes the behavior of plain concrete, and the model adopted for the reinforcement (stirrups and bars are modeled as embedded cable – section 5.3.1), can exclude some minor concrete contribution to shear strength. Along a shear diagonal crack (Fig. 5.13), the effects of the aggregate interlock, dowel action and crack sliding are sensible to the percentage of transverse steel (ASCE-ACI Committee 445, 1999). It was demonstrated that the aggregate interlock increases with a normal compressive force opposing to the crack opening (Walraven 1981), and the effect induced by the dowel action is higher when a small spacing between the stirrups is adopted. The adoption of embedded cables to simulate the steel bars neglects the crack sliding resistance offered by the bars crossing the cracks. Kolmar (1986) developed a shear retention factor model to take into account the percentage of reinforcement crossing the crack plane. The values of β and $G_{f,s}$ used for the numerical simulation in section 5.3 (Table 5.2) are plotted versus the $\left(E_{fw}\rho_{fw} + E_{sw}\rho_{sw}\right)/\left(f_{cm}^{2/3}\right)$ in Fig. 5.14. $\left(E_{fw}\rho_{fw} + E_{sw}\rho_{sw}\right)/\left(f_{cm}^{2/3}\right)$ depicts the total stiffness of the shear reinforcement divided by the $f_{cm}^{2/3}$ which represent the influence of the concrete tensile strength as indicated in Dias and Barros (2013). By means of a statistical linear regression analysis, two equations were determined for each investigated parameter (β and $G_{f,s}$). Since a significant difference of behavior was found experimentally between 90° and 45° ETS installed bars, different equations were adopted for vertical (90°) and inclined (45°) strengthening. The coefficient of determination R^2 shows a dispersion of data in the range of 0.46 and 0.94.The regression lines corresponding to Eq. 5.13 to 5.16 are reported in Fig.5.13. For Eq. 5.16 the constant term (Y-intercept) was imposed equal to $G_{f,s}$ = 0.07: value of the shear fracture energy for the beam without any shear reinforcement (0S-Ref). The inclined

and vertical ETS bars are indicated with continuous and dotter line, respectively. Fig. 5.14a presents the regression corresponding to the parameter β : it is possible to notice that this parameter decrease with the increase of $\left(E_{fw}\rho_{fw}+E_{sw}\rho_{sw}\right)/\left(f_{cm}^{2/3}\right)$. Similar inclinations were obtained for vertical and inclined ETS bars; nevertheless, higher values were provided by Eqs. 5.13 and 5.14 for vertical (90°) ETS bars. Fig 5.14b presents the regression corresponding to the parameter , $G_{f,s}$: it is possible to notice that this parameter increase with the increase of $\left(E_{fw}\rho_{fw}+E_{sw}\rho_{sw}\right)/\left(f_{cm}^{2/3}\right)$. Higher values of $G_{f,s}$ and higher slope of the linear regression were obtained for inclined (45°) ETS bars.

$$\beta=-1.137\cdot\left[\left(E_{fw}\rho_{fw}+E_{sw}\rho_{sw}\right)/\left(f_{cm}^{2/3}\right)\right]+0.176 \qquad R^2=0.46 \qquad \text{for 90° ETS} \qquad (5.13)$$

$$\beta=-1.36\cdot\left[\left(E_{fw}\rho_{fw}+E_{sw}\rho_{sw}\right)/\left(f_{cm}^{2/3}\right)\right]+0.161 \qquad R^2=0.53 \qquad \text{for 45° ETS} \qquad (5.14)$$

$$G_{f,s}=2.15\cdot\left[\left(E_{fw}\rho_{fw}+E_{sw}\rho_{sw}\right)/\left(f_{cm}^{2/3}\right)\right]+0.07 \qquad R^2=0.94 \qquad \text{for 90° ETS} \qquad (5.15)$$

$$G_{f,s}=9.77\cdot\left[\left(E_{fw}\rho_{fw}+E_{sw}\rho_{sw}\right)/\left(f_{cm}^{2/3}\right)\right]+0.07 \qquad R^2=0.62 \qquad \text{for 45° ETS} \qquad (5.16)$$

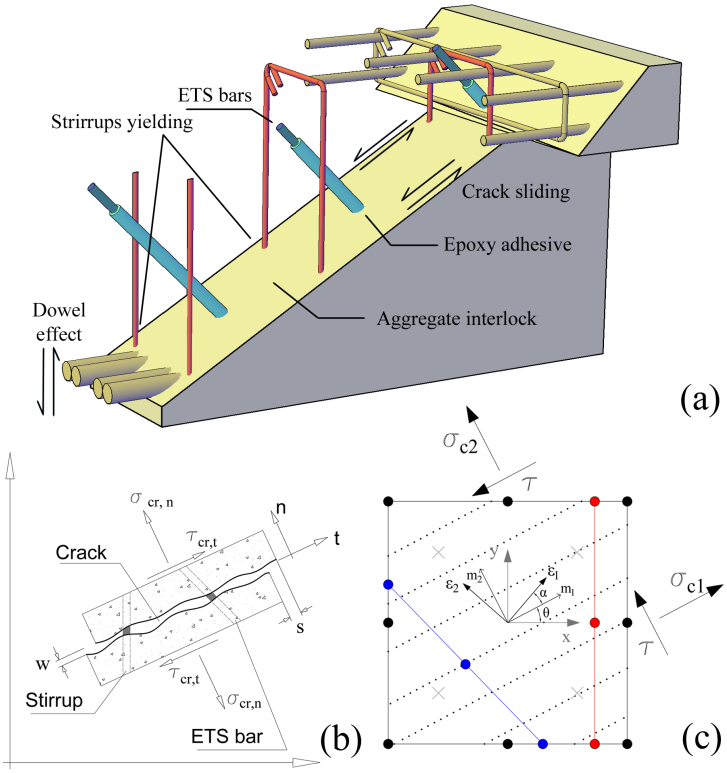

Fig 5.13 Forces acting along the crack (a); Crack stresses, relative displacements and local coordinate system of the crack (b); stress acting on the single finite element (c)

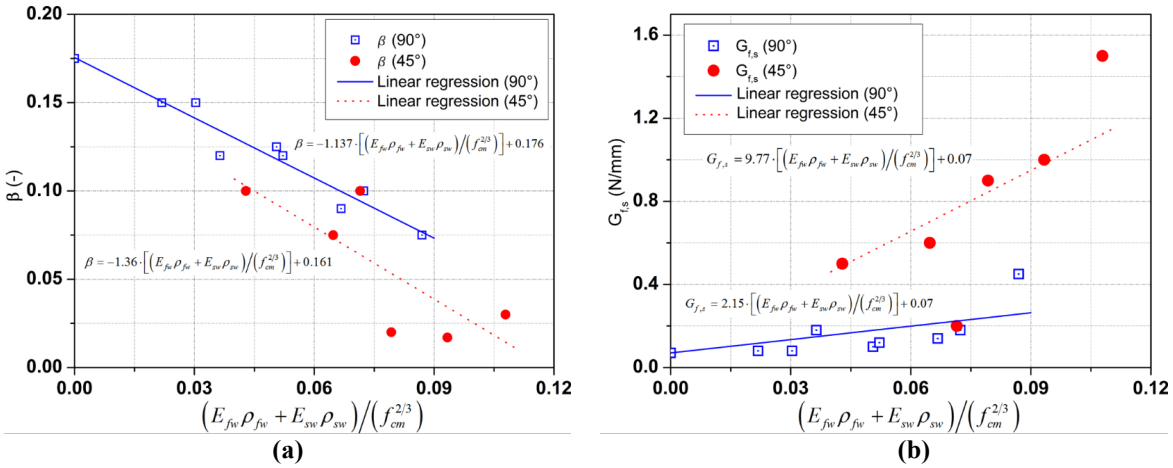

Fig. 5.14 β (a) and shear fracture energy $G_{f,s}$ (b) as a function of the total shear reinforcement stiffness and concrete compressive strength.

5.5.2 Accuracy of the simulation with the calculated values

The parameter values obtained with Eq. 5.13 to 5.16 were used to assess the accuracy of the presented equations on the estimation of the values β - $G_{f,s}$. These values are reported in Table 5.4 and are compared with the values obtained with the best fit of the experimental results (Table 5.2).

Table 5.4 Comparison between the values β and $G_{f,s}$ obtained by using Eq. 5.13 to 5.15 and obtained by inverse analysis (Table 5.2).

	β Table 5.2	β Eq. (5.13) Eq. (5.14)	$G_{f,s}$ Table 5.2	$G_{f,s}$ Eq (5.15) Eq. (5.16)
0S-REF	0.175	0.176	0.07	0.070
0S-S300-90	0.15	0.141	0.08	0.135
0S-S180-90	0.144	0.118	0.1	0.178
0S-S300-45	0.175	0.103	0.50	0.489
0S-E180-45	0.1	0.064	0.20	0.768
2-REF	0.15	0.151	0.08	0.117
2S-S300-90	0.12	0.116	0.12	0.182
2S-S180-90	0.1	0.093	0.18	0.225
2S-S300-45	0.075	0.073	0.6	0.702
2S-S180-45	0.017	0.034	1.00	0.981
4S-REF	0.1	0.134	0.22	0.148
4S-E300-90	0.09	0.100	0.14	0.213
4S-S180-90	0.075	0.077	0.45	0.256
4S-S300-45	0.02	0.053	0.9	0.844
4S-S180-45	0.030	0.014	1.5	1.124

The obtained load-deflection relationship and crack patterns are presented in Figs 5.15 and 5.16, respectively. As in section 5.3, the red color curves, including circle full markers, were obtained by using the parameter values in bold in Table 5.2, while the blue color curves, including square empty

markers, were obtained by using the parameter values calculated with Eq. 5.13 to 5.16. It is possible notice that, in most of the cases, these latter curves are very similar to the ones presented in section 5.3 as well as to the experimental results. Some of these simulations overestimate (for example beam 0S-S180-45 or 2S-S180-90) or underestimate (for example beam 2S-S300-45) the load carrying capacity of the beams, mainly when a meaningful difference between the values β and $G_{f,s}$ in Table 5.4 occurs. Nevertheless, it is possible to notice that in general, even with significant difference between the values β and $G_{f,s}$ in Table 5.4 for some of the beams, the predicted results provide satisfactory results. In some of the numerical simulations an underestimation of the maximum load carrying capacity can be attributed to numerical instabilities (e.g. 4S-S180-45). The crack patterns reported in Fig. 5.16 indicate a good agreement between numerical and experimental results. Moreover it was evidenced the possibility to increase the valued of $G_{f,s}$ and decrease the value of β with the increase of the total stiffness of the shear reinforcement. $\left(E_{fw}\rho_{fw}+E_{sw}\rho_{sw}\right)$. The presented equations (Eq. 5.13 to 5.15) intend to be a suitable tool to obtain a first estimation of the investigated parameters, for similar geometry of un-strengthened and ETS strengthened RC beams.

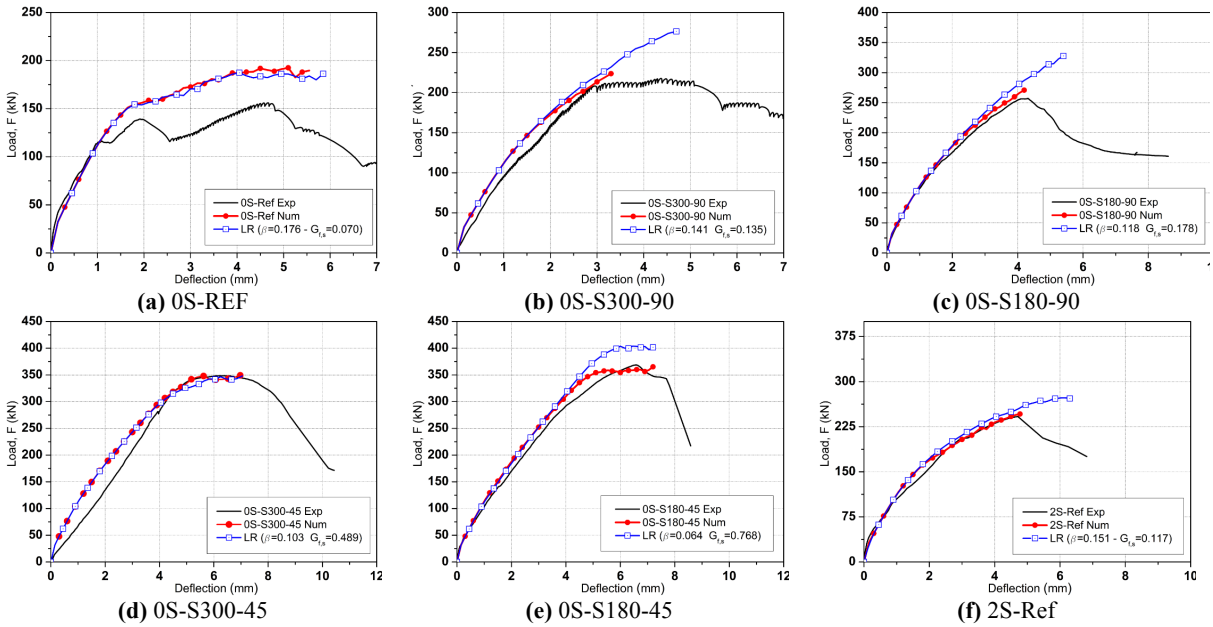

(a) 0S-REF **(b)** 0S-S300-90 **(c)** 0S-S180-90

(d) 0S-S300-45 **(e)** 0S-S180-45 **(f)** 2S-Ref

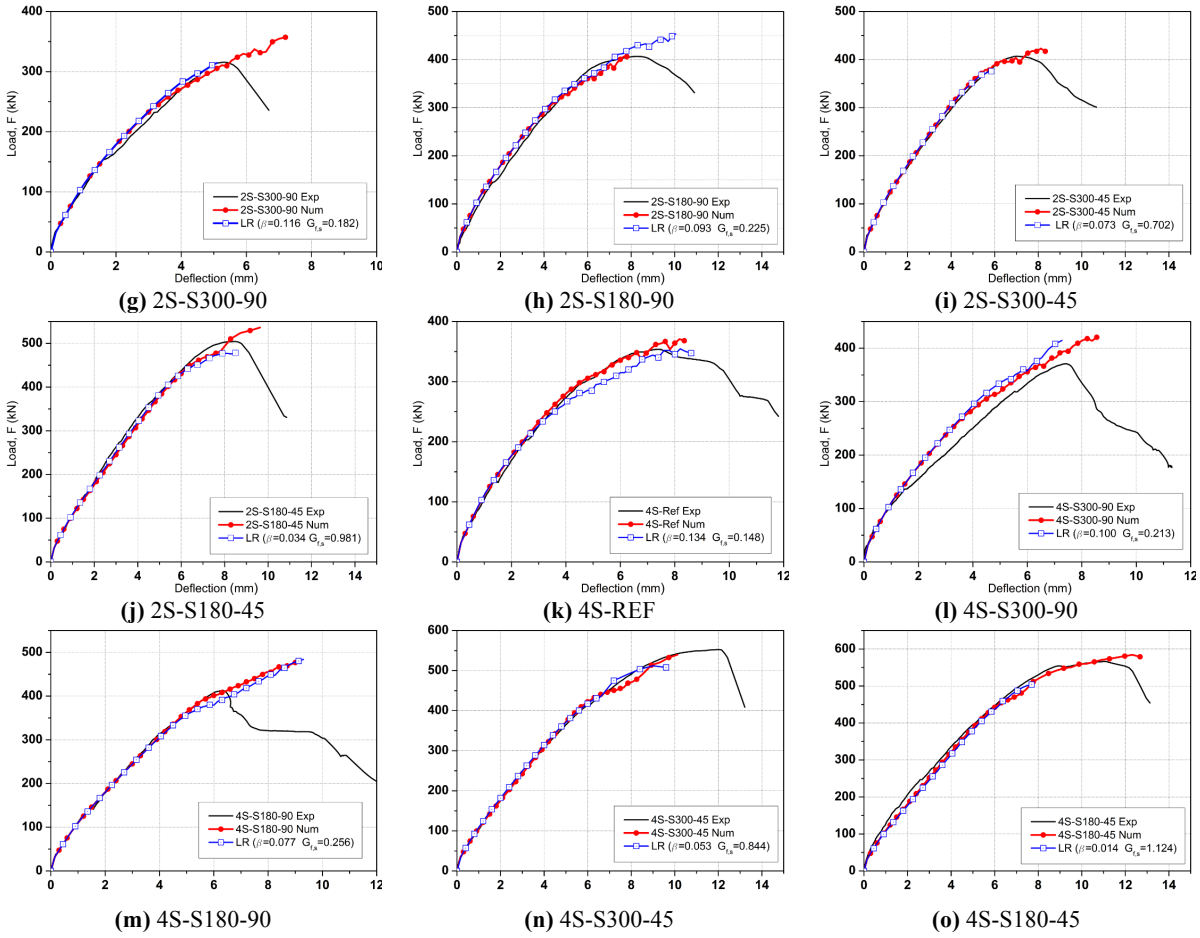

(g) 2S-S300-90 **(h)** 2S-S180-90 **(i)** 2S-S300-45

(j) 2S-S180-45 **(k)** 4S-REF **(l)** 4S-S300-90

(m) 4S-S180-90 **(n)** 4S-S300-45 **(o)** 4S-S180-45

Fig 5.15 Load-deflection of the numerical simulation obtained using the values provided by Eq. 5.13 to 5.16; comparison with experimental a values that best fit the experimental results

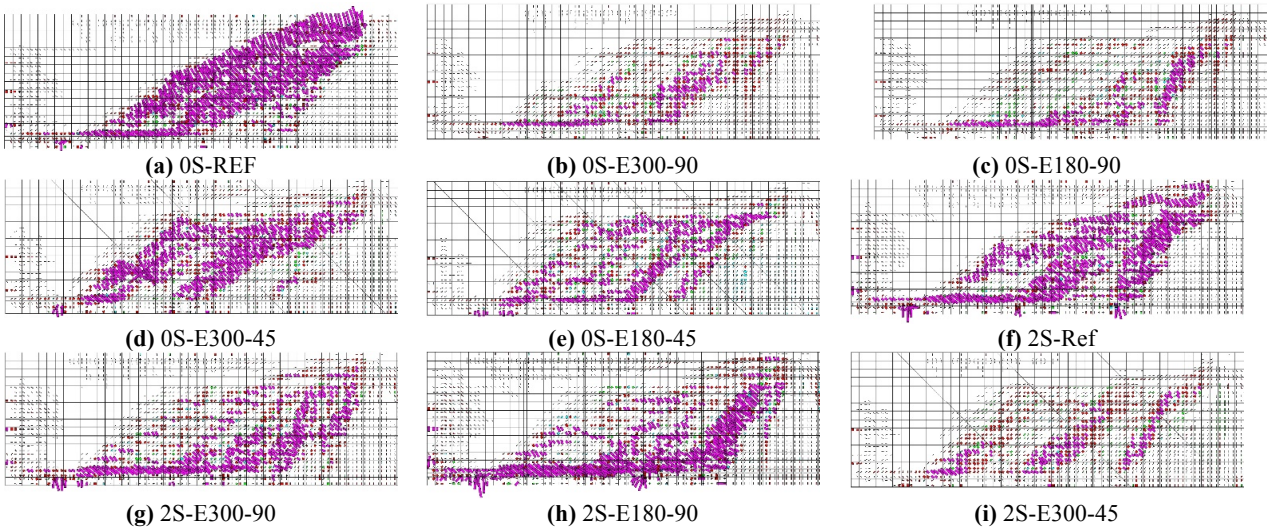

(a) 0S-REF **(b)** 0S-E300-90 **(c)** 0S-E180-90

(d) 0S-E300-45 **(e)** 0S-E180-45 **(f)** 2S-Ref

(g) 2S-E300-90 **(h)** 2S-E180-90 **(i)** 2S-E300-45

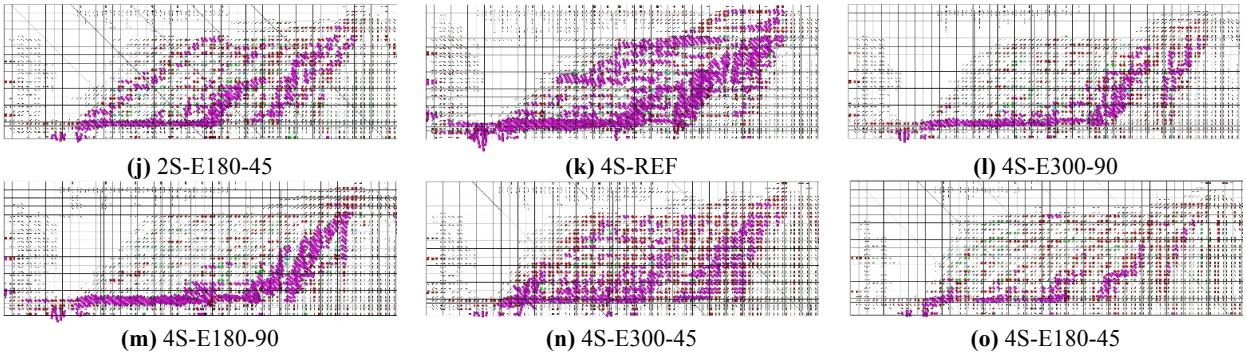

(j) 2S-E180-45 **(k)** 4S-REF **(l)** 4S-E300-90

(m) 4S-E180-90 **(n)** 4S-E300-45 **(o)** 4S-E180-45

Fig 5.16 Crack-Patterns of the numerical simulation obtained using the values provided by Eq. 5.13 to 5.16

5.6 Conclusion

This Chapter presents the relevant results of the numerical simulation performed on RC beams strengthened using steel ETS bars. The analysis capability of a multi-directional fixed smeared crack model FE program (FEMIX) to estimate the behavior of this type of elements up to failure was assessed. To simulate the degradation of the crack shear stress transfer after crack initiation, a shear crack softening diagram $\left(\tau_t^{cr} - \gamma_t^{cr}\right)$, was adopted and investigated as an alternative to the shear retention factor function. It was observed that the force-deflection relationship is sensible to the adopted values of the $\tau_t^{cr} - \gamma_t^{cr}$. The parameters that define the shear crack softening diagram β, $G_{f,s}$, $\tau_{t,p}^{cr}$ were identified by using an inverse analysis, since there is a lack of specific experimental tests dedicated to the assessment of those parameters. For each tested beam a different shear crack softening diagram was identified. It was in fact observed that the value of β and $G_{f,s}$ are influenced by the shear strengthening ratio (nevertheless a constant value of $\tau_{t,p}^{cr}$=1 MPa was used). The numerical simulations evidenced that by adopting a proper shear crack softening diagram a good prediction of the deformational behavior, load carrying capacity, crack pattern and reinforcement strain field of the tested beam can be obtained. It was also demonstrated that, due to the good bond performance between ETS bars and concrete during the experimental tests, the assumption of perfect bond between materials is reasonable and good results can be obtained. A parametric study to evaluate the influence of the parameters that define the shear-softening diagram $\tau_t^{cr} - \gamma_t^{cr}$, in RC beams was carried out. This study evidenced that the parameter β, $G_{f,s}$, $\tau_{t,p}^{cr}$ significantly affect the cracked stiffness of the tested beams. It was observed that the second branch (softening-branch) of the $\tau_t^{cr} - \gamma_t^{cr}$ diagram has a relevant role in the numerical model. The peak crack shear strain, $\gamma_{t,p}^{cr}$, which is as larger as smaller is β, is an important point in the diagram since it defines the entrance in the softening phase. A larger stiffness of the force-deflection response was

observed when the entrance in the softening phase is postponed (small value of β). It was also observed that the stiffness of the beams decreases by decreasing the values of $G_{f,s}$. A smaller value of β provided as well higher carrying capacity in the analyzed beam, nevertheless the values of $\tau_{t,p}^{cr}$ and $G_{f,s}$ seemed to have small influence on the estimation of the maximum load carrying capacity. The parametric study also showed that for the highest value of $\tau_{t,p}^{cr}$ (at constant values of $G_{f,s}$) an abrupt decay of the softening branch led to a brittle behavior of the deflectional response; on the other side the lowest value of $\tau_{t,p}^{cr}$ (at constant values of $G_{f,s}$) led to a very ductile behavior. The crack pattern was also influenced by different values of $\beta, G_{f,s}, \tau_{t,p}^{cr}$. It was also observed that by using the concept of shear retention factor, the numerical model is not able to simulate the stiffness degradation induced by the shear deformation, and an abnormal high load carrying capacity is estimated, while adopting a $\tau_t^{cr} - \gamma_t^{cr}$ softening diagram, the response of the beam, the failure mode and also the crack pattern are correctly estimated.

Finally, a linear regression model using the data of the presented numerical simulation was used to estimate the parameter $\beta, G_{f,s}$ of the $\tau_t^{cr} - \gamma_t^{cr}$ diagram. It was observed that the numerical simulation performed using the values obtained by linear regression showed a structural response similar to the experimental results in terms of both load-deflection relationship and crack pattern. The results would allow to use the introduced equations for a first estimation of the $\beta, G_{f,s}$ parameters for similar section geometries and material properties of beams strengthened using the ETS technique. Moreover and more important is was demonstrated the possibility to evaluate the β, $G_{f,s}$ as a function of the total transverse reinforcement stiffness and the concrete compressive strength. Nevertheless, more investigation is needed to provide a general rule for the estimation of the $\tau_t^{cr} - \gamma_t^{cr}$ diagram for RC un-strengthened and strengthened elements.

It is possible to conclude that by adopting the shear softening diagram in the multidirectional fixed smeared crack model, available in the FEMIX computer program, the numerical analysis was able to predict with higher accuracy the behavior of structures failing in shear and the numerical capability was improved.

6

Conclusions and future developments

6.1 Conclusions

The present thesis deals with the shear strengthening of RC beams using the Embedded Through-Section (ETS) technique. This technique consists in drilling holes through the beam cross section and introducing steel or carbon fiber reinforced polymer (CFRP) bars into these holes, and then bonded to the surrounding concrete with adhesive material. The objectives of the present work were to contribute to a better understanding of ETS shear strengthening system, its mechanical behavior and the parameters affecting its effectiveness, as well as to develop an analytical model to predict the contribution of ETS steel bars for the shear strengthening of RC beams. Moreover, a reliable FEM-based numerical strategy for RC beams failing in shear is provided by investigating the influence of the governing parameters of the crack shear softening diagram on the behavior of this type of elements. This shear-softening diagram is part of the constitutive law that simulates the crack shear stress transfer, already implemented in the multidirectional fixed smeared crack model available in the FEMIX computer program, which is based on the finite element method (FEM).

To accomplish those purposes, an experimental program was carried on RC T-cross section beams strengthened using steel and CFRP bars according to the ETS technique. The investigated parameter in the experimental program were the percentage of existing steel stirrups (ρ_{sw}), the percentage and inclination (90° and 45°) of ETS strengthening, as well as the material type used for ETS bars (steel and CFRP).

The obtained results demonstrated that this technique is able to increase significantly the load carrying capacity of RC beams failing in shear, as well as their ultimate deflection performance. The highest increase of load carrying capacity and shear strength were obtained by using inclined ETS bars (45° with respect to the longitudinal axis of the beams). By using this strengthening configuration, an increase of shear strength between 53% and 136% compared to the reference beam was obtained. For

vertical installed ETS bars the strengthening efficiency was lower and ranged between 5% and 68%. For both the inclinations, the level of effectiveness depended on the internal shear reinforcement arrangement, percentage and adopted material for ETS strengthening. As expected, from a technique that relies it efficiency on the adhesion between strengthening material and concrete, the bond played a relevant role. This evidence can justify the higher effectiveness of inclined ETS bars, since this strengthening configuration presented larger available bond length than the one offered by using vertical ETS bars; moreover 45° ETS bars presented favorable inclination, since they were almost orthogonal to the shear failure crack.

The experimental tests highlighted that the existing shear reinforcement ratio has a significant influence on the ETS effectiveness, which has decreased with the increase of ρ_{sw}. This was mainly notable in vertical ETS bars. As expected, the shear strength increased with the percentage of ETS bars (ρ_{fw}). It was also proved that the ETS technique assures higher effectiveness than the externally bonded reinforcement (EBR) and the near surface mounted (NSM) techniques. The deep embedment of the ETS bars into the concrete core is better confined by the surrounding concrete, resulting in a higher bond performance when compared to the aforementioned techniques. This enhanced bond allowed the steel yield strain to be exceeded, and the development of high tensile strains in CFRP bars, mainly in the inclined ETS bars. However, slip occurred for both type of strengthening material, especially in CFRP vertical bars.

Despite the high percentage of internal transverse strengthening, the stirrups have exceeded the steel yield strain. Regarding the strengthening material, it was possible to observe that for similar shear strengthening ratio, the inclined CFRP bars provided higher shear strengthening effectiveness than inclined steel bars, but lower increase of shear strength was obtained in the vertical strengthening configuration. However, in order to assess the most sustainable type of material for ETS strengthening, a cost-benefit analysis should be carried out.

Two analytical models were developed to estimate the steel ETS bars contribution for the shear strength of RC beams. The first model, denoted as “Empirical-based”, followed an empirical approach based on the concept of effective strain, supported on a function that depends of the total shear reinforcement stiffness and concrete compressive strength. The second model, denoted as “mechanical-based”, followed a mechanical approach supported on the physical laws governing the bond interface and stress transfer in concrete. When compared with the experimental values, the analytical values showed an average ratio $\left(V_f^{\exp} \middle/ V_f^{ana}\right)$ of 1.08 and 1.21 for the experimental-based and mechanical based models,

respectively. It was observed that the two approaches provided similar results in term of level of accuracy, indeed in terms of structural safety both of them indicated safe design for 90% of the analyzed beam by using a partial safety factor of γ_f =1.3. It is possible to observe that both models provided satisfactory results, and were able to evidence the different shear strengthening effectiveness between vertical and inclined ETS strengthening. Steel yielding was correctly detected in 45° installed bars by both of the models, and they were also capable of predicting a bond failure in case of vertical ETS bars. The experimental-based approach, which has the advantage to consider in his formulation the existing shear reinforcement ratio, provided a dispersion of results lower than the mechanical-based model. However, the mechanical model is conceptually more reliable since it considers a bond constitutive law to evaluate the contribution of a single ETS bar, as well as the concrete fracture by reducing the available resisting bond length with the progress of the concrete fracture. The main drawback of the latter model resides in neglecting the existing stirrups, and further research should be carried out in this regards. For a better assessment of the predictive performance of both models, more experimental data is also required.

The main effort in the numerical work was dedicated to investigate the shear softening constitutive model based on a bilinear shear crack-shear stress diagram $\left(\tau_t^{cr} - \gamma_t^{cr}\right)$ to simulate the degradation of the crack shear stress transfer after crack initiation. The performed inverse analysis for the identification of the values of β, $G_{f,s}$ and $\tau_{t,s}^{cr}$ that define the $\tau_t^{cr} - \gamma_t^{cr}$ diagram evidenced that those values varied by changing the percentage of transverse reinforcement. The values adopted to define the shear-softening diagram had main influence in the prediction of the deformational response of the simulated beams, by affecting the beam's stiffness at cracked stage, as well as the crack pattern at failure conditions. Smaller influence of the values adopted for these parameters was in general found in the estimation of maximum load carrying capacity of the beams. It is possible to affirm that a fundamental aspect of the $\tau_t^{cr} - \gamma_t^{cr}$ is the characterization of its softening branch; in fact, the numerical simulations evidenced the importance of the transaction point in which the element enters in the softening phase, and its ultimate crack shear strain. The performed numerical simulations have reproduced with high accuracy the deformational behavior of the experimental tests, as well as the crack pattern and strains in stirrups and ETS bars. In general, a fairly good prediction of the load carrying capacity was found. The study also compared the results obtained by adopting a $\tau_t^{cr} - \gamma_t^{cr}$ relationship and a shear retention factor whose value decreases with the increase of the strain normal to the crack according to a selected function. It was observed that by adopting a shear retention factor function the level of stiffness degradation

registered in the tested beam is not correctly simulated, and much higher ultimate load is estimated. Very good predictions are, however, capable of being assured if proper $\tau_t^{cr} - \gamma_t^{cr}$ is adopted. For deriving the values that define this diagram (mainly β, $G_{f,s}$), a linear regression model using the data of the presented numerical simulations was adopted. It was shown that numerical simulations performed using the values of β, $G_{f,s}$ obtained according to this strategy presented similar structural response in terms of load-deflection relationship and crack pattern to the ones obtained by using calibrated values, as well as to the experimental results. This evidence confirms the potential of evaluating with sufficient accuracy the β, $G_{f,s}$as a function of the total transverse reinforcement stiffness and the concrete compressive strength. It is possible to conclude that the adoption of a shear softening diagram can significantly improve the capability of the multidirectional fixed smeared crack model for the analysis of RC elements failing in shear.

This thesis demonstrates the high effectiveness of the ETS technique. Taking into account the high level of shear strengthening obtained in this experimental program, it can be concluded that ETS can assure ductile flexural failure mode in RC beams susceptible to brittle shear rupture, even in beams of quite high flexural reinforcement ratio. The ETS technique is more competitive than EBR and NSM techniques. Moreover, the ETS technique based on the use of steel bars is a cost competitive and sustainable solution for the shear strengthening of RC elements. Steel bars are much less susceptible than FRP bars to the detrimental effect of high temperature. It should also be remarked that corrosion can be avoided in ETS steel bars by providing a cement based cover at the bars' extremities, and these reinforcements are much better protected in case of fire.

6.2 Future developments

There is still few number of experimental tests dedicated to investigate the ETS technique for the shear strengthening of RC beams. Therefore, more experimental data are needed to contribute for a better understanding of the ETS technique, as well as to the assessment of the predictive performance of the proposed analytical models. Due to lack of time and financial support, the present work was not able to investigate the influence of the concrete compressive strength on the ETS effectiveness. All the strengthening techniques that rely their effectiveness on the bond between strengthening material and concrete evidenced the influence of the concrete compressive strength on the strengthening effectiveness. For this reason, experimental programs on RC elements with different compressive

strength should be carried out. However, it is expected that the higher is the compressive strength, the greater is the ETS effectiveness. The application of the ETS strengthening technique and its effectiveness on or pre-cracked or deteriorated RC elements due to corrosion or environmental aging should be also investigated, since these configurations represent possible scenarios for a strengthening application in civil construction. The influence of the bar diameter, surface treatment, and adhesive layer thickness, should be also investigated. The influence of the relative position between ETS bars and existing steel stirrups should be also studied, since the detrimental interaction effects seems to be dependent on this condition. The application of more than one ETS bar per cross section requires also further investigation due to an expected detrimental group effect.

The future developments of this work can also be oriented towards exploring the possibility offered by different materials. Different types of adhesive materials should be tested: the epoxy based material can be replaced by an inorganic mortar that would decrease the susceptibility of failure in case of fire. The bond of similar type of materials has already been assessed for Fabric-reinforced cementitious matrix FRCM (or Textile Reinforced Mortars-TRM), and due to the high confinement offered by the surrounding concrete to the bars installed following the ETS technique, a cement based adhesive can offer a possible sustainable and economic alternative to the epoxy based adhesive. A hybrid cement-based material with a percentage of epoxy adhesive can also be developed and tested. Pre-stressed steel or FRP ETS bars can also be applied to increase the service limit state conditions of existing RC beams. Hybrid GFRP-Steel bars (Seo, Park, You, & Kim, 2003), designed to obtain a pseudo ductile failure and to overcome the low elastic modulus of glass fibers can be considered as ETS strengthening solutions, after an economic evaluation. The hybridization process consists in adding steel as a high modulus material to enhance the Young's modulus to the GFRP. Since vertical CFRP bars evidenced low effectiveness, due to a lack of the available bond transfers length, an anchorage system can be developed to avoid a premature debonding in this type of application (anchorage system can be developed as well for steel ETS bars). By analogy with Manually Made-Near Surface Mounted (MM-NSM), (Jalali et al. 2012 - Chapter 1) it is possible to develop an ETS bar impregnated with resin only for the necessary length of embedment and characterized by a terminal part made of dry fibers, which can be fanned out over the concrete surface with the purpose of improving the resistance of the system. The available braiding technology can be used to develop this type of bars, or manually made solution by wrapping fiber sheets around a rigid core can be utilized. By adopting this type of solution, Hybrid EBR/ETS strengthening system can be developed for upgrade flexure and shear capacity of RC elements by analogy with Smith et al. (2011) where simple carbon fiber anchors were used to improve the bond of the flexural EBR strengthening.

Additional investigations are needed concerning the analytical models. In fact, the first model (*experimental-based*) presented in this work is based on a regression analysis of the experimental data and more data are needed for a better assessment of this type of approach. The second model (*mechanical-based*) adopts a simplified bond model initially developed for NSM strips. A proper constitutive law for steel and CFRP embedded bars in concrete should be developed and used in this model. As already evidenced in the previous paragraph, the influence of the internal shear reinforcement ratio should be taken into account in the model.

In regards to the numerical work carried out, a larger number of simulation on RC structural elements with different types of cross geometry and internal reinforcement should be carried out, mainly using the 3D version of this model, in order to identify a possible general criteria for the characterization of the shear-softening constitutive diagram.

References

ACI Committee 318, 2008. Building Code Requirements for Structural Concrete and Commentary (ACI 318-08), American Concrete Institute, Detroit.

ACI Committee 446, 1992. Fracture Mechanics of Concrete Structures. In Z. P. Bazant, ed. Proc. FraMCoS1. Breckenrige, p. 71.

ACI Committee 549, 2013. Guide to Design and Construction of Externally Bonded Fabric-Reinforced Cementitious Matrix (FRCM) Systems for Repair and Strengthening Concrete and Masonry Structures- ACI 549.4-13,

ACI Committee 440, 2008. Guide for the design and con- struction of externally bonded FRP systems for strengthening concrete structures. ACI440.2R, Farmington Hills, MI: American Concrete Institute, Detroit.

Angelakos, D., Bentz, E.C., Collins, M.P., 2001. Effect of concrete strength and minimum stirrups on shear strength of large members. ACI Structural Journal, 98(3), pp.290–300.

Anwarul Islam, A.K.M., 2009. Effective methods of using CFRP bars in shear strengthening of concrete girders. Engineering Structures, 31(3), pp.709–714.

Appleton, J., Gomes, A., 1997. Reforço de estruturas de betão armado por adição de armaduras exteriores. Revista Portuguesa de Engenharia de Estruturas, 41(Janeiro), pp.15–20.

Aprile, A., Benedetti, A., 2004. Coupled flexural-shear design of R/C beams strengthened with FRP. Composites Part B: Engineering, 35(1), pp.1–25.

ASCE, 1982. State-of-the-Art Report on Finite Element Analysis of Reinforced Concrete,

ASCE-ACI Committee 426, 1973. The Shear Strength of Reinforced Concrete Members. Journal of Structural Division, ASCE, 99(6), pp.1091–1187.

ASCE-ACI Committee 445 on Shear and Torsion, 1999. Recent Approaches to Shear Design of Structural Concrete.

Bakis, C. E., Bank, L.C., Brown, V. L., Cosenza, E., Davalos, J. F., Lesko, J. J., Machida, A., Rizkalla, S. H., Triantafillou, T. C., 2002. Fiber-Reinforced Polymer Composites for Construction—State-of-the-Art Review. Journal of Composites for Construction, 6(2), pp.73–87.

Barros, J.A.O., 1995. Comportamento do betão reforçado com fibras. Análise experimental e simulação numérica. Behavior of fiber reinforced concrete. Experimental analysis and numerical simulation. Phd Thesis, Faculty of Engineering, University of Porto, Portugal [in Portuguese].

Barros, J.A.O., Dias, S.J.E., Lima, J.L.T., 2007. Efficacy of CFRP-based techniques for the flexural and shear strengthening of concrete beams. Cement and Concrete Composites, 29(3), pp.203–217.

Barros, J.A.O., Trombini, E., Darlfé G.M., Aprile A., 2008. Exploring the possibilities of a new technique for the shear strengthening of RC elements. In Proceedings of the International Conference Challenges for Civil Construction , University of Porto, Portugal.

Barros, J.A.O., Costa, I.G., Ventura-Gouveia, A., 2011. CFRP Flexural and Shear Strengthening Technique for RC Beams: Experimental and Numerical Research. Advances in Structural Engineering, 14(3), pp.551–571.

Barros, J.A.O. and Dalfré, G.M., 2012. Assessment of the Effectiveness of the Embedded Through-Section Technique for the Shear Strengthening of Reinforced Concrete Beams. Strain, 49(1), pp.75–93.

Barros, J.A.O., Breveglieri, M., Ventura-Gouveia, A. Dalfré, G. M., Aprile, A., 2013a. Model to simulate the behavior of RC beams shear strengthenend with ETS bars. In Proceedings of the FraMCoS-8 Fracture Mechanics of Concrete and Concrete Structures. Toledo, Spain: CIMNE International Center for Numerical Methods in Engineering, pp. 505–516.

Barros, J.A.O., Baghi, H., Dias, S.J.E.,Ventura-Gouveia, A., 2013b. A FEM-based model to predict the behaviour of RC beams shear strengthened according to the NSM technique. Engineering Structures, 56(0), pp.1192–1206.

Barros, J.A.O., Dias, S.J.E., 2013. Assessment of the effectiveness of the NSM shear strengthening technique for deep T cross section RC beams. In Proceedings of the FRPRCS11, Guimarães, Portugal, 26-28 June 2013.

BASF Construction Chenical Italia Spa. Technical sheet MasterBrace BAR 8 CFS. http://www.master-builders-solutions.it

Baumann, T., Rüsch, H., 1970. Versuche zum Studium der Ver-dübelungswirkung der Biegezugbewehrung eines Stahlbetonbalkens. In DAfStb H.210. Wilhelm Ernst und Sohn, Berlin, pp. 43–83

Baumann, T., 1972. Zur frage der netzbewehrung von flächentragwerken. Bauingenieur, 47, pp.367–377.

Bazant, Z.P., Oh, B.H., 1983. No Crack band theory for fracture of concreteTitle. RILEM Publication SARL, 93(16), pp.155–177.

Bazant, Z.P., Kim, J.-K., 1984. Size Effect in Shear Failure of Longitudinally Reinforced Beams. ACI Journal, Proceedings, 81(5), pp.456–468.

Belarbi, A. Kuchma, A., Okeil, A.M., Bae, S-W, 2012. Design Equations for Shear Capacity of Concrete Girders Strengthened in Shear with Externally Bonded FRP Sheets. In APFIS. Hokkaido University Japan 2-4 February 2012, p. 8.

Berset, J.-D., 1992. Strengthening of reinforced concrete beams for shear using FRP composites. MSc Thesis-Massachusetts Institute of Technology.

Beschi, C., Meda, A., Riva, P., 2009. High Performance Fiber Reinforced Concrete Jacketing in a Seismic Retrofitting Application (ASCE). In Improving the Seismic Performance of Existing Buildings and Other Structures. San Francisco, United States, pp. 224–233.

Bianco, V., Barros, J.A.O., Monti, G., 2006. Shear Strengthening of RC beams by means of NSM laminates: experimental evidence and predictive models Report 06-DEC/E-18, Guimaraes.

Bianco, V., Barros, J.A.O., Monti, G., 2007. A new npproach for modelling the NSM shear strengthening contribution in reinforced concrete beams. In Proceedings of the FRPRCS-8. pp. 1–10.

Bianco, V., 2008. Shear Strengthening of RC beams by means of NSM CFRP strips: experimental evidence and analytical modeling. Phd Thesis - Univesity Roma la Sapienza.

Bianco, V., Barros, J.A.O., Monti, G., 2009a. Bond model of NSM CFRP in the context of the shear strengthening of RC beams. ASCE Journal of Structural Engineering, 135(6), pp.619–631.

Bianco, V., Barros, J.A.O., Monti, G., 2009b. Three dimensional mechanical model for simulating the NSM FRP strips shear strength contribution to RC beams. Engineering Structures, 31(4), pp.815–826.

Bianco, V., Barros, J.A.O., Monti, G., 2010. New approach for modeling the contribution of NSM FRP strips for shear strengthening of RC beams. Journal of Composites for Construction, 14(1), pp.36–48.

Bianco, V., Monti, G., Barros, J.A.O., 2011. Theoretical Model and Computational Procedure to Evaluate the NSM FRP Strips Shear Strength Contribution to a RC Beam. Journal of Structural Engineering, 137(11), pp.1359–1372.

Bianco, V., Barros, J.A.O., Monti, G., 2012. Three dimensional mechanical model to simulate the NSM FRP strips shear strength contribution to a RC beam: Parametric studies. Engineering Structures, 37(0), pp.50–62.

Bianco, V., Monti, G., Barros, J.A.O., 2014. Design formula to evaluate the NSM FRP strips shear strength contribution to a RC beam. Composites Part B: Engineering, 56(0), pp.960–971.

Bilotta, A. Ceroni, F., Di Ludovico, M., Nigro, E., Pecce, M., Manfredi, G., 2011. Bond Efficiency of EBR and NSM FRP Systems for Strengthening Concrete Members. Journal of Composites for Construction, 15(5), pp.757–772.

Binici, B., 2003. Punching shear strengthening of reinforced concrete slabs using fiber reinforced polymers. Ph.D. Dissertation, University of Texas at Austin.

Blanksvärd, T., Täljsten, B., Carolin, A., 2009. Shear Strengthening of Concrete Structures with the Use of Mineral-Based Composites. Journal of Composites for Construction, 13(1), pp.25–34.

De Borst, R., Nauta, P., 1985. Non-orthogonal cracks in a smeared finite element model. Engineering Computations, 2(1), pp.35–46.

Bousselham, A., Chaallal, O., 2004. Shear Strengthening Reinforced Concrete Beams with Fiber-Reinforced Polymer: Assessment of Influencing Parameters and Required Research. ACI Structural Journal, 101(2), pp.219–227.

Bousselham, A., Chaallal, O., 2006. Effect of transverse steel and shear span on the performance of RC beams strengthened in shear with CFRP. Composites Part B: Engineering, 37(1), pp.37–46.

Bousselham, A., Chaallal, O., 2008. Mechanisms of Shear Resistance of Concrete Beams Strengthened in Shear with Externally Bonded FRP. Journal of Composites for Construction, 12(5), pp.499–512.

Bresson, J., 1971. L'application du Béton plaqué. In Annales de l'I.T.B.T.P., No. 278.

C.S.L.P, 2009. Nuove Norme Tecniche per le Costruzioni DM 14 gennaio 2008 - Gazzetta Ufficiale n. 29 del 4 febbraio 2008,

CAN/CSA-S806-02, 2002. Design and construction of building components with fibrereinforced polymer, Rexdale, Canada.

Cao, S.Y., Chen, J. F., Teng, J. G., Hao, Z., Chen, J., 2005. Debonding in RC Beams Shear Strengthened with Complete FRP Wraps. Journal of Composites for Construction, 9(5), pp.417–428. Available at:

Carolin, A., Nordin, H., Täljsten, B., 2001. Concrete beams strengthened with prestressed near surface mounted reinforcement (NSMR). In International Conference on FRP Composites in Civil Engineering CICE 2001.

Carolin, A., Täljsten, B., 2005. Theoretical Study of Strengthening for Increased Shear Bearing Capacity. Journal of Composites for Construction, 9(6), pp.497–506.

Carpinteri, A., Gambarova, P., Ferro, G, Plizzari, Giovanni A (Eds.), 2007. Proceedings of the 6th International Conference of Fracture Mechanics of Concrete and Concrete Structures, FraMCoS. In Catania 18-21 June: Balkema (3 Volumes).

CEB-FIP Model Code 90, (1993) Bulletin d'Information N° 213/214, Final version printed by Th. Telford, London, (1993; ISBN 0-7277-1696-4; 460 pages).

Cedolin, L., Dei Poli, S., 1977. Finite Element Studies of Shear-Critical R/C Beams. Journal of the Engineering Mechanics Division, 103(3), pp.395–410.

Chaallal, O., Mofidi, A., Benmokrane, B., Neale, K., 2011. Embedded Through-Section FRP Rod Method for Shear Strengthening of RC Beams: Performance and Comparison with Existing Techniques. Journal of Composites for Construction, 15(5), pp.732–742.

Chaallal, O., Mofidi, A., 2011. Shear Strengthening of RC Beams with Externally Bonded FRP Composites: Effect of Strip-Width-to-Strip-Spacing Ratio. Journal of Composites for Construction, 15(5), pp.732–742.

Chaallal, O., Nollet, M.-J., Perraton, D., 1998. Strengthening of reinforced concrete beams with externally bonded fiber-reinforced-plastic plates: design guidelines for shear and flexure. Canadian Journal of Civil Engineering, 25(4), pp.692–704.

Chalioris, C.E., Papadopoulos, C., Pourzitidis, D.N., Fotis, D., Sideris, K.K., 2013. Application of a Reinforced Self-Compacting Concrete Jacket in Damaged Reinforced Concrete Beams under Monotonic and Repeated Loading. Journal of Engineering.

Chana, P.S., 1987. Investigation of the Mechanism of Shear Failure of Reinforced Concrete Beams. Magazine of Concrete Research, 39(12), pp.196–204.

Chen, J.F., Teng, J.G., 2003a. Shear Capacity of Fiber-Reinforced Polymer-Strengthened Reinforced Concrete Beams: Fiber Reinforced Polymer Rupture. Journal of Structural Engineering, 129(5).

Chen, J.F., Teng, J.G., 2003b. Shear capacity of FRP-strengthened RC beams: FRP debonding. Construction and Building Materials, 17(1), pp.27–41.

Chen, G.M., Teng, J. G., Chen, J. F., Rosenboom, O. A., 2010. Interaction between Steel Stirrups and Shear-Strengthening FRP Strips in RC Beams. Journal of Composites for Construction, 14(5), pp.498–509.

Chen, G.M., Teng, J.G., Chen, J.F., 2013. Shear Strength Model for FRP-Strengthened RC Beams with Adverse FRP-Steel Interaction. Journal of Composites for Construction, 17(1), pp.50–66.

Choudhury, R., Suntharavadivel, T.G., Keleher, P., Patil, A.., 2013. Shear strengthening of RC beam with external FRP bonding: A state-of-the-art review. In B. Samali, M. M. Attard, & C. Song, eds. From Materials to Structures: Advanced through Innovation. CRC Press, pp. 263–267.

CIDAR, 2006. Design guideline for RC structures retrofitted with FRP and metal plates: beams and slabs,

Collins, M.P., 1978. Toward a Rational Theory for RC Members in Shear. Journal of Structural Division, ASCE, 104(4), pp.649–666.

Collins, M.P., Kuchma, D.A., 1999. How safe are our large, lightly reinforced concrete beams, slabs and footings? ACI Structural Journal, 96(4), pp.482–490.

Collins, M.P., Mitchell, D., 1997. Prestressed concrete structures, Englewood Cliffs (NJ): Prentice-Hall, Inc.

Comité Euro-International du Béton, 1978. CEB-FIP Model Code for Concrete Structures. International System of Unified Standard Codes of Practice for Structures, Paris, V.II.

Cook, R.A., Doerr, G.T., Klingener, R.E., 1993. Bond stress model for design of adhesive anchors. ACI Structural Journal, 90(5), pp.514–524.

Cook, R.A., Kunz, J., Fuchs, W., Konz, R.C., 1998. Behaviour and desing of single adhesive anchors under tensile load in uncracked concrete. ACI Structural Journal, 95(1), pp.9–26.

Cook, R.A., Doerr, G.T., Klingener, R.E., 1998. Behavior and Design of Single Adhesive Anchors under Tensile Load in Uncracked Concrete. ACI Structural Journal, 95(1), pp.9–26.

Cook, R.A., Eligehausen, R., Appl, J.J., 2007. Overview: Behavior of Adhesive Bonded Anchors. Beton- und Stahlbetonbau, 102(S1), pp.16–21.

Costa, I.G., Barros, J.A.O., 2012. Evaluation of the influence of adhesive properties and geometry of cabon fiber laminates using pull-out tests, Report 12-DEC/E-08, University of Minho, Guimarães, PT

Cruz, J.S., Barros, J., 2004. Modeling of bond between near-surface mounted CFRP laminate strips and concrete. Computers & Structures, 82(17–19), pp.1513–1521.

Czaderski, C., 2002. Shear strengthening with prefabricated CFRP L-shaped plates. In Proceedings of the IABSE Symposium, Melbourne.

Czaderski, C., Motavalli, M., 2004. Fatigue behaviour of CFRP L-shaped plates for shear strengthening of RC T-beams. Composites Part B: Engineering, 35(4), pp.279–290.

Dalfré, G.M., Barros, J.A.O., Machado, D., 2011. Steel bar – concrete bond behavior in the context of the ETS shear strengthening technique for RC beams. In 53° Brazilan Confer- ence on Concrete – IBRACON.

Dei Poli, S., di Prisco, M., Gambarova, P., 1990. Stress Field in Web of RC Thin-Webbed Beams Failing in Shear. Journal of Structural Engineering, 116(9), pp.2496–2515.

Dias, S.J.E., 2008. Investigação experimental e analítica no reforço ao corte de vigas de betão armado com a técnica da inserção de laminados de CFRP. PhD - Thesis University of Minho.

Dias, S.J.E., Barros, J.A.O., 2011a. Experimental Behaviour of RC Beams Shear Strengthened with NSM CFRP Laminates. Strain, 48(1), pp.88–100.

Dias, S.J.E., Barros, J.A.O., 2012. NSM shear strengthening technique with CFRP laminates applied in high-strength concrete beams with or without pre-cracking. Composites Part B: Engineering, 43(2), pp.290–301.

Dias, S.J.E., Barros, J.A.O., 2010. Performance of reinforced concrete T beams strengthened in shear with NSM CFRP laminates. Engineering Structures, 32(2), pp.373–384.

Dias, S.J.E., Barros, J.A.O., 2013. Shear strengthening of RC beams with NSM CFRP laminates: Experimental research and analytical formulation. Composite Structures, 99(0), pp.477–490.

Dias, S.J.E., Barros, J.A.O., 2011b. Shear strengthening of RC T-section beams with low strength concrete using NSM CFRP laminates. Cement and Concrete Composites, 33(2), pp.334–345.

Dias, S.J.E., Barros, J.A.O., 2008. Shear Strengthening of T Cross Section Reinforced Concrete Beams by Near-Surface Mounted Technique. Journal of Composites for Construction, 12(3), pp.300–311.

Dussek, I.J., 1974. Strengthening of bridge beams and similar structures by means of epoxy-resin-bonded external reinforcement. Transport and research record, Washington, USA, pp.21–24.

El-Hacha, Raafat, Rizkalla, S.H., 2004. Near-surface-mounted fiber-reinforced polymer reinforcements for flexural strengthening of concrete structures. ACI Struct J, 101(5), pp.717–726.

Eligehausen, R., Appl, J.J., Lehr, B., Meszaros, J., Fuchs, W., 2004. Load-bearing Behavior and Design of Fastenings with Adhesive Anchors under Tension Loading – Part 1: Single Anchors with Large Axial and Edge Spacing). Beton und Stahlbetonbau, 99(7), pp.561–571.

Eligehausen, R., Popov, E.P., Bertero, V.V., 1983. Local Bond Stress-Slip Relationships of Deformed Bars Under Generalized Excitations. Report UCB/EERC-83/23. Berkeley: EERC, University of California.

El-Salakawy, E., Polak, M.A., Soudki, K.A., 2003. New strengthening technique for concrete slab column connections. ACI Structural Journal, 100(3), pp.297–304.

Esmaeeli, E., Barros, J.A., Baghi, H., 2013. Hybrid Composite Plates (HCP) for Shear Strengthening of RC Beams. In J. A. Barros & J. M. Sena-Cruz, eds. FRPRCS11, Guimarães, Portugal, 26-28 June.

Esmaeeli, E., Barros, J.A.O., Sena-Cruz, J., Varum, H.,Melo, J., 2015. Assessment of the efficiency of prefabricated hybrid composite plates (HCPs) for retrofitting of damaged interior RC beam–column joints. Composite Structures, 119, pp.24–37.

Esmaeeli, E., Barros, J.A.O., Baghi, H, Sena-Cruz, J.M., 2014. Development of hybrid composite plate (HPC) for the repair and strengthening of RC elements. In SHCC3-3rd International RILEM Conference on Strain Hardening Cementitious Composites (SHCC3-Delft). Dordrecht, NL.

European Committee for Standardization, 2001. EN 206-1 Concrete – Part 1: Specification, performance, production and conformity,

European Committee for Standardization, 2004. Eurocode 2: Design of concrete structures - Part 1-1: General rules and rules for buildings Eurocode.

European Committee for Standardization, ISO 527-2:2012. Plastics - Determination of tensile properties - Part 2: Test conditions for moulding and extrusion plastics.

European Committee for Standardization, UNI EN ISO 6892-1:2009 Metallic materials - Tensile testing - Part 1: Method of test at room temperature.

Federation Internationale du Béton (fib), 2001. Externally bonded FRP Reinforcement for RC Structures.

Fenwick, R.C., Paulay, T., 1968. Mechanisms of Shear Resistance of Concrete Beams. Journal of Structural Division, ASCE, 94(10), pp.2325–2350.

Fernàndez Ruiz, M., Muttoni, A., Kunz, J., 2010. Strengthening of Flat Slabs Against Punching Shear Using Post-Installed Shear Reinforcement. ACI Struct J, 107(4), pp.434–442.

fib, 2013. fib Model Code for Concrete Structures 2010, Ernst & Sohn.

Garcia, R., Hajirasouliha, I., Guadagnini, M., Helal, Y., Jemaa, Y., Pilakoutas, K., Mongabure, P., Chrysostomou, C., Kyriakides, N., Ilki, A., Budescu, M., Taranu, N.Ciupala, M.A., Torres, L., Saiidi, M., 2014. Full-Scale

Shaking Table Tests on a Substandard RC Building Repaired and Strengthened with Post-Tensioned Metal Straps. Journal of Earthquake Engineering, 18(2), pp.187–213. Available at: http://www.tandfonline.com/doi/abs/10.1080/13632469.2013.847874#.VPWjpfnz1VQ [Accessed March 3, 2015].

Van Gemert, D., 1996. Desing applications and durabilty of plate bonding technique. In R. K. Dhir & M. R. Jones, eds. Procedins: International Conference of Concrete Repair, Rehabilitation and Protection. Scotland, pp. 559–569.

Godat, A. L'Hady, A. Chaallal, O. Neale, K., 2012. Bond Behavior of the ETS FRP Bar Shear-Strengthening Method. Journal of Composites for Construction, 16(5), pp.529–530.

Godat, A., Neale, K.W., Labossière, P., 2007. Numerical Modeling of FRP Shear-Strengthened Reinforced Concrete Beams. Journal of Composites for Construction, 11(6), pp.640–649.

Gopalaratnam, V.S., Shah, S.P., 1985. Softening Response of Plain Concrete in Direct Tension. ACI Journal, Proceedings, 82(3), pp.310–323.

Grande, E., Imbimbo, M., Rasuolo, A., 2009. Effect of transverse steel on the response of RC beams strengthened in shear by FRP: Experimental study. Journal of Composites for Construction, 13(5), pp.405–414.

Gupta, P., Collins, M.P., 1993. Behaviour of Reinforced Concrete Members Subjected to Shear and Compression,

Haskett, M., Oehlers, D.J., Mohamed Ali, M.S., 2008. Local and global bond characteristics of steel reinforcing bars. Engineering Structures, 30(2), pp.376–383.

Hassan, T., Rizkalla, S.H., 2003. Investigation of Bond in Concrete Structures Strengthened with Near Surface Mounted Carbon Fiber Reinforced Polymer Strips. Journal of Composites for Construction, 7(3), pp.248–257.

Hassanzadeh, G., Sundqvist, H., 1998. Strengthening of bridge slabs on columns. Nordic Concrete Research, 21 (paper no.2).

Helal, Y., Garcia, Reyes, Pilakoutas, K., Guadagnini, M., Hajirasouliha, I., 2014. Strengthening of short splices in RC beams using Post-Tensioned Metal Straps. Materials and Structures. Available at: http://link.springer.com/10.1617/s11527-014-0481-6 [Accessed February 17, 2015].

Hofacker, I., Eligehausen, R., 2001. Post-installed rebars connection under seismic loading. In R. Eligehausen, ed. International Symposium on Connection between Steel and Concrete, Stuttgart, Germany. RILEM Publication S.A.R.L.

Hognestad, E., 1952. What do we know about diagonal tension and web reinforcement in concrete. University of Illinois Engineering Experiment Station, Urbana, Illinois.

Hoult, N.A., Lees, J.M., 2009. Modeling of an Unbonded CFRP Strap Shear Retrofitting System for Reinforced Concrete Beams. Journal of Composites for Construction, 13(4), pp.292–301.

Hu, H.-T., Lin, F.-M., Jan, Y.-Y., 2004. Nonlinear finite element analysis of reinforced concrete beams strengthened by fiber-reinforced plastics. Composite Structures, 63(3-4), pp.271–281.

Hu, H.-T., Schnobrich, W.C., 1990. Nonlinear Analysis of Cracked Reinforced Concrete. ACI Struct J, 87(2), pp.199–207.

Ionel, G., 1996. Two strengthening methods for prestressed damagad beams. In C. & Hall, ed. Proceedings of the International Conference Repair Rehabilitation and Protection, Scotland. pp. 571–581.

Jalali, M., Sharbatdar, M. K., Chen, J-F, Jandaghi Alaee. F., 2012. Shear strengthening of RC beams using innovative manually made NSM FRP bars. Construction and Building Materials, 36, pp.990–1000.

Jirsa, J., Kim, Y., Satrom, C.N., 2011. Shear strengthening of Bridge girders using CFRP sheets and anchors. fib Symposium Prague, pp.1137–1140.

Kaiser, H., 1989. Strengthening of reinforced concrete with CFRP plates. Ph.D. dissertation, ETH Zürich.

Kani, G.N.J., 1967. How Safe Are Our Large Reinforced Concrete Beams? ACI Journal, Proceedings, 64(3), pp.128–141.

Kani, G.N.J., 1964. The Riddle of Shear Failure and its Solution. ACI Journal, Proceedings, 61(4), pp.441–467.

Khalifa, A., Gold, W. J., Nanni A., Abel Aziz M., 1998. Contribution of Externally Bonded FRP to Shear Capacity of RC Flexural Members. Journal of Composites for Construction, 2(4), pp.195–202.

Khalifa, A., 1999. Shear performance of reinforced concrete beams strengthened with advanced composites. Ph.D. Thesis, Structural Engineering Department, Alexandria University, Egypt.

Khalifa, A., Nanni, A., 2000. Improving shear capacity of existing RC T-section beams using CFRP composites. Cement and Concrete Composites, 22(3), pp.165–174.

Khalifa, A., Nanni, A., 2002. Rehabilitation of rectangular simply supported RC beams with shear deficiencies using CFRP composites. Construction and Building Materials, 16(3), pp.135–146.

Kim, S.Y., Yang, K.H., Byun, H.Y., Ashour, A.F., 2007. Tests of reinforced concrete beams strengthened with wire rope units. Engineering Structures, 29(10), pp.2711–2722.

Kim, S, J., Smith, S.T., 2009. Behaviour of Handmade FRP Anchors under Tensile Load in Uncracked Concrete. Advances in Structural Engineering, 12(6), pp.845–865.

Kolmar, W., 1986. Beschreibung der kraftuebertragung über risse in nichtlinearen finite-element-berechnungen von stahlbetontragwerken. Darmstadt University of Technology, Germany.

Kolmar, W., Mehlhorn, G., 1984. Comparison of shear stiffness formulations for cracked reinforced concrete elements. In Proceedings: Computer aided analysis and design of concrete stucture, Part1. Spit,Yugoslavia, pp. 133–147.

Kuchma, D.A., Collins, M.P., 1998. Advances in understanding shear performance of concrete structures. Progress in Structural Engineering and Materials, 1(4), pp.360–369.

Kuchma, D.A., Su Kim, K., 2001. Stress limits and minimum reinforcement requirements in shear design provisions. Progress in Structural Engineering and Materials, 3(4), pp.317–325.

Kupfer, H., Mang, R., Karavesyrouglou, M., 1983. Failure of the Shear-Zone of R.C. and P.C. Girders—An Analysis with Consideration of Interlocking of Cracks. Bauingenieur, 57, pp.143–149.

Kwak, H.-G., Filippou, F.C., 1990. Finite element analysis of reinforced concrete structures under monotonic loads, Berkeley, California.

L'Hermite, R., 1967. L'application des colles et résines dans la conctruction. Le béton à coffrage portant. In Annales de l'I.T.B.T.P., No. 239.

Lee, D.O., Lim, D.H., 2008. Shear behavior of RC beams strengthened with NSM CFRP strips. In Proceedings of the 3rd ACF International Conference.

Lees, J.M., Winistörfer, A.U., Meier, U., 2002. External Prestressed Carbon Fiber-Reinforced Polymer Straps for Shear Enhancement of Concrete. Journal of Composites for Construction, 6(4), pp.249–256.

Li, A., Delmas, Y., 2001. CRFP contribution to shear capacity of strengthened RC beams. Engineering Structures, 23(10), pp.1212–1220.

Li, V.C., 1998. Repair and Retrofit with Engineered Cementitious Composites. In Procedins: FRAMCoS-3. Freiburg,Germany. p. Vol.3 pp 1715–1726.

Lima, J.L., Barros, J.A., 2011. Reliability analysis of shear strengthening externally bonded FRP models. Proceedings of the ICE - Structures and Buildings, 164(1), pp.43–56.

Lima, J.L.T., Barros, J.A.O., 2007. Design models for shear strengthening of reinforced concrete beams with externally bonded FRP composites: a statistical vs reliability approach. In FRPRCS-8 University of Patras, Patras, Greece, July 16-18, 2007. pp. 1–10.

De Lorenzis, L., Nanni, A., 2002. Bond between near-surface mounted fiber-reinforced polymer rods and concrete in structural strengthening. ACI Structural Journal, 99(2), pp.123–132.

De Lorenzis, L., Nanni, A., 2001. Shear strengthening of reinforced concrete beams with near-surface mounted fiber-reinforced polymer rods. ACI Structural Journal, 98(1), pp.60–68.

De Lorenzis, L., Nanni, A., La Tegola, A., 2000. Flexural and Shear Strengthening of Reinforced Concrete Structures with Near Surface Mounted FRP Rods. In Advanced Composite Materials in Bridges and Structures, Proc. of 3rd Int. pp. 521– 528.

De Lorenzis, L., Teng, J.G., 2007. Near-surface mounted FRP reinforcement: An emerging technique for strengthening structures. Composites Part B: Engineering, 38(2), pp.119–143.

Lutz, L.A., Gergely, P., 1967. Mechanichs of Bond and Slip of Deformed Reinforcement. ACI Journal, pp.711–721.

Maekawa, K., Pimanmas, A., Okamura, H., 2003. Nonlinear mechanics of reinforced concrete, CRC Press.

Mahrenholtz, C., 2012. Seismic Bond Model for Concrete Reinforcement and the Application to Column-to-Foundation Connections. Phd Thesis - Universität Stuttgart.

Malek, A.M., Saasatmanesh, H., 1998. Ultimate Shear Capacity of Reinforced Concrete Beams Strengthened with Web-Bonded Fiber-Reinforced Plastic Plates. ACI Struct J, 95(4), pp.391–399.

Manos, G.C., Theofanous, M., Katakalos, K., 2014. Numerical simulation of the shear behaviour of reinforced concrete rectangular beam specimens with or without FRP-strip shear reinforcement. Advances in Engineering Software, 67, pp.47–56.

Martinola, G., Meda, A., Plizzari, G.A., 2007. An application of high performance fiber reinforced cementitious composites for R/C beams strengthening. In FraMCos-6 Catania (Italy), Proceedings.

Mattock, A.H., Hawkins, N.M., 1972. Shear transfer in reinforced concrete recent research. PCI Journal, 17(2), pp.55–75.

Mazaheripour, H., Barros J.A.O., Sena-Cruz, J.M., Pepe, M., Martinelli, E., 2013. Experimental study on bond performance of GFRP bars in self-compacting steel fiber reinforced concrete. Composite Structures, 95(0), pp.202–212.

Meier, U., 1987. Bridge repair with high performance composite materials. Material & Technik, 4, pp.125–128.

Meier, U., 1992. Carbon Fiber-Reinforced Polymers: Modern Materials in Bridge Engineering. Structural Engineering International, 2(1), pp.7–12.

Meier, U., Deuring, M., Meier, H., 1992. Strengthening of structures with CFRP laminates: Research and applications in Switzerland. In K. W. Neale & P. Labossiere, eds. Procedins: Advanced Composite Material in Bridges and Structures. Montreal.

Meisami, M.H., Mostofinejad, D., Nakamura, H., 2015. Strengthening of flat slabs with FRP fan for punching shear. Composite Structures, 119, pp.305–314.

Mofidi, A., Chaallal, O., Benmokrane, B., Neale, K., 2012. Experimental Tests and Design Model for RC Beams Strengthened in Shear Using the Embedded Through-Section FRP Method. Journal of Composites for Construction, 16(5), pp.540–550.

Mofidi, A., Chaallal, O., 2011. Shear Strengthening of RC Beams with EB FRP: Influencing Factors and Conceptual Debonding Model. Journal of Composites for Construction, 15(1), pp.62–74.

Mohamed Ali, M.S., Oehlers, D.J., Griffith, M.C.. Seracino, R., 2008. Interfacial stress transfer of near surface-mounted FRP-to-concrete joints. Engineering Structures, 30(7), pp.1861–1868.

Mohamed Ali, M.S., Oehlers, D.J., Seracino, R., 2006. Vertical shear interaction model between external FRP transverse plates and internal steel stirrups. Engineering Structures, 28(3), pp.381–389.

Monti, G., Liotta, M., 2007. Tests and design equations for FRP-strengthening in shear. Construction and Building Materials, 21(4), pp.799–809.

Moody, K.G., Viest, I.M., Elster, R.C., Hognestad, E., 1954. Shear Strength of Reinforced Beams, Part-1: Test of Simple Beam. ACI Journal, Proceedings, 51(4), pp.317–332.

Mörsch, E., 1908. Der Eisenbetonbau, seine Theorie und Anwendung,

Mostakhdemin Hosseini, M.R., Dias, S.J.E., Barros, J.A.O., 2014. Effectiveness of prestressed nsm cfrp laminates for the flexural strengthening of rc slabs. Composite Structures, 111, pp.249–258.

Naaman, A.E., Reinhardt, H.W., 2006. Proposed classification of HPFRC composites based on their tensile response. Materials and Structures, 39(5), pp.547–555.

Nakai, H., Asai, H., Noritake, K., 1994. Studies on characteristics of beams using. Aramid tendons. In Bridge assessment management and desing. Proceedings of the centenary year bridge conference, Cardiff, 26-30 September.

Nanni, A., Di Ludovico, M., Parretti, M., 2004. Shear Strengthening of a PC Bridge Girder with NSM CFRP Rectangular Bars. Advances in Structural Engineering, 7(4).

National Research Council 2004, 2012. Guide for design and construction of externally bonded FRP systems for strengthening existing structures CNR-DT200.

Nielsen, M.P., 1999. Limit Analysis and Concrete Plasticiy, CRC Press.

Nielsen, M.P., Braestrup, M.W., 1975. PLASTIC SHEAR STRENGTH OF REINFORCED CONCRETE BEAMS. Dan Selsk Bygningsstat Medd, 46(3), pp.61–99.

Niwa, J., Yamada, K., Yolozawa, K., Okamura, M., 1986. Reevaluation of the Equation for Shear Strength of RC-Beams without Web Reinforcement. Proceedings, Japan Society of Civil Engineering,, 5(372), pp.1986–1988.

Oehlers, D.J., Haskett, M., Wu, C., Seracino, R. 2008. Embedding NSM FRP plates for Improved IC debonding resistance. Journal of Composites for Construction, 12(6), pp.635–642.

Okamura, H., Higai, T., 1980. Proposed Design Equation for Shear Strength of R.C. Beams without Web Reinforcement. Proceedings, Japan Society of Civil Engineering, 300, pp.131–141.

Owa, S.,Yamamoto, Y.,Kondo, T., Fogstad, C., 2012. Study on Strength and Ductility of Post-installed Adhesive Anchoring System –Comparison and analysis of experimental values, various values in ultimate strength and design strength. In 15WCEE / 15th World Conference on Earthquake Engineering, Lisbon.

Park, R., Paulay, T., 1975. Reinforced Concrete Structures, Wiley 1 edition (July 1975).

Paulay, T., 1971. Coupling Beams of Reinforced Concrete Shear Walls. Journal of the Structural Division, 97(3), pp.843–862.

Pellegrino, C., Modena, C., 2002. Fiber Reinforced Polymer Shear Strengthening of Reinforced Concrete Beams with Transverse Steel Reinforcement. Journal of Composites for Construction, 6(2), pp.104–111.

Pellegrino, M., Modena, C., 2006. Fiber-Reinforced Polymer Shear Strengthening of Reinforced Concrete Beams: Experimental Study and Analytical Modeling. ACI Struct J, 103(5), pp.720–728.

Rahal, K.N., Rumaih, H.A., 2011. Tests on reinforced concrete beams strengthened in shear using near surface mounted CFRP and steel bars. Engineering Structures, 33(1), pp.53–62.

Ramirez, J.A., Breen, J.E., 1991. Evaluation of a Modified Truss-Model Approach for Beams in Shear. ACI Structural Journal, 88(5), pp.562–572.

Reineck, K.-H., 1991a. Model for Structural Concrete Members without Transverse Reinforcement,

Reineck, K.-H., 1991b. Ultimate Shear Force of Structural Concrete Members without Transverse Reinforcement Derived from a Mechanical Model. ACI Structural Journal, 88(5), pp.592–602.

Richart, F.E., 1927. An investigation of web stresses in reinforced concrete beams. Bulletin (University of Illinois (Urbana-Champaign campus)., p.76.

RILEM Technical Committee 201, 2006. Report 36: Textile Reinforced Concrete - State-of-the-Art Report. In Brameshuber, W.

Ritter, W., 1899. Die Bauweise Hennebique (Construction Techniques of Hennebique). Schweizerische Bauzeitung, 33(7), pp.41–61.

Rizzo, A., De Lorenzis, L., 2009. Behavior and capacity of RC beams strengthened in shear with NSM FRP reinforcement. Construction and Building Materials, 23(4), pp.1555–1567.

Rots, J.G., 2002. Comparative study of crack models. In A. A. Hendriks, M.A.N., Rots, J.G., ed. Third DIANA World Conference. Tokyo, Japan 9-11 October: Taylor & Francis, pp. 17–28. Available at:

Rots, J.G., 1988. Computational modeling of concrete fracture. PhD Thesis, Delft University of Technology, The Netherlands.

Rots, J.G., Nauta, P., Kusters, G.M.A., Blaawendraad, J., 1985. Smeared crack approach and fracture localization in concrete. HERON, 30(1), pp.1–48.

Rots, J.G., de Borst, R., 1987. Analysis of Mixed-Mode Fracture in Concrete. Journal of Enigineering Mechanichs, ASCE, 113(11), pp.1739–1758.

Sayed, A.M., Wang, X., Wu, Z., 2014. Finite element modeling of the shear capacity of RC beams strengthened with FRP sheets by considering different failure modes. Construction and Building Materials, 59, pp.169–179.

Sena-Cruz, J.M., Barros, J.A.O., Azevedo, A. F. M., Ventura-Gouveia, A. 2007. Numerical simulation of the nonlinear behavior of RC beams strengthened with NSM CFRP strips. In Proceedings of CMNE/CILAMCE Congress. FEUP, Porto, Portugal, 13 15 June, 2007.

Sena-Cruz, J.M., 2004. Strengthening of concrete structures with near-surface mounted CFRP laminate strip. Department of Civil Engineering, University of Minho.

Sena-Cruz, J.M., Barros, J.A.O., 2004. Bond Between Near-Surface Mounted Carbon-Fiber-Reinforced Polymer Laminate Strips and Concrete. Journal of Composites for Construction, 8(6), pp.516–527.

Seo, D.-W., Park,K-T, You, Y-J, Kim, H-Y, 2003. Enhancement in Elastic Modulus of GFRP Bars by Material Hybridization. Engineering, 5, pp.865–869.

Seo, S.-Y., Feo, L., Hui, D., 2013. Bond strength of near surface-mounted FRP plate for retrofit of concrete structures. Composite Structures, 95, pp.719–727.

Seracino, R., Jones, N.M., Ali, M.S., Page, M.W., Oehlers, D.J. 2007. Bond Strength of Near-Surface Mounted FRP Strip-to-Concrete Joints. Journal of Composites for Construction, 11(4), pp.401–409.

Shehata, I., 1996. Structural repair of RC beams in shear. In Proceedings of the International Conference on Concrete Repair, Rehabilitation and Protection, Scotland. Chapman & Hall, pp. 615–622.

Shioya, T., Iguro, M., Nojiri, Y., Akiayma, H., Okada, T., 1989. Shear Strength of Large Reinforced Concrete Beams, Fracture Mechanics: Application to Concrete.

Silman Associated, 2001. Fallingwater. Available at: http://www.silman.com/services/historic-preservation/fallingwater/.

Sissakis, K., Sheikh, S.A., 2007. Strengthening Concrete Slabs for Punching Shear with Carbon Fiber-Reinforced Polymer Laminates. ACI Struct J, 104(1), pp.49–59.

Smith, S.T., Hu, S., Kim, S.J., Seracino, R., 2011. FRP-strengthened RC slabs anchored with FRP anchors. Engineering Structures, 33(4), pp.1075–1087.

Standards Australia, 2008. HB 305-2008 Design handbook for RC structures retrofitted with FRP and metal plates: beams and slabs,

Talbot, A.N., 1909. Tests of Reinforced Concrete Beams: Resistance to Web Stresses Series of 1907 and 1908. Bulletin 29, University of Illinois Engineering Experiment Station, Urbana, III.

Täljsten, B., 1994. Plate Bonding. Strengthening of Existing Concrete Structures with Epoxy Bonded Plates of Steel or Fibre Reinforced Plastic. Ph.D. Thesis, Lulea University of Technology, Sweden.

Täljsten, B., 2003. Strengthening concrete beams for shear with CFRP sheets. Construction and Building Materials, 17(1), pp.15–26.

Taylor, H.P.J., 1974. The Fundamental Behaviour of Reinforced Concrete Beams in Bending and Shear. Shear in Reinforced Concrete, SP-42, American Concrete Institute, SP-74, pp.43–77.

Teng, J.G., Chen, J. F., Smith, S. T., Lam, L., 2003. Behaviour and strength of FRP-strengthened RC structures: a state-of-the-art review. Proceedings of the ICE - Structures and Buildings, 156(1), pp.51–62.

Teng, J.G., De Lorenzis, L., Wang, B., Li, R, Wong, T.L., Lam, L., 2006. Debonding Failures of RC Beams Strengthened with Near Surface Mounted CFRP Strips. Journal of Composites for Construction, 10(2), pp.92–105.

Teng, J.G., Zhang, S.S., Dai, J.G., Chen, J.F., 2013. Three-dimensional meso-scale finite element modeling of bonded joints between a near-surface mounted FRP strip and concrete. Computers & Structures, 117, pp.105–117.

Teng, S., Kong, F.-K., Poh, S.P., Guan, L.W., Kang-Hai, T., 1996. Performance of Strengthened Concrete Deep Beams Predamaged in Shear. ACI Structural Journal, 92(2), pp.159–170.

Tepfers, R., 1973. A Theory of Bond Applied to Overlapped Tensile Reinforcemet Spices for Deformed Bars. Chalmers University of Technology.

Thürlimann, B., Grob, J., 1976. Ultimate strength and design of reinforced concrete beams under bending and shear,

Triantafillou, T., 1998. Shear Strengthening of Reinforced Concrete Beams Using Epoxy-Bonded FRP Composites. ACI Struct J, 98(2), pp.107–115.

Triantafillou, T., Antonopoulos, C.P., 2000. Design of concrete flexural members strengthened in shear with FRP. Journal of Composites for Construction, 4(4), pp.198–205.

Triantafillou, T.C., Papanicolaou, C.G., 2006. Shear strengthening of reinforced concrete members with textile reinforced mortar (TRM) jackets. Materials and Structures, 39(1), pp.93–103.

Triantafillou, T.C., Plevris, N., 1992. Strengthening of RC beams with epoxy-bonded fibre-composite materials. Materials and Structures, 25(4), pp.201–211.

Valerio, P., Ibell, T.J., Darby, A.P., 2007. Deep embedment of FRP bars for shear strengthening of prestressed concrete bridges. In Proceedings of Fibre-Reinforced Polymers for RC Structures (FRPRCS-8). pp. 2007–07–01, Patras.

Valerio, P., Ibell, T.J., Darby, A.P., 2009. Deep embedment of FRP for concrete shear strengthening. Proceedings of the ICE - Structures and Buildings, 162(5), pp.311–321.

Vecchio, F.J., Collins, M.P., 1986. The Modified Compression Field Theory for Reinforced Concrete Elements Subjected to Shear. ACI Journal, Proceedings, 83(2), pp.219–231.

Ventura-Gouveia, A., 2011. Constitutive models for the material nonlinear analysis of concrete structures including time-dependent effects. Universidade do Minho.

Ventura-Gouveia, A., Barros, J.A.O., Azevedo, A. F. M., Sena-Cruz, J.M., 2008. Multi-Fixed smeared 3D crack model to simulate the behavior of fiber reinforced concrete structures. In Torres Marques et al., ed. CCC2008-Challenges for Civil Construction. FEUP, Porto, p. 11.

Ventura-Gouveia, A., Barros, J.A.O., Azevedo, A. F. M., Sena-Cruz, J.M., 2006. Relatório 06-DEC/E-20 Implementação da técnica do arc-length e métodos relacionados no programa de elementos finitos FEMIX,

Vintzeleou, E.N., Tassios, T.P., 1986. Mathematical Models for Dowel Action under Monotonic Conditions. Magazine of Concrete Research, 38, pp.13–22.

Walraven, J.C., 1981. Fundamental Analysis of Aggregate Interlock. Journal of the Structural Division, 107(11), pp.2245–2270.

Withey, M.O., 1908. Bulletin of the University of Wisconsin, Engineering Series. Bulletin of the University of Wisconsin, Engineering Series, 88(3), pp.1–66.

Withey, M.O., 1907. Tests of Plain and Reinforced Concrete Series of 1906. Bulletin of the University of Wisconsin, Engineering Series, 4(1), pp.1–66.

Wittmann, F.H., 1998. Application of Fracture Mechanics to Optimize Repair System and Protective Coatings for Reinforced Concrete Structures. In Procedins: FRAMCoS-3. Freiburg,Germany. p. Vol.3 1707–1714.

Yang, K.-H., Byun, H.-Y., Ashour, A.F., 2009. Shear strengthening of continuous reinforced concrete T-beams using wire rope units. Engineering Structures, 31(5), pp.1154–1165.

Yoon, Y.S., Cook, W.D., Mitchell, D., 1996. Minimum Shear Reinforcement in Normal and High Strength Concrete Beams. ACI Structural Journal, 93, pp.576–584.

Yuan, H., Teng, J.G., Seracino, R., Wu, Z.S., Yao, J., 2004. Full-range behavior of FRP-to-concrete bonded joints. Engineering Structures, 26(5), pp.553–565.

Zhang, S.S., Teng, J.G., 2014. Finite element analysis of end cover separation in RC beams strengthened in flexure with FRP. Engineering Structures, 75, pp.550–560.

Zsutty, 1968. Beam Shear Strength Prediction by analysis of Existing Data. ACI Structural Journal, 65, pp.943–951.

Annex A

Annex A: Literature Review- Bond Test

Specimen ID (Experimental Program)	Mat	ϕ	f_{cm}	l_b/ϕ	l_b	t	F_{pull}	τ_{avg}	F.T.	Adh.
Dalfè et al. (2011)										
S_L5_E2(1)	S	8	28.4	6.25	50	2	21.8	17.3		Sikadur 32N
S_L5_E5(1)	S	8	28.4	6	48	5	20.2	16.7		Sikadur 32N
E_L5_E2(1)	S	8	28.4	6.25	50	2	15.9	12.6		S&P - Resin 50
E_L5_E5(1)*	S	8	28.4	3.5	28	5	9.4	13.4		S&P - Resin 50
S_L5_E2(1)	S	12	28.4	4	48	2	29.8	16.5		Sikadur 32N
S_L5_E2(2)	S	12	28.4	4.33	52		24.2	12.3		Sikadur 32N
S_L5_E4(1)	S	12	28.4	4.17	50	4	23.7	12.6		Sikadur 32N
S_L5_E4(2)	S	12	28.4	4.25	51		19.6	10.2		Sikadur 32N
S_L5_E6(1)	S	12	28.4	4.25	51	6	30.2	15.7		Sikadur 32N
S_L5_E6(2)	S	12	28.4	4.33	52		27.4	14.0		Sikadur 32N
S_L7.5_E2(1)	S	12	28.4	6.25	75	2	46.4	16.4		Sikadur 32N
S_L7.5_E2(2)	S	12	28.4	6.33	76		35.8	12.5		Sikadur 32N
S_L7.5_E4(1)	S	12	28.4	6.08	73	4	42.0	15.3		Sikadur 32N
S_L7.5_E4(2)	S	12	28.4	6.33	76		41.2	14.4		Sikadur 32N
S_L7.5_E2(1)	S	12	28.4	6.33	76	6	39.9	13.9		Sikadur 32N
S_L7.5_E2(2)	S	12	28.4	6.25	75		41.5	14.7		Sikadur 32N
E_L5_E2(1)	S	12	28.4	4.42	53	2	19.3	9.7		S&P - Resin 50
E_L5_E2(2)	S	12	28.4	4.17	50		30.9	16.4		S&P - Resin 50
E_L5_E4(1)	S	12	28.4	4.42	53	4	26.1	13.0		S&P - Resin 50
E_L5_E4(2)	S	12	28.4	4.67	56		25.6	12.1		S&P - Resin 50
E_L5_E6(1)	S	12	28.4	4.67	56	6	28.6	13.5		S&P - Resin 50
E_L5_E6(2)	S	12	28.4	5	60		30.0	13.3		S&P - Resin 50
E_L7.5_E2(1)	S	12	28.4	6	72	2	28.6	10.5		S&P - Resin 50
E_L7.5_E2(2)	S	12	28.4	6.42	77		34.3	11.8		S&P - Resin 50
E_L7.5_E4(1)	S	12	28.4	6.25	75	4	37.8	13.4		S&P - Resin 50
E_L7.5_E4(2)	S	12	28.4	6.83	82		37.5	12.1		S&P - Resin 50
E_L7.5_E2(1)	S	12	28.4	6.33	76	6	40.5	14.1		S&P - Resin 50
E_L7.5_E2(2)	S	12	28.4	6.5	78		37.6	12.8		S&P - Resin 50
Godat et al. (2012)[a]										
C1-1.50d-9.5B-15d	C-SC	9.5	20.7	15.1	143	15	35.7	8.4	C-S	
C1-1.50d-12.7B-15d	C-SC	12.7	20.7	11.3	143	15	57.0	7.5	C-S	
C2-1.25d-5S-15d	C-S	9.5	42.7	15.1	143	12	80.4	18.8	P-O	
C2-1.50d-5S-15d	C-S	9.5	42.7	15.1	143	15	91.2	22.3	P-O	
C2-2.00d-5S-15d	C-S	9.5	42.7	15.1	143	19	78.5	18.4	P-O	
C2-1.50d-9.5S-5.0d	C-S	9.5	42.7	5.05	48	15	42.8	29.9	P-O	
C2-1.50d-9.5S-7.5d	C-S	9.5	42.7	7.47	71	15	57.4	26.9	P-O	
C2-1.50d-9.5S-10.0d	C-S	9.5	42.7	10	95	15	63.4	22.3	P-O	
C2-1.50d-9.5S-12.5d	C-S	9.5	42.7	12.5	119	15	71.0	20.1	P-O	
C2-1.50d-9.5S-17.5d	C-S	9.5	42.7	17.5	166	15	100.7	20.3	P-O	
C2-1.50d-9.5S-20.0d	C-S	9.5	42.7	20	190	15	102.4	18.1	P-O	
C2-1.50d-9.5S-25.0d	C-S	9.5	42.7	25.1	238	15	114.7	16.1	R-Y	
C2-1.50d-9.5S-30.0d	C-S	9.5	42.7	30	285	15	128.3	15.1	R-Y	

Specimen ID (Experimental Program	Mat	ϕ	$f_{cm,cube}$	l_b/ϕ	l_b	t	F_{pull}	τ_{avg}	F.T.	Adh.
Valerio et al. (2009) Note – for this experimental program the the cube compressive strenth is indicated										
Steel 8	S	8	55-60	1.9	15	1		37.0	SH	Hilti 500
Steel 8	S	8	55-60	3.8	30	1		36.0	R-Y	Hilti 500
Steel 8	S	8	55-60	5.6	45	1		27.0	R-Y	Hilti 500
Steel 8	S	8	55-60	7.5	60	1		20.0	R-Y	Hilti 500
Steel 8	S	8	55-60	9.4	75	1		16.0	R-Y	Hilti 500
Steel 8	S	8	55-60	1.9	15	1		37.0	SR	Araldite
Steel 8	S	8	55-60	3.8	30	1		27.0	SR	Araldite
Steel 8	S	8	55-60	5.6	45	1		26.0	R-Y	Araldite
Steel 8	S	8	55-60	7.5	60	1		21.0	R-Y	Araldite
Steel 8	S	8	55-60	9.4	75	1		16.0	R-Y	Araldite
Steel 8	S	8	55-60	1.9	15	1		10.0	SR	Hilti 150
Steel 8	S	8	55-60	3.8	30	1		17.0	SR	Hilti 150
Steel 8	S	8	55-60	5.6	45	1		26.0	R-Y	Hilti 150
Steel 8	S	8	55-60	7.5	60	1		21.0	R-Y	Hilti 150
Steel 8	S	8	55-60	9.4	75	1		16.0	R-Y	Hilti 150
Carbon 7.5	C	7.5	55-60	2.0	15	1		36.0	IS	Hilti 500
Carbon 7.5	C	7.5	55-60	4.0	30	1		32.0	IS	Hilti 500
Carbon 7.5	C	7.5	55-60	6.0	45	1		28.0	IS	Hilti 500
Carbon 7.5	C	7.5	55-60	8.0	60	1		24.0	IS	Hilti 500
Carbon 7.5	C	7.5	55-60	10.0	75	1		25.0	IS	Hilti 500
Carbon 7.5	C	7.5	55-60	2.0	15	1		33.0	IS	Araldite
Carbon 7.5	C	7.5	55-60	4.0	30	1		22.0	IS	Araldite
Carbon 7.5	C	7.5	55-60	6.0	45	1		28.0	IS	Araldite
Carbon 7.5	C	7.5	55-60	8.0	60	1		30.0	IS	Araldite
Carbon 7.5	C	7.5	55-60	10.0	75	1		31.0	IS	Araldite
Carbon 7.5	C	7.5	55-60	2.0	15	1		17.0	IS	Hilti 150
Carbon 7.5	C	7.5	55-60	4.0	30	1		17.0	IS	Hilti 150
Carbon 7.5	C	7.5	55-60	6.0	45	1		16.0	IS	Hilti 150
Carbon 7.5	C	7.5	55-60	8.0	60	1		19.0	IS	Hilti 150
Carbon 7.5	C	7.5	55-60	10.0	75	1		19.0	IS	Hilti 150
Carbon 6	C	6	55-60	2.5	15	1		33.0	IS	Hilti 500
Carbon 6	C	6	55-60	5.0	30	1		30.0	IS	Hilti 500
Carbon 6	C	6	55-60	7.5	45	1		37.0	IS	Hilti 500
Carbon 6	C	6	55-60	10.0	60	1		23.0	IS	Hilti 500
Carbon 6	C	6	55-60	12.5	75	1		21.0	IS	Hilti 500
Glass 9	G	9	55-60	1.7	15	1		25.0	IS	Hilti 500
Glass 9	G	9	55-60	3.3	30	1		27.0	IS	Hilti 500
Glass 9	G	9	55-60	5.0	45	1		24.0	IS	Hilti 500
Glass 9	G	9	55-60	6.7	60	1		20.0	IS	Hilti 500
Glass 9	G	9	55-60	8.3	75	1		16.0	R-Y	Hilti 500
Glass 9	G	9	55-60	1.7	15	1		36.0	IS	Araldite
Glass 9	G	9	55-60	3.3	30	1		4.0	IS	Araldite
Glass 9	G	9	55-60	5.0	45	1		27.0	IS	Araldite
Glass 9	G	9	55-60	6.7	60	1		22.0	R-Y	Araldite
Glass 9	G	9	55-60	8.3	75	1		25.0	IS	Araldite
Glass 9	G	9	55-60	1.7	15	1		16.0	IS	Hilti 150
Glass 9	G	9	55-60	3.3	30	1		16.0	IS	Hilti 150
Glass 9	G	9	55-60	5.0	45	1		17.0	IS	Hilti 150
Glass 9	G	9	55-60	6.7	60	1		17.0	IS	Hilti 150
Glass 9	G	9	55-60	8.3	75	1		17.0	IS	Hilti 150
Aramind 9	A	9	55-60	1.7	15	1		17.0	IS	Hilti 500
Aramind 9	A	9	55-60	3.3	30	1		14.0	IS	Hilti 500
Aramind 9	A	9	55-60	5.0	45	1		10.0	IS	Hilti 500

Specimen ID (Experimental Program	Mat	ϕ	f_{cm}	l_b/ϕ	l_b	t	F_{pull}	τ_{avg}	F.T.	Adh.
Aramind 9	A	9	55-60	6.7	60	1		7.0	IS	Hilti 500
Aramind 9	A	9	55-60	8.3	75	1		7.0	IS	Hilti 500
Aramind 9	A	9	55-60	1.7	15	1		26.0	IS	Araldite
Aramind 9	A	9	55-60	3.3	30	1		20.0	IS	Araldite
Aramind 9	A	9	55-60	5.0	45	1		18.0	IS	Araldite
Aramind 9	A	9	55-60	6.7	60	1		17.0	IS	Araldite
Aramind 9	A	9	55-60	8.3	75	1		13.0	IS	Araldite
Aramind 9	A	9	55-60	1.7	15	1		7.0	IS	Hilti 150
Aramind 9	A	9	3.3	3.33	30	1		6.0	IS	Hilti 150
Aramind 9	A	9	5.0	5	45	1		8.0	IS	Hilti 150
Aramind 9	A	9	6.7	6.67	60	1		8.0	IS	Hilti 150
Aramind 9	A	9	8.3	8.33	75	1		5.0	IS	Hilti 150
Owa et al. (2012)[a]										
1	S	19	16.5	10	190	25	150.5	13.3	R-Y	Hilti gen
2	S	19	16.5	10	190	25	152.9	13.5	R-Y	Hilti gen
3	S	19	16.5	10	190	25	153.1	13.5	R-Y	Hilti gen
4	S	19	16.5	7	133	25	128.7	16.2	C-C	Hilti gen
5	S	19	16.5	7	133	25	117.5	14.8	C-C	Hilti gen
6	S	19	16.5	7	133	25	123.2	15.5	C-C	Hilti gen
7	S	19	35.5	7	133	25	152.4	19.2	R-Y	Hilti gen
8	S	19	35.5	7	133	25	144.3	18.2	R-Y	Hilti gen
9	S	19	35.5	7	133	25	138.4	17.4	R-Y	Hilti gen
Mahrenholtz (2012)[a]										
Post-installed										
expPI20-w0.0-d16ucr-1	S	16	20.2	5	80	20		30.1		
expPI20-w0.0-d16ucr-2	S	16	20.2	5	80	20		26.2		
expPI20-w0.4-d16-cr-1	S	16	24.1	5	80	20		22.0		
expPI20-w0.4-d16-cr-2	S	16	24.1	5	80	20		24.4		
expPI20-w0.4-d16-s0.25-con-1	S	16	18.7	5	80	20		15.9		
expPI20-w0.4-d16-s0.25-cyc-1	S	16	18.7	5	80	20		14.5		
Cast in place										
expPI20-w0.0-d16ucr-1	S	16	19.2	5	80	--		7.7		
expPI20-w0.0-d16ucr-2	S	16	19.2	5	80	--		7.8		

Notation:

Table heading: Mat - material, ϕ - ETS bar diameter, f_{cm} - average compressive strength, l_b/ϕ - ratio between the embedded length and the bar diameter, t - adhesive thickness, F_{pull}: Pullout force, τ_{avg} - average stress, F.T. - Type of Failure, Adh - Type of Adhesive.

Bar material: S – steel, C – CFRP, G – GFRP, A – AFRP, C-SC – sand coated CFRP, C-S – smooth CFRP.

Type Failure: C-S - concrete splitting, P-O - pull out, R-Y - rupture of yielding, SR - shearing in resin, IS - interlaminar shear, CC - concrete corn.

[a] For Godat et al. (2012), Owa et al. (2012), Mahrenholtz (2012) the hole diameter was indicated instead of the thickness of the adhesive layer.

Annex B

Annex B: Bond-based constitutive law and Calculation of f_{ctm}^{*}

B.1 Bond-based constitutive law

For a generic, transfer length $L_{Rfi} \le L_{Rfe}$, the relevant bond-based constitutive law $V_{fi}^{bd}\left(L_{Rfi},\delta_{Li}\right)$ is considered as in Bianco et al. (2011) neglecting the post-peak branch, and it is valid for values of $V_{fi}^{bd} \le V_{f1}^{bd}$:

$$V_{fi}^{bd}\left(L_{Rfi},\delta_{Li}\right) = L_p \cdot J_3 \cdot \lambda \cdot \left\{C_1 \cdot \left[\cos\left(\lambda \cdot L_{Rfi}\left(\delta_{Li}\right)\right) - 1\right] - C_2 \cdot \sin\left(\lambda \cdot L_{Rfi}\left(\delta_{Li}\right)\right)\right\} \tag{A.1}$$

With the bond transfers length function of the δ_{Li} as follows:

$$L_{Rfi}\left(\delta_{Li}\right) = \frac{1}{\lambda} \cdot arc\cos\left(1 - \frac{\lambda^2}{\tau_0 \cdot J_1} \cdot \delta_{Li}\right) \tag{A.2}$$

For the resisting bond length $\left(L_{Rfi} \le L_{Rfe}\right)$, the imposed end slip defining the extremities of the bond based law is defined by the equation:

$$\delta_{Li}\left(L_{Rfi}\right) = C_1 \cdot \sin\left(\lambda \cdot L_{Rfi}\right) + C_2 \cdot \cos\left(\lambda \cdot L_{Rfi}\right) + \left(\tau_0 \cdot J_1 / \lambda^2\right) \tag{A.3}$$

With bond modelling constants (Bianco 2009; Bianco et al. 2009; Bianco et al. 2012) for a ETS bar embedded in a concrete prism:

$$\frac{1}{\lambda^2} = \frac{\delta_1}{\tau_0 \cdot J_1};\ J_1 = \frac{L_p}{A_{fw}}\left[\frac{1}{E_{fw}} + \frac{A_{fw}}{A_c \cdot E_c}\right];\ J_2 = \frac{E_{fw} \cdot E_c \cdot A_c}{E_c \cdot A_c + E_{fw} \cdot A_{fw}}\ \ J_3 = \frac{E_{fw} \cdot A_{fw} \cdot E_c \cdot A_c}{L_p\left(A_c \cdot E_c + A_{fw} \cdot E_{fw}\right)};$$

$$C_1 = \delta_1 - \frac{\tau_0 \cdot J_1}{\lambda^2};\ C_2 = -\frac{\tau_0 \cdot J_1}{\lambda^2};\ C_3 = \frac{V_f^y \cdot J_1}{L_p \cdot \lambda} \tag{A.4}$$

B.2 Calculation of f_{ctm}^{*}

The simplified model described in considered and equivalent bond length to account the concrete fracture by means of η and f_{ctm}^{*}. The concrete mean tensile strength, f_{ctm}^{*} is the value, beyond which concrete is not fractured and the average available resisting bond length is not reduced $(\eta = 1)$. The value of f_{ctm}^{*} can be determinate by imposing the equality $V_{fi}^{bd} = V_{fi}^{cf}$ between the concrete fracture capacity V_{fi}^{cf} and the corresponding maximum value of the bond transferred force V_{fi}^{bd}. This latter will be attained for a transfer length that is equal to L_{Rfi} (Eq. A.2). In general it can be written:

$$V_{fi}^{cf}\left(L_{Rfi}\right) = V_{fi}^{bd}\left(L_{Rfi}\right) \tag{A.5}$$

The concrete fracture capacity can be calculated by spreading f_{ctm} thorough the semi-conical surface with o the cone, orthogonally to it in each point and integrating, as demonstrated by (Bianco 2009) the calculation can be reduced to the evaluation of the area of the ellipse intersection of the cone with the crack plane. Since in the present work the interaction between the ETS bars along the axis is not evaluated the cone opening was limited by the spacing of the ETS bars along the longitudinal axis $\left(s_{fw} \cdot \sin\beta_f\right)/\left(\sin\left(\theta+\beta_f\right)\right)$ and by $b_w/4$ in the orthogonal direction.

$$V_{fi}^{cf} = f_{ctm} \cdot \pi \cdot \min\left\{L_{Rfi} \cdot \tan\alpha; \frac{b_w}{4}\right\} \cdot \frac{\sin\left(\theta+\beta_f\right)}{2} \cdot \left(\begin{array}{l} \min\left\{\dfrac{s_{fw} \cdot \sin\beta_f}{2 \cdot \sin\left(\theta+\beta_f\right)}; \dfrac{L_{Rfi} \cdot \sin\alpha}{\sin\left(\beta_f+\theta+\alpha\right)}\right\} \\ + \min\left\{\dfrac{s_{fw} \cdot \sin\beta_f}{2 \cdot \sin\left(\theta+\beta_f\right)}; \dfrac{L_{Rfi} \cdot \sin\alpha}{\sin\left(\beta_f+\theta-\alpha\right)}\right\} \end{array} \right) \tag{A.6}$$

The bond transferred force is given by Eq. A.1, adopting simplification in Eq. (A.4). Since $J_3 = 1/J_1$, J_3 will be eliminated and substituted, whenever it appears, by $1/J_1$; since $\dfrac{1}{\lambda^2} = \dfrac{\delta_1}{\tau_0 \cdot J_1}$, C_1 vanishes and C_2 can be written as $C_2 = -\delta_1$, it results:

$$V_{fi}^{bd}\left(L_{Rfi}\right) = L_p \cdot \frac{1}{J_1} \cdot \lambda \cdot \delta_1 \cdot \sin\left(\lambda \cdot L_{Rfi}\right) \tag{A.7}$$

Substituting this latter in Eq. A.5 the f_{ctm}^{*} in Eq. 4.21 is obtained.

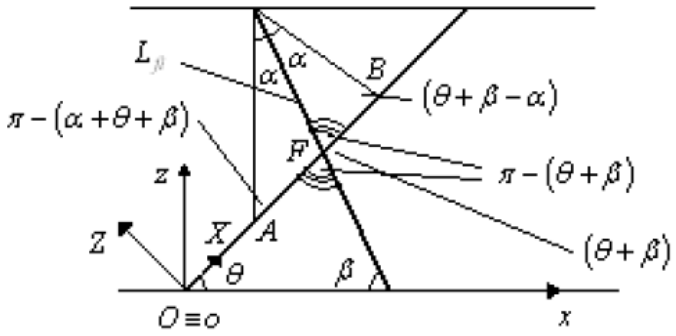

Fig.B.1 Determination of the major semi-axis

Annex C

Annex C: Preliminary numerical study on rectangular RC beams strengthened with ETS steel bars

C.1 Introduction

The performance of the proposed model presented in Chapter 5 was assessed in a preliminary study by simulating the experimental tests carried out by Barros and Dalfé (2012). The main aspect of this experimental program was presented in Chapter 2. The experimental program was formed by a series of beams with a cross section of 150x300 mm2, with a total length of 2450 mm and a shear span length of 900 mm. The longitudinal tensile steel reinforcement consist of two steel bars of 25 mm diameter. The internal shear reinforcement and the ETS strengthening arrangement are represented in Fig. C.1. The values for the characterization of the main properties of the materials used in the present work were obtained from experimental tests and can be found in Barros and Dalfré (2012).

ID	Shear strengthening system	Shear strengthening arrangements
Reference	----------	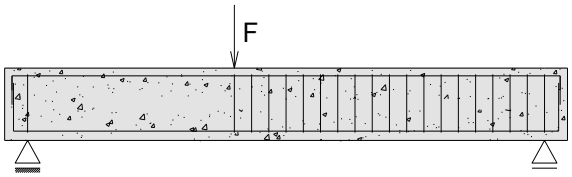
S300.90	Stirrups (2ϕ6 mm, 2 arms, 300 mm spacing)	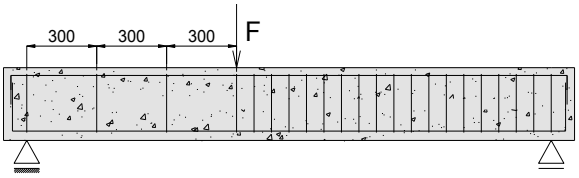
E300.90	ETS strengthening bars at 90° (3ϕ10 mm, 300 mm spacing)	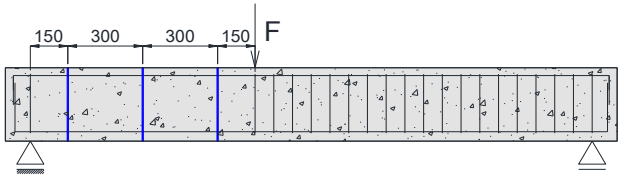

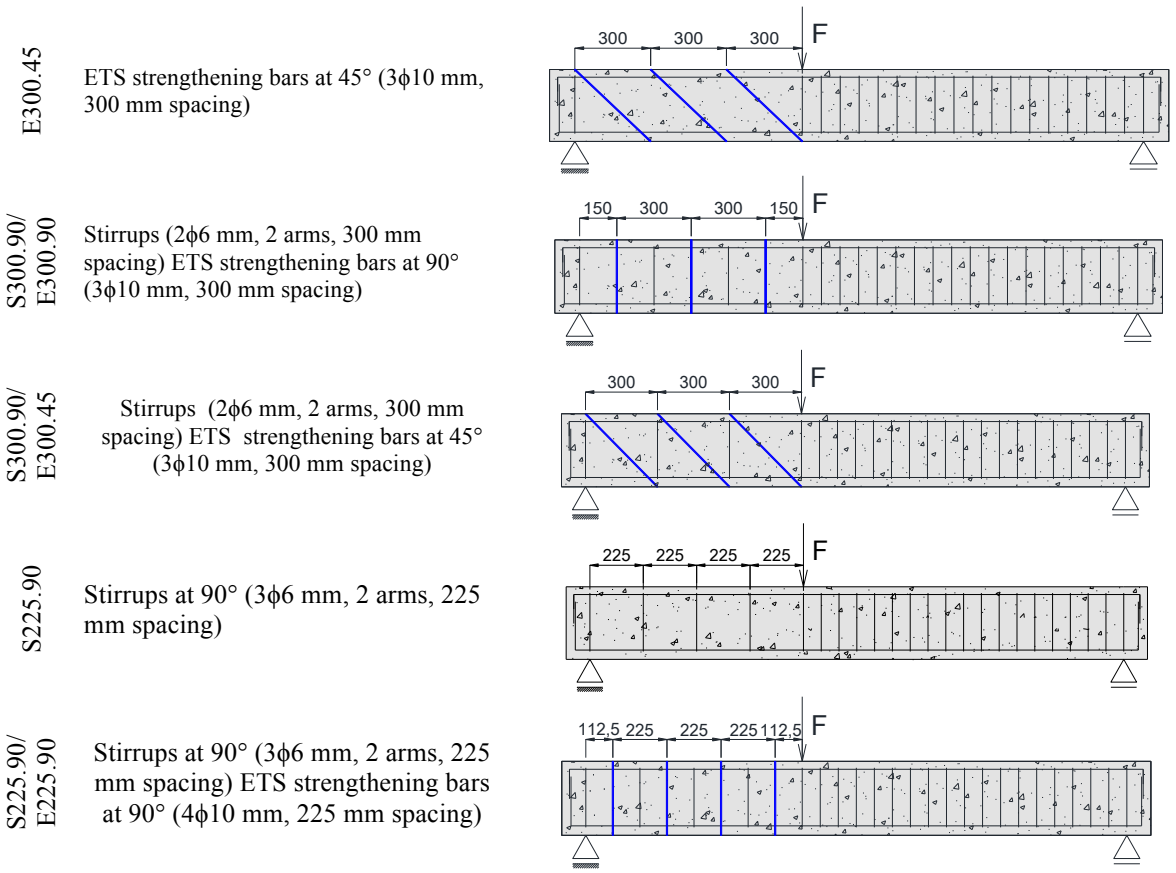

Fig. C.1 Shear reinforcement and strengthening arrangement.

C.2 Finite element mesh, integration schemes and constitutive laws for the materials

To simulate the crack initiation and the fracture mode I propagation of reinforced concrete, the trilinear tension-softening diagram represented in Fig. 5.2 was adopted. To distinguish concrete elements in tension softening and in tension stiffening, distinct values were considered for the concrete of the elements in the first two rows of finite element mesh (elements considered in tension stiffening). The values that define these diagrams are indicated in Table C.1. In this table is also included the data necessary to define the shear-softening diagram represented in Fig. 5.3, adopted to simulate the degradation of crack shear stress transfer after crack initiation. The adopted values were obtained by inverse analysis by fitting the experimental results as best as possible. An example of a finite element mesh used for the simulation of the S225.90/E225.90 beam is represented in Fig. C.2. The beams are modelled with a mesh of 8-noded serendipity plane stress finite elements. A Gauss-Legendre integration scheme with 3×3 IP is used in all concrete elements. The longitudinal steel bars, stirrups and the ETS strengthening bars are modelled with 3-noded perfect bonded embedded cables (one degree-of-freedom per each node) and a Gauss-Legendre integration scheme with 3 IP (integration point) is used.

Table C.1 Values of the parameters of the concrete constitutive model

Poisson's ratio (ν_c)	0.15
Initial Young's modulus (E_c)	31100 N/mm^2 (Batch 1) 30590 N/mm^2 (Batch 2)
Compressive strength (f_c)	30.78 N/mm^2 (Batch 1) 28.81 N/mm^2 (Batch 2)
Trilinear tension-stiffening diagram [(1)]	f_{ct} = 2.0 N/mm^2 ; G_f = 0.06 N/mm ξ_1 = 0.01; α_1 = 0.5; ξ_2 = 0.5; α_2 = 0.2
Trilinear tension-softening diagram [(1)]	f_{ct} = 1.8 N/mm^2 ; G_f = 0.05 N/mm ξ_1 = 0.01; α_1 = 0.4; ξ_2 = 0.5; α_2 = 0.2
Parameter defining the mode I fracture energy available to the new crack [4]	n = 2
Parameters for defining the softening crack shear stress-shear strain diagram of concrete in the tension-stiffening	$\tau_{t,p}^{cr}$ = 1.38 N/mm^2; $G_{f,s}$=0.5 N/mm; β =0.2
Parameters for defining the softening crack shear stress-shear strain diagram of concrete in the tension-softening	$\tau_{t,p}^{cr}$ = 1.38 N/mm^2; $G_{f,s}$=0.7 N/mm; β =0.2
Crack bandwidth, l_b	*Square root of the area of Gauss integration point*
Threshold angle [4]	α_{th} = 30º
Maximum number of cracks per integration point	2

(1) $f_{ct} = \sigma_{n,1}^{cr}$; $\xi_1 = \varepsilon_{n,2}^{cr} / \varepsilon_{n,u}^{cr}$; $\alpha_1 = \sigma_{n,2}^{cr} / \sigma_{n,1}^{cr}$; $\xi_2 = \varepsilon_{n,3}^{cr} / \varepsilon_{n,u}^{cr}$; $\alpha_2 = \sigma_{n,3}^{cr} / \sigma_{n,1}^{cr}$ (see Fig. 5.2)

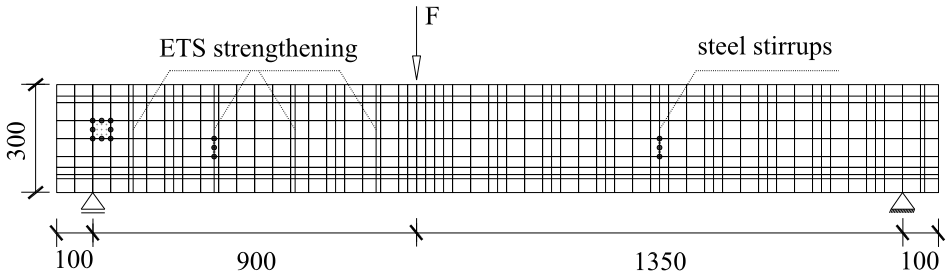

Fig. C.2 Finite element mesh (dimensions are in mm)

For modeling the behavior of the longitudinal steel bars, stirrups and ETS bars, the stress-strain relationship represented in Fig. 5.5 was adopted. The curve (under compressive or tensile loading) is defined by the points PT1=(ε_{sy},σ_{sy}), PT2=(ε_{sh},σ_{sh}) and PT3=(ε_{su},σ_{su}), and a parameter p that defines the shape of the last branch of the curve. Unloading and reloading linear branches with slope $E_s = \left(\sigma_{sy} / \varepsilon_{sy}\right)$ are assumed in the present approach. The values of the parameters of the constitutive model for the steel are indicated in Table C.2.

Table C.2 Values of the parameters of the steel constitutive model.

Steel bar diameter (mm)	PT1 $\varepsilon_{sy}[-]$ $\sigma_{sy}(MPa)$	PT2 $\varepsilon_{sh}[-]$ $\sigma_{sh}(MPa)$	PT3 $\varepsilon_{su}[-]$ $\sigma_{su}(MPa)$	p
6	2.750×10^{-3} 559.14	2.000×10^{-2} 708.14	5.000×10^{-2} 708.93	1
10	2.660×10^{-3} 541.60	2.405×10^{-2} 643.23	5.000×10^{-2} 643.23	1
12	2.350×10^{-3} 484.68	2.302×10^{-2} 655.00	5.000×10^{-2} 655.53	1
25	2.270×10^{-3} 507.68	3.450×10^{-3} 608.75	2.052×10^{-2} 743.41	1

C.3 Simulations and discussion

The experimental and the numerical relationships between the applied load and the deflection at the loaded section for the tested beams are compared in Fig. C.3. In these figures a horizontal line corresponding to the maximum experimental load (in dash) is also included. The crack patterns of these beams at the end of the analysis (at the end of the last converged load increment) are represented in Fig.C.4. These figures show that the numerical model is able to capture with good accuracy the deformational response of the beams and captured with good precision the localization and profile of the shear failure crack. Fig. C.5 also shows that the numerical simulations fit with good accuracy the strains measured in the steel stirrups and ETS strengthening bars, which means that the assumption of perfect bond between composite materials and surrounding concrete is acceptable, at least in the design point of view for the serviceability and ultimate limit states. Similar level of accuracy was obtained in the simulations of the other beams. At the moment of the shear failure, the longitudinal steel bars have already yielded in some of the beams, which is quite well predicted by the numerical models, since vertical completely open cracks were formed (flexural cracks)

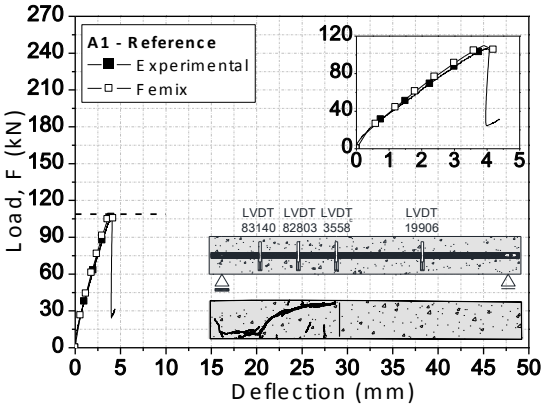

(a) Reference

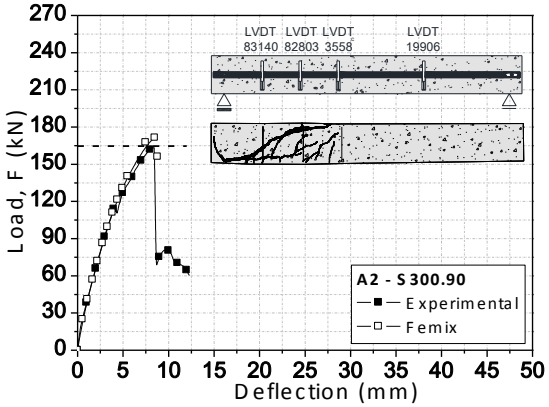

(b) S300.90

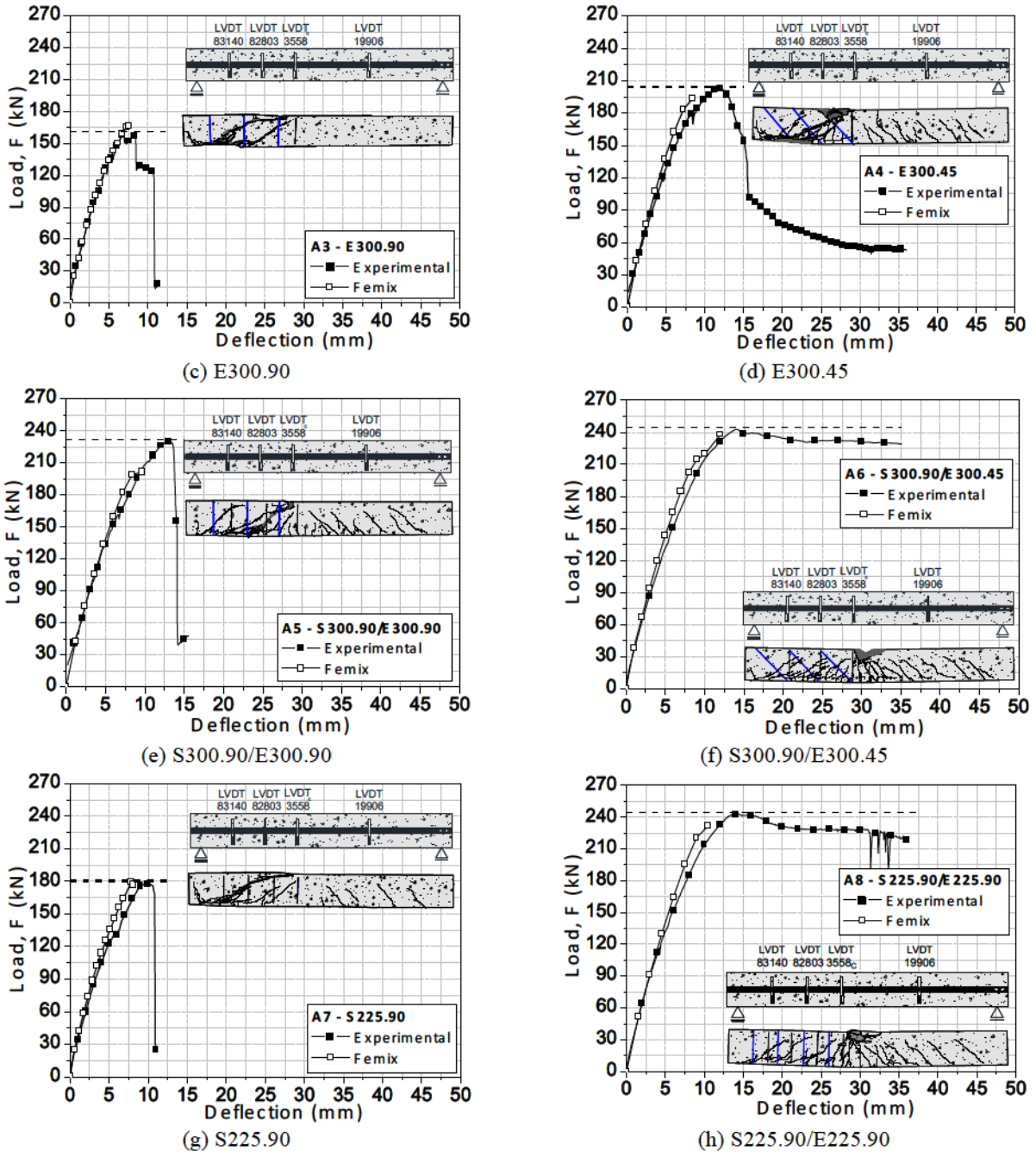

(c) E300.90 (d) E300.45

(e) S300.90/E300.90 (f) S300.90/E300.45

(g) S225.90 (h) S225.90/E225.90

Fig. C.3 Comparison between experimetal and numerical results

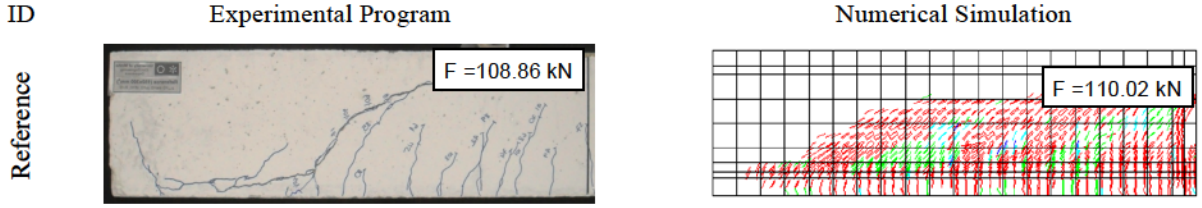

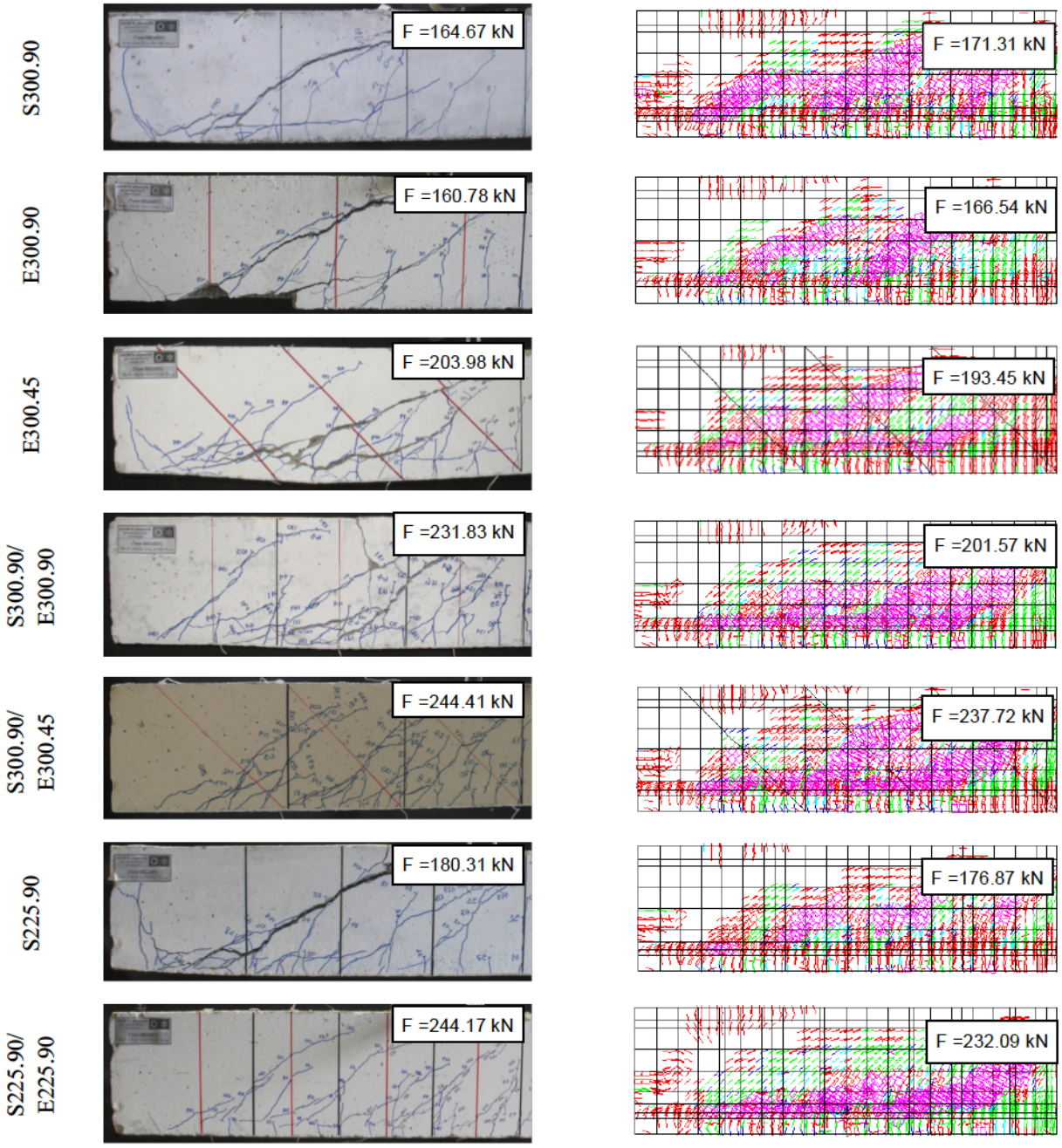

Fig. C.4 Experimental and numerical crack pattern

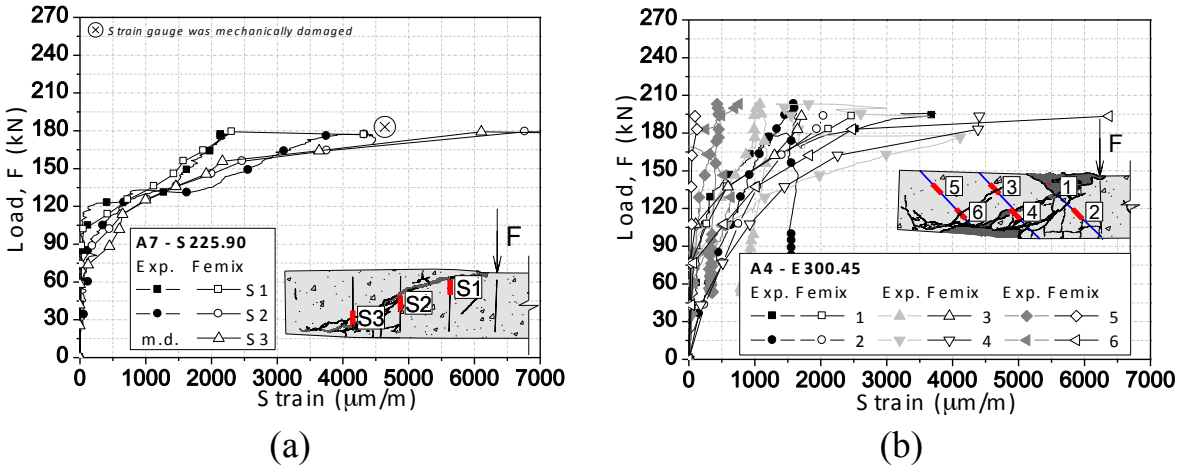

(a) (b)

Fig. C.5 Load *vs.* strains in the shear reinforcement of the beams: (a) S225.90, and (b) E300.45.